OCT 2 5 1946

VOLUME 104 NUMBER 2

THE ASTROPHYSICAL JOURNAL

AN INTERNATIONAL REVIEW OF SPECTROSCOPY AND ASTRONOMICAL PHYSICS

Founded in 1895 by GEORGE E. HALE *and* JAMES E. KEELER

Edited by

OTTO STRUVE
Managing Editor

S. CHANDRASEKHAR
Associate Managing Editor

Yerkes Observatory of the University of Chicago

PAUL W. MERRILL
Mount Wilson Observatory of the Carnegie Institution of Washington

HARLOW SHAPLEY
Harvard College Observatory
Cambridge, Massachusetts

N. U. MAYALL
Lick Observatory
University of California

SEPTEMBER 1946

RECTIFICATION OF THE LIGHT-CURVES OF ECLIPSING VARIABLES *Henry Norris Russell* 153
A STUDY OF THE EXTENDED ENVELOPE SURROUNDING THE WOLF-RAYET COMPONENT OF V 444 CYGNI . . . . . *Zdeněk Kopal and Martha B. Shapley* 160
THE INFRARED SPECTRUM OF υ SAGITTARII . *Jesse L. Greenstein and Paul W. Merrill* 177
ON THE RADIATIVE EQUILIBRIUM OF A STELLAR ATMOSPHERE. XII *S. Chandrasekhar* 191
ON THE HELIUM CONTENT OF THE SUN . . . . . *Martin Schwarzschild* 203
ULTRAVIOLET ABSORPTION SPECTRUM OF AIR IN THE REGION $\lambda\lambda$ 600–2000 *J. J. Hopfield* 208
ON THE DIRECTION OF ROTATION IN SPIRAL NEBULAE *Bertil Lindblad and Rolf Brahde* 211
STRUCTURE AND MASS OF COMETARY NUCLEI . . . . *B. Vorontsov-Velyaminov* 226
DWARF M STARS FOUND SPECTROPHOTOMETRICALLY: SECOND LIST *A. N. Vyssotsky, E. M. Janssen, W. J. Miller, S. J., and M. E. Walther* 234
MOTIONS AND ABSOLUTE MAGNITUDES OF DWARF M STARS . *A. N. Vyssotsky* 239
ON THE INTERSTELLAR REDDENING IN THE REGION OF THE NORTH POLAR SEQUENCE AND THE NORMAL COLOR INDICES OF A-TYPE STARS *W. W. Morgan and W. P. Bidelman* 245
SPECTROGRAPHIC OBSERVATIONS OF FOURTEEN ECLIPSING BINARIES *Otto Struve* 253
SPECTROSCOPIC OBSERVATIONS OF θ AQUILAE . . *Carlos U. Cesco and Otto Struve* 282
SPECTROSCOPIC OBSERVATIONS OF ζ^1 URSAE MAJORIS . . . *Carlos U. Cesco* 287
THE RADIAL VELOCITIES OF FIFTY GLOBULAR STAR CLUSTERS . *N. U. Mayall* 290
NOTES
SOME REMARKS ON THE NOVA PHENOMENON . . . . . *Svein Rosseland* 324
NOTE ON THE SPECTRAL AND LUMINOSITY CLASSIFICATION OF STARS FROM SPECTRA OF LOW DISPERSION . . . . . *Bertil Lindblad* 325
THE OCCURRENCE OF CYCLES IN *He* I . . . . . *Anne B. Underhill* 327
REVIEWS 330
ERRATUM 332

THE UNIVERSITY OF CHICAGO PRESS
CHICAGO, ILLINOIS, U.S.A.

September 1946 Vol. 104, No. 2

THE ASTROPHYSICAL JOURNAL

AN INTERNATIONAL REVIEW OF SPECTROSCOPY AND ASTRONOMICAL PHYSICS

Edited by

OTTO STRUVE
Managing Editor

S. CHANDRASEKHAR
Associate Managing Editor

Yerkes Observatory of the University of Chicago

PAUL W. MERRILL
Mount Wilson Observatory of the Carnegie Institution of Washington

HARLOW SHAPLEY
Harvard College Observatory
Cambridge, Massachusetts

N. U. MAYALL
Lick Observatory
University of California

With the Collaboration of the American Astronomical Society

Collaborating Editors:

1944-46	1945-47	1946-48
JOEL STEBBINS Washburn Observatory	CECILIA H. PAYNE-GAPOSCHKIN Harvard College Observatory	C. S. BEALS Dominion Astrophysical Observatory, Victoria
A. N. VYSSOTSKY Leander McCormick Observatory	H. N. RUSSELL Princeton University	LUIS E. ERRO Astrophysical Observatory, Tonantzintla
W. W. MORGAN Yerkes Observatory	R. H. BAKER University of Illinois	O. C. WILSON Mount Wilson Observatory

The Astrophysical Journal is published bimonthly by the University of Chicago at the University of Chicago Press, 5750 Ellis Avenue, Chicago, Illinois, during July, September, November, January, March, and May. ¶The subscription price is $10.00 a year; the price of single copies is $2.00. Orders for service of less than a full year will be charged at the single-copy rate. ¶Postage is prepaid by the publishers on all orders from the United States and its possessions, Argentina, Bolivia, Brazil, Chile, Colombia, Costa Rica, Cuba, Dominican Republic, Ecuador, Guatemala, Haiti, Republic of Honduras, Mexico, Morocco (Spanish Zone), Nicaragua, Panama, Paraguay, Peru, Rio de Oro, El Salvador, Spain (including Balearic Islands, Canary Islands, and the Spanish Offices in Northern Africa; Andorra), Spanish Guinea, Uruguay, and Venezuela. ¶Postage is charged extra as follows: for Canada and Newfoundland, 42 cents on annual subscriptions (total $10.42); on single copies, 7 cents (total $2.07); for all other countries in the Postal Union, 96 cents on annual subscriptions (total $10.96), on single copies 16 cents (total $2.16). ¶Patrons are requested to make all remittances payable to The University of Chicago Press, in United States currency or its equivalent by postal or express money orders or bank drafts.

The following are authorized agents:

For the British Empire, except North America, India, and Australasia: The Cambridge University Press, Bentley House, 200 Euston Road, London, N.W. 1, England. Prices of yearly subscriptions and of single copies may be had on application.

Claims for missing numbers should be made within the month following the regular month of publication. The publishers expect to supply missing numbers free only when losses have been sustained in transit, and when the reserve stock will permit.

Business correspondence should be addressed to The University of Chicago Press, Chicago 37, Illinois.

Communications for the editors and manuscripts should be addressed to: Otto Struve, Editor of THE ASTROPHYSICAL JOURNAL, Yerkes Observatory, Williams Bay, Wisconsin.

Line drawings and photographs should be made by the author, and all marginal notes such as co-ordinates, wave lengths, etc., should be included in the cuts. It will not be possible to set up such material in type.

One copy of the corrected galley proof should be returned as soon as possible to the editor, Yerkes Observatory, Williams Bay, Wisconsin. Authors should take notice that the manuscript will not be sent to them with the proof.

The cable address is "Observatory, Williamsbay, Wisconsin."

The articles in this journal are indexed in the *International Index to Periodicals*, New York, N.Y.

Applications for permission to quote from this journal should be addressed to The University of Chicago Press, and will be freely granted.

Entered as second-class matter, July 31, 1940, at the Post-Office at Chicago, Ill., under the act of March 3, 1879.
Acceptance for mailing at special rate of postage provided for in United States Postal Act of October 3, 1917, Section 1103, amended February 28, 1925.

[PRINTED IN U.S.A.]

THE ASTROPHYSICAL JOURNAL

AN INTERNATIONAL REVIEW OF SPECTROSCOPY AND ASTRONOMICAL PHYSICS

VOLUME 104 SEPTEMBER 1946 NUMBER 2

RECTIFICATION OF THE LIGHT-CURVES OF ECLIPSING VARIABLES

HENRY NORRIS RUSSELL
Princeton University Observatory

Received July 1, 1946

ABSTRACT

The usual methods of solution for the elements of an eclipsing binary involve rectification of the observed light-curve to remove the effects of variation outside the eclipses. Rectification for the effects of ellipticity and gravity-darkening may be made by *division* of the observed intensities by a certain factor. The process is exact only if the photometric ellipticities of the components are the same, but it is legitimate under the assumptions on which the intermediary model is based. Rectification for reflection demands the *addition* of a certain quantity to the observed intensity. When the minima are sufficiently unequal in depth, this quantity may be found from the term in cos θ in the empirical expression for the light outside eclipse. Otherwise, an approximate method, depending on the observed duration of eclipse, may be employed. These corrections depend upon the spectral types of the components. Formulae and tables for them are given.

1. If, in an eclipsing pair of stars, the components are spherical and each of constant surface brightness, except for darkening toward the limb in accordance with a definite law, the light will be constant and the light-curve horizontal, except for the effects of eclipse. Let L_1 be the light of the large star, L_2 that of the smaller, and take $L_1 + L_2$ as the unit. The light received from the system during the occultation (L_1 in front) will then be $l^o = 1 - \alpha^o L_2$, and during the transit (L_2 in front) $l^t = 1 - \tau(k)\alpha^t L_1$, when α^o and α^t define the extent of obscuration at the given phase and τ is the fraction of the light of L_1 lost at internal tangency.[1] Methods and tables for solving the problem when α is given as a function of the orbit-longitude θ are well known.

The components will actually be ellipsoidal in form; their surface brightness will be greater on the sides facing each other, and it will vary with the local intensity of gravity on their surfaces. If any of these effects is sensible, the light outside eclipse will not be constant. Before applying the ordinary methods of solution, this curve must be "rectified" so as to convert it into one which is horizontal between eclipses.

It was shown in 1912[2] that (on the assumption that the components are similar in form and each of uniform apparent surface brightness) rectification for ellipticity could be precisely made by *dividing* the observed light of the system by the light which would be received at the same moment from the two stars together if no eclipse occurred; and also that to rectify for "reflection" a certain quantity should be *added* to the observed

[1] This is called Q (k, 1) in *Ap. J.*, **36**, 392, 1912.

[2] Russell, *Ap. J.*, **36**, 65–69, 1912.

light. Both corrections are usually small, and it is then practically indifferent in what order they are made.

It has since been shown that when limb-darkening is present, the same methods may be employed[3] (with certain small outstanding errors) and that rectification for the gravity effect may in practice be combined with that for ellipticity.[4] There has, however, been considerable inconsistency in recent publications on the subject, aggravated by a serious mistake in a recent paper by the writer,[5] for which apologies are here offered. The erroneous statement is that rectification is to be made by division alone (p. 6).

2. A discussion of the subject, starting "from scratch" and containing considerable new material, may be in order.

The observed light of any eclipsing system is exactly defined by the equation

$$l = l_2(1 - \alpha^o) + l_1(1 - \tau\alpha^t). \tag{1}$$

Here l_1 and l_2 represent the light which would be received from each component separately at any phase, including all effects of unevenness of form or surface brightness; and α^o and $\tau\alpha^t$ represent the fractions by which l_2 and l_1 are diminished under the actual circumstances of eclipse for a given longitude θ. Note that $\alpha^o = 0$, except during the occultation, and that $\alpha^t = 0$, except during the transit; so that, outside eclipse, $l = l_1 + l_2$; during occultation $l^o = l_1 + l_2 - \alpha^o l_2$; during transit $l^t = l_1 + l_2 - \tau\alpha^t l_1$. Then

$$\alpha^o = \frac{l_1 + l_2 - l^o}{l_2}, \qquad \text{and} \qquad \tau\alpha^t = \frac{l_1 + l_2 - l^t}{l_1}. \tag{2}$$

There is good theoretical reason for believing that the expressions

$$\left.\begin{aligned} l_1 &= A_0' + A_1' \cos\theta + A_2' \cos 2\theta\,, \\ l_2 &= A_0'' + A_1'' \cos\theta + A_2'' \cos 2\theta\,, \end{aligned}\right\} \tag{3}$$

should be valid except for small terms of the second order in A_1'/A_0', A_2'/A_0', etc. Such terms will be neglected throughout this discussion. Then we may write

$$l_1 + l_2 = A_0 + A_1 \cos\theta - A_2 \cos 2\theta\,. \tag{4}$$

The values of A_0, A_1, and A_2 may be determined from the observations outside eclipse, and equation (4) may be used to extrapolate $l_1 + l_2$ during the eclipses—with an uncertainty which may be considerable if the eclipses occupy a large part of the period.

Apart from this, $l_1 + l_2 - l$ may be regarded as an observational datum, though not a directly observed quantity; but l_1 and l_2 are not separately known.

If, however, their ratio is constant, we may set

$$l_1 = L_1(l_1 + l_2)\,, \qquad l_2 = L_2(l_1 + l_2)\,, \qquad L_1 + L_2 = 1\,. \tag{5}$$

Then

$$L_2\alpha^o = \frac{l_1 + l_2 - l^o}{l_1 + l_2}, \qquad \text{and} \qquad L_1\tau\alpha^t = \frac{l_1 + l_2 - l^t}{l_1 + l_2}. \tag{6}$$

These equations express the process of rectification by division, the divisor being the calculated light cleared of eclipses. If it is permissible, the further solution proceeds conventionally—including the determination as to which of the eclipses is an occultation and which a transit.

[3] Russell and Shapley, *Ap. J.*, **36**, 400, 1912.

[4] Russell, *Ap. J.*, **90**, 658, 1939.

[5] *Ap. J.*, **102**, 6, 1945.

3. The variation due to ellipticity and gravity effect is given by the equation[6]

$$l = l_0 (1 - \tfrac{1}{2} C \sin^2 i \cos 2\theta) \tag{7}$$

where

$$C_1 = \frac{(15 + x_1)(1 + y_1)}{15 - 5x_1} \epsilon_1 , \tag{8}$$

when ϵ is the geometrical ellipticity of the equator and x and y the coefficients of limb- and gravity-darkening. Condition (5) then reduces to $C_1 = C_2$. Dynamical theory gives $\epsilon_1 = \frac{3}{2}(m_2/m_1) r_1^3$, and x and y depend on the effective temperature of the star. If the components are unequal, it is probable that C_1 and C_2 are different, and exact rectification by division is impossible. In this case ϵ_1 and ϵ_2 probably also differ, which greatly complicates the geometry of the eclipses, so that Kopal's new functions are required for a solution.

To avoid this, an intermediary method, consisting of two similar ellipsoids, is used in the first approximation. In such a case it is usually assumed, at least in the first solution, that the "darkening," x, is the same. These two assumptions, adopted to obtain a workable conventionalized model, are exactly those which justify the process of rectification by division. They do not interfere with subsequent correction of the elements by the method of false position.

4. The reflection effect (for spherical stars, according to Milne) is given by

$$l_1 = L_1' + f_1 (0.28 + 0.35 \cos \epsilon_1 + 0.07 \cos 2\epsilon_1) , \tag{9}$$

when $f_1 = (E_1/E_2) L_2 r_1^2$; L_1 and L_2 are the monochromatic luminosities of each star as seen from the other; E_1 and E_2 the luminous efficiencies of their radiation; L_1' the light cleared of reflection-effect; and ϵ_1 the phase-angle at the center of star 1 between the other star and the observer. Then $l_1 = L_1$ when $\epsilon = 0$, and

$$\left.\begin{aligned} l_1 &= L_1 + f_1 (-0.42 - 0.35 \sin i \cos \theta + 0.07 \sin^2 i \cos 2\theta) , \\ l_2 &= L_2 + f_2 (-0.42 + 0.35 \sin i \cos \theta + 0.07 \sin^2 i \cos 2\theta) . \end{aligned}\right\} \tag{10}$$

It is impossible to satisfy condition (5); and the terms in $\cos \theta$ must be removed before rectification by division can be attempted. This may be done by adding to l_1 and l_2 the quantities

$$\left.\begin{aligned} x &= f_1 (0.28 + 0.35 \sin i \cos \theta + 0.07 \sin^2 i \cos 2\theta) , \\ x_2 &= f_2 (0.28 - 0.35 \sin i \cos \theta + 0.07 \sin^2 i \cos 2\theta) . \end{aligned}\right\} \tag{11}$$

This amounts to adding to the hemisphere of each star remote from the other a distribution of brightness identical with that added by "reflection" on the near hemisphere. This additional light will never be eclipsed by any sensible amount—though a minute fraction may be, under special conditions. With this addition, the rectified intensity outside eclipse is $l_1 + l_2 + x_1 + x_2$ and inside, $l + x_1 + x_2$. The modified curve can be exactly rectified by addition if

$$(l_1 + x_1) / (l_1 + l_2 + x_1 + x_2) = \text{const} . \tag{12}$$

If ellipticity is also present, equations (9)–(12) should be modified by quantities of the order of the product of the ellipticity and reflection effects. Neglecting these, in the first approximation, we have

$$+ x_1 = L_1 [1 - 0.14 f_1 - (\tfrac{1}{2} C_1 - 0.14 f_1) \sin^2 i \cos 2\theta] . \tag{13}$$

[6] *Ibid.*, p. 4.

To the first order, the condition for rectification by division then becomes

$$C_1 - 0.28 f_1 = C_2 - 0.28 f_2 .$$

If the components are equal in size and brightness, this relation will be satisfied. In the "typical" Algol system, $r_1 > r_2$, $L_2 > L_1$, $m_2 > m_1$, and C_2 and f_2 are much less than C_1 and f_1. The difference in C will have to be ignored, in the first approximation, for geometrical reasons. That in f does not make things worse. Rectification by addition of the partial correction for reflection, combined with division to eliminate ellipticity and the rest of the reflection, appears, therefore, to be the best policy.

Equations (2) are now replaced by

$$a^o = \frac{l_1 + l_2 - l^o}{l_2 + x_2} \quad \text{and} \quad \tau a^t = \frac{l_1 + l_2 - l^t}{l_1 + x_1} . \tag{14}$$

The first of these applies to the eclipse centered on $\theta = 0$. At this phase $x_2 = 0$; and even when $\theta = 40°$, it has only 5 per cent of its maximum value, so that the additive part of the rectification has a very small effect on the calculated a. Its important effect is on the values of L_1 and L_2, which are reduced to those of the brighter sides of the components. Cases are known in which the back of a totally eclipsing companion observed during a total eclipse is only half as bright as the illuminated side. If the brightness of the former were used in calculating the secondary eclipse, gross errors would result.

5. If we set

$$l_1 + l_2 = A_0 + A_1 \cos\theta + A_2 \cos 2\theta , \tag{15}$$

equation (10) gives

$$A_1 = 0.35 (f_2 - f_1) \sin i . \tag{16}$$

Substituting in equation (11) and setting $\sin i = 1$ (neglecting second-order terms), we have

$$x_1 + x_2 = - A_1 \cos\theta + \frac{f_2 + f_1}{f_2 - f_1} A_1 (0.8 + 0.2 \cos 2\theta) . \tag{17}$$

If J is the surface brightness for the effective wave length,

$$\frac{f_2}{f_1} = \frac{J_1}{E_1^2} \Big/ \frac{J_2}{E_2^2} . \tag{18}$$

On black-body assumptions, J/E^2 depends only on the temperature. With $C_2 = 1.438$ and Kuiper's temperatures we obtain the results given in Table 1. The units of J and E

TABLE 1

λ	Sp.	B0	B5	A0	A5	F0	F5	G0	dG5	dK0	dM0
5290.....	log J.....	1.44	1.05	0.67	0.35	0.17	−0.08	−0.23	−0.46	−0.67	−1.54
(vis).....	log (J/E²).	3.12	1.81	0.93	0.41	0.18	−0.07	−0.19	−0.35	−0.45	−0.66
4250.....	log J.....	1.24	0.85	0.38	0.02	−0.22	−0.54	−0.71	−0.98	−1.26	−2.35
(photo).....	log (J/E²).	2.37	1.29	0.45	0.01	−0.18	−0.40	−0.48	−0.56	−0.62	−0.62

correspond to $C_2/\lambda T = 4$ (at which E is very near maximum) or to 6800° ($F_{2.5}$) for visual and 8500° (A_5) for photographic observations.

Except at the lowest temperatures, f is greater for the cooler star, and $l_1 + l_2$ will be greatest when this star is eclipsed—that is, near the secondary minimum. If the com-

ponents are equal in temperature, $f_1 = f_2$ and $A_1 = 0$, as is well known. If both stars have spectra later than G5, A_1 will be small visually and negligible photographically, even though they may differ considerably in surface brightness. In all such cases $(f_2 + f_1)/(f_2 - f_1)$ is large, and equation (17) is useless for rectification.

The limit for effective application comes when this factor is about 4, or when $f_c = 0.6 f_h$[7]. For total radiation this is also the limiting value of J_c/J_h. For monochromatic radiation J_c/J_h varies with the spectral class, as shown in Table 2. Rectification by

TABLE 2

$f_c = 0.6 f_h$

Sp_h	B0	B5	A0	A5	F0	F5	G0	dG5	dK0
(vis) J_c/J_h	0.91	0.83	0.78	0.66	0.61	0.51	0.47	0.28	.....
(photo) J_c/J_h . .	0.85	0.76	0.66	0.54	0.47	0.26	.....	.....	.....

equation (17) is effective in most cases among the hotter stars, but not at all for the cooler ones. This conclusion appears to be new.

In practice, the observed spectrum of the combined light will usually be that of the hotter star. There are exceptions (ζ Aurigae!); but, if radial velocities are available, there will be no uncertainty. The value of J_h is then known. With sufficient accuracy for the purpose, it may be assumed that J_c/J_h equals the ratio of the depths of the minima (rectified for ellipticity). The values of J_c and f_c/f_h may then be found from Table 1.

6. When the depths of minima are more nearly equal than the limits given in Table 2, the coefficient A_1 is useful only for removing the term $A_1 \cos\theta$. The remaining terms may be written

$$\Delta x = (f_h + f_c)(0.28 + 0.07 \cos 2\theta), \tag{19}$$

setting $\sin i = 1$, as above. It is easily verified that

$$\frac{f_h + f_c}{L_h + L_c} = \frac{f_h + f_c}{(f_h f_c)^{1/2}} \cdot \frac{(J_h J_c)^{1/2}}{J_h + J_c} \cdot \frac{(J_h + J_c)\, r_h r_c}{J_h r_h^2 + J_c r_c^2} \cdot r_h r_c . \tag{20}$$

In the case here considered, f_c/f_h lies between 0.6 and 1; so that the first factor in equation (20) lies between 0.52 and 0.5. The value of J_c/J_h is between f_c/f_h and 1, except for late spectral types; hence the product of the first two factors will be very close to 1. The third factor may be written

$$\frac{(J_1 + J_2)\, r_1 r_2}{J_1 r_1^2 + J_2 r_2^2} .$$

When we set

$$J_1 = \bar{J}(1 + j) \qquad J_2 = \bar{J}(1 - j), \qquad \text{and} \qquad r_2 = k r_1$$

this becomes

$$\frac{2k}{1 + k^2} \Big/ \left(1 + j \frac{1 - k^2}{1 + k^2}\right), \tag{21}$$

in which j may have either sign but is usually less than 0.3. Finally, from the basic equation of the eclipse theory,

$$r_1^2 (1 + pk)^2 = \cos^2 i + \sin^2 i \sin^2 \theta ,$$

[7] The subscripts h and c apply to the hotter and cooler components; b and f to the brighter and fainter and 1 and 2 to the larger and the smaller.

it follows that

$$\sin^2 i \sin^2 \theta' = r_1 r_2 (1 - p_0)(2 + k + k p_0),$$

where θ' corresponds to external tangency ($p = 1$) and p_0 to $\theta = 0$. For

$p_0 = 0$ (shallow partial eclipse), $\quad \sin^2 \theta' = (2 + k)\, r_1 r_2 \operatorname{cosec}^2 i$;

$p_0 = -1$ (grazing total), $\quad \sin^2 \theta' = 4 r_1 r_2 \operatorname{cosec}^2 i$;

$p_0 = -\frac{1}{k}$ (central eclipse) $\quad \sin^2 \theta' = \left(2 + k + \frac{1}{k}\right) r_1 r_2 \operatorname{cosec}^2 i$.

We may then write

$$\frac{f_h + f_c}{L_h + L_c} = F_1 F_2 \sin^2 \theta', \tag{22}$$

where

$$F_2 = \frac{1 + k^2}{1 + k^2 + j(1 - k^2)}$$

and for shallow partial eclipses,

$$F_1 = \frac{2k}{(1 + k^2)(2 + k)},$$

for grazing total eclipses,

$$F_1 = \frac{k}{2(1 + k^2)},$$

for central eclipses,

$$F_1 = \frac{2k^2}{(1 + k^2)(1 + k)^2}.$$

Table 3 gives, with argument k, the values of F_1 for these three cases, of F_2 for $j = \pm 0.3$.

TABLE 3

k	1.0	0.8	0.6	0.5	0.4
F_1 (shallow partial)	0.333	0.348	0.339	0.320	0.288
F_1 (grazing total)	0.250	0.244	0.221	0.200	0.172
F_1 (central)	0.250	0.241	0.209	0.178	0.141
F_2: $j = +0.3$	1.00	0.94	0.88	0.85	0.82
F_2: $j = -0.3$	1.00	1.07	1.16	1.22	1.28
Depth	0.50	0.39	0.26	0.20	0.14

The last line gives the depth of total eclipse $k^2/(1 + k^2)$ for uniform disks of equal J. For $p_0 = 0$, the depth should be a little less than half as great.

With Table 3 as a guide, it appears that values of k less than 0.6 will come into consideration only if the eclipses are very shallow. Otherwise, we may set $F_1 = 0.23$ for complete eclipses, with an average error of less than 10 per cent; and $F_1 = 0.29$ for partial eclipses, with errors that may rise to 20 per cent. The additional error contributed by F_2 will average less than 5 per cent, since j will usually be considerably less numerically than 0.3. We have, then, for the average correction Δx to be added for rectification for reflection,

$$\left.\begin{aligned} \Delta x &= (0.064 + 0.016 \cos 2\theta) \sin^2 \theta' \quad \text{(total eclipse)}, \\ \Delta x &= (0.080 + 0.020 \cos 2\theta) \sin^2 \theta' \quad \text{(partial eclipse)}. \end{aligned}\right\} \tag{23}$$

The difference of the two is hardly significant. On the average $\sin^2 \theta'$ will be about 0.3. The rectification correction will therefore usually be 2 or 3 per cent of the total light. This summary correction need be applied only in the first approximate solution. This, if determinate, will give values of L_1, L_2, r_1, and r_2, from which a second and much better approximation may be derived and applied if it differs sensibly from the first.

7. If the effects of ellipticity and reflection are both small, it is theoretically indifferent which is removed first. But when the ellipticity is large, it is very difficult to estimate either the duration or the depths of the minima from the unrectified light-curve; and a preliminary rectification for ellipticity should be made first. Rectification of this curve for reflection may then be made. Many such systems have late-type spectra, and the method of section 6 must be employed. Strictly speaking, the smaller equatorial radii should be used in calculating the reflection. The formulae in terms of $\sin \theta'$ make a considerable, though not a complete, approach toward doing this.

This rectification introduces a small term in $\cos 2\theta$, which must be removed by another division in order to get a completely rectified curve. This costs little labor.

For some systems of the W Ursae Majoris type it is difficult to separate the effects of ellipticity and eclipse; and it is good policy to derive two rectified curves depending on different assumed values of the ellipticity to see whether the observations are adequate to distinguish between the two.

8. The procedure recommended for rectification, in the general case, may be summarized as follows:

a) Plot the observations, assembled on the period, using the datum (stellar magnitude or intensity) which is determined observationally with nearly the same probable error in all cases. Draw a freehand curve to represent them throughout the period.

b) Turn the readings of this curve into intensities, if necessary. Plot these. Estimate what portion of the curve is free from eclipse, and represent the intensities in this by the formula $l_1 + l_2 = A_0 + A_1 \cos \theta + A_2 \cos 2\theta$.

c) Rectify provisionally for ellipticity by dividing the observed intensity by $A_0 + A_2 \cos 2\theta$.

d) Redetermine the term $A_1 \cos \theta$ from this curve, if necessary.

e) Record the depths of the rectified minima as fractions of the rectified intensity $1 + A_1 \cos \theta$.

f) If the ratio of the depth of the secondary to the primary is less than the limiting values given in Table 2, as functions of the spectral class of the brighter star, rectify for reflection by adding the quantity $x_1 + x_2$ given by equation (17) to the intensities obtained in step *c*. Details of this process are described in section 5.

f') If the ratio of the depths exceeds this limit, add the correction $\Delta x\ (L_1 + L_2) - A \cos \theta$ to the results of step *c*, using equation (23). For details see section 6.

g) The resulting curve will show a small term, $A_2' \cos 2\theta$, with opposite sign from the original A_2. Remove this as in step *c*.

h) The resulting intensity-curve may then be discussed as usual. The photometric ellipticity, cleared completely of reflection, will be measured by $A_2 - A_2'$, and the geometrical ellipticity by $z = (4\epsilon/c)\ (A_2 - A_2')$.[8] When ellipticity and reflection are small, step *d* may be omitted, and step *g* abbreviated.

9. The present discussion confirms and emphasizes the conclusion that rectification for reflection always involves a process of addition and can never be accurately made by division alone. The writer's suggestion to the contrary[9] involves an inadvertent, but serious, error for which an explicit apology is herewith made.

[8] *Ap. J.*, **102**, 8, 1945.

[9] *Ibid.*, p. 6 (beginning of sec. 8).

A STUDY OF THE EXTENDED ENVELOPE SURROUNDING THE WOLF-RAYET COMPONENT OF V 444 CYGNI

ZDENĚK KOPAL AND MARTHA B. SHAPLEY
Harvard College Observatory
Received June 3, 1946

ABSTRACT

The light-curve of V 444 Cygni within the primary minimum has been analyzed by a new method which endeavors to determine the distribution of opacity in the semitransparent envelope surrounding the Wolf-Rayet component of this eclipsing system. The outcome of our analysis leads to the following conclusions:

1. The Wolf-Rayet component appears to be a diffuse object of opacity which gradually increases from the periphery inward. The light-curve exhibits no evidence of any abrupt change in opacity which could be ascribed to a completely opaque central core. The upper limits for possible dimensions of such a core are found to be 11⊙, 4.4⊙, and 2.7⊙ for orbital inclinations of 70°, 80°, and 90°, respectively. Considerations relative to the secondary minimum make it, however, probable that the real value of orbital inclination will not be less than 80°.

2. It seems very probable that the extinction of light of the O component passing through semitransparent layers of the W star is due to its scattering by free electrons. Under prevailing conditions the absorption by ionized metals appears to be about ten to a hundred times less effective in dimming blue light than the scattering by free electrons liberated by such ionization.

3. The electron densities (computed on the assumption that the light of the O star reaching us during its atmospheric eclipse has been wholly scattered) necessary to give rise to the observed extinction range from 2×10^{12} particles per cubic centimeter at the lowest levels which we were able to penetrate by our analysis, to roughly 10^9 electrons/cm^3 at heights where the extinction just begins to make itself felt. These values turn out to be compatible with electron densities of the order of 10^{11}–10^{12} particles/cm^3, which were inferred from purely spectroscopic evidence for radiating layers of Wolf-Rayet stars.

4. If the envelope surrounding the Wolf-Rayet component of V 444 Cygni is in dynamical equilibrium and remains electrically neutral on a microscopic scale, it can be shown that its electron gas would dissipate completely within an astronomically insignificant interval of time. This demonstrates that the envelope cannot be regarded as a neutral equilibrium phenomenon and suggests that its free electrons may share the outward motion of ejected ions whose lines dominate the spectrum of the W star.

I. INTRODUCTION

The recently discovered eclipsing variable, V 444 Cygni,[1] has proved to represent a rare combination of a Wolf-Rayet star of spectral class WN5, attended by an early-type component of spectrum O6, according to Victoria classification. A precise photoelectric light-curve of this system, produced recently by Kron and Gordon,[2] has confronted us with several anomalous features; in particular, the apparent constancy of light between eclipses was hard to reconcile with the great width of the primary minimum, which was, moreover, found to be more than twice as wide as the secondary one. Attempts at an interpretation of the light-curve on the basis of a conventional model, consisting of components that appear in projection as opaque sharp-edged disks, led only to a limited success (see Fig. 1). A deeper analysis of the situation compelled Kopal[3] and Russell[4] to conclude that, in order to explain the approximate constancy of combined light of V 444 Cygni between eclipses, on the one hand, and the conspicuous disparity in durations of the two minima, on the other, we have to regard its Wolf-Rayet component as surrounded by an extensive semitransparent envelope which is capable of dimming the light of the O star that passes through it at the time of primary minimum, but whose own luminosity is so small a fraction of the total light of the star that no appreciable loss of light results when the O component passes in front of it. A great difference in width of the alternate minima discloses immediately that the conditions in the W envelope

[1] Discovered by S. Gaposchkin, *Pub. A.A.S.*, **10**, 52, 1940.
[2] *Ap. J.*, **97**, 311, 1943.
[3] *Ap. J.*, **100**, 204, 1944.
[4] *Ap. J.*, **100**, 213, 1944.

must depart widely from thermodynamical equilibrium[5]—a fact that should cause little surprise to the students of Wolf-Rayet stars. Conversely, should such departures be characteristic of stellar extended atmospheres in general, unequal width of the alternate minima should be the principal characteristic of all eclipsing systems having such a star as a component. If this star were hot enough for the opacity of its semitransparent layers to arise from continuous absorption by metallic ions, we should also expect the "effective" radius of the diffuse star (as deduced from the light-curve) to be smaller, the longer the effective wave length, λ, of observations. The same should be true at the other ex-

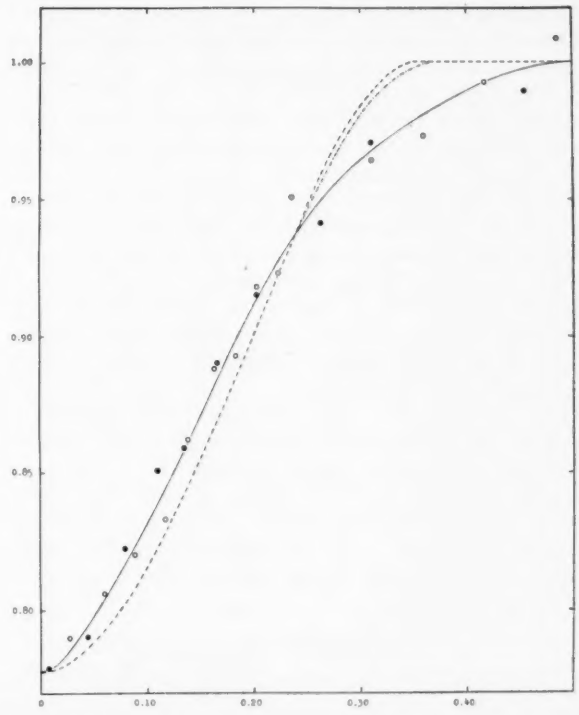

FIG. 1.—The light-curve of V 444 Cygni within primary minimum, according to the photoelectric observations by Kron and Gordon.

Full and open circles indicate positions of the individual normal points on the ascending and descending branch of the light-curve, respectively. The rectified luminosity of each normal (*abscissae*) is plotted against the phase, in fractions of a day (*ordinates*). The full line on this figure shows a curve, drawn freely to follow the course of observed normals, and interpreted in this investigation. The broken line represents the best theoretical light-curve which could be obtained on the assumption that the Wolf-Rayet component appears in projection as a sharp-edged disk of uniform surface brightness (after Russell, *Ap. J.* **100**, 213, 1944); while the dotted-and-dashed line shows the possible departures from such a solution if the W star were completely darkened at limb.

treme—if the envelope were cold and its extinction were due to dust or molecules, whose absorption varies also as some negative power of λ (between λ^{-1} and λ^{-4}).[6] If, on the other hand, the central star were hot enough to keep its envelope ionized—but not much hotter than the sun—theoretical considerations make it probable that negative

[5] If the envelope were to emit exactly as much light as it absorbs, a passage of its companion in front of and behind semitransparent layers should obviously be accompanied by the same loss of light, and, in consequence, the alternate minima should be equally wide. Departures from thermodynamical equilibrium in the envelope will naturally disturb this situation.

[6] Cf., e.g., Greenstein, *Harvard Circ.*, No. 422, 1937.

hydrogen ions would constitute the main source of opacity, which varies (within the spectral range of ordinary observations) as some positive power of λ.[7] In brief, it seems reasonable to expect that the effective radii of absorbing envelopes of stars hotter than the sun will appear smaller in visual than in photographic light; whereas for stars cooler than the sun the converse should be sure. If, however, the form of the light-curve within minima arising from atmospheric eclipses were found to be frequency-independent, the case would be strong for the scattering of light, in the envelope, on particles of dimensions large in comparison with λ or—for hot stars—on free electrons.

These considerations make it perhaps abundantly clear that appropriate photometric investigations of such eclipsing systems as V 444 Cygni can be expected to throw considerable light on the structure and nature of absorption processes in the extended envelope of its Wolf-Rayet component; but owing, perhaps, to the difficulties inherent in such a proposition, this aspect of the problem has so far not been approached by any previous worker on the subject. In the present paper such an investigation will be given. Our main aim will be to determine the whole march of opacity-distribution in semitransparent layers surrounding the W star from the observed data directly and without recourse to any a priori assumption restricting its course. We shall try to decide whether or not the W star possesses any opaque core or what its maximum permissible dimensions may be. We shall also attempt to give a physical interpretation to the observed opacities and to infer the kind, as well as the density, of particles constituting the semitransparent envelope of the W star. In Section II, which follows, equations that relate the observed loss of light to the structure of obscuring semitransparent layers will be set up, and solved by approximate means. Their solution will be closely analogous to a process employed recently in an investigation of ζ Aurigae;[8] in point of fact, the whole method to be outlined in this section can be regarded as a generalization of the former procedure to cases in which the curvature of isophotes, on the apparent disk of the star undergoing eclipse, impressed by the obscuring layers of its mate, cannot be ignored. Section III will contain an application of this type of analysis to the primary minimum of V 444 Cygni, while the fourth and last section will be devoted to a physical interpretation of the results obtained. The conclusions arrived at in the course of this investigation have already been summarized in the abstract; so that in what follows our task will be to substantiate them in detail.

II. EQUATIONS OF THE PROBLEM

Let us consider, quite generally, an eclipsing system whose one (say the primary) component is surrounded by a radially symmetrical envelope of gradually decreasing opacity. When, in the neighborhood of superior conjunction, its companion passes behind such semitransparent layers, a loss of light results which we may conveniently refer to as an "atmospheric eclipse." Suppose, for the sake of simplicity, that the disk of the component undergoing eclipse initially exhibits uniform surface brightness. Once the eclipse begins, the obscuring medium will disturb this uniform brightness by impressing upon it a characteristic distribution, such that the isophotes will form a family of circles concentric with the primary star. If the secondary's disk were divided into elementary segments by such circles, the light emitted by all parts of an element lying between the radii r and $r + dr$ from the primary's center will emerge from the semitransparent envelope with its original intensity reduced by the factor $e^{-\tau}$, where τ denotes the optical depth of the semitransparent layers along the line of sight.

The fractional light, f, of the secondary component, that remains visible during eclipse by semitransparent layers surrounding its mate, can then be expressed as

$$f = \frac{2}{\pi r_2^2} \int_{\delta - r_2}^{\delta + r_2} \Lambda(r)\, r \cos^{-1} \frac{r^2 + \delta^2 - r_2^2}{2\delta r}\, dr, \qquad (1)$$

[7] Cf. Chandrasekhar, *Ap. J.*, **102**, 223, 1945.

[8] Kopal, *Ap. J.*, **103**, 310, 1946.

where δ denotes the apparent separation of centers of both components; r_2, the radius of the secondary star; and $\Lambda(r) \equiv \exp(-\tau)$. The reader may notice that when $\Lambda(r) = 1$ (transparent atmosphere), f reduces to unity; and also that $\Lambda(\delta) \to f(\delta)$ when $r_2 \to 0$—the two functions being identical if the secondary component can be regarded as a luminous point.

As is well known, the fractional light, l, of our system during eclipse can be written as

$$l = L_1 + fL_2 , \tag{2}$$

where $L_{1,2}$ denote fractional luminosities of the respective components (normalized so that $L_1 + L_2 = 1$). Equation (2), differentiated with respect to δ, yields

$$\frac{\partial l}{\partial \delta} = \frac{\partial f}{\partial \delta} L_2 , \tag{3}$$

while from equation (1) it follows that

$$\frac{\partial f}{\partial \delta} = -\frac{2}{\pi r_2} \int_0^{\pi} \Lambda(\cos\theta) \cos\theta \, d\theta , \tag{4}$$

where

$$r^2 = \delta^2 + r_2^2 - 2\delta r_2 \cos\theta \tag{5}$$

defines our new independent angular variable θ. Combining equations (3) and (4), we arrive at the following fundamental equation of our problem in the nondimensional form:

$$\frac{r_2}{L_2} \frac{\partial l}{\partial \delta} = -\frac{2}{\pi} \int_0^{\pi} \Lambda(\cos\theta) \cos\theta \, d\theta , \tag{6}$$

which relates the slope of the observed light-curve to the unknown optical depth of semi-transparent layers surrounding the primary star.

In order to solve equation (6) for Λ, we propose, first, to replace the integral on its right-hand side by a sum of a finite number of terms in accordance with some formula for approximate numerical integration. In the present case we find it particularly convenient to employ one, originally due to Bronwin,[9] which asserts that, if Λ is a function of degree not in excess of $2n - 1$, then

$$\int_0^{\pi} \Lambda(\cos\theta) \cos\theta \, d\theta = \frac{\pi}{n} \sum_{j=1}^{n} a_j \Lambda(a_j) , \tag{7}$$

where

$$a_j = \cos \frac{2j-1}{n} \pi .$$

Inserting this in equation (6), we find that this latter equation can be approximated by

$$\frac{r_2}{L_2} \frac{\partial f}{\partial \delta} \doteq -\frac{2}{n} \sum_{j=1}^{n} a_j \Lambda(a_j) \tag{8}$$

with unlimited accuracy, provided only that n is taken sufficiently large.

In passing from equation (6) to equation (8), we have replaced the original integral equation by an algebraic equation involving a series of n particular values of Λ as unknowns. An equation of the form (8) can naturally be set up for every point of the light-curve at which the value of $\partial l/\partial\delta$ can be determined (numerically or otherwise). Since

[9] *Phil. Mag.*, **34**, 262, 1849.

the argument of Λ depends on both r and δ, the discrete values of Λ occurring in each equation of the form (8) will *not*, however, correspond to the same set of distances from the center of the primary star—which means that, if we regard the corresponding Λ's as unknowns, a set of m such equations will represent a diophantine system containing $m \times n$ unknowns.

This apparent indeterminacy may, however, be resolved in the following namner: A representation of the integral in equation (6) by a weighted sum of n unequally spaced ordinates tacitly presumes the Λ-function to be a polynomial of degree not in excess of $2n - 1$ if a representation of the integral equation (6) by an equivalent system of linear algebraic equations is to be exact. Suppose, now, that, out of the array of $m \times n$ ordinates of the diophantine system, we single out $2n$ of them as unknown, while expressing all others in terms of these unknowns by means of an interpolation polynomial of $(2n - 1)$th degree; for, though the magnitude of each ordinate is unknown, its position with respect to any other one is specified as soon as δ and r_2 are fixed.

A recourse, at this stage, to the interpolation polynomial reduces in one stroke the originally diophantine system to a set of m linear equations containing $2n$ unknown values of Λ. If $m = 2n$, this system will possess a definite solution; if $m > 2n$, it becomes overdeterminate and may be solved by the method of least squares. When values of the unknowns are ultimately inserted back in our interpolation polynomial, the latter represents an nth approximation to $\Lambda(r)$, whose accuracy may be increased arbitrarily by taking n sufficiently large.

The above-described method for solving our fundamental equation (6) consists, in brief, in replacing the original integral equation by an equivalent system of linear algebraic equations by means of a convenient summation formula and in reducing subsequently the number of the unknowns by expressing $n(m - 2)$ of them as interpolates in terms of a selected pivotal set of $2n$ points. This procedure requires the unknown function Λ to be continuous within the whole domain considered; for, if so, both steps represented by the quadrature formula (7) and the subsequent interpolation are easily justified, and our method can be shown to lead to a rigorous solution when n is allowed to increase beyond any limit. The fact that a quadrature formula with unequally spaced ordinates is employed guarantees, at any stage, the best possible results with the minimum number of terms.

A postulate of continuity of Λ is tantamount to a requirement that the opacity in the semitransparent envelope should vary continuously with the distance r from the center of the parent-star. Should, at any phase, the pencil of light passing through such semitransparent layers encounter an opaque core, it would encounter a sudden increase in opacity; and if the limb of this core were sharp, the Λ-function would discontinuously drop to zero. The method which we outlined above for solving equation (8) would then lose a formal justification, though the computational procedure would continue to work long enough to disclose the situation. We hope, indeed, to find out in this way whether or not the Wolf-Rayet component of V 444 Cygni possesses any sharp-edged core.

The physical advantages of the transformation which we have just effected will be immediately apparent. In passing from $l(\delta)$ to $\Lambda(\delta)$, we have replaced a distended beam of light emitted by the secondary component and emerging from semitransparent layers of its mate by an equivalent beam of a point source, which, unlike $l(\delta)$, can be related to the extinction coefficient $\kappa(r)$ of the obscuring layers by a series of rigorous analytical operations. It follows from the definition of optical depth, τ, that

$$\Lambda(\delta) = \exp(-\tau) = \exp\left\{-\int_{-\sqrt{r_A^2-\delta^2}}^{\sqrt{r_A^2-\delta^2}} \kappa(r)\, ds\right\}, \tag{9}$$

where r_A denotes the extent of the semitransparent envelope, and ds the element of the line of sight. Since

$$s^2 = r^2 - \delta^2$$

and, hence

$$ds = \frac{r\,dr}{\sqrt{r^2 - \delta^2}},$$

equation (9), on taking logarithms, may be easily re-written as

$$\log \Lambda(\delta) = -\int_{\delta}^{r_A} \frac{\kappa(r)\,dr^2}{(r^2 - \delta^2)^{\frac{1}{2}}}. \tag{10}$$

This equation can, by a suitable substitution, be transformed to one of Abel's type and formally inverted;[10] its solution being

$$\kappa(r) = \frac{1}{\pi}\int_{r}^{r_A} \frac{d}{d\delta}(\log \Lambda)\frac{d\delta}{(\delta^2 - r^2)^{\frac{1}{2}}}. \tag{11}$$

This last equation expresses κ explicitly as a function of r in terms of quantities that can be deduced from the observed data, and hence the solution of our problem is now complete. An ill-determinate character of r_A is not really troublesome in this connection; for beyond certain limiting value of δ, $\log \Lambda$ and hence the integrand in equation (11) become effectively zero. Any increase of the upper limit of our integral would then clearly add nothing to its numerical value.

III. APPLICATION TO V 444 CYGNI

Before proceeding to apply the foregoing theory to the light-curve of V 444 Cygni within primary minimum, the simplifying assumptions inherent to its derivation may be briefly recapitulated. First, it is obvious that the type of analysis as developed so far is easy of application only when the relative luminosity and dimensions of the star undergoing atmospheric eclipse can be ascertained independently of the light-curve—say, from the spectroscopic evidence. For V 444 Cygni this is fortunately the case.[11] Second, our assumption that the disk undergoing eclipse appears uniformly bright can likewise be justified on physical grounds; for it is generally accepted that the limb-darkening of O-type stars is small, if any, while the distortion caused by axial rotation and tidal action of the W star is too small to produce any noticeable gravity-darkening.[12] Last but not least, throughout Section II a tacit assumption was made that the envelope surrounding the W star possess radial symmetry. It is true that if an envelope of such relative dimensions were to be a configuration of equilibrium, its distortion would necessarily be considerable. Reasons can, however, be listed (cf. Sec. IV) as to why this envelope is unlikely to be in any kind of equilibrium, which makes the degree of its distortion rather unpredictable. Under such circumstances, an assumption of radial symmetry can be justified, at least on grounds of simplicity.

Within these limitations an application of the method developed in the preceding section to Kron and Gordon's photoelectric light-curve of V 444 Cygni may now proceed, and Table 1 summarizes the relevant observational data. Its successive columns indicate (1) the number of the respective normal; (2) the phase $(t - t_0)$, in days, reckoned from mid-primary minimum (positive and negative values correspond to the ascending and

[10] For details of this inversion cf., e.g., Sec. III of n. 8.

[11] A simultaneous determination of orbital elements and the structure of a semitransparent envelope surrounding one (or both) components from the photometric evidence is also possible in principle but would require much more precise observations than those available so far.

[12] A nonuniform intrinsic distribution of brightness over the disk undergoing eclipse could, moreover, be taken into account by a simple variation of our method, without encountering any fundamental obstacles.

descending branch of the light-curve, respectively); (3) the phase-angle of the secondary component in its relative orbit, reckoned from the moment of superior conjunction and computed from

$$\theta = (2\pi/P)(t - t_0),$$

where $P = 4^d21238$ denotes the period of orbital revolution; (4) the difference Δm in magnitudes between the star HD 193514 and V 444 Cygni, as observed with a potassium-hydride cell by Kron and Gordon;[2] (5) the corresponding fractional light, l, of the system; and (6) the rectified light, l_r, corrected for the effects of ellipticity and reflection as shown between minima.[13]

TABLE 1

No.	Phase	θ	Δm	l	l_r	δ (90°)	δ (80°)	δ (70°)
1	0^d008	0°.68	0^m295	0.7621	0.7790	0.0119	0.1739	0.3422
2	− .028	− 2.39	.280	.7727	0.7899	.0417	.1783	.3442
3	.044	3.76	.279	.7734	0.7906	.0656	.1853	.3475
4	− .060	− 5.13	.258	.7885	0.8060	.0894	.1947	.3522
5	.080	6.84	.236	.8046	0.8224	.1191	.2096	.3599
6	− .089	− 7.61	.239	.8024	0.8200	.1323	.2186	.3648
7	.110	9.40	.199	.8325	0.8507	.1633	.2367	.3749
8	− .118	−10.08	.220	.8151	0.8328	.1750	.2446	.3795
9	.136	11.62	.188	.8410	0.8591	.2014	.2637	.3909
10	− .139	−11.88	.184	.8441	0.8623	.2059	.2670	.3930
11	− .164	−14.02	.152	.8694	0.8880	.2423	.2951	.4109
12	.166	14.19	.149	.8718	0.8903	.2451	.2974	.4124
13	− .184	−15.73	.145	.8750	0.8934	.2711	.3185	.4265
14	.204	17.43	.119	.8962	0.9148	.2995	.3422	.4429
15	− .204	−17.43	.115	.8995	0.9181	.2995	.3422	.4429
16	− .224	−19.14	.109	.9045	0.9231	.3279	.3666	.4603
17	− .261	−22.31	.076	.9325	0.9510	.3796	.4122	.4942
18	.264	22.56	.087	.9230	0.9413	.3837	.4158	.4970
19	− .311	−26.58	.060	.9462	0.9640	.4475	.4736	.5420
20	.312	26.66	.053	.9524	0.9704	.4487	.4747	.5429
21	− .360	−30.77	.049	.9559	0.9729	.5116	.5329	.5900
22	− .418	−35.72	.025	.9773	0.9933	.5838	.6006	.6465
23	.455	38.89	.028	.9746	0.9896	.6278	.6422	.6820
24	− .486	−41.53	.007	.9936	1.0081	.6630	.6756	.7107
25	− .570	−48.71	.015	.9863	0.9984	.7514	.7601	.7846
26	.599	51.19	.024	.9782	0.9894	.7793	.7868	.8082
27	− .620	−52.99	.001	.9991	1.0099	.7985	.8054	.8247
28	− .663	−56.66	.003	.9972	1.0068	.8354	.8408	.8563
29	.693	59.23	.014	.9872	0.9959	.8592	.8638	.8769
30	.762	65.12	.003	.9972	1.0013	.9072	.9101	.9185
31	−0.799	−68.28	0.006	0.9945	1.0003	0.9290	0.9312	0.9376

An interpretation of certain features of the composite spectrum of V 444 Cygni led Beals[14] to conclude that its O component is approximately 1.75 mag. brighter than the W star, with an uncertainty of 0.2 or 0.3 mag.[15] This implies that the ratio of luminosities, $L_W/L_O = 0.20 \pm 0.04$, which renders for the fractional luminosity of the O component the value $L_O = 0.83 \pm 0.03$. The radius of this star was likewise estimated by Beals, from its absolute magnitude and effective temperature, to be $4.2\odot$. Values derived previously from the light-curve all came out somewhat larger. Since, however, we do not wish to bias our present investigation by postulating any eclipsing properties of the W star (which all previous investigations of the light-curve necessarily entailed), we prefer in what follows to adopt Beals's estimate, which is wholly independent of the

[13] See eq. (5.1) of n. 3. [14] *M.N.*, **104**, 205, 1944. [15] Private communication to one of us.

light-curve. As, according to Wilson,[16] the projected semimajor axis $(a_O + a_W) \sin i$ of the relative orbit of V 444 Cygni is close to $35.8\odot$, the fractional radius r_O of the O star should then be approximately equal to (4.2/35.8) csc i, or 0.115 csc i—the last digit being admittedly uncertain.

Spectroscopic observations cannot, unfortunately, throw any light on the actual value of the orbital inclination, i. Previous investigations by Kopal[3] and Russell[4] converged to the conclusion that i should be in the neighborhood of 80°. Since, however, both these investigations were again partly based on assumed eclipsing properties of the W component, we do not wish to adopt their outcome without scrutiny, and we propose to carry out our analysis for assumed orbital inclinations of 70°, 80°, and 90°, between which the actual inclination is reasonably certain to lie. The last three columns of Table 1 then give the values of fractional apparent separation, δ, of centers of both components, at each phase, computed from

$$\delta^2 = \sin^2 \theta \sin^2 i + \cos^2 i ,$$

for $i = 70°$, 80°, and 90°, respectively. The radius of the relative orbit of the system will hereafter be adopted as our unit of length.

To begin with, let us adopt, first, the intermediary value of $i = 80°$ and assume, furthermore, that a variation of $\Lambda(\delta)$ over a range of δ in which the atmospheric effect runs from transparency to complete opacity can be satisfactorily represented by a function of not more than sixth degree. If so, equation (8) can be explicitly written as

$$0.139 \frac{\partial l}{\partial \delta} = -\frac{2}{3} \sum_{j=1}^{3} \cos \frac{2j-1}{6} \pi \, \Lambda \left(\cos \frac{2j-1}{6} \pi \right). \qquad (12)$$

The reader may notice that, since for $j = 2$ the coefficient of Λ becomes zero, the summation on the right-hand side of equation (12) actually consists of only two terms. Next, let us select a number of points along the light-curve—say, for $\delta = 0.20$, 0.25, 0.30, ... , 0.75—and determine, by numerical differentiation, the values of $\partial l/\partial \delta$ at these points on a curve drawn freehand to follow the course of observed normals. These values are given in Table 2.

TABLE 2

δ	$\partial l/\partial \delta$	δ	$\partial l/\partial \delta$	δ	$\partial l/\partial \delta$
0.20	0.940	0.40	0.394	0.60	0.125
.25	.865	.45	.300	.65	.088
.30	.657	.50	.223	.70	.044
0.35	0.500	0.55	0.163	0.75	0.009

TABLE 3

δ	r_1	r_3	δ	r_1	r_3
0.20	0.115	0.306	0.50	0.405	0.603
.30	.208	.405	.60	.504	.702
0.40	0.306	0.504	0.70	0.603	0.802

The distances $r_{1,3}$ from the center of the W star corresponding to arguments $a_{1,3}$ in equation (12) can be found from equation (5) if we insert $r_2 = r_O = 0.115$ and $\cos \theta_{1,3} = \pm \sqrt{3}/2$. Then let us single out from the above array six values of $\delta = 0.20, 0.30, \ldots,$ 0.70, with the corresponding values of $r_{1,3}$ given in Table 3, and adopt the values of

[16] *Ap. J.*, **91**, 379, 1940.

$\Lambda(r_1)$ as our fundamental set of unknowns. Consistently with our foregoing restrictions, the $\Lambda(r)$'s for arguments other than these r_1's can evidently be expressed in terms of our six fundamental unknowns by means of an interpolation polynomial of fifth degree. In this way the twelve values of $\partial l/\partial\delta$ listed above supply us with twelve equations of condition for six unknown values of $\Lambda(r_1)$. Their least-squares solution leads to six normal equations of the form

$$\begin{array}{rrrrrrr}
\Lambda_1 & \Lambda_2 & \Lambda_3 & \Lambda_4 & \Lambda_5 & \Lambda_6 & \\
1.0423 + 0.3067 & - 1.4093 & + 0.1594 & - 0.1541 & + 0.0753 & = & -0.2474 \\
+ 3.4050 & - 2.5874 & - 0.3225 & - 1.3061 & + 0.6481 & = & -0.3656 \\
+ 7.1707 & - 2.3507 & + 0.0338 & - 1.0630 & = & & 0.1615 \\
+ 5.1361 & - 1.3872 & - 1.1422 & = & & & 0.1124 \\
+ 6.0049 & - 1.4650 & = & & & & 2.0005 \\
+ 4.8255 & = & & & & & 1.9016\,,
\end{array}$$

which yield the results given in Table 4.

TABLE 4

r_1	$\Lambda(r_1)$	$(f-\Lambda)$	r_1	$\Lambda(r_1)$	$(f-\Lambda)$
0.115	0.652	+0.015	0.405	0.934	+0.001
.208	.774	.007	.504	.970	− .001
0.306	0.878	+0.003	0.603	0.989	0.000

TABLE 5

r_1	$\Lambda(r_1)$	$(f-\Lambda)$	r_1	$\Lambda(r_1)$	$(f-\Lambda)$
0.076	0.719	0.019	0.553	0.983	0.002
.161	.797	.009	.752	0 998	.001
0.355	0.927	0.004	0.951	1.001	0.000

TABLE 6

r_1	$\Lambda(r_1)$	$(f-\Lambda)$	r_1	$\Lambda(r_1)$	$(f-\Lambda)$
0.306	0.658	.....	0.603	0.979	0.002
.405	.871	0.012	.702	0.997	.001
0.504	0.948	0.005	0.802	1.000	0.000

An interpolation polynomial of fifth degree, passed through these points, should provide a close approximation to the actual run of the Λ-function—provided, of course, that the assumed orbital inclination of 80° is true. Since we cannot be sure of this, we propose, next, to repeat the same analysis for $i = 90°$—which represents the upper limit of possible orbital inclination—and $i = 70°$, which may probably be regarded as a lower limit. The numerical process is exactly parallel to one described above, the outcome being that, for $i = 90°$, we get the results summarized in Table 5, while for $i = 70°$, we have the results given in Table 6. An interpolation polynomial of fifth degree, passed through these points, should provide approximations to the actual run of the Λ-function similar to that already obtained for $i = 80°$.

Having thus determined Λ from the observed light-changes for three assumed values of orbital inclination, our next step should be to investigate to what extent these results

may perhaps be dependent on the particular type of analysis employed. Accordingly, we have added $\Lambda(r_1)$, corresponding to $\delta = 0.80$, to our fundamental set of unknowns for $i = 80°$ and have made recourse to an interpolation polynomial of sixth degree. On going through exactly the same procedure, we find that $\Lambda(0.702) = 1.003$, while all other unknowns have not changed by more than three units of the last place. As there appears to be no reason why the situation should be different for other values of orbital inclination, we conclude that our original six-ordinates scheme of accuracy was ample and that a fifth-degree interpolation polynomial passed through the six values of Λ listed in Tables 4, 5, and 6 will provide a satisfactory approximation to the actual run of the Λ-function during the atmospheric eclipse.

Our next point of concern should be to estimate the extent to which our results may be affected by an inaccurate knowledge of the fractional radius and luminosity of the O star. In order to find this out, we propose to compare the computed Λ's with the remaining fractional light, f, of the O star, that may be obtained from

$$f = \frac{(l_r - L_W)}{L_O},$$

where, as before, $L_O = 0.83$ and $L_W = 0.17$ are the fractional luminosities of the respective components and l_r is the rectified fractional light of the system as given in the sixth column of Table 1. If the O star, undergoing atmospheric eclipse, could be regarded as a luminous point, $f(\delta)$ should naturally be identical with $\Lambda(\delta)$. As could have been expected, a comparison of the computed Λ's and f's at the corresponding points (see the last columns of Tables 4, 5, and 6) reveals that these two are not exactly the same but that f only slightly exceeds Λ.[17] In more specific terms, a change in r_O from zero to 0.11 has made the computed Λ's differ from the f's not more than 1 per cent—a fortunate circumstance, which absolved us from the obligation to recompute all Λ's with slightly altered values of r_O in order to see what effect this might have on the results. The magnitude of the $(f - \Lambda)$ differences, as given in the last columns of Tables 4, 5, and 6, shows convincingly that the effects of such uncertainty in r_O as may reasonably be expected are likely to be negligible.

An uncertainty in estimated value of fractional luminosity of the O star, based on Beals's spectroscopic studies, exerts particularly simple effects: as L_O occurs only as a divisor on the left-hand side of our fundamental equation (6), any error in its estimated value will affect all computed Λ's in the same proportional amount but in the opposite direction. In consequence, an error in L_O (or, more appropriately, in the ratio r_O/L_O) will not affect the logarithmic derivative of Λ and, hence, the value of the absorption coefficient $\kappa(r)$ as defined by equation (11). It is mainly our ignorance of the actual value of orbital inclination i which prevents us from exploring the obscuring properties of the W envelope unambiguously and with considerable accuracy.

A study of the primary minimum alone is bound to leave i largely indeterminate. Its value could, in principle, be approximated more closely by resorting to the secondary minimum and analyzing the light-changes exhibited when the W core undergoes eclipse by the O component. Such an analysis would naturally presuppose a knowledge of the actual "law of darkening" over the apparent W disk. In order to get it, we should have to solve not only the equation of radiative transfer of proper light, I_W, of the W core scattered in the surrounding electron envelope in accordance with Rayleigh's law but also the equation of transfer of the O light, I_O^*, intercepted by the W envelope and scattered in the direction of the line of sight; for, in the present case, both the proper and the reflected radiations are likely to be of comparable relative importance. Both equations of transfer would have to be solved in plane polar co-ordinates (or, if the distortion of the envelope were to be taken into account, in spherical polars); for the curvature

[17] This inequality is bound to be true in general whenever the curvature of isophotes impressed upon the star's apparent disk by extinction in obscuring layers of its mate cannot be ignored.

of the layer of equal density in the W envelope obviously could not be ignored. Since the distribution of density and opacity in this envelope has already been inferred from an analysis of the primary minimum by methods outlined in Section II, the respective equations of transfer could indeed be solved uniquely; and since they are linear, their sum $I_W + I_0^*$ should yield the resultant law of darkening. At present, unfortunately, such solutions are still completely lacking. Solutions for the transfer problem, in atmospheres stratified in plane-parallel layers, of both ordinary and incident radiation scattered according to Rayleigh's law have only recently been obtained by Chandrasekhar;[18] and, while it is possible that his method may admit of a generalization to extended atmospheres[19] as well, the actual construction of the appropriate solutions will undoubtedly require a great deal of work.

The specific reason why we do not propose to attack this problem at present is a relatively low weight of existing observational evidence for the secondary minimum of V 444

TABLE 7

$i = 70°$

δ	$\Lambda(\delta)$	$\frac{d \log \Lambda}{d\delta}$	$10^{12}\kappa$	$10^{-12} N_e$	$10^{-13} N_i$ (80,000°)	$10^{-13} N_i$ (60,000°)	T_e	T_e
0.3000	0.640	5.56	1.225	1.856	2.387	1.856	80,000°	60,000°
.3125	0.682	4.73	1.030	1.560	2.189	1.702	34,700	30,200
.3250	0.719	4.00	0.869	1.317	2.010	1.563	21,700	19,700
.3375	0.752	3.39	0.734	1.112	1.848	1.437	15,100	13,200
.3500	0.781	2.86	0.623	0.944	1.702	1.324	11,900	11,300
.3625	0.807	2.41	0.530	0.803	1.570	1.221	9,700	10,200
.3750	0.829	2.01	0.454	0.688	1.453	1.130	8,300	8,700
.3875	0.848	1.69	0.391	0.592	1.349	1.005	6,800	7,100
.4000	0.864	1.44	0.339	0.514	1.256	0.977	6,000	5,800
.4125	0.878	1.25	0.296	0.448	1.172	0.912	5,300	5,400
.4250	0.891	1.10	0.258	0.391	1.095	0.852	4,700	4,800
.4375	0.903	0.97	0.226	0.342	1.025	0.797	4,300	4,300
.4500	0.914	0.88	0.198	0.300	0.959	0.746	3,900	3,900
.4625	0.924	0.77	0.173	0.262	0.897	0.698	3,500	3,500
.4750	0.932	0.68	0.151	0.229	0.838	0.652	3,100	3,100
.4875	0.939	0.59	0.133	0.201	0.784	0.612	2,900	2,900
.5000	0.946	0.53	0.116	0.176	0.735	0.571	2,700	2,700
.5125	0.952	0.47	0.102	0.155	0.690	0.536	2,500	2,500
.5250	0.957	0.42	0.090	0.136	0.647	0.503	2,300	2,300
.5375	0.962	0.36	0.079	0.120	0.606	0.471	2,200	2,200
.5500	0.966	0.32	0.069	0.105	0.568	0.441	2,100	2,100
.5625	0.969	0.29	0.061	0.092	0.533	0.414	1,900	1,900
.5750	0.973	0.26	0.054	0.081	0.500	0.390	1,800	1,800
.5875	0.976	0.24	0.047	0.071	0.468	0.364	1,700	1,700
.6000	0.979	0.22	0.041	0.062	0.437	0.340	1,600	1,600
.6125	0.982	0.20	0.036	0.054	0.408	0.318	1,500	1,500
.6250	0.985	0.19	0.031	0.047	0.380	0.295	1,400	1,400
.6375	0.987	0.18	0.026	0.039	0.348	0.270	1,300	1,300
.6500	0.989	0.17	0.022	0.033	0.317	0.249	1,300	1,300
.6625	0.991	0.17	0.018	0.027	0.286	0.225	1,200	1,200
.6750	0.993	0.16	0.014	0.021	0.253	0.199	1,100	1,100
.6875	0.995	0.14	0.011	0.016	0.217	0.176	1,000	1,000
.7000	0.997	0.12	0.007	0.011	0.179	0.140	920	920
.7125	0.998	0.10	0.005	0.007	0.138	0.119	850	850
.7250	0.999	0.07	0.002	0.004	0.094	0.075	790	790
.7375	0.999	0.04	0.001	0.002	0.048	0.038	740	740
0.7500	1.000	0.00	0.000	0.000	0.000	0.000	.....	.....

[18] *Ap. J.*, **100**, 117, 1944; **103**, 165, 1946.

[19] Cf. Chandrasekhar, *Ap. J.*, **101**, 95, 1945.

Cygni. As this minimum lasts less than half as long as the primary one, it is covered by only 10 normal points, as compared with 24 normals defining the primary minimum. In addition, since the amplitude of light-changes in the secondary minimum is almost half that of the primary one, the proportional errors of the individual normals constituting this minimum are about twice as large as those we worked with formerly. This all renders the observational weight of the secondary minimum only about one-fifth that of the primary one, which we feel is too low to offer an adequate basis for any elaborate investigation. For the time begin, all we can say is that a value of $i = 74°$, as obtained by Russell[4] on the assumption of complete ordinary darkening at limb for the W star,

TABLE 8

$i = 80°$

δ	$\Lambda(\delta)$	$\frac{d \log \Lambda}{d\delta}$	$10^{12}\,\kappa$	$10^{-12}\,N_e$	$10^{-13}\,N_i$ (80,000°)	$10^{-13}\,N_i$ (60,000°)	T_e	T_e
0.12	0.657	+2.17	1.179	1.786	2.342	1.821	80,000°	60,000°
.14	0.685	+2.02	1.017	1.541	2.176	1.692	48,400	39,200
.16	0.712	+1.88	0.878	1.330	2.021	1.572	32,800	27,800
.18	0.738	+1.76	0.757	1.147	1.876	1.459	23,800	20,700
.20	0.764	+1.63	0.650	0.985	1.739	1.352	18,100	16,100
.22	0.789	+1.51	0.557	0.844	1.610	1.251	14,000	12,700
.24	0.812	+1.38	0.475	0.720	1.487	1.156	11,300	10,300
.26	0.834	+1.26	0.403	0.611	1.369	1.065	9,200	8,500
.28	0.854	+1.13	0.340	0.515	1.257	0.978	7,600	7,100
.30	0.873	+1.00	0.285	0.432	1.152	0.896	6,400	6,000
.32	0.889	+0.85	0.239	0.362	1.055	0.820	5,500	5,200
.34	0.903	+0.70	0.201	0.305	0.967	0.752	4,700	4,500
.36	0.914	+0.60	0.170	0.258	0.889	0.692	4,100	3,900
.38	0.924	+0.53	0.145	0.219	0.820	0.639	3,700	3,500
.40	0.933	+0.48	0.123	0.186	0.756	0.589	3,300	3,100
.42	0.942	+0.43	0.104	0.157	0.695	0.541	2,900	2,800
.44	0.950	+0.39	0.087	0.132	0.636	0.495	2,600	2,500
.46	0.957	+0.35	0.072	0.110	0.580	0.451	2,400	2,300
.48	0.964	+0.31	0.059	0.090	0.525	0.408	2,100	2,100
.50	0.969	+0.27	0.048	0.072	0.472	0.367	1,900	1,900
.52	0.974	+0.24	0.038	0.057	0.420	0.327	1,700	1,700
.54	0.978	+0.21	0.029	0.044	0.369	0.288	1,600	1,600
.56	0.982	+0.18	0.022	0.033	0.320	0.249	1,400	1,400
.58	0.986	+0.15	0.016	0.024	0.272	0.212	1,300	1,300
.60	0.989	+0.12	0.011	0.017	0.226	0.176	1,100	1,100
.62	0.992	+0.09	0.007	0.011	0.182	0.141	1,000	1,000
.64	0.995	+0.07	0.004	0.007	0.138	0.105	880	880
.66	0.997	+0.04	0.002	0.004	0.093	0.070	770	770
.68	0.999	+0.02	0.001	0.002	0.047	0.035	670	670
0.70	1.000	0.00	0.000	0.000	0.000	0.000	.....	.....

should be regarded as a possible lower limit of the orbital inclination; for it is certain that a consideration of the appropriate law of darkening would bring i considerably closer to 90°.

The mere runs of the Λ-functions evaluated above for three different values of orbital inclination permit us also to draw certain conclusions regarding the existence or possible absolute dimensions of an opaque central core of the Wolf-Rayet component of V 444 Cygni. If this star possessed such a core of fractional radius (say) r_c, the Λ-function should have become zero for $r \leqslant r_c$. Actually, we found it to remain finite, for every assumed value of orbital inclination, up to the smallest value of r for which $\Lambda(r)$ was directly evaluated; and, if the extrapolation can be any guide, $\Lambda(r)$ would not vanish even at the moment of conjunction, when $r = \cos i$. This suggests that the W component is apparently a diffuse object of opacity gradually increasing from the periphery inward.

The light-curve does not seem to exhibit any indication of an abrupt change in opacity which might point to the existence of an opaque central core. The upper limits for possible dimensions of such a core are given by the smallest values of r for which $\Lambda(r)$ was directly evaluated and which are 0.306, 0.115, and 0.076, expressed in terms of the orbital radius of the eclipsing system—or 11⊙, 4.4⊙, and 2.7⊙—for inclinations of 70°, 80°, and 90°, respectively. These values are probably not much in excess of the actual extent of the luminous core of the W component, whose eclipse by the O star gives rise to the secondary minimum. The dimensions of this core have previously been estimated by Kopal[3] and by Russell[4] from formal aspects of the light-curve and conform in substance

TABLE 9

$i = 90°$

δ	$\Lambda(\delta)$	$\frac{d \log \Lambda}{d\delta}$	$10^{12}\kappa$	$10^{-12} N_e$	$10^{-12} N_i$ (80,000°)	$10^{-12} N_i$ (60,000°)	T_e	T_e
0.075.....	0.718	1.30	0.934	1.415	2.084	1.621	80,000°	60,000°
.100.....	0.741	1.26	.790	1.197	1.916	1.491	46,300	36,800
.125.....	0.764	1.21	.670	1.015	1.765	1.373	30,100	24,900
.150.....	0.787	1.14	.569	0.862	1.627	1.265	21,400	18,200
.175.....	0.809	1.06	.483	0.731	1.499	1.166	15,900	13,800
.200.....	0.830	0.98	.408	0.618	1.378	1.071	12,200	10,800
.225.....	0.850	0.90	.344	0.521	1.264	0.984	9,700	8,600
.250.....	0.869	0.82	.289	0.438	1.158	0.902	7,800	7,000
.275.....	0.886	0.72	.241	0.366	1.059	0.823	6,500	5,900
.300.....	0.901	0.63	.201	0.305	0.968	0.752	5,500	5,000
.325.....	0.914	0.55	.168	0.254	0.884	0.687	4,600	4,200
.350.....	0.926	0.47	.140	0.212	0.808	0.628	3,900	3,600
.375.....	0.936	0.41	.117	0.177	0.739	0.574	3,400	3,200
.400.....	0.945	0.36	.098	0.148	0.675	0.525	3,000	2,800
.425.....	0.953	0.32	.081	0.123	0.615	0.477	2,700	2,500
.450.....	0.960	0.28	.067	0.102	0.559	0.434	2,400	2,200
.475.....	0.967	0.25	.055	0.083	0.506	0.393	2,100	2,000
.500.....	0.973	0.22	.044	0.067	0.455	0.352	1,900	1,800
.525.....	0.978	0.19	.035	0.053	0.407	0.314	1,700	1,600
.550.....	0.982	0.17	.027	0.041	0.361	0.276	1,500	1,400
.575.....	0.986	0.14	.021	0.031	0.316	0.243	1,400	1,300
.600.....	0.990	0.12	.016	0.023	0.272	0.212	1,200	1,200
.625.....	0.993	0.10	.012	0.017	0.228	0.184	1,100	1,050
.650.....	0.995	0.08	.008	0.012	0.185	0.150	1,100	960
.675.....	0.997	0.06	.005	0.008	0.141	0.118	880	850
.700.....	0.998	0.04	.003	0.005	0.096	0.092	790	770
.725.....	0.999	0.02	.001	0.002	0.049	0.052	710	700
0.750.....	1.000	0.00	0.000	0.000	0.000	0.000	.....	.....

to the above limits. There exists, however, no evidence for the existence of any sharp boundary between the core and its envelope; according to all appearances, the transition between them is gradual.

Having determined Λ and discussed its possible sources of uncertainty, we may now proceed to complete our analysis by evaluating the extinction coefficients $\kappa(r)$ of the obscuring semitransparent layers of the W star by means of equation (11). Tables 7, 8, and 9 contain the details of such computations for $i = 70°$, 80°, and 90°, respectively. Their successive columns indicate (1) the distance, δ, from the center of the W star; (2) the value of $\Lambda(r = \delta)$ obtained by subtabulation of the pivotal Tables 4, 5, and 6; (3) the logarithmic derivative of $\Lambda(\delta)$ deduced from the preceding column by the process of numerical differentiation; and (4) the respective values of the extinction coefficient κ obtained by evaluating the right-hand side of equation (11) by quadratures. This coefficient is not a dimensionless quantity. Consistently with the system of units em-

ployed thus far, κ would pertain to the loss of light suffered by a ray along a path equal to the radius of the relative orbit of V 444 Cygni. In order to reduce it to absolute units, we have to divide the outcome of the quadrature by the orbital radius of V 444 Cygni, which, according to Wilson,[16] is equal to $35.8 \csc i \odot = 2.48 \csc i \times 10^{12}$ cm. The fourth columns of Tables 2–4 then contain such absolute values of κ, in cm^{-1}, which correspond to the distance $r = \delta$ from the center of the Wolf-Rayet star.

IV. DISCUSSION OF THE RESULTS

With these data on hand, we find ourselves in a position to inquire about the composition of the semitransparent envelope surrounding the W star and about the nature of particles giving rise to the observed extinction. The loss of light suffered by the O component during primary minimum may, in general, be due to either absorption or scattering, pure or combined. It is needless to stress the fact that all matter enveloping so hot a star as the Wolf-Rayet component must be wholly gaseous and highly ionized. The alternative choice of light-dimming agents then narrows down to absorption by ionized atoms or scattering on electrons liberated by such ionization.

Let us examine this latter possibility first and assume that all light of the O star passing through the semitransparent envelope of its mate has been wholly scattered on free electrons. If so, then the well-known formula of Thomson asserts that

$$\kappa(r) = \frac{8\pi}{3}\left(\frac{e^2}{mc^2}\right)^2 N_e(r), \tag{13}$$

where e denotes the specific charge of an electron; m, its mass; c, the velocity of light; and N_e, the number of electrons per cubic centimeter. Setting $e = 4.801 \times 10^{-10}$ e.s.u., $m = 9.105 \times 10^{-28}$ gm, and $c = 2.998 \times 10^{10}$ cm/sec, equation (13) yields

$$\kappa(r) = 0.660 \times 10^{-24} N_e(r), \tag{13.1}$$

and the values of κ as given in the fourth columns of Tables 7–9 can readily be converted into the number of free electrons per cubic centimeter required to produce the observed extinction. These values are listed in the fifth columns of the same tables. Their inspection reveals that, irrespective of the uncertainty in orbital inclination, the N_e's range from approximately 2×10^{12} electrons/cm^3 at the lowest levels which we were able to penetrate by our analysis to 10^9 electrons/cm^3 at altitudes where the extinction just begins to make itself felt. It may be mentioned in this connection that the electron densities in radiating layers of Wolf-Rayet stars, as inferred from purely spectroscopic investigations, are, according to Aller,[20] of the order of 10^{11}–10^{12} electrons/cm^3. On the other hand, the observed width of the secondary minimum of V 444 Cygni demonstrates that the radius of its luminous core cannot be much smaller than the values of δ in the top lines of the first columns in Tables 2–4, for which electron densities of the order of 10^{12} particles/cm^3 were encountered. We conclude, therefore, that a hypothetical electron gas, enveloping the W component of V 444 Cygni, of density inferred spectroscopically for these stars as a class, is sufficient to scatter enough light of the O star passing through it in the neighborhood of superior conjunction to give rise to the observed primary minimum.

Let us next examine the possibility that the extinction by the semitransparent envelope surrounding the W component may be due to continuous absorption by metallic ions. If so, then, according to Menzel,[21] the equation relating $\kappa(r)$ with the number N_i of absorbing ions in an electrically neutral atmosphere assumes the form

$$\kappa(r) = 2.67 \times 10^{24} \frac{k}{\nu^3 T^{1/2}} \{ e^{h\nu/kT} - 1 \} N_i^2, \tag{14}$$

[20] *Ap. J.*, **97**, 135, 1943.

[21] *Harvard Circ.* No. 417, 1936.

where ν denotes the frequency of light; h, the Planck constant; k, the Boltzmann constant; and T, the electron temperature of the W star. The effective wave length of the photoelectric observations by Kron and Gordon was close to 4500 A, which corresponds to $\nu = 6.66 \times 10^{14}$ sec^{-1}. Adopting, with Beals,[14] the temperature of the Wolf-Rayet star $T = 80{,}000°$ and setting $h = 6.62 \times 10^{-27}$ erg/sec and $k = 1.379 \times 10^{-16}$ erg/deg, we may utilize equation (14) for evaluating the ion numbers, N_i, necessary to account for the observed extinction. The results of such computations are given in the sixth columns of Tables 7–9; while the seventh columns of the same tables contain, in addition, the same ion numbers computed with $T = 60{,}000°$ (Aller's estimate[20]). A glance at these results reveals that the number of ions, per unit volume, necessary to produce the observed loss of light by absorption is from ten to a hundred times as large as the number of electrons, at corresponding levels, which would produce the same effect by scattering.[22] But an ionization of N atoms will necessarily liberate at least N electrons, whose scattering is bound to superpose upon atomic absorption. This leads us to conclude that, under conditions prevailing in the W envelope, the atomic absorption may be dismissed as insignificant for dimming the light of the O star that passes through the envelope in the neighborhood of superior conjunction. There seems to remain but little room for doubt that the bulk of the observed extinction must arise from electron-scattering.

We may extend our inquiry one step further and conjecture that, if this atmosphere of electron gas enveloping the W component were to be in dynamical equilibrium, its temperature-distribution, $T(r)$, should be related to the observed opacity by

$$N_e(r) \sim e^{-[mg(r)/kT(r)]r}, \tag{15}$$

where $g(r)$ denotes the gravitational acceleration at the respective level. The mass M of the W component is, according to Wilson,[16] approximately equal to $10\odot = 1.98 \times 10^{34}$ gm; and there is no doubt that the mass is stored predominantly in its luminous core. In consequence,

$$g(r) = G\frac{M}{r^2},$$

where $G = 6.68 \times 10^{-8}$ gm$^{-1}\cdot$cm$^3\cdot$sec^{-2} is the gravitational constant. Inserting this in equation (15), we may employ the latter for evaluating, from known electron densities, the temperatures necessary to sustain the envelope distended. On taking logarithms and inserting appropriate values of the constants involved, equation (15) may be clearly rewritten as

$$\frac{1}{r_1T_1} - \frac{1}{rT} = 2.926 \times 10^{-4} \log \frac{N_e(r)}{N_e(r_1)}, \tag{15.1}$$

where r_1 denotes the distance from the star's center, corresponding to a level at which the temperature T_1 is known. We may tentatively identify r_1 with the first entry in the first columns of Tables 7–9, which corresponds roughly to the dimensions of the luminous core of the W star, the temperature of which was estimated as 80,000° by Beals[14] and as 60,000° by Aller.[18] The last two columns of Tables 7–9 then indicate the whole march of the resultant temperature-distribution in the W envelope corresponding to $T_1 = 80{,}000°$ and 60,000°, respectively.[23] It may be noticed that the electron temperatures in outer

[22] It may be objected that an assumption of constant temperature of 80,000° throughout the envelope is likely to exaggerate the computed ion numbers, since in its outer portions the temperature will certainly be lower. The conclusion that, under the circumstances, the electron-scattering is much more effective in dimming light than is atomic absorption holds good, however, regardless of our uncertainty in temperatures prevailing in the outer parts of the envelope; for, in order to make the atomic absorption as effective as the electron-scattering, the temperature prevailing near the W core would have to be lowered to less than 10,000°—which seems out of the question.

[23] It should be emphasized, moreover, that the temperatures listed in the last columns of Tables 7–9 are maximum possible values, derived under the assumption that the envelope is wholly supported by

parts of the W envelope turn out to be relatively low and largely independent of our choice of T_1; as the reader may easily verify, the temperature of the electron gas near the periphery of the envelope is essentially given by

$$T \doteq -\frac{m g r}{k \log (N_r/N_1)} . \tag{16}$$

The next logical object of our inquiry should be the question of stability of an envelope characterized by such a temperature-distribution. A little consideration discloses that, owing to their small mass and high thermal velocities, the free electrons constituting the envelope can escape the gravitational field of the star with relative ease. This problem has been theoretically investigated by Milne[24] to a considerable detail, and his results may now be applied to the Wolf-Rayet component of V 444 Cygni.[25] If N denotes the total number of electrons per cubic centimeter, at the periphery of the W envelope characterized by a radius r_0[26] and temperature T_0, then, according to Milne,

$$\frac{dN}{dt} = -2N_e(r_0)\, r_0 \left(\frac{2\pi k T_0}{m}\right)^{\frac{1}{2}} e^{-q}(1+q) , \tag{17}$$

where q denotes the ratio of the gravitational potential energy of the electron, at $r = r_0$, to two-thirds of its mean kinetic energy. Now should the envelope be electrically neutral—i.e., should the loss of free electrons by diffusion be compensated for by the ejection of positive ions, then

$$q = \frac{m g(r_0)}{k T(r_0)}\, r_0 ;$$

but as the temperature at the periphery is essentially given by equation (16), this readily reduces to

$$q \doteq -\log (N_0/N_1) .$$

Now the radius r_0 characterizing the periphery of our envelope may be tentatively associated with the last entry in the first columns of Tables 2–4. If so, then, for $i = 80°$, $q \backsim 7$ or 8, and equation (17) yields

$$\frac{dN}{dt} = -2 \times 10^{38} \text{ electrons/sec} .$$

The total number of electrons in the envelope can be obtained by integrating $N_e(r)$, as given in the fifth column of Table 3 over the respective volume; hence we obtain

$$N = 3 \times 10^{48} \text{ electrons} .$$

A comparison of these two values shows that the electron population of the envelope would dissipate to less than one-half within 10^{10} seconds, or some 300 years—which is an astronomically insignificant interval of time; and, if the orbital inclination were higher than 80°, this time would be still shorter. Now the chances that an envelope character-

---

thermal agitation of the constituent electrons and that all light of the O star reaching us during its atmospheric eclipse has been scattered. A partial scattering would bring about a decrease of the computed extinction coefficients and hence of the temperatures; and the occurrence of any large-scale turbulent motions in the envelope, accounting for its partial support, would operate in the same direction.

[24] *Trans. Cambridge Phil. Soc.*, **22**, No. 26, 483, 1923.

[25] In Milne's discussion, the gravitational potential is supposed to be due to the parent-star alone. In the W envelope of V 444 Cygni, tidal effects arising from the secondary cannot be ignored. In consequence, Milne's eq. (17) will not be applicable literally, though the results it leads to in the present case will doubtless be of a correct order of magnitude.

[26] It is understood that this radius does not differ from the actual "boundary" by more than the mean free path of whirling electrons.

ized by such a lifetime could actually be observed are, of course, practically nil. In our opinion this result demonstrates, instead, the untenability of the premises on which it was based: namely, of our assumptions, underlying equations (15) and (17), that the extended envelope surrounding the Wolf-Rayet component of V 444 Cygni can be regarded as an electrically neutral phenomenon in dynamical equilibrium.[27] As H. N. Russell has pointed out in discussion to the junior writer, it is very much more probable that free electrons constituting the envelope share the outward motion of ejected ions—though the physical causes of ejection of particles which cannot absorb radiation still remain wholly obscure.

The outcome of all the foregoing discussion makes it reasonably safe to conclude that the main cause of extinction in the semitransparent envelope surrounding the Wolf-Rayet component is scattering on free electrons and that this electron gas cannot be in ordinary dynamical equilibrium. It is to be stressed that these conclusions invite further observational tests, summarized in the following points, the results of which should be highly revealing.

1. Since the electron-scattering is known to be frequency-independent, the deep minima of V 444 Cygni observed in light of different effective wave lengths should be equally wide and differ only in their vertical (magnitude) scales. A comparison of a blue and red light-curve could disclose at once whether or not this is actually the case.

2. As light scattered on free electrons becomes completely polarized if viewed at 90° from the direction of its propagation, the light of the O star, reaching us for several hours before and after mid-primary minimum, should exhibit a certain degree of polarization, varying with the phase and distributed symmetrically around the moment of conjunction. A ratio of polarized to unpolarized fractions of the O light during primary minimum should reveal the proportion of light scattered in the W envelope; and the variation of the degree of polarization with the phase might even disclose the longitude of the node of this binary system.[28]

3. The average electron velocities—whether radial or random—are almost certainly of the order of several hundred km/sec and therefore sufficient to wash out all traces of absorption lines from the scattered part of the O light. If so, the line spectrum of the O component would be expected to disappear for several hours before and after mid-primary minimum in polarized light, while remaining visible in its unpolarized fraction.

4. An estimate of the number of ions ejected, per unit of time, by the Wolf-Rayet star from the intensity of its bright bands should be of utmost value for further studies of dissipation of the hypothetical electron-gas envelope and of the intensity of its eventual electrostatic field.

It is a very fortunate circumstance that V 444 Cygni happens to be bright enough (8.0 mag.) and that its primary minimum lasts long enough (almost 24 hours) to make the observational studies along the above-described lines feasible. It is to be hoped that such studies will be undertaken in the near future; for it is scarcely an exaggeration to assert that further progress in our understanding of the nature of Wolf-Rayet stars in general will, to a large extent, depend upon further exploration of this remarkable eclipsing system.

In conclusion, the writers take pleasure in expressing their appreciation to Professors Henry Norris Russell and Donald H. Menzel for stimulating discussions of certain aspects of problems treated in this paper.

[27] The mean lifetime of the envelope can be greatly extended by allowing the envelope to accumulate a certain positive charge; for, if so, electrostatic forces will rapidly take control of q and, by increasing it, will slow down the diffusion of electrons. In such a case the structure of the envelope would, however, be governed by electrostatic rather than by gravitational forces, and the equations of ordinary dynamical equilibrium would be inapplicable.

[28] The writers owe this remark to Professor Russell.

THE INFRARED SPECTRUM OF υ SAGITTARII*

JESSE L. GREENSTEIN AND PAUL W. MERRILL
Yerkes Observatory
and
Mount Wilson Observatory
Received May 22, 1946

ABSTRACT

The spectrum of υ Sagittarii has been measured on Mount Wilson coudé plates, of dispersion 20 A/mm. Wave lengths for about 300 stellar lines are given in the region from $H\alpha$ to 8784 A. The strongest lines are those of the lighter elements, *N* I, *O* I, *He* I, *Ne* I, *Al* II, *Mg* II, and *Si* II. Hydrogen is weak. The identifications are far from complete. Peculiarities in the behavior of various elements are discussed. Emission lines present are $H\alpha$ and those of *Ca* II and [*Ca* II], *Fe* II and possibly [*Fe* II]. The emission lines do not share the orbital motion and show a velocity of −11 km/sec with respect to the center of mass. Their origin is tentatively ascribed to various regions of an extended nebulous envelope, which possess complex stream motions and rotations. No indications of a secondary absorption spectrum are found.

The rich spectrum of υ Sagittarii (HD 181615, 6; R.A. $19^h16^m.0$; Dec. $-16°8'$; mag. 4.6; spect. cApe) shows the star to be a peculiar object of high luminosity. Lines of *He* I, *Ne* I, and *N* I, as well as of the ionized metals, are strong; hydrogen and the neutral metals are very weak. The observed spectrum is that of a single star; since it shows velocity changes with a range of 100 km/sec, its source is considered a member of a spectroscopic binary system.[1] The other component has not been detected.

The spectrum has previously been studied in the ultraviolet,[2] photographic,[3] and visual regions.[4] A detailed investigation of the photographic and visual regions with 2.8 A/mm dispersion is in progress. The present investigation is based on plates taken with the first-order grating and the 32-inch camera of the Mount Wilson coudé spectrograph (dispersion 20.5 A/mm, emulsion Eastman IV-N).

The spectrum is rich in lines, but, because of the relatively high temperature of the star and because of turbulence, the lines are shallow and slightly widened. Strong atmospheric lines make complete measurement and identification difficult. The present investigation is designed to reveal the outstanding features of the spectrum on the available infrared plates; a complete list of accurate wave lengths will require a further investigation. Two plates were measured as completely as possible; they were so chosen that the orbital motion (and the solar reduction) result in a considerable difference in the measured wave lengths on the plate—about 1.7 A in the pair used. The displacement aided in the recognition of the stationary atmospheric lines. The plates are as shown in the accompanying tabulation. Every line certainly visible on the plates was measured, ex-

Plate	Date (1943)	Stellar Velocity
Ce 3177	Sept. 7	+29 km/sec
3223	Oct. 7	−35 km/sec
3121	July 21	+39 km/sec (for $\lambda > 8680$ A only)

* *Contributions from the Mount Wilson Observatory, Carnegie Institution of Washington*, No. 723.

[1] R. E. Wilson, *Lick Obs. Bull.*, **8**, 132, 1914. [2] J. L. Greenstein, *Ap. J.*, **91**, 438, 1940.

[3] W. W. Morgan, *Pub. Yerkes Obs.*, Vol. **7**, Part III, 1935.

[4] J. L. Greenstein, *Ap. J.*, **97**, 252, 1943, and unpublished data; P. W. Merrill, *Pub. A.S.P.*, **51**, 218, 1939, and unpublished data; also H. F. Weaver, *Ap. J.*, **98**, 131, 1943.

cept in the atmospheric bands. Within those regions, only lines not obviously atmospheric were measured. (The stellar lines are generally wider and shallower than the atmospheric lines.) In consequence, measures are extremely incomplete in the regions λλ 6867–6929, 7168–7319, 7592–7698, and 8110–8339. Approximately one-quarter of the spectrum is masked. The absence of certain strong lines is thus not conclusive proof of the absence of an element from the spectrum. For example, the strong group of *N* I lines at λλ 8184.8–8242.3 is missing from the table, although other *N* I lines are very strong. Some of the missing lines can be detected by special search. After the reductions were completed, a careful re-examination of the measured lines was made to establish their reality; the atmospheric lines were also searched for and eliminated by means of the *Revised Rowland Table*.

The identifications and wave lengths are based mainly on the *Revised Multiplet Table*.[5] They are not to be regarded as final; of approximately 300 lines, only 125 have completely satisfactory identifications. Laboratory data are poor for the ionized metals *Fe* II, *Ti* II, and *Cr* II, which give a large percentage of the lines in the blue. In the infrared, only a few lines of these elements can be identified. The elements best identified are the abundant lighter elements; they have one common (and unusual) feature, in that their lines arise from high excited levels, both normal and metastable. Unidentified lines may be those of the ionized metals; these lines may also arise from higher series in such elements as *N* I, *Al* II, and *Si* II. The frequency of lines in the infrared is about one per 6 A; in the ultraviolet, about one line per 1.5 A is observed. While the present IV-N plates have moderately good contrast and resolving power, lines in the infrared seem to be intrinsically less numerous and weaker. The same phenomenon is observed in the solar spectrum, but we must not conclude that some mechanism (such as emission, high opacity, or veiling by another spectrum) weakens the lines; strong absorption lines are, in fact, observed to be quite deep. Central absorptions for the strong *N* I lines at λλ 7424, 7442, and 7468 are 42 per cent; for λλ 8680, 8703, and 8712, 35 per cent. These are the values before correction for scattered light and finite instrumental resolving power. Lines of this depth show also that there is no appreciable light from an overlapping spectrum of another star. From a linear approximation to the solution of the equation of radiative transfer, we can compute the absorption in the center, A_c, of a strong line:

$$A_c = \frac{F_\nu\,(\text{continuum}) - F_\nu\,(\text{line})}{F_\nu\,(\text{continuum})}, \tag{1}$$

which is given approximately by

$$A_c = 1 - \frac{1}{1 + \frac{1}{4} u_0 \frac{\kappa}{\kappa_\nu} (1 - e^{-u_0})^{-1}}, \tag{2}$$

where

$$u_0 = \frac{h\nu}{kT_0}. \tag{3}$$

Now, in the infrared, at 8000 A, if we adopt[2] $T_0 = 10{,}000°$, we find $u_0 = 1.8$. If we further assume a black body, i.e., $\bar{\kappa} = \kappa_\nu$, then $A_c = 0.35$. The observed lines show at least this much absorption. The shallowness of the lines is a consequence of their location on the long-wave side of the energy-maximum of a black-body curve. A similar situation accounts for the shallowness of lines in the blue region of a B star.

Table 1 contains the wave lengths and identifications for all lines measured, excluding those found to be dominantly atmospheric. Strong lines measured on two plates are given to two decimal places, weaker lines to one place. Lines measured on only one plate are indicated by a colon. Probable errors of a tabular wave length are of the order of ±0.06 A for lines with intensity $I \geq 2$. The intensities are on an arbitrary scale, with

[5] C. E. Moore, *Revised Multiplet Table*, Princeton, 1945.

TABLE 1

WAVE LENGTHS AND IDENTIFICATIONS

λ	I	Identification	λ	I	Identification
6571.46	4	*Fe* II .41 [tr]	6769.4:	1–0	*N* I .57 (00d), *Ba* II .62 (10)
6573.9:	2n		6770.7	1n	
6576.1:	1–0		6777.0	1–0	*N* I .36 (00d)
6578.03	2	*C* II .03 (10)	6787.6	1	*C* II .09 (2)?, *Zr* II .15 (2)?
6581.2	1	*N* I 0.70 (0)?	6792.5	1	
6583.1:	3	*C* II 2.85 (9)	6811.0	1n	
6586.87	2	*Fe* II .69 (5)	6815.2	1–0	
6592.0:	0		6817.1	1	*Al* II 6.69 (1)
6599.3	5N	*Ne* I 8.95 (15)	6818.4:	1	*A* II .39 (4)?
6602.5	1	*Ne* I .91 [100]?	6819.7	1n	
6606.0:	0		6823.47	3	*Al* II .48 (5)
6610.1:	1N	*Al* II 9.64 (0.5), *N* II .58 (6)?, *N* I 2.63 (00)	6826.5:	1	
6622.43	3n	*N* I .53 (3)	6828.5	1	
6627.02	2	*Fe* II .28 (5), *N* I .02 (0)?	6829.9	1	
6631.8	0–1		6833.9:	1–0	*F* I 4.26 (12)?
6637.0:	1	*N* I .01 (4)	6837.27	3	*Al* II .14 (8)
6638.6:	0–1	*A* II .24 (8)? *A* II 9.72 (7)?	6841.72	2	
6642.9:	0n	*La* II .79 (100)	6845.5:	1–0	
6645.00	3	*N* I 4.96 (9), *N* I 6.52 (2)	6855.7	1	*F* I 6.02 (16)?, *V* II 6.03 (400)?
6647.5:	0n		6857.77	2	
6649.0:	1		6861.2:	1	*A* II .30 (4)?
6650.8:	1–0	*Fe* II 1.03 (1)	6862.6	1	*Sm* II .82 (150)?
6651.6:	1		6882.1	1n	Note 1
6653.51	3n	*N* I .41 (5), *O* I .78 (5)?	6906.04	2n	
6656.50	2	*N* I .61 (2)	6920.4	0	*Al* II 9.96 (0.5)
6660.60	3	*Si* II .49 (2)	6922.10	4	Atm+
6665.12	2N	*N* I 6.75 (0d), *A* II 6.36 (5)?	6924.40	2	Atm+
6668.9:	1n		6926.6:	1	*N* I .90 (1)
6671.94	4	*Si* II .88 (3)	6927.9	1	Atm+
6673.7	0–1		6929.54	4	*Ne* I .47 (10)
6678.28	7	*Ne* I .28 (9), *He* I .15 (6)	6932.01	3	Atm+
6679.7:	1N	*Ti* II 0.26 (1)?	6945.19	2	*N* I .22 (4)
6684.3	1	*A* II .36 (8)	6951.4	0–1	*N* I .50 (1)
6685.8	1–0n		6963.2	1–0	
6690.9:	1		6967.1:	1–0	*Fe* II 6.9 (2), *F* I 6.35 (10)?
6693.3	1–0		6972.6:	0	
6699.52	3	*Al* II .46 (0)?	6979.2:	0–1	*N* I .10 (1)
6701.9:	1n		6981.8:	2	*N* I 2.02 (00), *S* II .40 (4)
6706.3:	1	*N* I .20 (4)	6990.1:	0	Atm?
6708.81	2	*N* I .81 (4)	7002.2:	1	*O* I .22 (17), *O* I 1.93 (15)
6711.2:	0		7032.47	9n	*Ne* I .41 (10)
6713.3	1	*N* I .12 (1)	7035.9:	1–0	
6717.13	4	*Ne* I .04 [70]?	7039.85	2	Atm+*Sm* II .22 (600)
6719.5	1	*A* I .20 [100]?	7042.08	10	*Al* II .06 (10)
6720.9:	0		7045.3:	0	
6722.88	5N	*N* I 3.12 (9)	7056.69	9	*Al* II .60 (5)
6726.4	1n	*O* I .25 (5), *O* I .50 (2)	7059.1	1	*Ne* I .11 [200]
6728.8	0n		7063.56	6	*Al* II .64 (1)
6733.34	2n	*N* I .48 (6)	7065.43	5n	*He* I .19 (5), *He* I .72 (1)
6741.3	1–0	*N* I .29 (3)	7072.0	1	
6743.4:	1–0		7077.5:	0	*Eu* II .10 (3000)
6744.9:	1n		7094.2	1–0	
6750.1:	2	*C* II .22 (2)?	7100.3	1	
6751.95	2	*N* I 2.40 (4)	7125.6	1–0	
6757.2	1N	*N* I 8.60 (4), *A* II 6.61 (5)?			

TABLE 1—*Continued*

λ	*I*	Identification	λ	*I*	Identification
7127.9	2n	*F* I .88 (14)?	7488.94	2	*Ne* I .87 [500]
7132.0:	1n	*Al* II 1.29 (0)?	7492.4:	0	
7134.50	3	*Al* II .66 (0.5), *Fe* II .99 (5)	7495.67	3	
7135.63	3	Atm+	7499.88	3	*He* I .44 (p)
7140.1:	1–0	*N* II 9.8 (3), *S* II 9.79 (1)	7503.8:	1	*A* I .87 (700)
7143.4	1	Atm+	7506.6	1	
7145.5:	0		7508.9:	1	*S* II 9.03 (0)?
7154.95	5em	Note 2; [*Fe* II] 5.14?	7510.8:	1	
7169.0:	2	Atm+	7513.11	5	*Cr* II 2.70 (p)?
7216.7:	1	*N* II 7.0 (2)	7515.49	2n	*Fe* II .88 (6)
7220.2	1		7518.0:	1n	
7224.04	2	*Fe* II .51 (12); note 5	7525.3:	1n	
7236.47	1	*C* II .19 (8d)	7529.1	1	
7245.4:	2	*Ne* I .17 (10)	7533.0:	1–0	*Fe* II .42 (2); note 5
7256.9:	1N	*S* II .96 (1) +atm	7535.79	2	*Ne* I .78 [300]
7281.36	5	*He* I .35 (3)	7540.4	1–0	
7290.75	10em	[*Ca* II] 1.46; note 2	7543.7	1	*Ne* I 4.05 [100]?
7291.2:	5	[*Ca* II] 1.46; notes 2, 3	7546.2	1	
7291.77	10em	[*Ca* II] 1.46; note 2	7548.7	1	
7298.20	2n	*He* I 7.66 (p)?+atm	7550.9	1	
7305.1:	0		7566.3:	1	
7310.2:	1	*Fe* II .24 (6)	7574.0:	1–0	
7312.24	1	Atm, *Cr* II 1.60 (2)	7579.1	1n	*S* II 8.96 (10)
7320.3:	1em	Note 2; *Fe* II 0.70 (40 bl)?	7580.9:	0	*Cr* II .51 (p)
7323.21	7em	[*Ca* II] 3.88; note 2	7588.80	1Nd	*A* II 9.33 [250], *Kr* I 7.41 (1000)
7323.7:	4	[*Ca* II] 3.88; notes 2, 3			
7324.16	8em	[*Ca* II] 3.88; note 2	7617.0:	1–0	
7326.1:	1–0		7660.9:	2	
7342.9	1		7705.17	2	
7347.7	1	*Mn* II .72 (p)?	7711.23	3em	Note 2; *Fe* II .71 (15)?
7350.4:	1	Note 5	7711.4	1–0	*Fe* II .71 (15); note 5
7363.9:	1		7721.3:	1–0	
7365.9:	1	Note 5	7724.0:	1n	*A* I 3.76 (200), *A* I .21 (200)
7370.2:	1	*Mn* II 9.73 (p)?, *Eu* II .22 (2500)	7731.76	3	
7377.9:	1–0em	Doubtful; note 2	7743.0	1	
7385.9:	0		7748.6	1	
7391.5:	1		7755.8:	1	*F* I 4.70 (19)?
7393.7	1		7771.92	10	*O* I .96 (27)
7394.7	1	*Cr* II .81 (p)	7774.24	8	*O* I .18 (26)
7398.3	1n	*F* I .68 (17)?	7775.37	6	*O* I .40 (25)
7406.15	3	*Si* I 5.85 (300)?	7780.47	2	
7409.2	1n	*Si* I .11 (100)?	7783.0	1	
7415.7:	1–0	*Si* I 6.00 (250)?, *Mn* II .78 (p)?; note 5	7784.9:	1	
			7790.03	3N	
7423.64	10	*N* I .63 (7)	7793.4:	0	
7438.88	2	*Ne* I .90 [300]	7796.7:	1	
7442.27	10	*N* I .28 (8)	7801.0:	1–0	*F* I 0.22 (18)?
7444.2:	1		7816.3	1n	*He* I .16 (4), *Al* II 5.83 (1)
7447.04	1n		7818.3	1	
7449.2	2em	Note 2; *Fe* II .34 (6)	7821.0:	1	
7450.3:	2N	*Al* II 9.42 (5)	7845.8:	1	*Gd* II 6.35 (3000)?
7452.6	1em	Note 2; [*Fe* II] .50?	7849.54	3N	
7462.1	2em	Note 2; *Fe* II .38 (20)?	7851.8:	0em	Note 2; doubtful
7462.3	1	*Fe* II .38 (20); note 5	7851.9:	1	
7468.37	10	*N* I .29 (10)	7868.2:	0	*A* I .20 (40)?
7471.51	2n	*Al* II .41 (9), *O* I .36 (2)	7873.8:	0	
7478.8	1–0	*O* I 6.45 (12), *O* I 9.06 (8), *O* I 0.66 (8)	7877.09	4	*Mg* II .13 (−)
			7896.29	4	*Mg* II .37 (−)
7485.0:	1	*Cr* II .93 (p)?	7899.07	5	

TABLE 1—*Continued*

λ	*I*	Identification	λ	*I*	Identification
7907.9:.....	2N	Atm+	8504.0....	1	.....
7911.2.....	1n	Note 5	8508.8:.....	2	*Kr* I .87 (200)
7915.51....	4n	Atm+	8541.76....	15em	*Ca* II 2.09 (1500); notes 2, 4
7948.0.....	1n	*O* I 7.56 (12), *O* I 0.83 (10), *A* I .18 (400)	8543.2:.....	2em	*Ca* II 2.09; notes 2, 4
7967.29.....	2	*S* II .43 (10)+atm	8567.7.....	1n	*N* I .74 (4)
7982.1.....	1	.....	8571.9:.....	1	.....
8005.2:.....	0	*S* II .24 (1)+atm	8581.5:.....	1N	.....
8006.2:.....	1	*A* I .16 (600)+atm	8591.3.....	1	*Ne* I .26 [400]
8014.4:.....	1–0	*A* I .79 (800)+atm	8594.10....	3	*N* I .01 (6)
8046.3.....	1–0	Atm+	8597.2:.....	1–0	.....
8074.2:.....	1em	Doubtful; note 2	8598.4:.....	1	*H* .39
8115.3:.....	2n	*He* I .84 (p)?, *A* I .31 (4000)	8602.1:.....	0	.....
8119.0:.....	2n	*Al* II .72 (1.5)?, *A* II .18 [50], +atm	8609.2:.....	2	.....
8121.4.....	1n	*Al* II 2.08 (0.5)+atm	8621.2:.....	1–0	.....
8183.4:.....	2n	.....	8629.27....	3	*N* I .24 (8)
8232.4:.....	2N	*O* I 0.01 (10), *O* I .99 (13) +atm	8632.6:.....	1–0	*He* I .05 (p)?
8234.8:.....	2	*O* I 5.31 (5)?+atm	8634.8:.....	2	*Ne* I .65 [600]
8249.0.....	1	.....	8636.6:.....	1	.....
8307.7:.....	1n	Atm+	8640.86....	3	*Al* II .70 (8)
8314.57....	3n	*S* II .73 (10)+atm	8654.7:.....	4	*Ne* I .51 [400], *Ne* I .38 [1500]
8316.4.....	1n	Atm+	8655.74....	2	*N* I .88 (3)
8325.2:.....	1	.....	8661.66....	10em	*Ca* II 2.14 (1000); notes 2, 4
8357.3.....	1	Atm+	8663.0:.....	1em	*Ca* II 2.14 (1000); notes 2, 4
8362.3:.....	1n	*He* I 1.77 (4)+atm	8680.19....	5n	*N* I .24 (10), *Al* II .31 (3), *Ne* I 1.92 [500], *Ne* I 9.49 [500]
8377.63....	2n	*Ne* I .61 [800], *Ne* I 6.41 [200], +atm	8683.38....	3	*N* I .38 (8)
8385.3.....	1N	.....	8686.23....	3	*N* I .13 (7)
8394.7:.....	0n	Atm+	8695.0.....	1	.....
8400.3:.....	0	.....	8703.25....	4	*N* I .24 (6)
8407.88....	3N	*A* I 8.21 (3000)+atm	8711.71....	3	*N* I .69 (7)
8418.51....	2	*Ne* I .43 [400]+atm	8718.81....	3	*N* I .82 (6)
8421.0.....	1–0	.....	8722.6:.....	1–0	.....
8424.22....	3	*A* I .65 (2000)	8728.78....	2	*N* I .88 (1)
8431.5:.....	0	.....	8733.5:.....	0	.....
8439.2:.....	0–1	.....	8747.3:.....	1	*N* I .35 (0)
8444.5.....	1nd	*He* I 3.95 (p)?	8751.0:.....	0	*H* 0.48
8446.56....	2n	*O* I .35 (25), *O* I .76 (23)	8776.7:.....	2N	*He* I .47 (p)?, *Kr* I .79 (300)
8467.2:.....	0	*H* .26	8780.6:.....	1n	*Ne* I .62 [1200]
8469.5.....	2	.....	8784.0:.....	1n	*Ne* I 3.76 [1000]
8490.34....	3	.....			
8495.3:.....	3	*Ne* I .36 [500]			
8497.53....	12em	*Ca* II 8.02 (300); notes 2, 4			

NOTES TO TABLE 1

1. This line is apparently stationary but is not included in lists of atmospheric lines. The wave length given is the measured position on the plates, not reduced for the earth's motion.

2. The emission lines which have been identified are stationary (Merrill, *Pub. A.S.P.*, **56**, 42, 1944); consequently, all emission lines are given with wave lengths corrected for the earth's motion and for the γ-velocity of the binary system (Wilson, *Lick Obs. Bull.*, **8**, 132, 1914), to aid in identification. A correction of $+3.7 \times 10^{-4} \times \lambda$ in A should probably be applied to all tabulated emission-line wave lengths.

3. The forbidden [*Ca* II] lines (Merrill, *Pub. A.S.P.*, **55**, 242, 1943) are double, with a *minimum* halfway between the two components. It is not suggested that a forbidden absorption line occurs but that there is little or no emission by [*Ca* II] atoms near zero velocity.

4. The *Ca* II emission lines are broad and asymmetric. The measured position at the zero velocity is at a *maximum* of intensity, thus differing from the [*Ca* II] lines in which the zero velocity is at a minimum intensity. Weak and nearly completely resolved components are seen at velocity +40 km/sec.

5. These absorption lines, where identified as *Fe* II, show very discrepant wave lengths on the two plates measured. While the wave lengths are close enough to refer to the same line, the mean displacement is such that Ce 3177 gives +0.67 A compared to Ce 3223—i.e., if the shift is a Doppler effect, the mean velocity of these lines on Ce 3177 is +26 km/sec.

lines of $I = 1$–0 being almost certainly real. Symbols used are: "n," diffuse; "N," very diffuse; "d," double; "em," emission; "atm," atmospheric. Most of the intensities and wave lengths are from C. E. Moore;[5] those from other sources are indicated by brackets, ([]). Unsatisfactory identifications or minor contributors are shown by a question mark (?).

Elements identified are described in Table 2. Certain lines arise from levels of high excitation potential; the highest levels certainly present are indicated by the tabulated value of E. Some of the elements included in Table 2 present interesting features which are discussed individually.

H.—Paschen lines are extremely weak in absorption. *Hα* is a strong asymmetrical emission discussed below.

He I.—Lines arising from levels of principal quantum number, $n = 3$, are very weak compared to those from $n = 2$. For example, λ 7065 ($2^3P^o - 3^3S$) is strong, $I = 5n$, compared to λ 7816 ($3^3S - 7^3P^o$), $I = 1n$ (blend). Unfortunately, no computed f-values

TABLE 2

ELEMENTS IDENTIFIED IN υ SAGITTARII, INFRARED REGION

Element	Remarks	Element	Remarks
H	*Hα* emission; Paschen lines extremely weak compared to β Ori	*A* II	Present; $E = 18$ e.v.
		Ca II	Emission lines, permitted and forbidden
He I	Strong; $E = 22$ e.v.	*Ti* II	Doubtful
C II	Present; $E = 16$ e.v.	*V* II	Doubtful
N I	Very strong compared to β Ori; $E = 12$ e.v.	*Cr* II	Weak
		Mn II	Doubtful
N II	Weak; $E = 23$ e.v.	*Fe* II	Weak absorption and emission; possibly also forbidden emission
O I	Strong, but weaker than β Ori; $E = 11$ e.v.		
F I	Very doubtful	*Kr* I	Doubtful
Ne I	Strong; $E = 18$ e.v.	*Zr* II	Doubtful
Mg II	Strong; $E = 10$ e.v.	*Ba* II	Doubtful
Al II	Strong; $E = 14$ e.v.	*La* II	Doubtful
Si II	Strong	*Sm* II	Doubtful
S II	Present	*Eu* II	Weak
A I	Present; $E = 12$ e.v.	*Gd* II	Doubtful

exist for the transition from $n = 3$. The difference in Boltzmann factors between 2^3P^o and 3^3S is small. There is no strong evidence for effects due to metastability in υ Sagittarii. For example, λ 7281 ($2^1P^o - 3^1S$) is a strong line ($I = 5$) and arises from a normal level.

N I.—The multiplet $3s^4P - 3p^4P^o$ is not measured because of its location within a strong atmospheric band. Other doublet and quartet systems are well represented. An apparent peculiarity exists in the behavior of certain multiplets arising from a common electron transition, 3s – 3p. According to the estimated intensities in Table 1, the $3s^4P - 3p^4D^o$ group near λ 8680 appears weaker than the $3s^4P - 3p^4S^o$ group near λ 7470. The theoretical relative intensities, computed on the assumption of LS coupling, are given in Table 3, together with the laboratory intensities. They show that, in fact, the λ 8680 group should be stronger. The stellar intensities were measured (on two plates) and the equivalent widths are included in Table 3. It can be seen that there is approximate agreement of the measured widths with the theoretical ones and that the anomaly arises from a systematic underestimation of the line intensities toward the far infrared.

While Table 3 defines—very roughly—a curve of growth for *N* I, the data are too poor to give more than an order-of-magnitude determination of the turbulence. The strong lines demonstrate the existence of a rather flat portion of the curve where log

W/λ is of the order of -4.20. Using standard curves of growth, we can estimate a rough value of the atomic velocity for *N* I as 10 km/sec, which is quite reasonable for a star of very high luminosity. Objects with extended atmospheres, such as ϵ Aur or 17 Lep, possess larger turbulent velocities than does υ Sgr. It is interesting also to note that effects of metastability are not involved in the strength of the *N* I lines, since they arise from a normal lower level, from which transitions to the ground level ($2p^3\ {}^4S^o$) are possible. There is also no evidence for anomalies in the relative strength of doublet and quartet lines. The presence of *N* I is highly correlated with luminosity. Merrill has shown the strengthening of *N* I in α Cyg[6] when compared with α Lyr.

O I.—These lines are weak in the spectrum of υ Sgr, in comparison with β Ori or α Cyg. There is little doubt that the ratio *N* I/*O* I is greater in υ Sgr. The ionization equilibriums and the excitation factors are such that we can assume the abundance ratio of *N*/*O* to be also relatively greater in υ Sgr. If Lyman-line and continuous emission of hydrogen is abnormally weakening *O* I by ionization, it would enhance *O* II. However, the *O* II lines in the blue are weak compared to *N* II. The behavior of the *O* I quintet and triplets in the infrared is peculiar. The 3^5S^o level is metastable, the 3^3S^o is normal; the theoretical ratio of the two multiplets at λ 7774 ($3^5S^o - 3^5P$) and λ 8446 ($3^3S^o - 3^3P$) is 5/3. In β Ori and α Cyg the two groups are nearly equal, while in υ Sgr the individual

TABLE 3

INTENSITIES OF *N* I LINES

λ	*I* (Lab.)	Theoretical log *I*	Observed log W/λ	*I* (Table 1)	λ	*I* (Lab.)	Theoretical log *I*	Observed log W/λ	*I* (Table 1)
7423.....	7	−0.79	−4.16	10	8703.....	6	−0.40	−4.14	4
7442.....	8	−0.50	−4.22	10	8711.....	7	−0.29	−4.19	3
7468.....	10	−0.32	−4.16	10	8718.....	6	−0.37	−4.23	3
8683.....	8	0.00	−4.22	3	8729.....	1	−1.12	−4.48	2
8686.....	7	−0.40	−4.23	3	8747.....	0	−1.32	−4.60	1

quintet lines are stronger than the blended triplet. Because of the incomplete resolution, we give the measured equivalent widths of the total blend in each case. The quintet lines, λ 7774, have an equivalent width of 1.06 A, while the triplets, λ 8446, have a width of 0.18 A. The expected ratio, because of the effects of the curve of growth, is less than 5/3. A strong tendency may exist for λ 8446 to appear in emission, resulting in a weakening of the absorption feature. An anomaly similar to that of the triplets and singlets in *He* I may also be suggested as responsible for this effect. The strength of *O* I varies rapidly with luminosity,[6] but less rapidly than does that of *N* I; the behavior of the quintets and triplets should be studied in stars with peculiar atmospheres, such as those with emission lines. P. Swings[7] has shown that in P Cyg the *O* I lines occur in both emission and absorption. It is interesting to note that, in emission, λ 8446 is nearly as strong as λ 7774; in absorption, it is much weaker.

Rare gases.—Lines of these elements are usually weak in stellar spectra. In υ Sgr, *He* I and *Ne* I are very strong. Both *A* I and *A* II are present, and *Kr* I may be present. The lines arise from levels with high excitation potentials (from 23 e.v. for *He* I to 11 e.v. for *Kr* I), and it is the extremely high "excitation temperature" which accounts for the greater strength of such elements in υ Sgr than in normal supergiants. From other astrophysical data the abundances of *Ne* and *A* are known to be high; *Kr* is apparently relatively rare, since *Kr* II does not appear, in spite of a favorable stage of ionization, and *Kr* I is only weakly present.

[6] *Mt. W. Contr.*, No. 486; *Ap. J.*, **79**, 183, 1934.

[7] *Pub. A.S.P.*, **56**, 238, 1944.

Fe II.—The laboratory spectrum of *Fe* II is not rich in the infrared, almost all identified lines belonging to the multiplet $b^4D - z^4D^o$. We have found on high-dispersion spectra of υ Sgr that the profiles of the strong *Fe* II lines of the $b^4F - z^4D^o$ and $b^4F - z^4F^o$ multiplets are subject to peculiar doublings and asymmetries and are strongly variable. It is suggestive that most of the observed lines in the infrared have an upper level (z^4D^o) in common with the strong variable lines in the blue. The measured positions of the observed *Fe* II lines are variable, deviating considerably from the orbital velocities. Further, it is probable that some of the weak emission lines also arise from the same *Fe* II multiplet. If we assume that the emission lines are stationary while the absorption lines move with the star, we obtain the wave lengths in Table 4. Theoretical intensities are computed on the basis of LS coupling. It is apparent that the strong lines are present in emission, and some of them also in absorption. Table 4 suggests that incipient emission is present in all lines and that a small physical disturbance can change a line from emission to absorption. Since the emission is probably stationary, it is possible that the blend-

TABLE 4

WAVE LENGTHS AND INTENSITIES, *Fe* II, $b^4D - z^4D^o$

LABORATORY			THEORETICAL	ABSORPTION		EMISSION	
λ	*I*	*J*	*I*	λ	*I*	λ	*I*
7711.71	15	7/2–7/2	100	1.4	1–0	1.23	3
7462.38	20	5/2–5/2	50	2.3	1	2.1:	2
7307.97*	(50 bl)	3/2–3/2	23	.....	.....	.....	.....
7224.51*	12	1/2–1/2	15	4.04	2	.....	.....
7515.88	6	7/2–5/2	17	5.49	2	.....	.....
7320.70*	(40 bl)	5/2–3/2	20	.....	.....	0.3:	1
7222.39*	8	3/2–1/2	15	.....	.....	.....	.....
7655.47*	1	5/2–7/2	17	.....	.....	.....	.....
7449.34	6	3/2–5/2	20	.....	.....	9.2:	2
7310.24*	6	1/2–3/2	15	0.2:	1	.....	.....

* Lines marked with an asterisk are in regions of strong atmospheric absorption and may be blended or masked.

ing with overlying weak emission produces the doubling and asymmetry of the absorption lines in the blue and the discrepant wave lengths observed in the infrared. Other permitted *Fe* II lines seem to be present in emission in the region $\lambda < 6500$ A.

If the emission lines of *Fe* II arise in an extended envelope in parts of which *Ca* II and [*Ca* II] lines are produced, some unknown selective mechanism must be operating to excite emission from z^4D^o. The difference between the term value of z^4D^o and the ionization limit (to *Fe* III) is about 10.6 e.v.; since a Lyman-α quantum has only 10.16 e.v., coincidence with Lyman-α is probably not important. The z^4D^o levels are about 5.5 e.v. above the ground state of *Fe* II; and no resonance lines of the abundant atoms, such as *He* I, *N* I, *He* II, *Ne* I, etc., have significant coincidences.

The identification of the two emission lines, λ 7154.95 (5 em) and λ 7452.61 (1 em), as [*Fe* II], ($a^4F - a^2G$), suggested by P. Swings,[8] is still uncertain. The excitation potential of a^2G is 1.96 e.v., and there is a lower group of forbidden lines, $a^6D - a^4P$, at 1.66 e.v., which seems actually to be absent (although some of its lines fall in a region of strong atmospheric lines). It will be necessary to prove that the transition probability for [*Fe* II], λ 7155, is high before the identification with the stellar line is adopted. Observation of the infrared spectra of peculiar lines with strong [*Fe* II] would be useful.The

[8] *Pub. A.S.P.*, **56**, 242, 1944.

intensity of λ 7155 was measured and found to be equivalent to 0.31 A in the neighboring continuum; the intensity should eventually be followed for possible variability.

EMISSION-LINE VELOCITIES

Emission lines in the infrared have been reported[9] to be approximately stationary. The lines are not symmetrical; the profiles differ from line to line and may be variable. Measures of positions, made on all available plates by one observer, are in Table 5. To determine the velocity, the measures were corrected only for the reduction to the sun. (In Table 1 the wave lengths of the emission lines were also corrected for the γ-velocity of the system.) Data given include the date; the phase in the orbital motion[1] expressed as a fraction of the period; the predicted orbital velocity ("Pred."); the observed stellar velocity from the absorption lines ("Obs."); and the observed emission-line velocity,

TABLE 5

EMISSION-LINE VELOCITIES (KM/SEC)

PLATE NO.	DATE	PHASE	PRED.	OBS.	V (EM)		
					Hα	*Ca* II	[*Ca* II]
G 175	1928 July 24	0.07	+34	+39	+12:	.....	.....
Ce 852	1934 June 25	.75	+28	+33	− 8	.....	.....
2024	1939 May 4	.61	− 8	−13	+ 7	.....	.....
2025	May 4	.61	− 8	−11:	+ 7	.....	.....
2050	June 6	.85	+55	+56	+ 2	.....	.....
2066	July 31	.24	−18	.....	− 4	.....	.....
2109	Aug. 30	.46	−35	.....	+ 4	.....	.....
G 1769	1942 Sept. 5	.45	−33	−35	.....	−6	.....
Ce 3121	1943 July 21	.76	+33	+39	.....	−2	.....
3125	22	.77	+35	+40	.....	0	.....
3126	22	.77	+35	+42:	+ 3	0	+2
3176	Sept. 7	.11	+23	.....	.....	−2	+5
3177	8	.11	+22	+29	− 4	−2	+4
3209	21	.21	−10	.....	+10	−5	+5
3223	Oct. 7	0.33	−32	−35	+ 2	−3	+1
Mean	.....	.....	.....	.....	+ 2	−2	+3

V (em), for *H*, *Ca* II, and [*Ca* II]. Colons denote uncertain values. The predicted and observed absorption-line velocities agree well. There is little variation in the velocities of the emission lines. While the latter do not share the orbital motion of the observed star, they show a systematic velocity of −11 km/sec with respect to the center of mass of the system (γ-velocity = +12 km/sec). As a consequence, the emission-line wave lengths in Table 1 are systematically too small by about 0.3 A, if we assume that all emission lines share the characteristic motion of the bright lines *Hα*, *Ca* II, and [*Ca* II]. Such a correction strengthens the wave-length coincidence of λ 7155 with [*Fe* II].

Interpretation of these emission velocities is not simple. If there were a dominant expansion in the shell, self-reversal of the P Cygni type would shift the lines systematically to longer wave lengths rather than to shorter wave lengths (−11 km/sec), as observed. It is improbable that the [*Ca* II] lines originate in the same parts of the nebulous mass as do the *Ca* II and *Hα* lines. Nevertheless, all these lines show substantially the same type of motion and seem unaffected by the orbital motion of the observed star. The value of $a \sin i$ is 9×10^7 km; the radius of the star may be of the order of half this

[9] Paul W. Merrill, *Pub. A.S.P.*, **56**, 42, 1944.

quantity. The radiation giving rise to the emission lines can possess moderate dilution for *Hα* and *Ca* II and must be more highly diluted for [*Ca* II]. The distance from the center of mass of the system to the emitting material should eventually be correlated with the dynamical properties of the system. The *Hα* line, as will be shown below, possesses a peculiar asymmetry; the [*Ca* II] lines are apparently double. If the line structure is interpreted as a result of Doppler shift in two expanding jets of material, the jets, even at large distances, should be in slow rotation about the system, and the line patterns should change slowly with time. The pattern of the *Hα* emission line, except for an outburst discussed below, has not changed substantially on the plates available, that is, within fifteen years of rather scattered observation. It is certain that no notable change

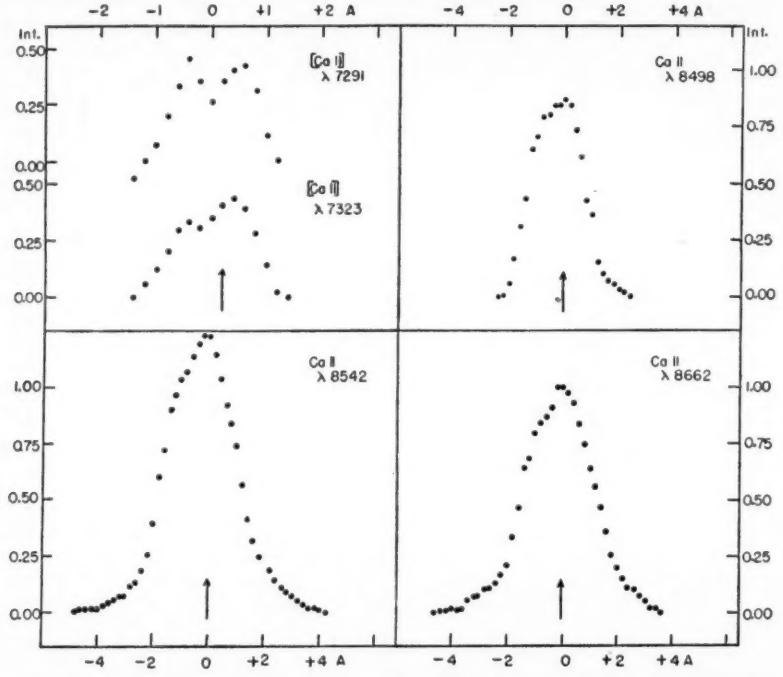

FIG. 1.—Profiles of forbidden and permitted lines of ionized calcium. The intensities are expressed in units of the intensity in the neighboring stellar continuum. The arrow marks the stationary position of each line.

took place in four years. The rotation of the nebulous mass must be slow, if the line profiles are to be explained by asymmetrical expanding jets. Two possibilities may be considered. On the one hand, let the material be gravitationally bound to the system; then, if the mass ratio of the two stars is 3/1 and if we assume a period of one hundred years, the distance is 2×10^{10} km. On the other hand, we may assume that the material is being permanently ejected from the star and is only conserving its initial angular momentum; then the distance is 6×10^{9} km. The resultant rotational width of the emission lines is either 40 km/sec or 16 km/sec (in the above two cases). The observed line widths are very much greater. The narrowest strong emission lines, those of [*Ca* II], have widths corresponding to about an 85-km/sec range of motion. This width could be rotational in origin, since such rotation could occur at large distances from the star, where the dilution of radiation would be about 10^{-4} or 10^{-5} and where, in consequence, strong forbidden lines could be emitted. This argument is not valid for the *Hα* line. The *Ca* II

lines are probably emitted close to the star in a more or less uniformly rotating mass, with range of velocity of 200 km/sec. The possibility of survival of jets of material in such a complex mass requires investigation.

EMISSION-LINE INTENSITIES

In Figure 1 we show the intensities and profiles of the *Ca* II lines. The forbidden lines are based on the mean of three plates. The permitted lines are plotted as observed on plate Ce 3209. The structure of all lines is slightly variable. In Figure 2, two profiles of

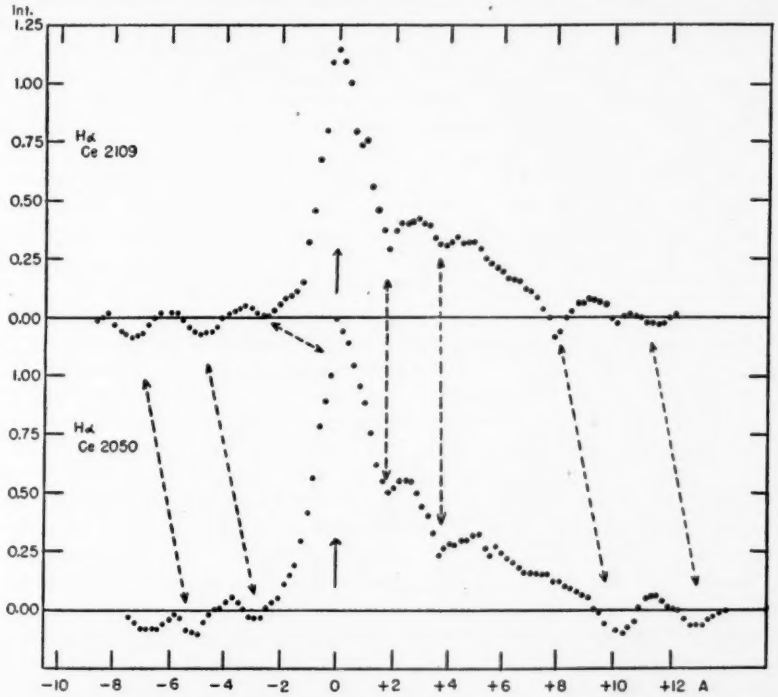

FIG. 2.—Profiles of *Hα* on two plates. Negative intensities indicate absorption lines. The dotted lines connect the corresponding stellar absorption lines on the two plates. The shifts of the absorption lines arise from orbital motion; the emission lines are stationary. The dips in the profiles near +2 and +3.7 A may possibly be stationary structural features of the emission line. The absorption feature at −2.7 A on Ce 2109 is the stellar absorption line of *Hα*; it is invisible when superposed on the strong emission maximum of Ce 2050.

Hα are shown, measured on the red plates, Ce 2050 and Ce 2109. (The infrared plates have lower resolution than the ordinary red-sensitive plates, and the detailed structure in *Hα* can best be studied on the red plates.) Visual inspection suggests that the relative intensity of the two components of a [*Ca* II] line varies slightly. Correlated with a strengthening of the longward component of [*Ca* II] is a strengthening of a nearly separated component on the longward side of the *Ca* II lines. Plates Ce 3126 and 3176 have strong longward [*Ca* II] components, at phases 0.77 and 0.11; plate Ce 3223 has a stronger shortward component of [*Ca* II] at phase 0.33 in the same cycle. The observational material is not sufficient to establish the regularity of these variations. On the original plates the dip in intensity at the center of the [*Ca* II] lines is more conspicuous than in Figure 1; the longward component of *Ca* II is an easily visible feature.

[*Ca II*].—The transitions are $4^2S - 3^2D$, excitation potential of upper level 3.14 e.v.

The theoretical intensity ratio of the lines λ 7291/λ 7323 is 3/2. The observed equivalent widths are 0.66 A and 0.65 A. The discrepancy is not significant, since a strong atmospheric line weakens the shortward wing of λ 7291. There is no obvious explanation of the apparent doubling. Known atmospheric lines or lines to be expected in the star are not sufficient to weaken the center of the forbidden line; self-absorption cannot be expected in forbidden lines. To produce such profiles, we might postulate two jets of material emitted nearly in the line of sight from opposite sides of an envelope surrounding the binary system. The points of ejection must not rotate with the stars. Such a hypothesis requires the presence of a distant third body, to establish a preferential direction of motion fixed in space. The widths of the lines correspond to a total range of about 85 km/sec of Doppler motion. An alternative possibility suggested by Dr. G. P. Kuiper is a ring of matter at a large distance from the stars; over a certain range of distance the pressure and dilution might be favorable for emission of the forbidden lines. Such a doughnut-shaped ring of moderate radial extension, if in rotation, would produce an emission line with a dip in the center, similar to that observed.

Ca II.—The transitions are $3^2D - 4^2P^o$, excitation potential of upper level 3.14 e.v. The lines λλ 8498, 8542, 8662, have theoretical intensities in the ratio 1/9/5; laboratory estimates agree roughly with this ratio. It is obvious that no such intensity ratio exists in the observed emission lines. Mean equivalent widths measured are 2.25, 3.67, and 3.46 A for λλ 8498, 8542, 8662, respectively. Photometric errors at the end of the plate may possibly account for the excessive strength of λ 8662 with respect to λ 8542, but an intensity ratio of 1/9 seems out of the question for λ 8498/λ 8542. Since these two lines arise from the same upper level, the explanation cannot involve a process of specific excitation of the upper level. Self-reversal by atoms of *Ca* II in a nebulous mass whose expansion is small would reduce the intensity-ratio of the observed lines. Exact interpretation of the measured intensities is complicated by the slight depression of these lines by the underlying *Ca* II absorption lines of the star. The number of *Ca* II atoms in the excited 3^2D state must be quite high; if the nebulous mass is sufficiently opaque to the light of λ 8662 to produce self-reversal, the emission by *Ca* II must occur fairly close to the star, where the dilution is moderate. The profiles of the *Ca* II lines are wide, showing a velocity range of 220 km/sec, which is large compared to the orbital range of the observed star. These velocities cannot represent dominantly an expansion because of the strong general self-reversal of the *Ca* II lines and the absence of a P Cygni absorption component. The maximum intensity of the line is near zero velocity, and no effects of the two jets or the thin rotating ring suggested by [*Ca* II] can be seen. The displaced longward component of *Ca* II, however, may be connected with the jet phenomenon.

The origin of the *Ca* II emission may be a mechanism similar to that suggested by A. B. Wyse.[10] The ionization of an atom of *Ca* II in the 3^2D state requires an energy of 82,050 cm^{-1}, which is less than that of Lyman-α, 82,260 cm^{-1}. Consequently, if *Ca* II (3^2D) has a sharp maximum probability of ionization at its series limit, an emission line at Lyman-α could depopulate 3^2D. Wyse suggested that a tendency might then exist for the emission of $3^2D - 4^2P^o$. Even a simple form of this theory, however, requires study of the properties of a complex cyclical mechanism. The lines $4^2S - 4^2P^o$ (H and K) are strong, in absorption, exhibiting no emission. If 4^2P^o is "overpopulated," the emission transitions downward strongly favor H and K emission; the ratio of the *f*-values (emission) of $4^2S - 4^2P^o$ to $3^2D - 4^2P^o$ is about 10/1. The observational evidence for self-reversal of $3^2D - 4^2P^o$ is strong; large numbers of upward transitions occur, therefore, even in the outer parts of the *Ca* II nebulous mass. These upward transitions depend on the number of quanta of radiation at λ 8600 in the nebula; the transitions induced by Lyman-α depend on the number of quanta of Lyman-α, which is probably small compared to that in the infrared. An ionization process has only small efficiency if it depends on line emission. The total *f*-value for ionization is small compared to that for line ab-

[10] *Pub. A.S.P.*, **53**, 184, 1941.

sorption,[11] even when integrated over the whole range of radiation capable of producing ionization; the Lyman emission line provides energy over only a small part of this ionizing range.

Hα.—The profiles of *Hα* (Fig. 2) are complex and should be studied for variability with phase. The equivalent widths of the observed line on the two red plates are 4.1 A on Ce 2109 and 5.0 A on Ce 2050, in units of the stellar intensity in the neighboring continuum. The asymmetry is very striking, appreciable emission appearing on both plates at −3 A and persisting to +12 A (−140 to +550 km/sec). Such velocities seem large compared to any known rotational velocities in the nebulous mass, and the predominantly positive velocity shifts suggest a jet fixed in space flowing outward from the star and in a direction away from the sun. Note the existence of dips in the intensity at about +2 and +3.7 A from the maximum. The stellar absorption lines shift on the two stationary profiles of *Hα* by about 90 km/sec between the two plates, but these two features remain fixed and seem to be present and similar on plates taken[12] in July and September, 1940. The two absorption features on the emission band have not been identified. They may not actually be absorption lines but may correspond to gaps in the emission-velocity distribution. The irregularities may be due to jets similar to those suggested to explain the [*Ca* II] lines. More detailed study at other phases in the orbit might show them to be stationary.

If the jet hypothesis is abandoned, the asymmetrical profile of *Hα* must be of complex origin. A tentative hypothesis may be advanced. In an ordinary expanding shell about a star, a P Cygni absorption line appears by the absorption of stellar radiation by gas in the line of sight between the star and the observer. No strong hydrogen absorption feature in υ Sgr is now directly observed at *Hα*. The absence of the violet wing of the *Hα* emission may, nevertheless, be a result of an analogous phenomenon in a large nebulous mass about the star. Assume that, close outside the stellar orbit, hydrogen gas, ejected from one or both stars, is in a state of rapid motion, either rotation or expansion. Orbital motion is not observed because of a uniform distribution of the nebulous material in a ring or shell about the stars. Ionization is high, and recombination produces emission. Such a mass could produce a uniform emission line with a maximum at zero velocity. At larger distances from the stars, but still at moderate dilution, there might be a surrounding ring of hydrogen expanding with large velocities. Such absorbing material between us and the inner hydrogen cloud would tend to weaken the shortward wing of the *Hα* line. The difficulties faced by such a hypothesis are obvious. A very delicate balance is required between the amounts of absorbing and emitting material; the velocity distributions in the inner and outer zones must be correctly chosen. The high velocity required, reaching 500 km/sec, is not probable for rotation and is not shown in expansion by *Ca* II or by [*Ca* II] at large distances from the system. Among the spectra available, only one plate (G 175, taken on July 24, 1928) shows a strong absorption component near *Hα*. The measured displacement with respect to the center of the bright line is −323 km/sec. This component, previously reported by J. S. Plaskett[13] at *Hβ*, *Hγ*, and *Hδ*, is weak or absent on later plates. Although this displaced absorption has now disappeared, it may be taken as evidence for the possibility that hydrogen atoms may acquire high expansion velocities in the complex system of υ Sgr.

The *Hα* line is strong in emission, but on all recent plates *Hβ*, *Hγ*, etc., are normal absorption lines. The intensity ratio between the emission at *Hα* and that at *Hβ* must be large (no recent measures are yet available). In emission nebulae a theoretical ratio for *Hα*/*Hβ* is about 2.5/1. The weakness of the *Hβ* emission on high-dispersion coudé plates suggests a ratio greater than 10/1.

[11] This point was raised by Dr. L. G. Henyey.

[12] J. L. Greenstein, *Ap. J.*, **97**, 252, Fig. 1, 1943.

[13] *Pub. Dom. Ap. Obs.*, **4**, 11, 1927.

THE SECONDARY SPECTRUM

In the ultraviolet and blue no sign of a secondary component of υ Sgr has been detected. It is possible that the invisible secondary is a hot, small star; in that case the bolometric correction and the intrinsic weakness of the lines of an early star would combine to mask completely the spectrum of the secondary. The lines of υ Sgr are quite deep in the blue, reaching perhaps 60 per cent central absorption; on that account the overlapping continuum of the secondary must also be faint. The depths in the infrared indicate that the secondary is faint in that region also. Nevertheless, the considerable number of unidentified absorption lines in Table 1 should be investigated for the possibility that they originate in a late-type secondary.

R. E. Wilson has determined the mass function[1] to be $1.582\odot$. If the mass ratio, m_2/m_1, is less than $\frac{1}{3}$, the primary becomes excessively massive. The value of K_2 is there-

TABLE 6

EXPECTED STRONG LINES IN THE INFRARED

λ	Solar Intensity	Element	λ	α Cyg Intensity	Element
6575.0	4	*Fe* I	8374.4	4	*H*
6592.9	6	*Fe* I	8392.4	5	*H*
6593.9	4	*Fe* I	8413.3	6	*H*
6643.6	5	*Ni* I	8438.0	7	*H*
6678.0	5	*Fe* I	8446.5	9	*O* I
6717.7	5	*Ca* I	8467.3	7	*H*
6767.8	4	*Ni* I	8502.5	7	*H*
7664.9	6	*K* I	8545.4	7	*H*
7699.0	5	*K* I	8598.4	8	*H*
8435.0	1	*Ti* I	8665.0	9	*H*
8435.7	1	*Ti* I			
8675.8	1	*Fe* I			
8688.6	2	*Fe* I			

fore probably less than three times K_1, or about 150 km/sec. On plate Ce 3223 the primary had a velocity near the minimum value, -32 km/sec or -44 km/sec with respect to the γ-axis; the velocity difference of the secondary with respect to the primary is about $+180$ km/sec or less and would result in shifts of $+5$ A at λ 8600. If the spectral type of the secondary were between A and M, the dominant absorption lines might be those of the *Ca* II triplet. Inspection of Table 1 reveals no absorptions shifted longward by this amount. If the mass ratio is closer to unity, the velocity shifts are smaller, and the lines may be hidden in the *Ca* II emission bands. The study of the sun[14] and a few stars[6] in the infrared yields a list of other possible strong lines given in Table 6. Most of the lines are in regions free from strong atmospheric bands.

Examination of Table 1 has not revealed any lines in υ Sgr that can reasonably be identified with those in Table 6. Various reasonable velocity displacements can be assumed, which would result in red shifts of the line between $+1$ and $+5$ A. No significant coincidences seem to exist; consequently, there is at present no evidence for a late-type companion to υ Sgr.

[14] C. E. St. John *et al.*, *Revision of Rowland's Preliminary Table of Solar Spectrum Wave Lengths*, Carnegie Institution of Washington, 1928.

ON THE RADIATIVE EQUILIBRIUM OF A STELLAR ATMOSPHERE. XII

S. CHANDRASEKHAR
Yerkes Observatory
Received June 3, 1946

ABSTRACT

In this paper the theory of diffuse reflection, given in an earlier paper of this series, is further developed to allow for the scattering of radiation in accordance with a general phase function.

1. *Introduction.*—In an earlier paper[1] of this series the problem of diffuse reflection by a semi-infinite plane-parallel atmosphere has been considered, allowing for the anisotropy of the scattered radiation in accordance with the phase functions $\lambda(1 + x \cos \Theta)$ and $\frac{3}{4}(1 + \cos^2 \Theta)$, where Θ denotes the angle of scattering. In this paper we propose to extend this discussion to include all cases in which the phase function can be expressed as a series with a finite number[2] of terms in Legendre polynomials in $\cos \Theta$.

2. *The reduction of the equation of transfer.*—The equation of transfer appropriate to the problem of diffuse reflection of a parallel beam of radiation by a plane-parallel atmosphere has already been written down in Paper IX (eq. [2]). We shall now suppose that the phase function $p(\cos \Theta)$, which occurs in this equation, can be expressed as a finite series in the form

$$p(\cos \Theta) = \sum_{l=0}^{N} \varpi_l P_l(\cos \Theta), \tag{1}$$

where $\varpi_l, l = 0, \ldots, N$ are a set of $N + 1$ constants and P_l denotes the Legendre polynomial of order l in the argument specified. For this phase function the equation of transfer is

$$\left.\begin{aligned} \cos \vartheta \frac{dI(\tau, \vartheta, \varphi)}{d\tau} = I(\tau, \vartheta, \varphi) - \frac{1}{4\pi} \int_0^{\pi} \int_0^{2\pi} I(\tau, \vartheta', \varphi') \sum_{l=0}^{N} \varpi_l \\ \times P_l(\cos \vartheta \cos \vartheta' + \sin \vartheta \sin \vartheta' \cos [\varphi' - \varphi]) \sin \vartheta' d\vartheta' d\varphi' \\ - \tfrac{1}{4} F e^{-\tau \sec \beta} \sum_{l=0}^{N} \varpi_l P_l(-\cos \vartheta \cos \beta + \sin \vartheta \sin \beta \cos \varphi). \end{aligned}\right\} \tag{2}$$

Expanding the Legendre functions in equation (2) in accordance with the addition theorem, we have

$$\left.\begin{aligned} \mu \frac{dI(\tau, \mu, \varphi)}{d\tau} = I(\tau, \mu, \varphi) - \frac{1}{4\pi} \int_{-1}^{+1} \int_0^{2\pi} I(\tau, \mu', \varphi') \sum_{l=0}^{N} \varpi_l \\ \times \left[P_l(\mu) P_l(\mu') + 2 \sum_{m=1}^{l} \frac{(l-m)!}{(l+m)!} P_l^m(\mu) P_l^m(\mu') \cos m(\varphi' - \varphi)\right] d\mu' d\varphi' \\ - \tfrac{1}{4} F e^{-\tau \sec \beta} \sum_{l=0}^{N} (-1)^l \varpi_l \Big[P_l(\mu) P_l(\cos \beta) \\ + 2 \sum_{m=1}^{l} (-1)^m \frac{(l-m)!}{(l+m)!} P_l^m(\mu) P_l^m(\cos \beta) \cos m\varphi\Big], \end{aligned}\right\} \tag{3}$$

where we have written μ and μ' for $\cos \vartheta$ and $\cos \vartheta'$, respectively.

[1] *Ap. J.*, **103**, 165, 1946. Referred to hereafter as "Paper IX."

[2] The necessity of this restriction to a finite number of terms will become apparent in § 3 (see eq. [7]).

The form of equation (3) suggests that we seek a solution of the form

$$I(\tau, \mu, \varphi) = I^{(0)}(\tau, \mu) + \sum_{m=1}^{N} I^{(m)}(\tau, \mu) \cos m\varphi , \tag{4}$$

where, as the notation indicates, $I^{(0)}$ and $I^{(m)}$ are functions of τ and μ only. With the substitution (4), equation (3) breaks up into the following equations:

$$\left.\begin{aligned} \mu \frac{dI^{(0)}}{d\tau} = I^{(0)} - \frac{1}{2}\int_{-1}^{+1} I^{(0)}(\tau, \mu') \sum_{l=0}^{N} \varpi_l P_l(\mu) P_l(\mu')\, d\mu' \\ - \tfrac{1}{4} F e^{-\tau \sec\beta} \sum_{l=0}^{N} (-1)^l \varpi_l P_l(\mu) P_l(\cos\beta) , \end{aligned}\right\} \tag{5}$$

and

$$\left.\begin{aligned} \mu \frac{dI^{(m)}}{d\tau} = I^{(m)} - \frac{1}{2}\int_{-1}^{+1} I^{(m)}(\tau, \mu') \sum_{l=m}^{N} \varpi_l \frac{(l-m)!}{(l+m)!} P_l^m(\mu) P_l^m(\mu')\, d\mu' \\ - \tfrac{1}{2} F e^{-\tau \sec\beta} \sum_{l=m}^{N} (-1)^{l+m} \varpi_l \frac{(l-m)!}{(l+m)!} P_l^m(\mu) P_l^m(\cos\beta) \\ (m = 1, \ldots, N) . \end{aligned}\right\} \tag{6}$$

We shall now show how these equations can be solved.

3. *The solution of equation* (5) *in the* n*th approximation.*—Following the general method developed in the earlier papers of this series, we replace the integral which occurs on the right-hand side of equation (5) by a sum according to Gauss's formula for numerical quadratures and reduce the integrodifferential equation to a system of linear equations. In the nth approximation the equivalent linear system is of order $2n$, corresponding to the Gaussian division of the interval $-1 \leqslant \mu \leqslant 1$ according to the zeros of $P_{2n}(\mu)$. It therefore follows that in our present context, in which the Legendre polynomials $P_l(\mu')$ with a maximum degree N occur under the integral sign, we must seek solutions in approximations n such that

$$4n - 1 > 2N . \tag{7}$$

Conversely, if we limit ourselves to solutions of the equation of transfer in the nth approximation, we are not entitled to include in an expansion of the phase function in Legendre polynomials terms of order higher than $2n - 1$.

Assuming, then, that condition (7) is fulfilled, the system of $2n$ linear equations, to which equation (5) is equivalent in the nth approximation, is

$$\left.\begin{aligned} \mu_i \frac{dI_i^{(0)}}{d\tau} = I_i^{(0)} - \frac{1}{2}\sum_j \sum_{l=0}^{N} a_j I_j^{(0)} P_l(\mu_j) \varpi_l P_l(\mu_i) \\ - \tfrac{1}{4} F e^{-\tau \sec\beta} \sum_{l=0}^{N} (-1)^l \varpi_l P_l(\cos\beta) P_l(\mu_i) \qquad (i = \pm 1, \ldots, \pm n) , \end{aligned}\right\} \tag{8}$$

where the various symbols have their usual meanings.

In solving the system of equations represented by equation (8), we first seek the general solution of the associated homogeneous system

$$\mu_i \frac{dI_i}{d\tau} = I_i - \frac{1}{2}\sum_j \sum_{l=0}^{N} a_j I_j P_l(\mu_i) \varpi_l P_l(\mu_i) \qquad (i = \pm 1, \ldots, \pm n) \tag{9}$$

and then add to it a particular integral of the nonhomogeneous system.

To obtain the different linearly independent solutions of the system (9), we follow a procedure which has now become standard. Thus, setting

$$I_i = g_i e^{-k\tau} \qquad (i = \pm 1, \ldots, \pm n), \quad (10)$$

we find that the constants g_i must be expressible in the form

$$g_i = \frac{\sum_{l=0}^{N} \varpi_l \xi_l P_l(\mu_i)}{1 + \mu_i k} \qquad (i = \pm 1, \ldots, \pm n), \quad (11)$$

where the ξ_l's ($l = 0, \ldots, N$) are certain constants independent of i which have to be determined in conformity with the equation

$$\sum_{l=0}^{N} \varpi_l \xi_l P_l(\mu_i) = \sum_{l=0}^{N} \sum_{\lambda=0}^{N} \varpi_l P_l(\mu_i)\, D_{l,\lambda} \varpi_\lambda \xi_\lambda, \quad (12)$$

where

$$D_{l,\lambda} = \frac{1}{2} \sum_j \frac{a_j P_l(\mu_j) P_\lambda(\mu_j)}{1 + \mu_j k}. \quad (13)$$

Since equation (12) must be valid for all i, we must require that

$$\xi_l = \sum_{\lambda=0}^{N} D_{l,\lambda} \varpi_\lambda \xi_\lambda \qquad (l = 0, \ldots, N). \quad (14)$$

We shall now show how equation (14) determines the ξ's apart from a constant of proportionality and leads also to the characteristic equation for k.

First, we may observe that $D_{l,\lambda}$ defined as in equation (13) satisfies a simple recursion formula. For, writing $D_{l,\lambda}$ in the form

$$D_{l,\lambda} = \frac{1}{2} \sum_j a_j P_l(\mu_j) P_\lambda(\mu_j) \left(1 - \frac{k\mu_j}{1 + \mu_j k}\right) \quad (15)$$

and remembering that, since

$$l + \lambda \leqslant 2N < 4n - 1, \quad (16)$$

$$\left.\begin{aligned} \frac{1}{2} \sum_j a_j P_l(\mu_j) P_\lambda(\mu_j) &= \frac{1}{2} \int_{-1}^{+1} P_l(\mu) P_\lambda(\mu)\, d\mu \\ &= \frac{\delta_{l,\lambda}}{2l+1}, \end{aligned}\right\} \quad (17)$$

we have

$$\left.\begin{aligned} D_{l,\lambda} &= \frac{\delta_{l,\lambda}}{2l+1} - \tfrac{1}{2} k \sum_j \frac{a_j P_\lambda(\mu_j)}{1 + \mu_j k} \mu_j P_l(\mu_j) \\ &= \frac{\delta_{l,\lambda}}{2l+1} - \frac{k}{2(2l+1)} \sum_j \frac{a_j P_\lambda(\mu_j) [(l+1) P_{l+1}(\mu_j) + l P_{l-1}(\mu_j)]}{1 + \mu_j k} \\ &= \frac{\delta_{l,\lambda}}{2l+1} - \frac{k}{2l+1} [(l+1) D_{l+1,\lambda} + l D_{l-1,\lambda}]. \end{aligned}\right\} \quad (18)$$

In other words,

$$(2l+1) D_{l,\lambda} = \delta_{l,\lambda} - k [(l+1) D_{l+1,\lambda} + l D_{l-1,\lambda}]. \quad (19)$$

Using the recursion formula (19) in equation (14), we have

$$(2l+1)\,\xi_l = \sum_{\lambda=0}^{N} \{\delta_{l,\lambda} - k\,[\,(l+1)\,D_{l+1,\lambda} + lD_{l-1,\lambda}\,]\}\,\varpi_\lambda \xi_\lambda\,, \tag{20}$$

or, again using equation (14),

$$(2l+1)\,\xi_l = \varpi_l \xi_l - k\,[\,(l+1)\,\xi_{l+1} + l\xi_{l-1}\,]\,. \tag{21}$$

Alternatively, we can write

$$\xi_{l+1} = -\frac{2l+1-\varpi_l}{k\,(l+1)}\,\xi_l - \frac{l}{l+1}\,\xi_{l-1} \qquad (l=0,\,\ldots\,,\,N-1)\,. \tag{22}$$

From equation (22) it follows that all the ξ's can be determined successively in terms of ξ_0. To remove this arbitrary constant of proportionality in the ξ's, we shall assume in our further work (as it will entail no loss of generality) that

$$\xi_0 = 1\,. \tag{23}$$

With this choice of ξ_0, the remaining ξ's are all uniquely determined by equation (22). Thus,

$$\xi_1 = -\frac{1-\varpi_0}{k}\,; \qquad \xi_2 = \frac{(1-\varpi_0)\;(3-\varpi_1)}{2k^2} - \tfrac{1}{2}\,; \qquad \text{etc.} \tag{24}$$

It is to be particularly noted that the ξ_l's ($l > 0$) determined in this manner are, in general, functions of k. We shall accordingly write

$$\xi_l = \xi_l\,(k) \qquad (l=1,\,\ldots\,,\,N)\,. \tag{25}$$

The characteristic equation for k now follows from equation (14) by considering the case $l = 0$. Thus,

$$1 = \sum_{\lambda=0}^{N} D_{0,\lambda}\varpi_\lambda \xi_\lambda\,, \tag{26}$$

or, more explicitly,

$$1 = \frac{1}{2}\sum_j \frac{a_j \sum_{\lambda=0}^{N} \varpi_\lambda \xi_\lambda P_\lambda\,(\mu_j)}{1+\mu_j k}\,. \tag{27}$$

Equation (27) is of order n in k^2 and accordingly admits, in general, $2n$ distinct nonvanishing roots, which must occur in pairs, as

$$\pm k_a \qquad (a=1,\,\ldots\,,\,n)\,. \tag{28}$$

However, an important exception arises when $\varpi_0 = 1$; for, in this case, $k = 0$ is a root[3] and equation (27) admits of only $(2n-2)$ distinct nonvanishing roots. On the other hand, when $\varpi_0 = 1$, it may be readily verified that we also have the integral

$$I_i = b\left(\tau + \frac{\mu_i}{1-\frac{1}{3}\varpi_1} + Q\right) \qquad (i=\pm 1,\,\ldots\,,\,n)\,, \tag{29}$$

where b and Q are arbitrary constants. To avoid frequent repetition we shall suppose that $\varpi_0 \neq 1$ unless we explicitly state otherwise.

[3] Note that $\frac{1}{2}\sum_j \sum_{\lambda=0}^{N} a_j \varpi_\lambda \xi_\lambda P_\lambda(\mu_j) = \frac{1}{2}\sum_j a_j \varpi_0 = 1$.

Returning to equations (9) and (10), we have now shown that the homogeneous system (9) admits $2n$ linearly independent integrals of the form

$$I_i = \text{constant} \frac{\sum_{l=0}^{N} \varpi_l \xi_l (\pm k_a) P_l (\mu_i)}{1 \pm \mu_i k_a} e^{\mp k_a \tau} \qquad \begin{pmatrix} i = \pm 1, \ldots, \pm n \\ a = 1, \ldots, n \end{pmatrix}. \quad (30)$$

To complete the solution we need a particular integral of the nonhomogeneous system (8). Again this can be found by our standard procedure.

Setting

$$I_i^{(0)} = \tfrac{1}{4} F h_i e^{-\tau \sec \beta} \qquad (i = \pm 1, \ldots, \pm n), \quad (31)$$

we readily verify that the constants h_i must be expressible in the form (cf. eq. [11])

$$h_i = \frac{\sum_{l=0}^{N} \varpi_l \gamma_l P_l (\mu_i)}{1 + \mu_i \sec \beta} \qquad (i = \pm 1, \ldots, \pm n), \quad (32)$$

where the γ_l's ($l = 0, \ldots, N$) are certain constants to be determined in accordance with the equation (cf. eq. [14])

$$\gamma_l = \sum_{\lambda=0}^{N} E_{l,\lambda} \varpi_\lambda \gamma_\lambda + (-1)^l P_l (\cos \beta) \quad (l = 0, \ldots, N) \quad (33)$$

where (cf. eq. [13])

$$E_{l,\lambda} = \frac{1}{2} \sum_j \frac{a_j P_l (\mu_j) P_\lambda (\mu_j)}{1 + \mu_j \sec \beta}. \quad (34)$$

The E_λ's satisfy a recursion formula similar to the $D_{l,\lambda}$'s. We have

$$(2l+1) E_{l,\lambda} = \delta_{l,\lambda} - \sec \beta \left[(l+1) E_{l+1,\lambda} + l E_{l-1,\lambda} \right]. \quad (35)$$

Using this formula in equation (33), we obtain

$$\left.\begin{aligned} (2l+1) \gamma_l = \varpi_l \gamma_l - \sec \beta \Big[\sum_{\lambda=0}^{N} \{ (l+1) E_{l+1,\lambda} + l E_{l-1,\lambda} \} \varpi_\lambda \gamma_\lambda \Big] \\ + (-1)^l (2l+1) P_l (\cos \beta) \end{aligned}\right\} \quad (36)$$

Again, using equation (33), we have

$$\left.\begin{aligned} (2l+1) \gamma_l = \varpi_l \gamma_l - \sec \beta \left[(l+1) \{ \gamma_{l+1} + (-1)^l P_{l+1} (\cos \beta) \} \right. \\ \left. + l \{ \gamma_{l-1} + (-1)^l P_{l-1} (\cos \beta) \} \right] + (-1)^l (2l+1) P_l (\cos \beta). \end{aligned}\right\} \quad (37)$$

Hence,

$$(2l+1) \gamma_l = \varpi_l \gamma_l - \sec \beta \left[(l+1) \gamma_{l+1} + l \gamma_{l-1} \right]. \quad (38)$$

It is therefore seen that the γ's satisfy a recursion formula of the same form as the ξ's (cf. eq. [21]). Accordingly, we may write

$$\gamma_l = \gamma_0 \xi_l (\sec \beta), \quad (39)$$

where γ_0 is a constant of proportionality. This can be determined from equation (33) by considering the case $l = 0$. We have

$$\gamma_0 = \gamma_0 \sum_{l=0}^{N} E_{0,\lambda} \varpi_\lambda \xi_\lambda (\sec \beta) + 1, \quad (40)$$

or

$$\gamma_0 = \frac{1}{1 - \sum_{\lambda=0}^{N} E_{0,\lambda}\varpi_\lambda \xi_\lambda (\sec\beta)} . \tag{41}$$

This is related to the characteristic equation (26) in a manner which enables us to write at once that (cf. paper IX, p. 171)

$$\gamma_0 = H^{(0)}(\cos\beta)\, H^{(0)}(-\cos\beta) , \tag{42}$$

where

$$H^{(0)}(\mu) = \frac{1}{\mu_1 \ldots . \mu_n} \frac{\prod_{i=1}^{\tau}{}^{*} (\mu + \mu_i)}{\prod_{a=1}^{n} (1 + k_a\mu)} = \frac{(-1)^n}{\mu_1 \ldots . \mu_n} \frac{P(-\mu)}{R^{(0)}(-\mu)} . \tag{43}$$

Thus equation (8) admits a particular integral of the form

$$I_i^{(0)} = \tfrac{1}{4} F \gamma_0 e^{-\tau \sec\beta} \frac{\sum_{l=0}^{N} \varpi_l \xi_l (\sec\beta) P_l(\mu_i)}{1 + \mu_i \sec\beta} \quad (i = \pm 1, \ldots . , \pm n) . \tag{44}$$

Combining equations (30) and (44), we obtain the general solution of the nonhomogeneous system (8). We have

$$\left.\begin{aligned} I_i^{(0)} = \tfrac{1}{4} F \Bigg\{ & \sum_{a=1}^{n} \frac{M_a e^{-k_a\tau}}{1 + \mu_i k_a} \Big[\sum_{l=0}^{N} \varpi_l \xi_l (+k_a) P_l(\mu_i) \Big] \\ & + \sum_{a=1}^{n} \frac{M_{-a} e^{+k_a\tau}}{1 - \mu_i k_a} \Big[\sum_{l=0}^{N} \varpi_l \xi_l (-k_a) P_l(\mu_i) \Big] \\ & + \frac{\gamma_0 e^{-\tau \sec\beta}}{1 + \mu_i \sec\beta} \Big[\sum_{l=0}^{N} \varpi_l \xi_l (\sec\beta) P_l(\mu_i) \Big] \Bigg\} \quad (i = \pm 1, \ldots . , \pm n) \end{aligned}\right\} \tag{45}$$

where $M_{\pm a}$ $(a = 1, \ldots . , n)$ are the $2n$ constants of integration.

If we are dealing with a plane-parallel atmosphere of optical thickness τ_1, the boundary conditions which determine the constants $M_{\pm a}$ are

$$I_{-i}^{(0)} = 0 \quad \text{at} \quad \tau = 0 \quad \text{and} \quad i = 1, \ldots . , n , \tag{46}$$

and

$$I_i^{(0)} = 0 \quad \text{at} \quad \tau = \tau_1 \quad \text{and} \quad i = 1, \ldots . , n . \tag{47}$$

On the other hand, if we are dealing with diffuse reflection from a semi-infinite atmosphere, the boundedness of the solution for $\tau \to \infty$ requires that $M_{-a} = 0$ $(a = 1, \ldots . , n)$. The solution then has the form

$$\left.\begin{aligned} I_i^{(0)} = \tfrac{1}{4} F \Bigg\{ & \sum_{a=1}^{n} \frac{M_a e^{-k_a\tau}}{1 + \mu_i k_a} \Big[\sum_{l=0}^{N} \varpi_l \xi_l (+k_a) P_l(\mu_i) \Big] \\ & + \frac{\gamma_0 e^{-\tau \sec\beta}}{1 + \mu_i \sec\beta} \Big[\sum_{l=0}^{N} \varpi_l \xi_l (\sec\beta) P_l(\mu_i) \Big] \Bigg\} \quad (i = \pm 1, \ldots . , n) , \end{aligned}\right\} \tag{48}$$

and the constants M_a are now determined by the boundary condition at $\tau = 0$, namely, equations (46). Moreover, in this case, the angular distribution of the emergent radiation is given by

$$\left.\begin{aligned} I^{(0)}(0, \mu) = \tfrac{1}{4}F\Bigg\{ \sum_{a=1}^{n} \frac{M_a}{1+\mu k_a}\Bigg[\sum_{l=0}^{N} \varpi_l \xi_l(k_a) P_l(\mu)\Bigg] \\ + \frac{\gamma_0}{1+\mu \sec\beta}\Bigg[\sum_{l=0}^{N} \varpi_l \xi_l(\sec\beta) P_l(\mu)\Bigg]\Bigg\}. \end{aligned}\right\} \quad (49)$$

This completes our discussion of equation (5).

4. *The solution of equation (6) in the nth approximation.*—Considering, next, equation (6), we have the following system of linear equations to which it is equivalent in the nth approximation:

$$\left.\begin{aligned} \mu_i \frac{dI_i^{(m)}}{d\tau} = I_i^{(m)} - \frac{1}{2}\sum_j \sum_{l=m}^{N} a_j I_j^{(m)} P_l^m(\mu_j)\, \varpi_l \frac{(l-m)!}{(l+m)!} P_l^m(\mu_i) \\ - \tfrac{1}{2}F e^{-\tau\sec\beta} \sum_{l=m}^{N} (-1)^{l+m} \varpi_l \frac{(l-m)!}{(l+m)!} P_l^m(\mu_i) P_l^m(\cos\beta) \\ (i = \pm 1, \ldots, \pm n\ ;\ m = 1, \ldots, N). \end{aligned}\right\} \quad (50)$$

The general solution of this system can be found by a procedure analogous to that which was adopted for the solution of the system (8).

Thus it can be shown that the system of homogeneous equations associated with equation (50) admits integrals of the form

$$I_i = \text{constant} \frac{\sum_{l=m}^{N} \varpi_l \frac{(l-m)!}{(l+m)!} \xi_l^m P_l^m(\mu_i)}{1+\mu_i k} e^{-k\tau} \quad (51)$$

where the ξ_l^m's are constants to be determined in accordance with the equation

$$\xi_l^m = \sum_{\lambda=m}^{N} D_{l,\lambda}^m \xi_\lambda^m \varpi_\lambda \frac{(\lambda-m)!}{(\lambda+m)!} \qquad (l = m, \ldots, N\ ;\ m = 1, \ldots, N), \quad (52)$$

where

$$D_{l,\lambda}^m = \frac{1}{2}\sum_j \frac{a_j P_l^m(\mu_j) P_\lambda^m(\mu_j)}{1+\mu_j k}. \quad (53)$$

Using the recursion formula

$$(2l+1)\, D_{l,\lambda}^m = \frac{(l+m)!}{(l-m)!}\, \delta_{l,\lambda} - k\,[(l-m+1)\, D_{l+1,\lambda}^m + (l+m)\, D_{l-1,\lambda}^m], \quad (54)$$

which the $D_{l,\lambda}^m$'s may be verified to satisfy, it can be readily deduced from equation (52) that

$$(2l+1)\, \xi_l^m = \varpi_l \xi_l^m - k\,[(l-m+1)\, \xi_{l+1}^m + (l+m)\, \xi_{l-1}^m], \quad (55)$$

or

$$\xi_{l+1}^m = -\frac{2l+1-\varpi_l}{k(l-m+1)}\, \xi_l^m - \frac{l+m}{l-m+1}\, \xi_{l-1}^m. \quad (56)$$

Equation (56) determines the ξ_l^m's apart from a constant of proportionality which we shall make determinate with the choice

$$\xi_m^m = 1 \,. \tag{57}$$[4]

Thus, we find from equation (56) that

$$\left.\begin{aligned} &\xi_{m+1}^m = -\frac{2m+1-\varpi_m}{k}\,; \\ &\xi_{m+2}^m = \frac{(2m+1-\varpi_m)\,(2m+3-\varpi_{m+1})}{2k^2} - \frac{2m+1}{2}\,; \\ &\text{etc.} \end{aligned}\right\} \tag{58}$$

The characteristic equation now follows from equation (52) by putting $l = m$. We have

$$1 = \sum_{\lambda=m}^{N} D_{m,\lambda}^m \xi_\lambda^m \varpi_\lambda \frac{(\lambda-m)\,!}{(\lambda+m)\,!}, \tag{59}$$

or, more explicitly,

$$1 = \frac{1}{2}\sum_j \frac{a_j \sum_{\lambda=m}^{N} \xi_\lambda^m \varpi_\lambda \frac{(\lambda-m)\,!}{(\lambda+m)\,!} P_m^m(\mu_j) P_\lambda^m(\mu_j)}{1+\mu_j k}\,. \tag{60}$$

Equation (60) is of order n in k^2 and admits, in general, $2n$ distinct nonvanishing roots, which must occur in pairs, as

$$\pm k_a^m \qquad (a = 1, \ldots, n\,;\ m = 1, \ldots, N)\,. \tag{61}$$

The $2n$ linearly independent solutions of the homogeneous system associated with equation (50) are, therefore,

$$\left.\begin{aligned} &I_i = \text{constant} \frac{\sum_{l=m}^{N} \varpi_l \frac{(l-m)\,!}{(l+m)\,!} \xi_l^m(\pm k_a^m) P_l^m(\mu_i)}{1 \pm \mu_i k_a^m} e^{\mp k_a^m \tau} \\ &(a = 1, \ldots, n\,;\ i = \pm 1, \ldots, \pm n\,;\ m = 1, \ldots, N)\,. \end{aligned}\right\} \tag{62}$$

Similarly, it can be shown that equation (50) admits a particular integral of the form

$$\left.\begin{aligned} &I_i^{(m)} = \tfrac{1}{2} F e^{-\tau \sec\beta} \frac{\sum_{l=m}^{N} \varpi_l \frac{(l-m)\,!}{(l+m)\,!} \gamma_l^m P_l^m(\mu_i)}{1+\mu_i \sec\beta} \\ &(i = \pm 1, \ldots, \pm n\,;\ m = 1, \ldots, N)\,, \end{aligned}\right\} \tag{63}$$

where the constants γ_l^m are to be determined in accordance with the equation

$$\gamma_l^m = \sum_{\lambda=m}^{N} E_{l,\lambda}^m \gamma_\lambda^m \varpi_\lambda \frac{(\lambda-m)\,!}{(\lambda+m)\,!} + (-1)^{l+m} P_l^m(\cos\beta)\,, \tag{64}$$

[4] It may be noted that, in applying equation (56) for the case $l = m$, we must put $\xi_{m-1}^m = 0$, as the ξ's are not defined for $l < m$.

where

$$E^m_{l,\lambda} = \frac{1}{2}\sum_j \frac{a_j P^m_l(\mu_j) P^m_\lambda(\mu_j)}{1+\mu_j \sec\beta}. \tag{65}$$

The $E^m_{l,\lambda}$'s defined in this manner satisfy the recursion formula

$$(2l+1)E^m_{l,\lambda} = \frac{(l+m)!}{(l-m)!}\delta_{l,\lambda} - \sec\beta\,[(l-m+1)E^m_{l+1,\lambda} + (l+m)E^m_{l-1,\lambda}], \tag{66}$$

with which we can deduce from equation (64) that the γ^m_l's satisfy the relation

$$(2l+1)\gamma^m_l = \varpi_l\gamma^m_l - \sec\beta\,[(l-m+1)\gamma^m_{l+1} + (l+m)\gamma^m_{l-1}]. \tag{67}$$

This is of exactly the same form as the recursion formula satisfied by the ξ^m_l's. Hence, we may write

$$\gamma^m_l = \gamma^m_m \xi^m_l(\sec\beta) \qquad (l = m, \ldots N), \tag{68}$$

where the constant of proportionality γ^m_m can be found from equation (64) by considering the case $l = m$. We find

$$\gamma^m_m = \frac{P^m_m(\cos\beta)}{1 - \sum_{\lambda=m}^{N} E^m_{m,\lambda}\xi^m_\lambda(\sec\beta)\varpi_\lambda \dfrac{(\lambda-m)!}{(\lambda+m)!}}. \tag{69}$$

The relation of this equation to the characteristic equation (59) is such that we can write

$$\gamma^m_m = \gamma^m_0 P^m_m(\cos\beta), \tag{70}$$

where

$$\gamma^m_0 = H^{(m)}(\cos\beta)\,H^{(m)}(-\cos\beta), \tag{71}$$

and

$$H^{(m)}(\mu) = \frac{1}{\mu_1 \ldots \mu_n}\frac{\prod_{l=1}^{n}(\mu+\mu_i)}{\prod_{a=1}^{n}(1+k^m_a\mu)} = \frac{(-1)^n}{\mu_1 \ldots \mu_n}\frac{P(-\mu)}{R^{(m)}(-\mu)}. \tag{72}$$

The particular integral (63) can therefore be written in the form

$$I^{(m)}_i = \tfrac{1}{2}F e^{-\tau\sec\beta}\gamma^m_0 P^m_m(\cos\beta)\frac{\sum_{l=m}^{N}\varpi_l\dfrac{(l-m)!}{(l+m)!}\xi^m_l(\sec\beta)P^m_l(\mu_i)}{1+\mu_i\sec\beta} \tag{73}$$
$$(i = \pm 1, \ldots, \pm n;\ m = 1, \ldots, N).$$

Finally, combining equations (62) and (63), we can write the general solution of equation (50) in the form

$$I_i^{(m)} = \tfrac{1}{2}FP_m^m(\cos\beta)\left\{\sum_{\alpha=1}^{n}\frac{M_\alpha^m e^{-k_\alpha^m\tau}}{1+\mu_i k_\alpha^m}\left[\sum_{l=m}^{N}\varpi_l\frac{(l-m)!}{(l+m)!}\xi_l^m(+k_\alpha^m)P_l^m(\mu_i)\right]\right.$$
$$+\sum_{\alpha=1}^{n}\frac{M_{-\alpha}^m e^{+k_\alpha^m\tau}}{1-\mu_i k_\alpha^m}\left[\sum_{l=m}^{N}\varpi_l\frac{(l-m)!}{(l+m)!}\xi_l^m(-k_\alpha^m)P_l^m(\mu_i)\right]$$
$$\left.+\frac{\gamma_0^m e^{-\tau\sec\beta}}{1+\mu_i\sec\beta}\left[\sum_{l=m}^{N}\varpi_l\frac{(l-m)!}{(l+m)!}\xi_l^m(\sec\beta)P_l^m(\mu_i)\right]\right\} \tag{74}$$
$$(i=\pm1,\ldots,\pm n\ ;\ m=1,\ldots,N).$$

The boundary conditions which determine the constants of integration $M_{\pm\alpha}^m$ ($\alpha = 1, \ldots, n$) are the same as for $I_i^{(0)}$ (cf. eqs. [46] and [47]). In particular, for the case of a semi-infinite atmosphere, the solution is

$$I_i^{(m)} = \tfrac{1}{2}FP_m^m(\cos\beta)\left\{\sum_{\alpha=1}^{n}\frac{M_\alpha^m e^{-k_\alpha^m\tau}}{1+\mu_i k_\alpha^m}\left[\sum_{l=m}^{N}\varpi_l\frac{(l-m)!}{(l+m)!}\xi_l^m(+k_\alpha^m)P_l^m(\mu_i)\right]\right.$$
$$\left.+\frac{\gamma_0^m e^{-\tau\sec\beta}}{1+\mu_i\sec\beta}\left[\sum_{l=m}^{N}\varpi_l\frac{(l-m)!}{(l+m)!}\xi_l^m(\sec\beta)P_l^m(\mu_i)\right]\right\} \tag{75}$$
$$(i=\pm1,\ldots,\pm n\ ;\ m=1,\ldots,N),$$

where the constants M_α^m ($\alpha = 1, \ldots, n$) are to be found from the conditions

$$I_{-i}^{(m)} = 0 \quad \text{at} \quad \tau = 0 \quad \text{and for} \quad i = 1, \ldots, n\,. \tag{76}$$

With this we have completed the formal solution of the equation of transfer. It is seen how solutions to any desired accuracy can always be found.

5. *Diffuse reflection in accordance with the phase function* $1 + \varpi_1 P_1(\cos\Theta) + \varpi_2 P_2(\cos\Theta)$.—As an illustration of the general theory developed in the preceding sections we shall consider the case of diffuse reflection by a semi-infinite plane-parallel atmosphere scattering radiation in accordance with the phase function

$$p(\cos\Theta) = 1 + \varpi_1 P_1(\cos\Theta) + \varpi_2 P_2(\cos\Theta)\,. \tag{77}$$

For this phase function the solution has the form

$$I(\tau,\mu) = I^{(0)}(\tau,\mu) + I^{(1)}(\tau,\mu)\cos\varphi + I^{(2)}(\tau,\mu)\cos 2\varphi\,. \tag{78}$$

Considering, first, the solution for $I^{(0)}(\tau, \mu)$, we have (cf. eq. [24])

$$\xi_0 = 1\ ; \qquad \xi_1 = 0\ ; \qquad \text{and} \qquad \xi_2 = -\tfrac{1}{2}\,. \tag{79}$$

The corresponding characteristic equation is

$$1 = \frac{1}{2}\sum_j \frac{a_j[1-\tfrac{1}{2}\varpi_2 P_2(\mu_j)]}{1+\mu_j k}, \tag{80}$$

or, somewhat differently,

$$1 = \tfrac{3}{4}\varpi_2\sum_{j=1}^{n}\left(\frac{4+\varpi_2}{3\varpi_2} - \mu_j^2\right)\frac{a_j}{1-\mu_j^2 k^2}\,. \tag{81}$$

Equation (81) admits of only $(2n-2)$ distinct nonvanishing roots for k^2. We must accordingly make use of the integral (29) in writing the general solution for $I_i^{(0)}$.

The solution for $I_i^{(0)}$ has the form

$$I_i^{(0)} = \frac{3\varpi_2}{16} F\left[\left(\frac{4+\varpi_2}{3\varpi_2} - \mu_i^2\right)\sum_{\alpha=1}^{n-1} \frac{M_\alpha e^{-k_\alpha \tau}}{1+\mu_i k_\alpha} + X + \left(\frac{4+\varpi_2}{3\varpi_2} - \mu_i^2\right)\frac{\gamma_0 e^{-\tau \sec\beta}}{1+\mu_i \sec\beta}\right] \quad (i = \pm 1, \ldots, \pm n). \tag{82}$$

The angular distribution of the emergent radiation $I^{(0)}(0, \mu)$ and the boundary conditions which determine the constants of integration M_α $(\alpha = 1, \ldots, n-1)$ and X can both be expressed in terms of the function

$$G(\mu) = \left(\frac{4+\varpi_2}{3\varpi_2} - \mu^2\right)\sum_{\alpha=1}^{n-1} \frac{M_\alpha}{1-\mu k_\alpha} + X + \left(\frac{4+\varpi_2}{3\varpi_2} - \mu_i^2\right)\frac{\gamma_0}{1-\mu \sec\beta}. \tag{83}$$

Thus

$$I^{(0)}(0,\mu) = \frac{3\varpi_2}{16} FG(-\mu), \tag{84}$$

and

$$G(\mu_i) = 0 \qquad (i = 1, \ldots, n). \tag{85}$$

Comparing the foregoing solutions with those considered in paper IX, § 8 (see particularly eqs. [169]–[173]), it is apparent that in this case we can obtain a closed expression for $G(\mu)$ which does not explicitly involve the constants of integration. By an analysis similar to that in paper IX, § 8, we find that (cf. paper IX, eqs. [184], [188], and [189])

$$I^{(0)}(0,\mu) = \frac{3\varpi_2}{16} FH^{(0)}(\mu) H^{(0)}(\cos\beta) \frac{\cos\beta}{\cos\beta+\mu} \left\{\xi\left(\sqrt{\frac{4+\varpi_2}{3\varpi_2}} + \cos\beta\right)\right. \times\left(\sqrt{\frac{4+\varpi_2}{3\varpi_2}} + \mu\right) + (1-\xi)\left(\sqrt{\frac{4+\varpi_2}{3\varpi_2}} - \cos\beta\right)\left.\left(\sqrt{\frac{4+\varpi_2}{3\varpi_2}} - \mu\right)\right\}, \tag{86}$$

where

$$\xi = \frac{P\left(+\sqrt{\frac{4+\varpi_2}{3\varpi_2}}\right) R\left(-\sqrt{\frac{4+\varpi_2}{3\varpi_2}}\right)}{P\left(+\sqrt{\frac{4+\varpi_2}{3\varpi_2}}\right) R\left(-\sqrt{\frac{4+\varpi_2}{3\varpi_2}}\right) - P\left(-\sqrt{\frac{4+\varpi_2}{3\varpi_2}}\right) R\left(+\sqrt{\frac{4+\varpi_2}{3\varpi_2}}\right)}. \tag{87}$$

Considering, next, the solution for $I^{(1)}(\tau, \mu)$, we have

$$\xi_1^1 = 1 \qquad \text{and} \qquad \xi_2^1 = -\frac{3-\varpi_1}{k}. \tag{88}$$

The characteristic equation (60) now becomes

$$1 = \frac{1}{2}\sum_{j=1}^{n} \frac{a_j(1-\mu_j^2)}{1-\mu_j^2 k^2}\left[\varpi_1 + \varpi_2(3-\varpi_1)\mu_j^2\right]. \tag{89}$$

The corresponding solution for $I_i^{(1)}$ is

$$I_i^{(1)} = \frac{\varpi_1}{4} F(1-\mu_i^2)^{1/2} \sin\beta \left\{\sum_{\alpha=1}^{n} \frac{M_\alpha^1 e^{-k_\alpha^1 \tau}}{1+\mu_i k_\alpha^1}\left[1 - \frac{\varpi_2(3-\varpi_1)}{\varpi_1}\frac{\mu_i}{k_\alpha^1}\right]\right. + \left.\frac{\gamma_0 e^{-\tau\sec\beta}}{1+\mu_i\sec\beta}\left[1 - \frac{\varpi_2(3-\varpi_1)}{\varpi_1}\mu_i\cos\beta\right]\right\} \quad (i = \pm 1, \ldots, \pm n). \tag{90}$$

From the similarity of this solution with equation (54) in paper IX, we conclude that, in this case also, closed expressions for $I^{(1)}(0, \mu)$ can be found which do not require an explicit solution for the constants of integration. We have (cf. paper IX, eq. [108])

$$\left.\begin{aligned} I^{(1)}(0, \mu) = \frac{\varpi_1}{4} F (1-\mu^2)^{1/2} \sin\beta\, H^{(1)}(\mu)\, H^{(1)}(\cos\beta) \frac{\cos\beta}{\cos\beta+\mu} \\ \times\left[1 - \frac{\varpi_2(3-\varpi_1)}{\varpi_1}\left\{\frac{\sigma}{\rho}(\cos\beta+\mu) + \mu\cos\beta\right\}\right], \end{aligned}\right\} \quad (91)$$

where σ and ρ are defined as in paper IX, equations (90) and (91), with $\varpi_2(3-\varpi_1)/\varpi_1$ replacing $x(1-\lambda)$.

Finally, considering the solution for $I^{(2)}(\tau, \mu)$, it is seen that the characteristic equation is (cf. paper IX, eq. [193])

$$1 = \tfrac{3}{8}\varpi_2 \sum_{j=1}^{n} \frac{a_j (1-\mu_j^2)^2}{1-\mu_j^2 k^2} \quad (92)$$

and, further, that the equation that has to be solved belongs to the class considered in paper IX, § 4.[5] We can accordingly write (cf. paper IX, eq. [191])

$$I^{(2)}(0, \mu) = \frac{3\varpi_2}{16} F \sin^2\beta \sin^2\vartheta\, H^{(2)}(\mu)\, H^{(2)}(\cos\beta) \frac{\cos\beta}{\cos\beta+\mu}. \quad (93)$$

It is therefore seen that in this case, as in the cases considered in paper IX, expressions for the angular distribution of the emergent radiation can be found which do not require an explicit solution of the constants of integration. Whether this is generally possible is not so easily answered, though it is a simple matter to write down a variety of special phase functions for which this can, in fact, be accomplished. We hope to return to these and related questions in the near future.

And, finally, there is the question of the relationship between our method (particularly in those cases in which we are able to eliminate the constants of integration) and Ambarzumian's,[6] in which integral equations are derived for the functions describing the angular distribution of the emergent radiation. An examination of this relationship leads to interesting developments in the solution of a large class of functional equations by a systematic method of approximation. But to go into these matters here will take us too far from the main objective of this paper.

[5] Indeed, this is generally true of the case $m = N$.

[6] *J. Phys. Acad. Sci. U.S.S.R.*, **8**, 64, 1944.

ON THE HELIUM CONTENT OF THE SUN

MARTIN SCHWARZSCHILD
Rutherfurd Observatory, Columbia University
Received May 27, 1946

ABSTRACT

Under the assumption that the sun consists of hydrogen, helium, and Russell mixture, it is shown that the sun contains approximately 40 per cent of helium.

1. *Introduction.*—For a star with a given mass and composition, there exists generally only one equilibrium configuration. In this configuration all physical quantities (as, for example, the luminosity and the radius) are completely determined. Therefore, if, for a star, the mass M, the luminosity L, and the radius R are found from observations, two parameters of the composition (as, for example, the hydrogen content X and the helium content Y) can be determined under the condition that the rest of the composition and all physical laws determining the equilibrium configuration are known.

Until recently, the law of energy generation was not known, and therefore, not two, but only one, composition parameter could be determined from M, L, and R. Thus, by using the mass-luminosity equation, the only relation between M, L, and R not involving the rate of energy generation—the hydrogen content X—was determined under suitable assumptions about the helium content Y.[1]

Now, however, the law of energy generation is known for main-sequence stars like the sun,[2] and hence X and Y can both be determined on the assumption that the rest of the composition consists of Russell mixture. Two equations are necessary, each involving M, L, and R, which are known from observations, and X and Y, which are to be found. The mass-luminosity equation may be used as the first of these equations. A second equation can be derived by setting the luminosity equal to the total energy production by the carbon cycle throughout the star.

Both the mass-luminosity equation and the energy-output equation contain numerical coefficients which have to be evaluated by integrating the appropriate differential equations of the stellar interior before these equations can be used for the determination of X and Y[3].

2. *Internal structure.*—The differential equations for the stellar interior have been ntegrated under the following approximations:

a) The composition (and consequently the molecular weight, μ) is constant throughout the star.
b) The radiation pressure is negligible.
c) The star consists of a convective core with $\gamma = \frac{5}{3}$, and an envelope in radiative equilibrium with an absorption coefficient given by $\kappa = \kappa_0 \rho^{0.75} T^{-3.5}$, where the exponents

[1] Eddington, *M.N.*, **92**, 364, and 471, 1932; B. Strömgren, *Zs. f. Ap.*, **4**, 118, 1932, **7**, 222, 1933; *Ap. J.*, **87**, 520, 1938.

[2] Bethe, *Phys. Rev.*, **55**, 434, 1939; *Ap. J.*, **92**, 118, 1940.

[3] Of the available integrations, those of Cowling (*M.N.*, **96**, 42, appendix, 1935) do not take account of the variation of the guillotine factor and hence do not give an accurate formula for the central temperature. The integrations of Blanch, Lowan, Marshak, and Bethe (*Ap. J.*, **94**, 37, 1941) were made for $Y = 0$, and therefore are not sufficiently general for the present purpose. The integrations of Henrich (*Ap. J.*, **96**, 106, 1942) are sufficiently general for the present investigation and do take account of the variation of the guillotine factor. However, because of the special form in which the latter was accomplished, Henrich's integrations were found inadequate for another investigation (on the rotation of the sun). Therefore, new integrations were performed, as described in Section 2, and subsequently used not only for the rotation problem but also for the investigation reported here.

were chosen so as to fit the absorption values given by Morse[4] as closely as possible for the temperatures and densities occurring in the sun.

d) The entire energy generation from nuclear sources occurs within the convective core.

To simplify the integrations, the dimensionless variables, p, t, q, and x, were used, which are defined by

$$P = p\,\frac{GM^2}{4\pi R^4}, \qquad T = t\,\frac{\mu H}{k}\,\frac{GM}{R}, \qquad M(r) = qM. \qquad r = xR. \tag{1}$$

With these variables, the three basic differential equations are

$$\frac{dp}{dx} = -\frac{p}{t}\,\frac{q}{x^2}, \qquad \frac{dt}{dx} = -\frac{C}{x^2}\,\frac{p^{1.75}}{t^{8.25}}, \qquad \frac{dq}{dx} = +\frac{p}{t}\,x^2, \tag{2}$$

where the eigen-value parameter C is defined by

$$C = \frac{3\kappa_0}{4ac}\left(\frac{k}{\mu HG}\right)^{7.5}\left(\frac{1}{4\pi}\right)^{2.75}\frac{LR^{1.25}}{M^{5.75}}. \tag{3}$$

The integration of the above equations was started off by using an analytical development from the surface to a point, $\log(1/x - 1) = -0.80$. From there the integration was carried inward by numerical methods. For the numerical integration the following logarithmic variables were used: $\log p$, $\log t$, $\log q$, and $\log(1/x - 1)$. Since the eigen-value C is not known beforehand but has to be determined by fitting the radiative envelope to the convective core (represented by the polytrope of index 1.5), six separate integrations were performed. In each integration a value of C was chosen as close to the true eigen-value as could be estimated from the previous integrations. The last three integrations were computed with six-place logarithms. In the final integration it was found that all variables could be fitted to the convective core with an accuracy of better than one in the fifth place. Hence the value for C used in this integration is the true eigen-value,

$$\log C = -5.51674. \tag{4}$$

The corresponding final solution is given in Table 1. The errors of all logarithmic quantities in this table are estimated never to exceed one unit in the fifth place.

The values of all variables at the interface between the convective core and the radiative envelope are listed below:

$$\left.\begin{aligned} &\log\left(\frac{1}{x_f} - 1\right) = +0.85825, \qquad x_f = 0.121725 = \frac{\text{radius of core}}{\text{R}};\\ &\log p_f = +2.19453, \qquad \log t_f = -0.04260, \qquad \log q_f = -0.92689;\\ &\xi_f = 1.12009, \qquad \theta_f = 0.80928\ (\xi \text{ and } \theta \text{ variables of the polytrope } 1.5). \end{aligned}\right\} \tag{5}$$

With the help of these quantities, the following formulae for the central temperature and central density can be derived:

$$T_c = \frac{t_f}{\theta_f}\,\frac{\mu H}{k}\,\frac{GM}{R}; \qquad \rho_c = \frac{p_f}{4\pi\theta_f^{1.5}t_f}\,\frac{M}{R^3} = 79.04\,\bar{\rho}; \tag{6}$$

or, with M and R in solar units,

$$T_c = 25.89\times 10^6\times\mu\,\frac{M}{R}; \qquad \rho_c = 111.6\,\frac{M}{R^3}. \tag{6'}$$

[4] *Ap. J.*, **92**, 27, 1940.

3. *Mass-luminosity equations.*—If the eigen-value C found by the integration is introduced into equation (3), the mass-luminosity equation is obtained. To use this equation for the determination of X and Y, it is necessary to express the molecular weight, μ, and the absorption coefficient, κ_0, as functions of the composition. The expression for μ is

$$\frac{1}{\mu} = 2X + \tfrac{3}{4}Y + \tfrac{1}{2}(1 - X - Y), \tag{7}$$

TABLE 1

$\log\left(\frac{1}{x}-1\right)$	$\log q$	$.05\frac{d\log q}{d\log\left(\frac{1}{x}-1\right)}$	$\log t$	$.05\frac{d\log t}{d\log\left(\frac{1}{x}-1\right)}$	$\log p$	$.05\frac{d\log p}{d\log\left(\frac{1}{x}-1\right)}$	$\frac{d\log p}{d\log t}-1$
−1.00	−0.00000	−0.00000	−1.67342	+0.05000	−5.12135	+0.23571	3.714
−0.95	0.00000	.00000	1.62342	.05000	−4.88564	.23571	3.714
−0.90	0.00001	.00000	1.57342	.05000	−4.64992	.23571	3.714
−0.85	0.00001	.00000	1.52342	.05000	−4.41421	.23571	3.714
−0.80	0.00002	.00001	1.47342	.05000	−4.17851	.23571	3.714
−0.75	0.00003	.00001	1.42342	.05000	−3.94280	.23570	3.714
−0.70	0.00005	.00002	1.37342	.05000	−3.70711	.23569	3.714
−0.65	0.00008	.00004	1.32343	.05000	−3.47142	.23568	3.714
−0.60	0.00012	.00006	1.27343	.04999	−3.23575	.23566	3.714
−0.55	0.00019	.00009	1.22344	.04999	−3.00011	.23562	3.713
−0.50	0.00030	.00014	1.17346	.04998	−2.76451	.23557	3.713
−0.45	0.00047	.00021	1.12348	.04997	−2.52897	.23550	3.713
−0.40	0.00072	.00031	1.07352	.04996	−2.29353	.23537	3.711
−0.35	0.00111	.00047	1.02357	.04993	−2.05824	.23520	3.710
−0.30	0.00169	.00070	0.97366	.04989	−1.82317	.23493	3.709
−0.25	0.00255	.00103	0.92379	.04984	−1.58842	.23454	3.706
−0.20	0.00379	.00149	0.87399	.04976	−1.35415	.23397	3.702
−0.15	0.00558	.00213	0.82428	.04965	−1.12055	.23317	3.696
−0.10	0.00813	.00301	0.77471	.04948	−0.88792	.23203	3.689
−0.05	0.01170	.00419	0.72534	.04926	−0.65663	.23046	3.678
0.00	0.01664	.00576	0.67622	.04895	−0.42718	.22832	3.664
+0.05	0.02338	.00781	0.62748	.04853	−0.20023	.22546	3.646
+0.10	0.03245	.01043	0.57921	.04797	+0.02343	.22168	3.621
+0.15	0.04448	.01374	0.53159	.04724	+0.24277	.21681	3.590
+0.20	0.06019	.01782	0.48480	.04631	+0.45662	.21066	3.549
+0.25	0.08040	.02275	0.43904	.04516	+0.66361	.20306	3.496
+0.30	0.10598	.02858	0.39457	.04374	+0.86222	.19389	3.433
+0.35	0.13785	.03530	0.35165	.04207	+1.05086	.18313	3.353
+0.40	0.17687	.04287	0.31052	.04014	+1.22798	.17085	3.256
+0.45	0.22383	.05115	0.27145	.03797	+1.39212	.15725	3.141
+0.50	0.27935	.05995	0.23465	.03561	+1.54214	.14265	3.006
+0.55	0.34382	.06902	0.20028	.03312	+1.67724	.12748	2.849
+0.60	0.41739	.07809	0.16844	.03056	+1.79706	.11221	2.672
+0.65	0.49990	.08687	0.13915	.02802	+1.90178	.09732	2.473
+0.70	0.59094	.09511	0.11237	.02556	+1.99199	.08325	2.257
+0.75	0.68987	.10260	0.08798	.02324	+2.06867	.07032	2.026
+0.80	0.79585	.10918	0.06583	.02109	+2.13308	.05874	1.785
+0.85	0.90790	.11474	0.04574	.01914	+2.18664	.04862	1.540
+0.90	1.02496	.11919	0.02749	.01739	+2.23080	.03995	1.297
+0.95	−1.14588	−0.12246	−0.01088	+0.01585	+2.26700	+0.03266	1.060

and the guillotine factor is found from the tables given by Morse,[4]

$$\log\left(\frac{t}{\bar{g}}\right) = +0.6 + \log p^{0.25}. \tag{8}$$

This formula represents the logarithm of the guillotine factor with an accuracy of ±.25 for the temperatures and densities occurring in the sun. Introducing the above expression for the guillotine factor into the equation for the absorption coefficient, one gets

$$\kappa = \kappa_0 \rho^{0.75} T^{-3.5} = 10^{25}(1+X)(1-X-Y). \tag{9}$$

It is estimated that the value of κ_0 is not uncertain by more than a factor 1.5, if the Russell mixture gives a fair representation of the relative abundances of the heavier elements in the sun.

By introducing these values of κ_0 and μ into equation (3) and by expressing L, M, and R in solar units, the following mass-luminosity equation is found:

$$(2X+\tfrac{3}{4}Y+\tfrac{1}{2}[1-X-Y])^{7.5}(1+X)(1-X-Y)=1.34\,\frac{M^{5.75}}{LR^{1.25}}. \quad (10)$$

By applying this equation to the sun ($L = M = R = 1$), a relation between X and Y is obtained which is shown in Figure 1. To indicate the uncertainty in this relation, two further curves are given in the same figure, representing the mass-luminosity relation for values of κ_0 two-thirds and one and one-half times the adopted value.

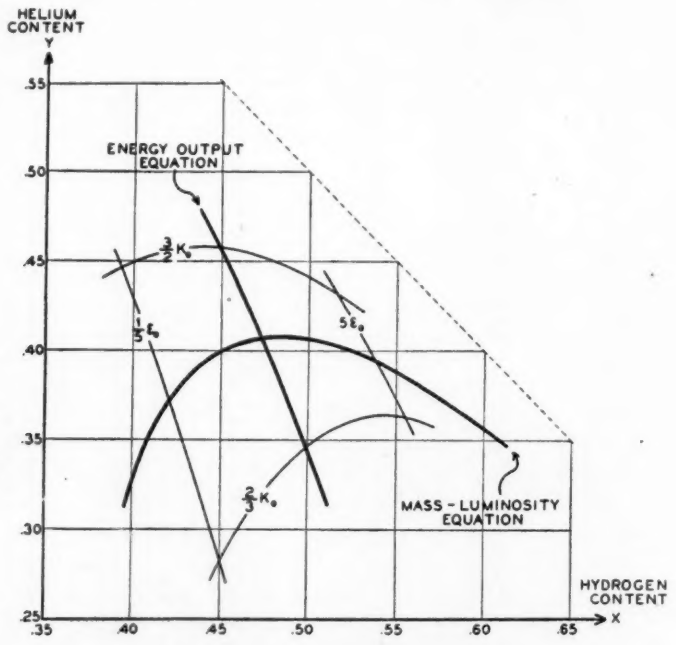

Fig. 1.—Helium-hydrogen diagram for sun

4. *Energy-output equation.*—The second equation necessary for the determination of X and Y is derived by integrating the energy production over the entire core. The rate of energy generation[2] by the carbon cycle is given by

$$\epsilon=\frac{Eh_{12}}{m_{12}t_{12}}(1-X-Y)\frac{X}{0.35}\frac{\rho}{80}\left(\frac{T}{2\times10^7}\right)^{17}=\epsilon_0\rho T^{17}, \quad (11)$$

where

$$\left.\begin{aligned} E &= 4\times10^{-5}\text{ ergs} = \text{total energy released per cycle};\\ m_{12} &= 2\times10^{-23}\text{ gm} = \text{mass of one } C^{12}\text{ nucleus};\\ t_{12} &= 2.5\times10^{6}\text{ years} = \text{average lifetime of one } C^{12}\text{ nucleus if}\\ &\qquad \rho=80,\quad T=2\times10^{7}\,K,\quad \text{and } X=0.35;\\ h_{12} &= 0.02 = \text{carbon content of Russell mixture.}\end{aligned}\right\} \quad (11')$$

The integration over the core gives

$$L = \int_0^{r_f} \epsilon_0 \rho^2 T^{17} 4\pi r^2 dr .$$

This can be transformed into

$$\frac{L}{M} = \epsilon_0 \rho_c T_c^{17} \frac{p_f}{\theta_f^{1.5} t_f} \left(\frac{x_f}{\xi_f}\right)^3 \int_0^{\xi_f} \theta^{20} \xi^2 d\xi = \frac{\epsilon_0 \rho_c T_c^{17}}{47} . \tag{12}$$

The last equation shows directly the relation between the energy production per gram at the center and the average energy production per gram for the entire star. The denominator in this equation depends solely on the temperature exponent in the energy-generation law. This dependence is shown in the accompanying table.

Temperature exponent	15	17	19
Denominator	41	47	54

By introducing ϵ_0 from equation (11) and ρ_c and T_c from equation (6) and by using solar units for L, M, and R, the energy-output equation is found in the following form:

$$\frac{(2X + \frac{3}{4}Y + \frac{1}{2}[1 - X - Y])^{17}}{(1 - X - Y)X} = 1800 \frac{M^{19}}{LR^{20}} . \tag{13}$$

By applying this equation to the sun ($L = M = R = 1$), a second relation between X and Y is obtained, which is shown in Figure 1. To indicate the uncertainty in this relation (caused by the uncertainty of the nuclear cross-sections corresponding to the carbon cycle, the carbon content of the Russell mixture, and the numerical coefficient in equation [6] for T_c), two further curves are shown in the same figure, which represent the energy-output equation for values of ϵ_0, five and one-fifth times the adopted value.

5. *Conclusions.*—From Figure 1, it is seen that, for the sun, the mass-luminosity equation and the energy-output equation are satisfied simultaneously by

$$X = 0.47 , \qquad Y = 0.41 , \qquad 1 - X - Y = 0.12 .$$

These values[5] give, according to equations (6) and (7),

$$\mu = 0.76 , \qquad T_c = 19.8 \times 10^{6\circ} \text{ K} .$$

It also can be seen from Figure 1 that, in spite of the uncertainty in κ_0 and particularly in ϵ_0, it appears certain that the hydrogen content lies between 35 and 60 per cent, the helium content between 25 and 50 per cent, and the content of Russell mixture does not exceed 30 per cent. These conclusions are based on the assumption that the Russell mixture gives a fair representation of the relative abundances of the heavier elements in the sun, so that the use of Morse's table for the guillotine factor is justified.

The above results show that the introduction of an appreciable helium content removes the discrepancy, found earlier,[6] between the observed luminosity and the rate of energy generation by the carbon cycle.

[5] This set of values is in fair agreement with one of the sets given by Henrich, *Ap. J.*, **83**, 192, Table 2, 1943.

[6] *Ap. J.*, **94**, 37, 1941.

ULTRAVIOLET ABSORPTION SPECTRUM OF AIR IN THE REGION λλ 600–2000

J. J. HOPFIELD
Applied Physics Laboratory, Johns Hopkins University
Received July 2, 1946

ABSTRACT

A series of absorption spectra of air contained in a vacuum-grating spectrograph was taken. A range of air pressures was used. A hot spark in a Pyrex glass capillary served for the continuous light-source. Spectra selected from this series are assembled into a spectrogram which gives a fairly complete picture of light-absorption by air in the region λλ 600–2000.

Judging from these results, one can hope to find transparent windows to the light of the sun and stars in the extreme ultraviolet from new altitudes made available to physicists using modern rockets to transport equipment. Thus, one can infer that the atmosphere at high altitudes is more transparent in the region λλ 1000–1300 than in the region λλ 1300–1700 and that another region of transparency begins at λ 1700 and extends to the visible region. Lyman-α, the resonance line of atomic hydrogen, lies in a favorable place for observation through one of the more transparent windows.

With the advent of large rockets, such as the German V-2, weighing 15 tons and capable of reaching altitudes of 100 miles or more, one is stimulated to explore the spectrum of the sun and stars in the extreme ultraviolet, infrared, and X-ray region, using spectrographs carried aloft by these rockets. By such explorations, such questions as the following might be answered: (*a*) Does the light from the chromosphere of the sun follow the blackbody radiation law for a body having a temperature of 6000° K? (*b*) Does the spectrum of the sun's corona outshine the continuum to give a bright-line spectrum in the extreme ultraviolet? (*c*) What is the state of matter in the sun's corona to give such lines? (*d*) Can one observe and measure the X-ray spectrum of the sun, which has never been observed at the earth's surface on account of an ocean of air (equivalent to a depth of 8,570 meters at a pressure of 1 atm.) that surrounds it?

To answer these questions, one should know how transparent the atmosphere at various altitudes is to the various radiations emitted by the sun. Since the atmosphere is made up mostly of ordinary air, the absorption spectra of air would help to answer these questions. The ultraviolet absorption spectrum of air has been known for many years. It has been mentioned by several observers, including the present author, but at no time, to my knowledge, has it been fully published. To the end that the absorption spectrum of air as obtained in the laboratory may serve as a guide to the ultraviolet spectrum of the sun from high altitudes, it is published in the present form.

The absorption spectrum of air in the region λλ 600–2000 was obtained with a vacuum-grating spectrograph at the University of California about twenty years ago. The spectrograph had a concave reflection grating of 50-cm radius, and this was ruled with about 30,000 lines per inch. The dispersion in the first order was about 15 A/mm. The distance from the slit to the grating was 50 cm, and from the grating to the photographic plate 50 cm also. Thus the chamber of the spectrograph served as a 100-cm *absorption cell* for holding air, and one could photograph its absorption spectrum. By varying the pressure in the chamber from 1 atm. to low values, one could vary the equivalent air thickness for absorption at one atmosphere from 100 cm to a value as small as 0.0019 cm; and these values, as will be shown later, are comparable to the absorption of the air for sunlight at altitudes of 72 km and more than 120 km, respectively.

The source of the continuum which forms the background for recording absorption spectra was a condensed spark discharge in a capillary glass tube, with its open end immediately in front of the slit and with the axis of the capillary aimed at the center of the

PLATE III

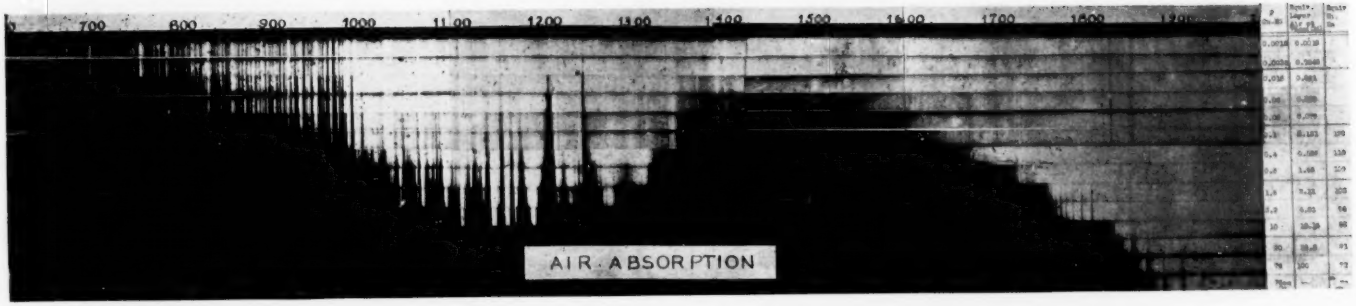
700
800
900
1000
1100
1200
1300
1400
1500
1600
1700
1800
AIR ABSORPTION

grating. About 15 sparks were enough for a fully exposed spectrum. Schumann film was used for the pictures. The discharge tube opened into the spectrograph through the slit, but discharge tube and spectrograph were evacuated by a separate pump to the pressures desired.

The absorption spectrum of air shown in Plate III was assembled from spectra taken with different pressures of air in the spectrograph. The region covered by these spectra is λλ 600–2000.

The spectra of the plate are numbered in the first column of Table 1. The pressure of the air in the spectrograph is given in the second column. Using the pressures in the second column over the path of absorption, which is 100 cm (as already mentioned), one can deduce the equivalent thickness of air at 760 mm that would give about the same light-absorption. This equivalent air thickness is given in the third column, and it is obviously $(P/76) \times 100$ cm, where P is the air pressure in the spectrograph in centimeters of mercury and the length of "absorption cell" is 100 cm. Finally, the fourth column gives the approximate altitude above which this equivalent air thickness (third column) may be found,[1,2] Kurrelmeyer's table gives the pressure and temperature of the

TABLE 1

Spectrum Number	P, in Spectrograph (Centimeters of Mercury)	Equivalent Air Thickness in Centimeters, at 1 Atm.	Equivalent Height above Earth (in Kilometers)	Spectrum Number	P, in Spectrograph (Centimeters of Mercury)	Equivalent Air Thickness in Centimeters, at 1 Atm.	Equivalent Height above Earth (in Kilometers)
1.....	0.0015	0.0019	.....	8.....	0.8	1.05	109
2.....	0.0035	0.0046	.....	9.....	1.6	2.11	103
3.....	0.016	0.021	.....	10.....	3.2	4.21	96
4.....	0.03	0.039	.....	11.....	10.0	13.16	86
5.....	0.06	0.079	.....	12.....	20.0	26.3	81
6.....	0.1	0.131	128	13.....	76.0	100.0	72
7.....	0.4	0.526	115	14.....	76 cm O_2	.....	.....

atmosphere at a given altitude in the range of altitude from 20 to 120 km. The manner of relating the equivalent air thickness in the spectrograph (third column) to the equivalent air thickness above a point whose altitude is h is given by

$$y = \frac{13.59\, P_h}{0.001205}, \tag{1}$$

where

y = Equivalent air thickness in cm at 76.0 cm of mercury and 20° C;

P_h = Pressure of air altitude h in cm of mercury;

13.59 = Density of mercury, grams per cubic centimeter;

0.001205 = Density of air, grams per cubic centimeter.

If one substitutes $P_h = 76$ in equation (1), one obtains $y = 8.57 \times 10^5$ cm, or 8,750 meters, the equivalent depth of the ocean of air that covers the earth to absorb the ultraviolet light of the sun. That the absorption of the air in the spectrograph for ultraviolet

[1] F. L. Whipple, *Rev. Mod. Phys.*, **15**, 246, October, 1943.

[2] The data of the fourth column are based on a table calculated by B. Kurrelmeyer from the data of Whipple.

light is small in comparison with the absorption of the total sea of air is evident not only in the ratio of 1 meter (spectrograph) to 8,570 meters air thickness given above but also by the point of cutoff of the spectrum's being at λ 1850 in the spectrograph instead of λ 3000, the limit of the sun's spectrum at sea-level. It has already been implied that this λ 1850 cutoff limit is expected to be found at a height of 75 km. One realizes that equivalent layers of *laboratory air* and air of the stratosphere and the ionosphere do not have the same temperature and composition. For example, the stratosphere is known to contain ozone to an altitude of 30 km, and possibly to 45 km or higher, and ozone is nearly opaque in the region of λ 2500. Also, Wulf and Denning[3] have calculated that O_2 is almost entirely dissociated into atoms above 100 km and that some oxides of nitrogen also are formed.

However, the ultraviolet absorption spectrum of atomic oxygen can be inferred from its resonance spectrum, which is known[4] to be a series of lines quite widely spaced and lying in the region λλ 1350–900. The absorption spectrum of *NO* also is known, and this is not strong for the equivalent thickness of layers of this gas found above about 100 km. Hence, if one disregards these and other complexities and regards only the "air component" of the atmosphere as approximated by the laboratory air, then one can make two inferences. (*a*) The atmosphere at high altitudes is much more transparent in the region λλ 1000–1300 than in the region λλ 1300–1700, which is the region of continuous absorption at the convergence limit of the Schumann-Runge bands of O_2. This system of bands is easily seen in absorption on the plate in the region λλ 1750–1950, and the band heads are indicated by lines at the bottom of the picture. (*b*) At the height of 86 km—roughly the height attainable by the Army rocket, the "WAC Corporal"— one might be able to extend the solar spectrum to λ 1800. (*c*) At heights above 96 km, the solar spectrum might be observable to λ 1750 and again in a second region of transparency that begins to show in the region λλ 1100–1200. (*d*) As one approaches a height of 128 km the first region of transparency lengthens, and the second one broadens and forms open windows to the light of the sun and stars.

Of particular interest is the spectrum line, λ 1215, Lyman-α which is the resonance line of atomic hydrogen. The plate shows this line in absorption because of the hydrogen liberated from the walls of the discharge tube by the hot spark. It lies in a favorable place for observation through one of the more transparent windows in this region. Lyman-β at λ 1025 is also observable through one of these windows. The possibility of observing these lines is of particular interest to astrophysicists. In short, this absorption spectrum of air encourages one to hope that at altitudes of 128–160 km one might be able to extend our knowledge of the spectrum of the sun's chromosphere from its present limit at about 2875[5] to a new value near λ 1600 and then after passing over a relatively dim region, to find it again as emission lines of the sun's corona in the region between λ 1350 and λ 1000. The resonance lines of *H*, *O*, and *N*, strong lines in the normal spectra of other elements, and the chief lines of the spectra of many elements in the first or higher states of ionization lie in this region.

With the advent of the new rockets which can rise to the top of the ocean of air which surrounds us, scientists are excited about the possibility of obtaining the entire spectrum of the sun and stars for the first time.

The work described in this paper was done in connection with the Contract NOrd 7386 with the U.S. Naval Bureau of Ordnance. The experimental part of the work was done, however, at the University of California at Berkeley in 1926.

[3] *Ter. Mag. and Atm. Electricity*, **43**, 283, 1938.

[4] Hopfield, *Ap. J.*, **59**, 114, 1924.

[5] Regener, *Phys. Zs.*, **35**, 788, 1934.

ON THE DIRECTION OF ROTATION IN SPIRAL NEBULAE

BERTIL LINDBLAD AND ROLF BRAHDE
Stockholm Observatory, Saltsjöbaden, Sweden
Received April 1, 1946

ABSTRACT

The question as to the true direction of tilt of spiral nebulae which are inclined toward the line of sight is the subject of a new discussion here. A photometric study of the distribution of intensity and color in indisputable cases, like NGC 4565, compared with typical cases, like NGC 7331, 4216, 4258, leads to a conclusion regarding the true tilt of the last-mentioned objects which is identical with the one derived by one of us in earlier papers. The importance of the "secondary" absorption on the distant half of the nebula is emphasized on the basis of new evidence. The results indicate that the dissolution of a system into spiral structure proceeds in such a way that the arms open up in the direction of rotation. The projection effects of the distribution of novae, variables, and globular clusters in M 31 are discussed. A comparison between the distributions supports strongly the contention that the brighter side of the nebula is the nearer one. Kinematical considerations, supporting the opinion that the spiral arms open up in the direction of rotation, are discussed for M 81 and M 33. The case of NGC 2681, which shows an outer diffuse spiral structure of a direction of winding opposite to that of the interior main spiral structure, illustrates conclusions drawn from dynamical theory. It is also of importance for the interpretation of NGC 3190, though this nebula is, no doubt, to be considered as a singular object on account of disturbing effects from its neighbor, NGC 3187.

I. INTRODUCTION

The theoretical discussion of the dynamics of the extragalactic nebulae has to start from certain fundamental data, among which the spectrographically determined rotations are of outstanding importance. In this connection it has early been recognized as one of the principal requirements that the relation between the direction of rotation of the nebula and the direction of winding of the spiral arms should be established with confidence. Pioneer work on this subject was carried out by V. M. Slipher,[1] who observed spectrographic rotations for six objects. For a few of these objects the direction of winding of the spiral arms can be seen; and, in order to solve the problem as to the relation between the direction of rotation and the direction of winding, it is necessary to know the orientation of the nebular plane in space. This depends on which side of the nebula, counted from the apparent major axis, is the nearer one. Slipher assumed the nearer side to be the one which shows the most prominent effects of occulting matter, and this led him to the conclusion that the spiral arms trail in the rotation.

While Slipher's assumption concerning the occulting matter is true for certain early-type spirals seen nearly edge-on, such as NGC 4594, it is by no means self-evident for nebulae in general, especially the advanced types of spiral nebulae. It was shown by one of us[2] that the interrelation between bright and dark matter in nebulae of the last-mentioned kind may be such that the part of the nebula on the farther side, reckoned from the apparent major axis, appears considerably fainter than the near side. It was recognized that photometric analysis, and especially observations of the distribution of color in typical nebulae, might be expected to yield considerable information about the interrelation of bright and dark matter. Photographic photometry of M 31 was begun at the Stockholm Observatory by Lindblad and Ramberg. During the stay of one of us as Morrison Research Associate at the Lick Observatory in 1939, an investigation of the distribution of intensity and color in certain typical nebulae—in the first place, the nebula NGC 7331—was begun and was completed at the Stockholm Observatory.[3] Photometry

[1] *Proc. Amer. Phil. Soc.*, **56**, 403, 1917; abstr. in *Pub. A.A.S.*, **4**, 232; *Pop. Astr.*, **29**, 272, 1921.

[2] *Ark. f. Mat., Astr. och Fys.*, Vol. **24A**, No. 21; *Stockholm Medd.*, No. 14, 1934.

[3] *Stockholms Obs. Ann.*, Vol. **13**, No. 8, 1941.

in red, blue, and ultraviolet revealed very considerable color effects produced by the tilt. Figures 1 and 2 reproduce the intensity-curves along the major and minor axis of the nebula. If we form apparent "centers of gravity" in violet light and in red light according to the observed intensity distribution in these colors, there appears a marked relative displacement between these centers at right angles to the apparent major axis of the nebula. Passing from violet to red, the center of gravity moves in the direction from the bright side to the faint side of the major axis. Moreover, the way in which the asymmetry of the light-distribution changes from one wave length to another, especially close to the nucleus, made it exceedingly probable that the side of higher intensity and lower color

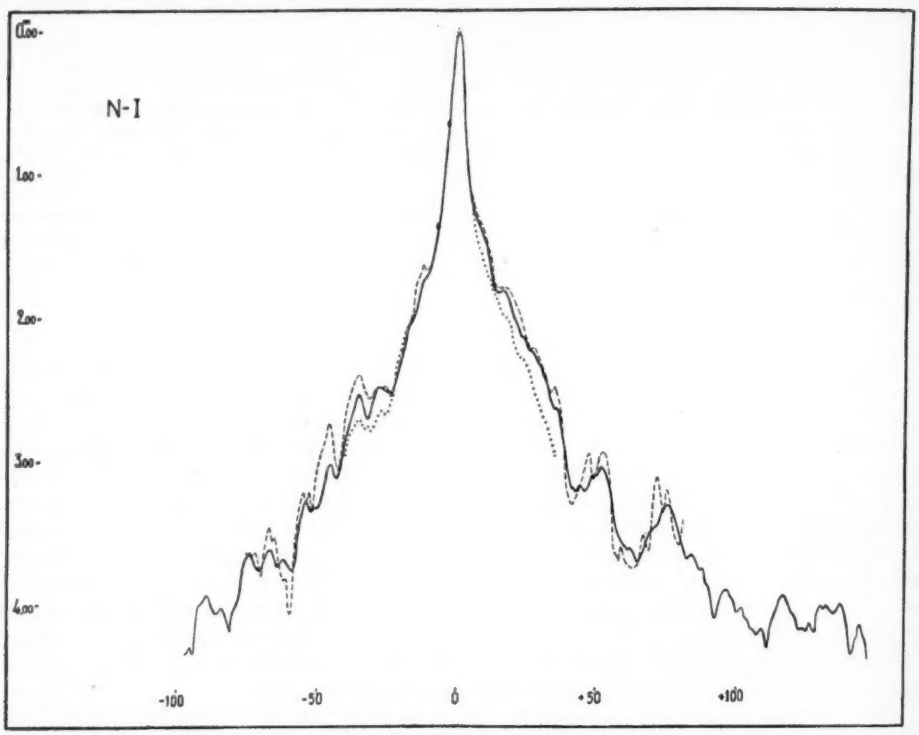

FIG. 1.—Intensity-curves along the major axis of NGC 7331. The full-drawn curve represents the blue spectral region; the broken-line curve the ultraviolet; the dotted curve the red.

is the nearer one. A detailed mathematical analysis,[4] aimed at disclosing the way in which bright and dark matter must be interrelated in order to produce the observed effects of intensity distribution and color, confirmed rather definitely the rule just mentioned. A review of various methods for obtaining the true direction of tilt was also given, which seemed to corroborate the conclusions drawn from the analysis of color.

An important contribution to the solution of the problem was given somewhat later by Hubble.[5] He was able to add several new spectrographic rotations; and on the basis of this material he could state with confidence that a general systematic connection exists between the direction of rotation, the direction of winding of the arms, and the type of obscuration, in such a way that there is a general unique relation between the direction

[4] *Stockholms Obs. Ann.*, Vol. **14**, No. 3, 1942.

[5] *Mt. W. Contr.*, No. 674; *Ap. J.*, **97**, 112, 1943.

of winding of the arms and the direction of rotation. The arms either "trail" or "ope up" in the direction of rotation. Hubble also tried to give a definite answer to the question as to which one of these alternatives is true. On this point he did not use such arguments as the internal distribution of color but selected a few nebulae in which the direction of winding of the arms was assumed to be traceable and in which, at the same time, the general appearance of the occultation by dark matter was considered to suggest in an obvious way the true direction of tilt. Only one of the nebulae—NGC 3190—is of the obvious "spindle" type, in which a streak of "primary" absorption cuts across a central system; but, unfortunately, in this case the true direction of winding of the arms is by

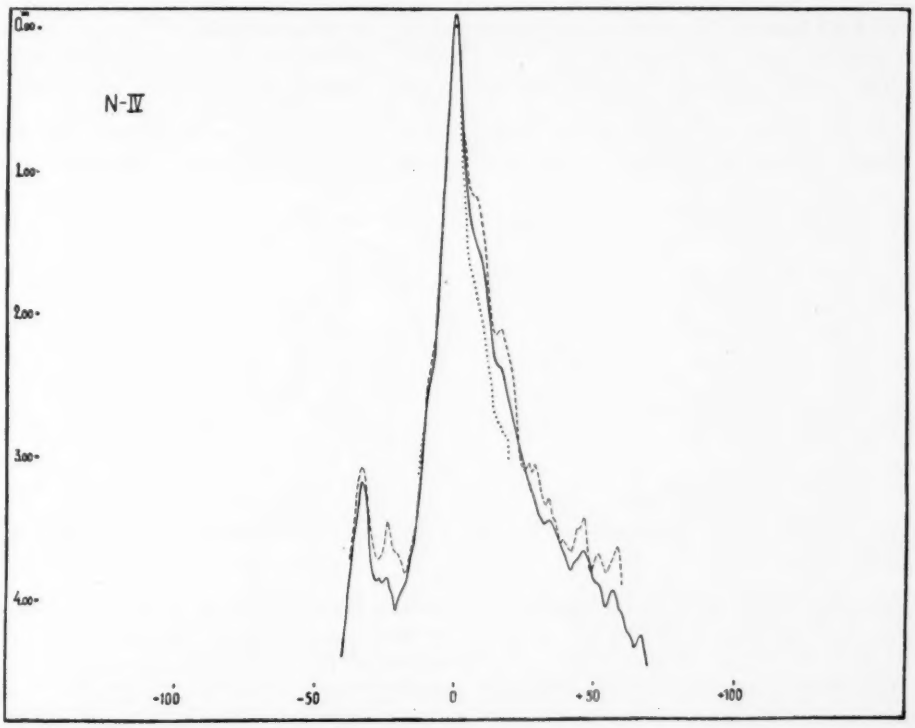

FIG. 2.—Intensity-curves along the minor axis of NGC 7331. Full-drawn curve blue; broken-line curve ultraviolet; dotted curve red.

no means certain, as will be further commented upon below. Concerning the other selected objects, Hubble assumed that the strongest lanes are "primary" lanes on the near side, and he accordingly deduced that the arms trail. However, in the nebulae NGC 4216, 4258, and 4527 the obscuration is of the same type as in NGC 7331, which was also adopted by Hubble as a typical case. In the case of NGC 7331 the color analysis by one of us had given an orientation in space opposite to that suggested by Hubble. Moreover, photometric plates of NGC 4216 taken in blue and red with the 40-inch reflector of the Stockholm Observatory showed obvious color effects in this nebula quite analogous to those observed in NGC 7331.

These circumstances have caused us to re-examine the inference drawn from the distribution of color, as well as certain other arguments, with the result that we feel obliged to maintain the opinion as to the direction of rotation expressed by one of us in previous papers. We shall first discuss some new facts about the distribution of color in a nebula

considerable inclination to the line of sight —the "real spindle" NGC 4565—in comparison with the nebulae NGC 7331, 4216, and 4258. The great Andromeda nebula will be briefly discussed from a point of view raised by Hubble concerning the apparent distribution of certain objects. Kinematical points of view will be taken up in connection with the nebulae M 81 and M 33. Dynamical considerations will be appealed to for explaining the double spiral structure of NGC 2681, which seems, moreover, to be of importance for the understanding of the apparent structure of NGC 3190.

II. NGC 4565 AND NGC 7331

The conclusion drawn from the study of the distribution of intensity and color in NGC 7331 that in this type the side of the nebula of relatively low color is the nearer one may be tested by investigating "real spindles," where there is no doubt as to the direction of tilt but where the tilt of the nebular plane against the line of sight is still sufficient to show a fair part of the nebular disk. We have therefore begun the comparative photometry in blue and red light of a few spindles, in the first place, NGC 4565 and 5746. The aim of this investigation is to discover whether or not general color effects like those

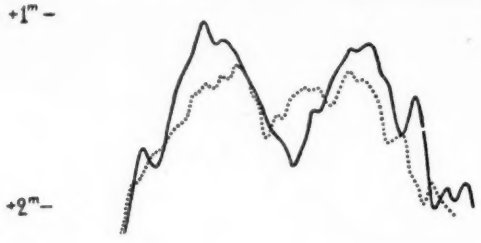

FIG. 3.—The intensity distribution in blue and red light along track *a* in Plate IV. Full-drawn curve blue; dotted curve red.

observed in NGC 7331 and 4216 may be found in NGC 4565 and 5746. In the latter cases we know without doubt which side is the nearer and which is the farther one and may thus determine the sign of the color effect with respect to the distance from the observer. Blue and red plates have been taken in the primary focus of the 40-inch reflector of the Stockholm Observatory. Sensitometer impressions were taken with exposure times of the same order as those used at the telescope. A detailed account of the photometric results will be given elsewhere.

In Plate IV the apparent disk of NGC 4565 on a moderately exposed photographic plate is compared with an inclosing oval figure which is symmetrical about the center. It is evident that in the parts of the spiral structure which are far from the center the real nebular disk is far from symmetrical with respect to the major axis; and the comparison with the symmetrical oval indicates clearly that there is, in addition to the central "primary" absorption lane, a considerable obstruction of the light from the parts of the spiral structure which are most distant from the observer. In other words, we have here a "secondary" absorption, according to the terminology introduced by one of us in earlier papers. A study of the distribution of intensity and color in the nebula fully corroborates this conclusion. A few tracings in blue and red light are reproduced as examples in Figures 3 and 4. The numbers correspond to the tracks indicated in Plate IV. In the photometry, surrounding stars have been used as points of reference, and great care has been taken to obtain a correct orientation in the comparison of the curves. The near side is to the right in the figures.

PLATE IV

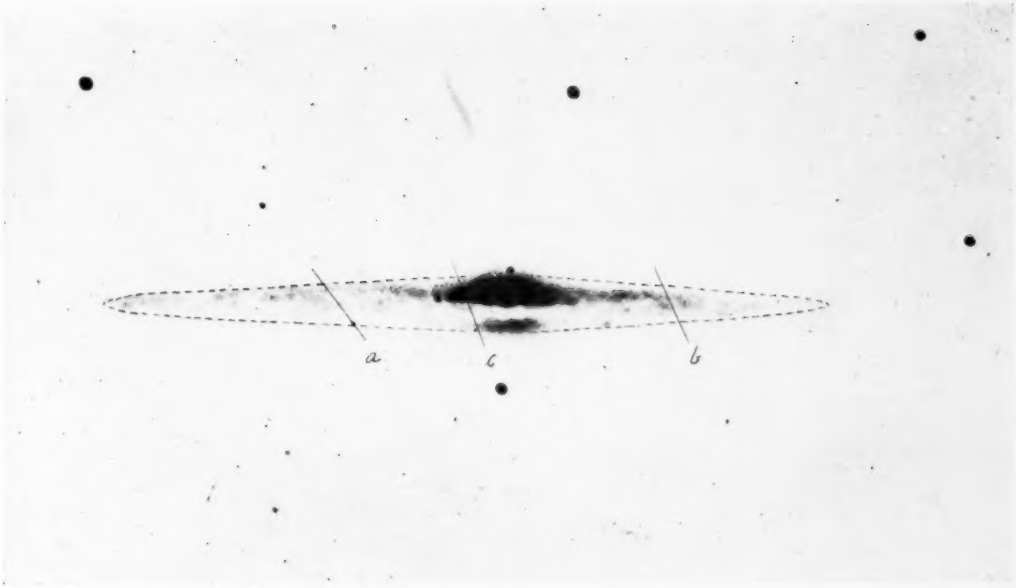

NGC 4565 Compared with a Symmetric Oval
The tracks of the photometric analysis in Figures 3, 4, and 5 are indicated

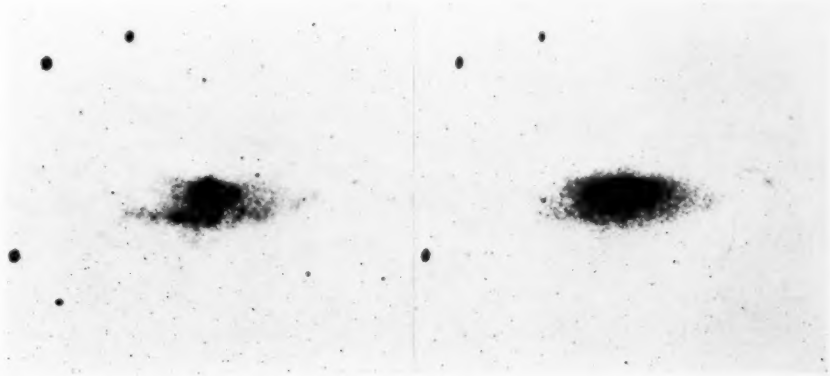

The Central Regions of NGC 7331 in Ultraviolet (*left*) and Red (*right*)

UNIV. OF MICH.

The most important inference to be drawn from the figures is that the results corroborate the conclusion arrived at from the study of NGC 7331, namely, that the edge of the spiral structure which is turned toward the observer has lower color, is "bluer," than the opposite, more distant part of the disk. In the case of NGC 4565 this conclusion has been established in a nebula for which the direction of tilt cannot be disputed, and the result gives very strong support to the conclusion concerning the direction of tilt of NGC 7331 which was obtained in earlier papers.

Tracings across the nuclear regions of NGC 4565, of course, record the strong "primary" absorption lane. The intensity-curves for blue and red light are shown in Figure 5. The color system is the same as that of Figures 3 and 4, so that a direct comparison of the color is possible for the three diagrams. In Figure 5 the depth of the central primary lane is much more pronounced in the blue than in the red light. There is thus a strong

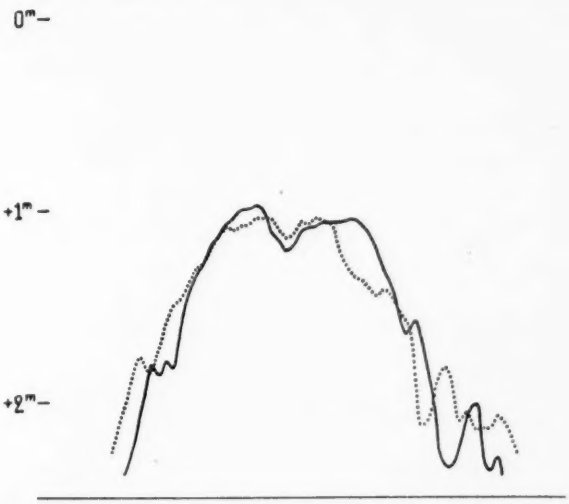

FIG. 4.—The intensity distribution in blue and red light along track *b* in Plate IV. Full-drawn curve blue; dotted curve red.

selective absorption here. Comparing Figure 5 with the tracings along the minor axis of NGC 7331 in Figure 2, we note the important difference that the one-sided absorption in this nebula is apparently very little selective and nearly the same in ultraviolet, ordinary photographic, and red light. This circumstance is of importance in view of the different interpretation of the effects in question, the absorption in NGC 4565 being on the near side, that of NGC 7331 on the farther side, reckoned from the nucleus. A theory explaining the apparently nonselective absorption in the case of NGC 7331 has been given elsewhere.[6] In Figure 5 spiral arms contribute to the intensity at three points—at the top, in the middle of the primary dark lane, and on the extreme right-hand slope. The last-mentioned near parts of the spiral structure contribute to give a fairly low average color to this slope, in agreement with the general effects of Figures 3 and 4.

A theoretical model intended to explain the facts mentioned may be described in a very simple way. We may state as a general postulate that the spiral arms and the spiral structure in general are associated with, and in a more or less irregular way surrounded and enveloped by, diffuse occulting matter. The model of a nebula of "late" type is illustrated schematically in the lower part of Figure 6, where the vertical intersections of nu-

[6] *Stockholms Obs. Ann.*, **14**, No. 3, 22, 1942.

cleus and spiral arms are indicated as full-drawn ovals, whereas the average distribution of the dark matter is indicated by dotted curves. It is evident that for an observer viewing the system at an oblique angle the optical depth of the spiral arms on the farther side is larger than that of the spiral arms on the near side. The evidence seems quite convincing that this simple picture gives, in principle, some of the essential features governing the law of distribution of intensity and color on the apparent disk of an average late-type nebula.

Though there is certainly a tendency of the dark matter, under equilibrium conditions, to concentrate extremely strongly toward the equatorial plane,[7] the general appearance of bright and dark matter in the spiral nebulae suggests that in the torn and complicated

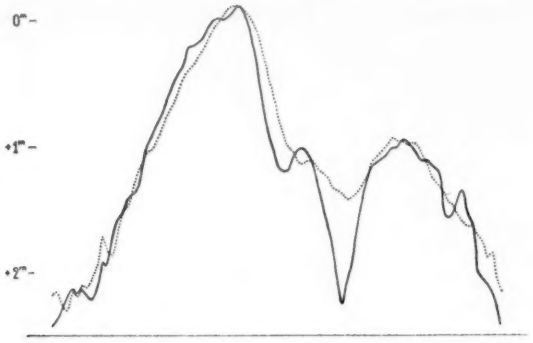

FIG. 5.—The intensity distribution in blue and red light along track *c* in Plate IV. Full-drawn curve blue; dotted curve red.

FIG. 6.—Schematic models of intersections through "early-" and "late-"type spirals. The dotted curves indicate the average distribution of dark matter.

spiral structure the clouds of dark matter have a dispersion at right angles to the equatorial plane which is at least comparable with that of the stars in the spiral arms. We may take into account the fact that these stars are, on the average, of early type and that, for instance in our surroundings of the galactic system, the dispersion of the dark matter at right angles to the galactic plane certainly exceeds the vertical dispersion of the massive early-type stars.[8]

The great importance of considering separately "early" and "late" types of spiral nebulae should be emphasized in this connection, as considerable confusion has arisen by mixing these types when the influence of a varying degree of tilt on the appearance of a nebula has been discussed.

In the early type of spirals, which is illustrated schematically in the upper part of Figure 6, the vast central bulge seems to be comparatively free from absorbing matter.

[7] Cf. *M.N.*, **94**, 231; *Stockholm Medd.*, No. 13, 1934; and results by L. Spitzer, *Ap. J.*, **95**, 329, 1942.

[8] Cf. results by Van Tulder, *B.A.N.*, No. 353, 1942.

Such matter appears to be concentrated in the thin spiral structure at the edge of the system; and in nebulae of sufficient tilt this matter is projected onto the central lens and gives the well-known "primary" lane of the type shown in NGC 4594. It is important to state that a primary lane of this kind will appear very much easier in early types of nebulae than in late types, and for this reason there will be a strong selection of early-type nebulae when nebulae are chosen to show this type of absorption.

In the late types the central system may be very small, and the spiral structure can be traced very close to the center. It is therefore natural that the occulting matter associated with the spiral structure will inclose the small nucleus rather thoroughly. There is little occasion here for the formation of "primary" lanes; and, instead, the "secondary" absorption, which may be characterized especially as an extinction of the spiral structure on the more distant side of the nebula, comes into play. It appears that a nebula like NGC 4565 occupies a kind of intermediary position between the early and late types. A primary absorption lane appears on the cental region because of the absorbing matter of the near part of the disk, which is projected onto the central bulge, whereas in the outer regions the absorption is mainly of the secondary type, as shown above.

III. GENERAL FEATURES OF THE DISTRIBUTION OF INTENSITY AND COLOR IN NGC 7331, 4216, 4258, AND 4088

The determination of the distribution of color in the nebula NGC 7331 allows us to draw roughly the "isochromes" in the central regions of this nebula. Such isochromes are

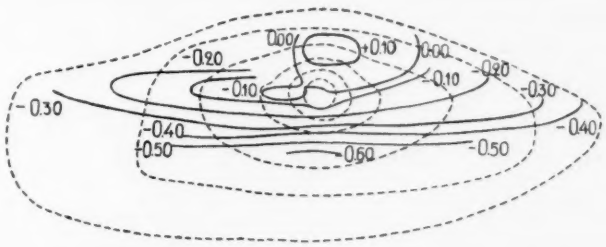

FIG. 7.—Isochromes (ultraviolet-red) and red isophotes (*dotted curves*) in the central regions of NGC 7331.

given here in Figure 7, together with the red isophotes,[9] which are indicated by dotted curves. Reproductions of the central region in ultraviolet and red are given in Plate IV. On the bright side of the nucleus the isochromes adhere closely to ellipses of great eccentricity, considerably greater than the eccentricity of the isophotic curves, and the change of color with the distance from the major axis is very rapid. On the fainter side a vast region of nearly constant color occurs close to the nucleus.

When we follow the *major axis* inward, we find that the color increases toward the center. This phenomenon may be due to a real change of the average color of the mixture of stars when we go inward or to an increase of selective absorption due to clouds of occulting matter surrounding the nucleus or, which seems most likely, to the combined action of both these causes. In any case we must expect, when we examine the color distribution along the *minor axis*, that there should be, by projection, a region of high color on the more distant part of the minor axis. Such a region is readily identified above the major axis in Figure 7. On the other hand, the run of the isochromes of low color close to the nucleus below the major axis clearly corresponds to a projection of the inner spiral

[9] Taken from *Stockholms Obs. Ann.*, **14**, No. 3, 4, 1942.

arm on the nucleus,[10] as may be seen by comparison with the left-hand picture of Plate IV. These results evidently confirm entirely the previous conclusions regarding the true direction of tilt of NGC 7331.

We turn our attention next to the nebula NGC 4216, the second nebula in Hubble's selection. Pictures of the nebula are given in Plate V, and intensity-curves for blue and red light along the tracks indicated in one of the pictures of Plate V are given in Figures

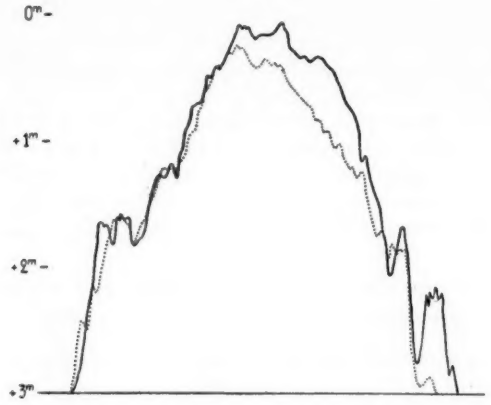

FIG. 8.—The intensity distribution in blue and red light along track *a* in Plate V. Full-drawn curve blue; dotted curve red.

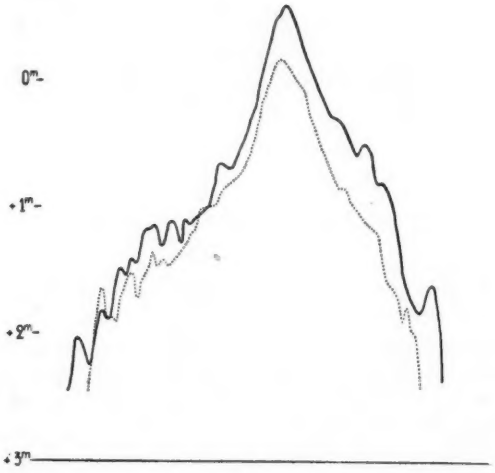

FIG. 9.—The intensity distribution in blue and red light along track *b* in Plate V. Full-drawn curve blue; dotted curve red.

8 and 9. On one side of the major axis the spiral structure is, on the average, much more intense than on the other side, where the intensity is weakened by a few strong and broad lanes. The bright side has, on the average, a lower color than the dark side; a point of great importance is that the distinct spiral arms which mark the border of the bright side are of very low average color. The distribution of color shows very considerable anal-

[10] Cf. also *ibid.*, **13**, No. 8, 26, 1941.

PLATE V

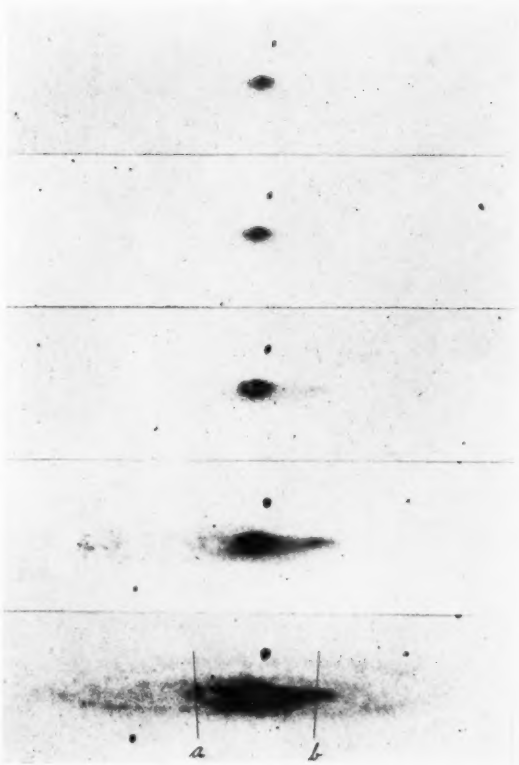

REPRODUCTIONS OF NGC 4216, PHOTOGRAPHED IN BLUE LIGHT
a and *b* indicate the tracks of the photometry in Figures 8 and 9

PLATE VI

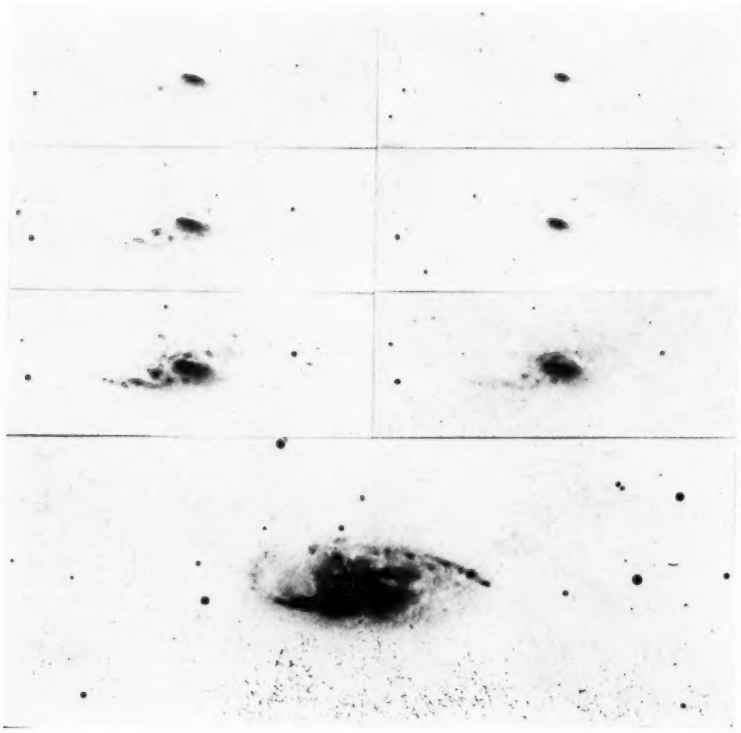

REPRODUCTIONS OF NGC 4258

The left-hand pictures and the bottom one, blue; the three right-hand pictures, red

PLATE VII

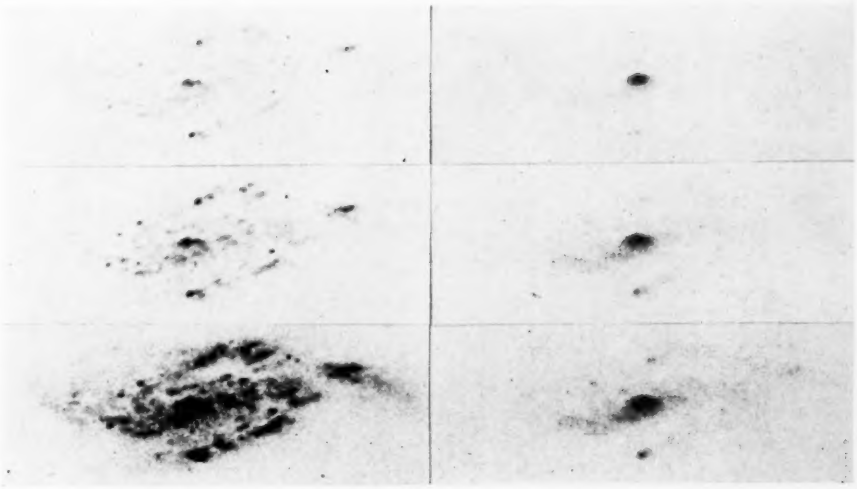

REPRODUCTIONS OF NGC 4088

Blue pictures to the left; red ones to the right. The blue pictures are from a Lick photograph

PLATE VIII

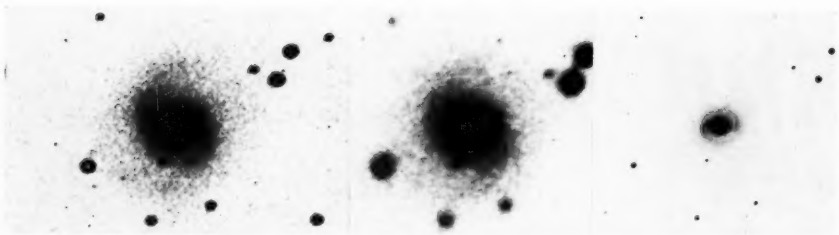

THE OUTER AND INNER SPIRAL STRUCTURE OF NGC 2681

In order from the left-hand side, picture taken with the 40-inch reflector; picture taken with the 16-inch astrograph; Mount Wilson picture of central structure.

NGC 3190 AND 3187

Mount Wilson photograph

ogy with NGC 7331. This is true also for the central regions of the two nebulae. A scrutiny of the regions close to the nucleus in NGC 4216 reveals that the true nucleus is small and appears to be surrounded by an annular formation of considerably lower color than the nucleus itself. Toward the fainter side of the nebula the "ring" is broken by absorption or partly hidden by the nucleus.

A comparison between NGC 4216 and NGC 4565 shows in the outer regions analogous color effects, if we suppose that the fainter side of NGC 4216 is the more distant one. Thus the comparison of NGC 4216 with NGC 7331 and NGC 4565 suggests strongly that the typical absorption effects in NGC 4216 are of the "secondary" type, i.e., more strongly developed on the distant half of the nebula than on the near half.

On the other hand, the central systems of NGC 4216 and NGC 4565 are found to be of very different nature, and it is evident that, of the two nebulae, NGC 4216 is, in reality, of a considerably later type than NGC 4565. This is borne out by the difference in the distribution of color in the nuclear regions. While in NGC 4565 the nucleus is surrounded by a discoidal central system of fairly advanced color, the nucleus in NGC 4216 is surrounded by the apparently annular formation of low color. The low color of this formation suggests that it belongs to the spiral structure and that it is rightly interpreted as a ring, which will be the case if the fainter half of the nebula is the more distant one. We may then understand that dark clouds may appear in immediate conjunction with this ring, so that the projection of the nucleus itself on the ring, combined with the absorption in these clouds, may cause the apparent break in the ring on the more distant side.

The differences of opinion regarding the direction of tilt of NGC 4216 seem to arise mainly from an apparent, extremely vast, central bulge, which is shown especially in reproductions in which the details of the intensity distribution in the central regions are obliterated by overexposure. In our opinion this apparent central system, which corresponds to a certain isophotic curve about the center, is, in reality, to be interpreted in quite another way. It marks simply the region of low optical depth in the spiral structure. This interpretation is supported, above all, by the fact that the region in question has a low color, nearly the same as other parts of the spiral structure.

The third nebula among the "safe cases" selected by Hubble is NGC 4258. In this case, too, it appears to be of paramount importance to consider the actual structure of the nuclear regions of the nebula rather than the run of the wider isophotes. As shown in Plate VI, there is, in reality, a very small, nearly spherical nucleus which is closely surrounded by spiral structure and dark clouds. The color analysis of the nebula shows the advanced color of the small nucleus itself. The light-distribution about the nucleus is asymmetrical, and, in particular, a small field on the minor axis close to the nucleus is considerably brighter than a similar field symmetrically situated with respect to the nucleus. The asymmetry is more pronounced in blue than in red light. These facts place the nebula NGC 4258 clearly in line with NGC 7331; and there is reason to assume that, of the two fields just mentioned, the brighter is the near one and the darker the more distant one. In reproductions in which the central region has reached full density down to a certain isophote the dark field makes the impression of a primary lane silhouetted against a central bulge. The analysis of the details of the distribution of intensity and color, however, gives quite another picture, as has just been explained.

The conditions of NGC 4258 are, moreover, plainly illustrated in a nebula of a closely related type, NGC 4088. In this nebula the small central system, shown in Plate VII, has a strikingly advanced color, compared with the surrounding spiral structure. The same contrast of intensity between two opposite fields adjacent to the nucleus appears in this nebula. The explanation of the phenomenon and the conclusion as to the direction of tilt are the same as for NGC 4258. Several details of various kinds strongly support this conclusion. The rotation of NGC 4088 is known, and, according to Hubble, the northeast end is approaching. The northwest side is directed toward us, according to the results

just obtained; and, as the spiral is "left-handed" (the sense of a spiral pattern being defined as "right-handed" if an object traveling inward along one arm moved in a clockwise direction, and "left-handed" in the opposite case), we conclude that the spiral arms open up in the direction of rotation. This is in accordance with the results for other nebulae mentioned above, for which spectrographic rotations have been determined—NGC 7331, 4216, and 4258.

IV. MESSIER 31

The great Andromeda nebula shows the effects of tilt in the distribution of intensity and color, which are, no doubt, of the same general kind as those observed in NGC 7331 and 4216. The interpretation of the main dark lanes as being of the "secondary" type does not seem to meet serious difficulties, though it is necessary to assume that the obstructing clouds occasionally reach fairly great heights above the spiral structure. The general asymmetry of light in the regions farther away from the center, the well-defined spiral arms on one side, and the obscuration of the arms on the other strongly suggest a close analogy with NGC 7331 and lead to the conclusion that the bright half of the nebula is the near one. This conclusion is much strengthened by Öhman's[11] discovery of effects

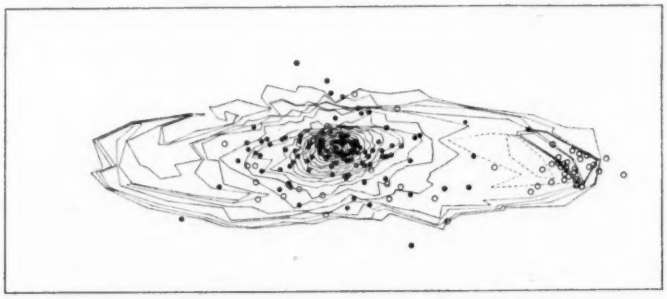

FIG. 10.—The apparent distribution of novae (*full circles*) and variables (*open circles*) in M 31. The background is the isophotic map of Lindblad and Ramberg.

of polarization in certain dark nebulae close to the central regions, as has been mentioned in earlier papers. The presence of "negative" polarization in clouds on the fainter side supports the result that this side is the more distant one.

Hubble has drawn attention to the inference which may be obtained from the apparent distribution of novae, variables, and globular clusters over the nebula, when we consider the effects of an extinction of light in the nebular disk on objects which are, as seen by us, situated below the disk. He finds in each case the number of objects to be greater on the brighter half than on the fainter half of the nebula and interprets this as an effect of projection which would indicate that the bright side is the more distant one. It seems to us, however, that it is scarcely possible to draw conclusions from the behavior of a certain class of objects, as long as we do not consider more exactly the law of distribution at right angles to the nebular plane of the class of objects considered, as well as of the dark matter. Instead, a comparative study for classes of objects which have different dispersion in the distance from the central plane of the disk may give safer results. Figures 10 and 11 illustrate a comparison between the distribution of novae and variables, on the one hand, with that of the globular clusters, on the other hand. Hubble's[12] material has been used; in the case of the novae the 14 novae given by Mayall[13] have been included,

[11] *Stockholms Obs. Ann.*, Vol. **14**, No. 4, 1942.

[12] *Mt. W. Contr.*, Nos. 376 and 452; *Ap. J.*, **69**, 103, 1929, and **76**, 44, 1932.

[13] *Pub. A.S.P.*, **43**, 217, 1931.

making the total number 100. The isophotic map of Lindblad and Ramberg has also been drawn in Figures 10 and 11, and, accordingly, these diagrams illustrate directly the projection of the objects over various parts of the nebular disk. The differences between the two pictures are considerable. Especially in the case of the variables it must, of course, be kept in mind that certain regions have been examined systematically, which has a direct effect on the distribution. If we confine ourselves to the regions around the center, however, we may probably assume that the main difference between the two pictures is due to a wider distribution at right angles to the equatorial plane for the clusters than for the novae and variables. Without doubt, the novae and variables are, on the average, strongly bound to a very flat formation; and it is quite in accordance with our ideas that the novae and variables should be more numerous on the near, bright side of the nebula than on the faint side. It is evident that the distribution of the novae and variables reproduces fairly well the skewness of the isophotic map, whereas the clusters have a tendency to fill out the upper regions of the spiral structure, even outside of the isophotic map. On the whole, they form a fairly uniform distribution within an ellipsoidal contour, which is nearly symmetrical with respect to the major axis of the nebula. The shift of the center

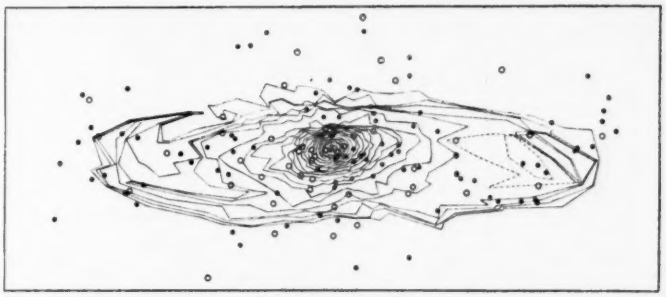

FIG. 11.—The apparent distribution of globular clusters in M 31. Open circles are clusters brighter than 16.5 mag.; full circles the fainter ones.

of gravity of the distribution upward in the pictures, when we pass from the novae and variables to the clusters, is entirely in accordance with the assumption that the lower, brighter part of the spiral disk is the nearer one, if the globular clusters have a wider dispersion at right angles to the equatorial plane than do the novae and variables. That the overweight of the clusters in the upper part of the picture when compared with the novae and variables is not still more marked may be due to various circumstances. The clusters, too, may show a considerable increase of frequency toward the plane of rotation, though their vertical distribution is, on the average, considerably wider than that of the novae and variables. It is also possible that the upper half of the nebular disk is actually, as a whole, less transparent than the lower half

V. DIFFERENTIAL MOTIONS IN SPIRALS REVEALED BY CERTAIN DARK TRACINGS; SYSTEMATIC MOTIONS IN M 33

For those nebulae discussed above for which the direction of winding of the spiral arms can be traced and the direction of rotation has been measured spectrographically, the direction of tilt derived by us is such that the spiral arms open up in the direction of rotation. The motion of the individual particles of an arm should be at least roughly in the direction of the arm. The state of motion, however, can also be described as a rotation superposed by an expansion which proceeds like a wave motion around the system in such a way that the points at which an arm separates from the central system stay approximately fixed in space. The *relative displacement* between a point of the central system

and an originally coinciding point of an adjacent spiral arm follows a certain arc which is determined by the law of areas in the motion. The question may be raised as to whether this relative motion can be checked in a direct way.

Attention has been drawn in earlier papers to a certain kind of narrow and very much elongated formations of obstructing material which pass like dark strings over the spiral structure. They were first found[14] in M 81 and are of special interest in relation to the regular structure of this nebula; but similar transverse dark "strings" have been observed in a number of other nebulae as well.

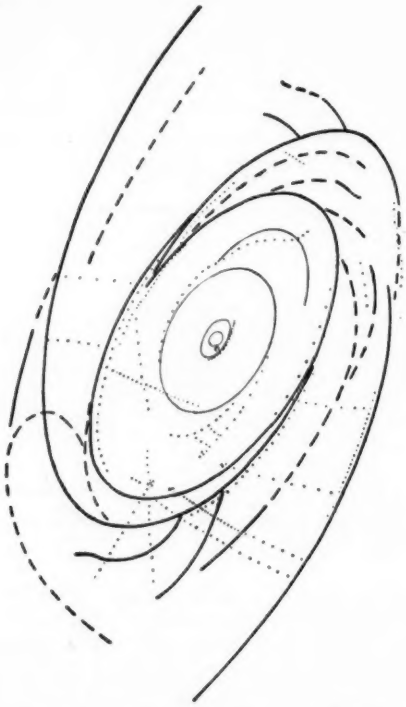

FIG. 12.—Schematic picture of M 81. The heavy full-drawn and broken curves represent spiral arms and the limits of the central system. Faint full-drawn curves indicate, approximately, certain isophotes in the central system. The dotted curves indicate lanes of dark matter.

In M 81 the most clearly marked dark strings proceed in such a way that they mark very nearly the direction of relative separation between originally adjacent parts of matter in a motion of the kind just described. They are readily identified in the right-hand part of the schematic Figure 12. It is readily understood that dark nebulae may lie in the region of separation between an arm and the central system and that such a nebula may become very much extended between these two as the separation proceeds. The appearance of the markings of this kind in M 81 and in other nebulae in a fairly similar way is thus in general agreement with conditions to be expected on the basis of the present results.

Important contributions to the study of internal motions in nebulae are the measurements of velocities of emission nebulae in spirals. Such measurements have been per-

[14] *Ark. f. Mat., Astr. och Fys.*, Vol. **27**B, No. 13; *Stockholm Medd.*, No. 47, 1940.

formed by Horace Babcock[15] for the Andromeda nebula and by Mayall and Aller[16] for M 33. Dingens[17] has tried to use the velocity for an emission nebula close to the minor axis of M 31 for determining the tilt of the nebula, on the supposition that the nebula moves away from the center of the system. Oort[18] has investigated Mayall and Aller's material for M 33 and has made solutions for the systematic radial and rotational velocities. Oort's line of thought is that, "if emission nebulosities which are situated in the arms of a spiral show radial motion with respect to the center of the system, we may safely assume that this motion will be away from the center and not toward it. Therefore, if such a radial motion is large enough to be measured, it will make it possible to decide which side of the system is turned toward us." For the emission nebulae in the innermost zone within 16′ from the center, he sets for the average radial motion $\Pi = pR$ away from the center; and for the tangential motion $\Theta = tR$, Θ being counted positive in the direction of the arms. From a least-squares solution for ten objects and for an assumed inclination of 33° between the nebular plane and the line of sight, Oort obtains

$$p = +4.30 \pm 2.25\ (m.e.), \qquad t = +6.99 \pm 1.91\ (m.e.).$$

The positive signs of p and t are valid if the eastern side of the spiral is directed toward us. For the opposite orientation of the spiral in space, both p and t would be negative. In order that p may be positive, the angular rotation t will be in the direction of the arms. The systematic radial motion is still uncertain, but Oort concludes that in any case the results do not seem compatible with a rotation in the opposite direction, accompanied by considerable outward motions. The nebulae of greater distance from the center show no indication of any systematic motion away from the center but a rotational motion in agreement with Mayall and Aller's results. Oort emphasizes the importance of further observations of radial velocities in the nebulae.

VI. DYNAMICAL CONSIDERATIONS RELATED TO NGC 2681 AND 3190

The dynamical theory of the formation of spiral structure which has been developed by one of us in recent years starts from the theory of asymptotic orbits in regions of unstable circular motions. Such regions of instability may be expected in a general way where matter is strongly concentrated to the plane of rotation and where considerable radial density gradients occur. If we take as a model the simple quasi-spheroidal case, we should expect an exterior region of instability at a certain degree of flattening of the system. With a still greater degree of flattening, the system is likely to become unstable for certain kinds of wave motions. The most important of these are the two-dimensional waves of the sectorial harmonic type, which may be shown to exist for a rotating quasi-spheroidal stellar system as well as for a liquid spheroid. The critical wave is probably the second-order harmonic, which may be expressed, if r and θ are polar co-ordinates in the rotating system, and ω the angular velocity of rotation,

$$\delta r = r \cos(\omega t + 2\theta).$$

This wave is the one which, according to Bryan, makes the McLaurin spheroid unstable at the meridian eccentricity,

$$e = 0.9529.$$

The wave proceeds with the angular speed $\omega/2$ against the rotation; it may be expected to eject particles by a certain resonance effect in asymptotic orbits where the points of ejection follow the wave (cf. *Stockholms Obs. Ann.*, **13**, No. 10, 1941, and **14**, No. 1, 1942).

[15] *Lick Obs. Bull.*, **19**, 41, 1940. [16] *Lick Obs. Contr.*, Ser. II, No. 1; *Ap. J.*, **95**, 5, 1942.

[17] *Mededeel. kon. vlaamsche ac.*, **5**, No. 4, 20, 1943.

[18] Unpublished result kindly communicated by Professor Oort.

The nebula NGC 2681 has been found to possess an outer diffuse spiral structure which may possibly be interpreted as the result of an ejection by an unstable sectorial wave of the kind just described. The nebula has a regular, well-defined inner spiral structure attached to a small, intensely luminous central system, as shown in the right-hand picture in Plate VIII. The exterior structure, for which the entire inner spiral structure serves as central system, appears at long exposures as shown in the two pictures to the left in Plate VIII. A particularly interesting feature is that the outer diffuse spiral structure shows a direction of winding opposite to that of the interior regular spiral structure.

The theoretical picture, Figure 13, gives the loci of the ejected matter in asymptotic orbits for a meridian eccentricity of the spheroid,

$$e = 0.980 ,$$

and for a motion of the points of ejection with the angular speed $\omega/2$ against the rotation. The arrows indicate the direction of motion if the rotation of the central system occurs in the positive direction.

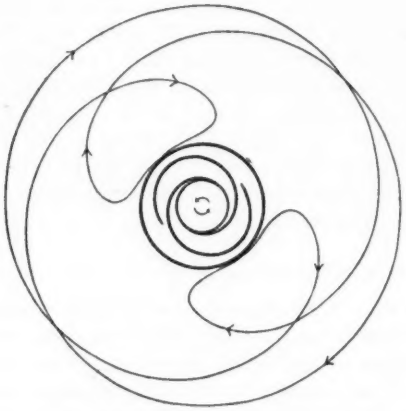

FIG. 13.—Theoretical spiral arms of outer and inner structure in NGC 2681

In spite of the diffuse character of the outer structure of NGC 2681, there is a remarkable correspondence between the structure in Plate VIII and the outer-curve system of Figure 13. As the outgoing branch must be supposed to be most clearly defined, the rotation of the nebula in Plate VIII must be the same as in Figure 13, i.e., from right to left in the upper part of the figure.

The interior arms correspond well to asymptotic spiral orbits for a meridian eccentricity,

$$e = 0.950 ,$$

of the respective small central system. These orbits are given in the central region of Figure 13, in order to match the interior arms in the right-hand picture of Plate VIII. The points of ejection are fixed in space, and the arms open up in the direction of the rotation.

The process by which the points of ejection may become fixed in space in the interior parts has been discussed in earlier papers. In many cases the disturbing gravitational field of a distant massive object may contribute effectively to this end.

In the nebula NGC 3190, which is the first nebula in Hubble's selection, there is probably an exterior disturbance from the nebula NGC 3187, the neighboring peculiar barred

spiral which shows plain indications of being, in its turn, heavily disturbed by NGC 3190. The two nebulae are reproduced in Plate VIII from a Mount Wilson photograph. A comparison between NGC 2681 and NGC 3190 suggests that the last mentioned nebula has a massive right-handed spiral structure analogous to the interior spiral structure of NGC 2681. As the rotation, according to Hubble, occurs in the positive direction, this would be in agreement with our rule that the spiral arms open up in the direction of rotation. An outer faint spiral arm to the left, which appears to form a continuation of the dark primary lane and which, according to Hubble, indicates a left-handed spiral structure, may perhaps belong to an outer structure similar to that of NGC 2681. There is a considerable amount of conjecture in such a hypothesis, and the present reasoning shows that the case of NGC 3190 is not sufficiently clear to be used as a criterion for a general rule concerning the relation between spiral structure and direction of rotation.

In the face of the evidence from sources which we are inclined to consider as conclusive and which have been indicated in previous parts of the present paper, little weight can be attached to cases of more enigmatic nature. Still, a few words may be said here concerning nebulae in which the spiral arms may not be clearly made out but in which a certain S-shape of the nebulae as a whole may possibly indicate the direction of winding. The inner parts of NGC 3190 present such a case, which has just been discussed. Among other cases may be mentioned NGC 4565, for which no spectrographic rotation seems to have been determined as yet, and NGC 5746. For this nebula Hubble mentions certain indications that the arms are right-handed (in the sense defined by Hubble), but he finds the arms difficult to trace and places the nebula among the doubtful cases. A certain trace of an S-shape, as judged from the general intensity distribution of the object, however, in comparison with spirals of great tilt in which the arms may be traced, would rather seem to indicate a left-handed pattern. From the present material, however, we do not wish to press this point as far as direct evidence is concerned. The distribution of color in the nebula seems to show a general agreement with NGC 4565 and thus indirectly confirms the results obtained in the present work. The effects of color are slight, however, which is, no doubt, due to the fact that NGC 5746 must be classed in an earlier nebular type than NGC 4565.

STRUCTURE AND MASS OF COMETARY NUCLEI

B. VORONTSOV-VELYAMINOV
Sternberg Astronomical Institute, Moscow, U.S.S.R.
Received January 4, 1946

ABSTRACT

The different characteristics of the cometary nuclei are apparently contradictory because of an improper terminology to describe the relevant facts. A terminology which avoids these difficulties is suggested and its physical meaning explained.

Attention is drawn to the fact that the linear diameter of the solid nucleus can be determined only from the spectrograms, where the Fraunhofer spectrum is present; at the same time, the nuclei are too small to be measured on the spectrograms. Their reflecting surface can be calculated from the luminosity contributed by the Fraunhofer spectrum and the rate of evaporation, determined from the variation of the monochromatic luminosity of a comet. The mass of the nucleus can be calculated by estimating the loss of the gases determined from the comet's luminosity and knowing the gas content of meteorites.

The comparison of all such results obtained for comets Halley and Peltier 1936a leads to the following conclusions: The solid nuclei are some 25–60 km in diameter and are composed of blocks some 160 m in diameter, which are nearly in contact. The mass is 3×10^{19} gm. The evaporation of sodium and other problems are also discussed.

I. PRESENT STATE OF THE PROBLEM

Some writers believe that the cometary nuclei are of meteoric nature. Apparently, this opinion is supported by the known relation existing between comets and meteoric swarms. Others believe the nuclei to be monoliths, as small as 1 km in diameter or even less, arguing that such was the starlike nucleus of the Pons-Winnecke comet when observed close to the earth in 1927[1] and that the hypothetical radiation pressure exerted by the nucleus upon the ejected molecules leads to a very small radius of its "sphere of action."[2] It appears, however, that no effort has actually been made to study the structure and the mass of the nuclei or to reconcile such data with the widely quoted statement that the gases in comets are liberated from their nuclei under the heating effect of the sun.

It appears further that not much attention has been given to the fact that the enormous range displayed by the luminosities of comets must be related to the structure and mass of their nuclei. The true luminosities of comets (at $r = \Delta = 1$) have a range of at least 10^6. Therefore, the data obtained for the nucleus of one comet cannot be directly combined with those obtained for another. The apparent discrepancies can be quite illusory and may be caused not only by the real dispersion of nuclear characteristics but by fundamental differences of nuclear characteristics provided by various methods. This may be similar to the differences in stellar temperatures obtained from the absorption lines (temperature of the reversing layer) and from the continuous spectrum (temperature of the photosphere).

II. THE METHOD OF ATTACK

We can get an idea of the real nature of the nucleus and avoid the apparent discrepancies, if we do not confuse the concepts and terms used in connection with this problem. I suggest the following terminology:

a) *The photometric nucleus* is the luminous condensation as it appears to an observer. Its dimensions and luminosity depend on the observational conditions.[3] Generally speak-

[1] F. Baldet, *C.R.*, **185**, 39, 1927; V. M. Slipher, *Bull. Lowell Obs.*, **86**, 3, 1927.

[2] S. Orlov, *The Nature of Comets*, Moscow, 1944 (in Russian); and *Russ. A. J.*, **14**, 135, 1925.

[3] H. D. Curtis, *Pub. A.S.P.*, **22**, 117, 1910.

ing, it has nothing in common with the true volume occupied by the solid matter of the nucleus or with its reflective efficiency.

b) The stellar nucleus is sometimes observed inside the photometric nucleus (as in the case of the Pons-Winnecke comet in 1927). It can be smaller than the volume occupied by the solid matter of the nucleus and represents only the core of the latter.

c) The nucleus as origin of the Fraunhofer spectrum is due to reflected sunlight. It can be studied only on slit spectrograms and is determined by that surface of solid matter of the nucleus which is exposed to sunlight.

d) The nucleus as origin of the "continuous spectrum" does not always have the same origin as the Fraunhofer spectrum, since it is usually observed on slitless spectrograms. Apparently, it is much like the photometric nucleus, its dimensions depending upon the exposure time, etc. Besides, it may be caused by emission of gas, such as the continuous spectrum of H_2 or the fluorescence spectrum of Na_2, etc. Sometimes it may be produced simply by the overlapping of monochromatic images.

e) The nucleus of the mechanical theory of comets and of its modifications is generally treated as a point source of emanation of particles and of forces acting on these particles.

f) The nucleus as a bearer of the comet's mass is treated in celestial mechanics. Its upper limit in the case of Lexell's and Brock's comets, which caused no perceptible planetary perturbations, is estimated as 10^{23} gm. This is by far the highest limit and may be compared with the latest estimates of S. Orlov,[2] which represent the smallest values hitherto suggested. According to Orlov, treatment of the hypothetical repulsive force exerted by the nuclei of large comets, such as Halley's 1882 II, leads to a mass of $10^{13} - 10^{15}$ gm.

Other existing estimates[4] of nuclear masses are also very tentative. For instance, the apparent repulsive force acting upon the nucleus, which is difficult to observe (if it exists at all), may be ascribed to light-pressure upon the small particles of the meteoric nucleus (Russell, Dugan, and Stewart) or to the recoil caused by the impulse of gases emanating from the nucleus (Ambarzumian and Krochmal[5]) or to the perturbations caused by meteoric masses moving behind the nucleus (Dubiago[6]). All these effects may coexist and cannot be properly separated.

g) The nucleus as the source of the gases is responsible for the coma and the tail. An estimate of the comet's mass based on data of meteoric swarms—the Perseids and the Leonids—can be made. It is not of high accuracy, particularly because of the doubtful estimate of the mass of the meteors. The necessary data were taken from Watson.[7] The width of the Perseid swarm was accepted as being 1.1×10^8 km, and the distribution of meteors along the orbit was considered to be uniform. The minimum resulting mass of the swarm then is 5×10^{16} gm. It is unlikely that the earth passes centrally through the ring composed of meteors, and a considerable fraction of the initial cometary mass must still remain in its nucleus, since the comet still exists. Hence it appears that 10^{18} gm is the lower limit for the initial mass of Tuttle's 1862 comet.

For the Leonids, the meteoric cluster was estimated as having dimensions of $(7 \times 10^5) \times (3 \times 10^9)$ km. The resulting mass is 1.5×10^{14} gm. Allowing for the noncentral crossing of the cluster by the earth, for the dissipation of meteors behind the cluster, and for the concentration of the meteors toward the center of the cluster which did not strike the earth, the minimum mass of Tempel's comet of 1866 may be estimated as 10^{16} gm. Unfortunately, the masses of these comets cannot be checked by other methods. However, these estimates tend to bring the masses of relatively bright comets closer to the upper limit adopted by the majority of writers.

[4] Bobrovnikoff, *Pub. Lick. Obs.*, **17**, 471, 1930.

[5] *Scientific Notices of the Leningrad University*, Vol. **12**, No. 82, 1941 (in Russian).

[6] *Russ. A.J.*, **19**, 50, 1942.

[7] *Between the Planets* ("Harvard Books on Astronomy"), 1941.

In order to compare and discuss the results, the nucleus of Halley's comet can alone be used at present, for the necessary observational data are lacking for all other comets.

III. THE NUCLEUS OF HALLEY'S COMET

The following methods for investigating the nature of cometary nuclei are almost free from arbitrary hypotheses:

a) *The width of the Fraunhofer spectrum*, D_{F_s}, gives the diameter of the space occupied by solid matter responsible for the noticeable reflection of sunlight.

b) *The integrated luminosity far from the sun*, L_∞, gives an upper limit to the area that reflects sunlight. The actual area may be smaller, since the monochromatic emissions are also present there, as manifested by the "violet type" of spectrum of comets when far from the sun.

c) *The luminosity of the Fraunhofer spectrum*, L_{F_s}, gives the best information about the surface of the particles exposed to the sun.

d) *The number of molecules emanating from the nucleus* can be estimated from the comet's monochromatic luminosity. This leads to an estimate of the mass of the nucleus, since the volume of gases in meteorites is known.

e) *The rate of evaporation* of the molecules can be evaluated from the observed monochromatic luminosity of the comet on the basis of the kinetic theory of matter. This leads to a determination of the surface area of the solid particles which produce the gases.

No stellar nucleus was present in Halley's comet. Its nucleus was invisible when projected on the sun's disk. This is usually interpreted[4] as meaning that the diameter of the nucleus was less than 50 km. If the nucleus is semitransparent like a cluster, at least in its outer parts, and if we take into account the effects of irradiation, etc., meteoric clusters with true diameters as large as 150 km or more can escape detection when projected on the solar disk. On the other hand, H. D. Curtis[3] observed that the photometric nucleus diminished to 480 km when the comet approached the earth. No doubt, this is an upper limit to the monolithic part of the nucleus or to its dense portion, if it is of meteoric nature. However, this has nothing to do with the mass or with the surface of the solid matter inside the comet.

Now we pass to the methods enumerated above. The width of the Fraunhofer spectrum D_{F_s} cannot be determined from slitless spectrograms, not only because the continuum present there cannot be entirely identified with the former but because of purely photographic widening. On the small scale of such spectrograms this leads to an impossibly high linear diameter of the nuclear strip. The values of D_{F_s} were estimated for all comets, for which appropriate data based on slit spectra are available. They range from 1 to 10,000 km. However, from these fragmentary data it is difficult to be sure of the reality of the measured D_{F_s}. The data on Halley's comet are more conclusive. The abrupt fluctuations of D_{F_s} on consecutive days and its rapid decrease as the comet approached the earth demonstrate that the measured D_{F_s} is spurious, though the image of the comet on the slit was as large as could be achieved with existing telescope . The variations of D_{F_s} must be due mainly to the quality of guiding and to photographic effects but not to the gradual decrease of brightness along the radius of the nucleus, as the edges of the Fraunhofer spectrum are sharp on almost all spectrograms. The continuous slitless spectra of the nuclei of planetary nebulae obtained with the 72-inch reflector[8] (where certainly no motion perpendicular to the dispersion was allowed) are 2".2 wide. If such a strip were due to a cometary nucleus, at a distance $\Delta = 1$, D_{F_s} would be estimated as 1500 km, thus confirming the theory that the true D_{F_s} of Halley's comet was less than 960 km (the lowest value measured).

The luminosity far from the sun, at $r = 3.4$, was 15 mag. for the comet, 15.5 mag.

[8] Zanstra, *Pub. Dom. Ap. Obs.*, Vol. **4**, No. 15, 1931.

for the "nucleus." If the albedo of the nucleus is the same as that of Ceres, the surface exposed to the sun would be 1.3×10^{13} cm^2.

The luminosity of the Fraunhofer spectrum, L_{Fs}, is not known. An effort to estimate this quantity was made from the reproductions published. In May, L_{Fs} appears to have been fainter by 3 mag. than the integrated luminosity of the whole slit spectrum. The latter is also unknown, since the width of the slit projected on the comet's head and the distribution of brightness in the coma are unknown. The integrated magnitude of the comet being 5 (at $\Delta = 1$), we assume that L_{Fs} is 10 mag.

The phase angle for Halley's comet at the period considered is $a = 56°$. The correction for the phase angle was accepted as being the same as for Mercury: $m = m_0 + 0.015a$. The resulting visual magnitude L_{Fs} is 9.2. With an albedo equal to that of Ceres, the surface of the nucleus exposed to the sun is 3×10^{13} cm^2.

It is to be noted that, even if our estimate were wrong by as much as a factor of 10 (which seems impossible), the resulting surface area of the nucleus would be in error by a factor of only 3, and the mass (if monolithic) by a factor of only 2. The visual L_{Fs} for Peltier's comet of 1936 (a comet of comparable physical appearance, according to Wellmann's and Richter's data[9]) was 4 mag. fainter than the integrated luminosity of the head.

The number of the molecules emanating from the nucleus can be calculated from the number N of molecules present in the comet's head. The energy emitted by N molecules in a band with average frequency ν is

$$E = N f \frac{\pi e^2}{h\nu \cdot \mu} \rho_\nu h\nu W ,$$

where f is the oscillator strength, W is the dilution factor, and

$$\rho_\nu = \frac{8\pi h\nu^3}{c^3} \left(e^{h\nu/kT} - 1 \right),$$

e is the charge, and μ the mass of an electron.

If q_ν is the relative sensitivity of the human eye and Q the mechanical equivalent of light, the monochromatic magnitude of a comet is

$$m = -2.5 \log \left(E q_\nu \frac{10^{10}}{Q} \right), \qquad (1)$$

since the illumination produced by a star of $m = 0$ is 2×10^{-10} phots.

The oscillator strength for the resonance bands observed in comets is close to unity. Formula (1) can be written in the form

$$\log N = -0.4m - \log q_\nu + 2 \log r + 1.754 + \frac{10.38}{\lambda} + 3 \log \lambda + 2 \log \Delta , \quad (2)$$

r being expressed in astronomical units.

For visual observations the luminosity of the comet's head can be attributed mainly to the band λ 5100 of C_2 (in the majority of comets the continuous spectrum is weak and the sodium lines are not prominent).

The fact that actually some of the visual light of the comets is emitted in other bands of C_2 may be compensated by assuming that the monochromatic luminosity is equal to the visual luminosity. Then

$$\log N = 32.56 - 0.4m + 2 \log r \quad \text{for } \lambda 5800 \text{ of } C_2 , \qquad (3)$$

$$\log N = 32.29 - 0.4m + 2 \log r \quad \text{for } \lambda 5900 \text{ of } Na , \quad (3')$$

[9] *Zs. f. Ap.*, **14**, 77, 1937.

the latter formula being used for comets which, like 1882 I, were bright in sodium when close to the sun. If $m = m_0 + 2.5n \log r$, then

$$\log N = 32.56 - 0.4m_0 - (n-2)\log r \qquad \text{for } C_2 . \quad (4)$$

The quantities m_0 and n are determined from the usual photometric observations. However, we must account for the fact that not all of the molecules of C_2 present contribute to the luminosity of comets. Some of the molecules must be ionized. Unfortunately, we do not know the density distribution in the coma. In the brightest, innermost portions near the nucleus, the gases are rather dense. At the boundary of the coma the density is so low that the free path of the molecule is larger than the diameter of the comet's head, so that the ionized molecules cannot recombine with the free electrons. Possibly the ordinary ionization formula will give approximately the proper amount of the ionization for the mean concentration n_0:

$$\frac{n^+ n_e}{n_0} = \left(\frac{2\pi m k T_0}{n^3}\right)^{3/2} e^{-\chi/kT} \left(\frac{R_0}{2r}\right)^2 ,$$

or

$$\log n^+ = 7.90 - 0.420V + 0.5 \log n_0 - \log r , \quad (5)$$

V being the ionization potential in volts. For C_2 an ionization potential of 12 volts was adopted, that is,

$$\left.\begin{aligned} \log n^+ &= 2.87 + 0.5 \log n_0 - \log r , \\ n_0 &= \frac{3}{4}\frac{N}{\pi R^3} . \end{aligned}\right\} \quad (6)$$

The radius of the comet's head, R, generally varies, and only in the case of Halley's comet can it be represented analytically[2] in the form

$$R = R_0 \sqrt{r} . \quad (7)$$

Thus, the total number of the C_2 molecules, practically equal to that of the ionized molecules, is given by

$$\left.\begin{aligned} \log N^+ = 8.21 - 0.420V + 1.5 \log R_0 + 0.5\,(32.56 - 0.4m_0) \\ - 0.5\,(n-1.5)\log r , \end{aligned}\right\} \quad (8)$$

or

$$\log N^+ = 19.45 + 1.5 \log R_0 - 0.2m_0 - 0.5\,(n-1.5)\log r . \quad (9)$$

Similarly for *Na*,

$$\log N^+ = 22.21 + 1.5 \log R_0 - 0.2m_0 - 0.5\,(n-1.5)\log r . \quad (9')$$

For Halley's comet, at perihelion, log N = 30.86 and log N^+ = 32.4 for C_2.

Let τ be the lifetime of a molecule or the duration of its stay in the comet's head. Then, during one revolution in its orbit with period P, the number M of the molecules lost by the comet is

$$M = 2\int_0^{P/2} \frac{N}{\tau}\, dt . \quad (10)$$

Substituting

$$r = \frac{q(1+e)}{1 + e\cos v} \qquad \text{and} \qquad dt = \frac{r^2 dv}{\sqrt{\mu q (1+e)}} ,$$

we can change the variable.

The analytical form of τ is unknown. We can assume (*a*) τ = const., which includes the case that τ varies slightly with r, and (*b*) $\tau = \tau_0 r^2$ according to Wurm's[10] hypothesis.

Formula (10) may also be applied to parabolic comets and to the number M^+ of ionized molecules lost. Of the set of formulae thus deduced, we shall quote the following for C_2:

Ellipse, τ = const.:

$$M^+ = \frac{3.27 \times 10^{21-0.2m_0}}{\tau} R_0^{3/2} [q(1+e)]^{-0.5n+2.25} \int_0^{\pi} \frac{dv}{(1+e\cos v)^{-0.5n+2.75}}; \quad (11)$$

Ellipse, τ = const.:

$$M = \frac{4.23 \cdot 10^{34-0.4m_0}}{\tau} [q(1+e)]^{3.5-n} \int_0^{\pi} \frac{dv}{(1+e\cos v)^{2-n}}. \quad (12)$$

As a mean value of n for comets we can adopt $n = 4$. Then for τ = const. and an ellipse:

$$\log M = 35.12 - 0.2m_0 + 0.5 \log [q(1+e)] - \log \tau + \log\left(1+\frac{e^2}{2}\right), \quad (13)$$

and

$$M^+ = \frac{3.27 \cdot 10^{21-0.2m_0}}{\tau} R_0^{3/2} [q(1+e)]^{1/4} \int_0^{\pi} \frac{dv}{(1+e\cos v)^{3/4}}. \quad (14)$$

The value of τ is uncertain. We shall adopt τ = 1 day, which is probably of the right order and in conformity with S. Orlov's computations. Then, for C_2 in Halley's comet, log M = 33.09. Assuming $\tau = 1^d \times r^2$, one obtains log M = 33.55. During the thirty known revolutions of Halley's comet it lost $10^{34.03}$ neutral molecules. The minimum corresponding value for M^+ is 10^{36}.

The diminution of brightness of Halley's comet is hardly perceptible, so that the number of C_2 molecules which can volatilize in its nucleus is certainly larger than 10^{37}.

The analysis of existing data on the gases in stony meteorites gives 1.7×10^{19} atoms of C per cm^3, on the average. Probably 8×10^{18} molecules of C_2 per cm^3 is an upper limit for the following reasons: (*a*) The iron meteorites contain a smaller volume of gases; (*b*) not all C-atoms form C_2 molecules, since CN and CH molecules also exist in comets; (*c*) in the laboratory some of these molecules may have been liberated from the glass tube; and (*d*) it is likely that the gas liberated from meteorites in the laboratory originates mainly from chemical reactions under the influence of high temperature, which is not the case with cometary nuclei in interplanetary space.

It is of interest that the gases liberated from stones found on the earth are nearly identical (as regards their volume and chemical composition) with those liberated from stony meteorites. The gases liberated are mainly H_2 and CO_2. Then follow CO, N_2 (found in the tails of comets), and CH_4. Of these, CO_2 and CH_4 can represent the parent-molecules expected but not observed in comets. It appears, however, that the molecules of the tail, CO and N_2, may volatilize from the nucleus directly and may not be due to the dissociation of parent-molecules, as is the case for the molecules of the coma. However, it was found recently that CN also emanates from the meteorites.

Thus the minimum volume of solid matter in the nucleus of Halley's comet is $10^{37}/(8 \times 10^{18}) \approx 10^{18}$ cm^3. The lower limit of the nuclear mass is 3×10^{18} gm.

The loss of CO^+ molecules through the tail, estimated by a similar method for the Morehouse and Halley comets (which were of the same luminosity), is approximately 10^{31} per revolution. The same amount is obtained from Schwarzschild and Kron's[11] calculations made by a different method. This leads to 10^{17} gm as the lower limit for the

[10] *Zs. f. Ap.*, **9**, 62, 1934.

[11] *Ap. J.*, **34**, 342, 1911.

nuclear mass, or to a higher value, if the loss of the neutral *CO* molecules is taken into account.

The rate of evaporation of gases from the nucleus can be treated as follows: According to the kinetic theory of matter, the approximate rate of evaporation from solid bodies per square centimeter per second is

$$n = n_0 \sqrt{\frac{kT}{2\pi m}}\, e^{-L/RT}, \tag{15}$$

L being the heat of vaporization and n_0 the concentration of the molecules. We assume that for the nucleus

$$T = \frac{T_0}{\sqrt{r}} = \frac{350^\circ}{\sqrt{r}}. \tag{16}$$

Thus

$$n = n_0 \sqrt{\frac{kT_0}{2\pi m}}\, r^{-1/4} e^{-(L/RT_0)\sqrt{r}}. \tag{17}$$

The effective value of L, according to Levin,[12] can be determined from the photometric observations of a comet. For Halley's comet we evaluate $L = 8530$ cal/mol, which is of the same order as the mean L determined in the laboratory for different solids and gases.

Let S be the surface of the nucleus which emits gases under the heating effect, and τ, the lifetime of the molecules. Then for C_2 or Na:

$$n \cdot S \cdot \tau = N^+. \tag{18}$$

From equation (9) we get

$$\log(\tau \cdot S) = -3.87 - 0.2 m_0 + \log r + 1.5 \log R_0 + \frac{L}{700}\sqrt{r}. \tag{19}$$

With $\tau = 1^d$, we get $S = 6.0 \times 10^{15}$ cm^2.

IV. MODEL OF THE COMETARY NUCLEUS

In the accompanying table the results for the nucleus of Halley's comet are summarized. The data determined directly are printed in italics; the others, calculated from these on the assumption that the nucleus is a solid sphere, are in roman type.

	Surface	Diameter	Mass
Transit before the sun	$<3\times10^{14}$ cm^2	$<5\times10^6$ cm	.....
Width of the Fraunhofer spectrum	$<10^{14}$	$<10^7$	$<10^{21}$
Integrated luminosity far from the sun	1.3×10^{13}	2×10^6	2×10^{19}
Luminosity of the Fraunhofer spectrum	3×10^{12}	3×10^6	3×10^{19}
Loss of C_2	10^{13}	2×10^6	3×10^{18}
Loss of CO^+	$>3\times10^{11}$	$>3\times10^5$	$>10^{17}$
Evaporation of gases	$>6\times10^{15}$	$>4\times10^7$	.....

Thus the nucleus of Halley's comet must be regarded as a dense cluster of meteoric blocks, whose distances from each other are comparable to their dimensions. The diameter of the nucleus is of order of 30 km and its mass 3×10^{19} gm.

The largest diameter compatible with the above data is 60 km, corresponding to a mass of 2×10^{20} gm, which would guarantee a sufficient quantity of gases which are lost by the nucleus.

[12] *Russ. A.J.*, **21**, 48, 1943.

Let the nucleus consist of n particles of radius r. Then

$$\log n = \tfrac{3}{2} \log S_{Fe} - \log S - \log 2\sqrt{\pi}\,, \tag{20}$$

and

$$\log n = \log S - 2 \log r - \log 4\pi\,. \tag{21}$$

With $S_{Fe} = 3 \times 10^{13}$ cm^2 and $S = 6 \times 10^{15}$ cm^2, it follows that $r = 80$ meters and $n = 10^7$. Actually, the number of particles must be much larger, and the dispersion of their sizes must be considerable, since the inner portions of the nucleus cannot be sufficiently heated by the sun to emit a large quantity of gas and since S refers to the outer portions of the nucleus.

There are indications that the outer surface of the nucleus becomes larger at perihelion, which appears plausible if the Keplerian law of areas and tidal effects is taken into account. It is then probable that, besides the usual phase effect, there exists a geometrical effect, depending upon the projection of an elongated nucleus upon the celestial sphere relative to the sun and to the observer. The emanation of gases proceeds inside the fragmentary nucleus, though it must be more prominent on the sunlight side.

Owing to the rotation of the nucleus and to the liberation of its particles, fresh surfaces of the meteorites, still rich in gases, are continuously exposed to the sun and produce gases. The small surface of the monolithic nucleus cannot produce the observed rate of evaporation of gases, nor can the concentration of gases at the surface be rapidly renewed. In such a case, short-period comets would tend to decrease in brightness much more rapidly than observed. The diffusion of gases through the stones is negligible, and its effect is replaced by exposing a fresh surface to the sun.

The model described tends to increase the lifetime of the cometary nuclei before their disintegration, on account of the tidal and other disturbing effects discussed recently by A. Dubiago. The resulting lifetime would be measured by thousands of years, in agreement with the most plausible estimate. The disintegration of comets is due mostly to the accelerated mechanical disintegration of their nuclei rather than to their degassing. The emanation of gases far from the center of the nucleus, particularly in its rarified outer regions, probably would remove the mystery of the high initial velocities of the molecules which are necessary for the mechanical theory of comets.

The observations needed for an accurate study of the cometary nuclei have been formulated. A number of results concerning other comets and the evaporation of sodium in comets have been obtained by the author. They are similar to the results discussed above but meet with certain difficulties.

A more detailed presentation of this investigation was published in *Russ. A.J.* **22,** 317, 1945.

DWARF M STARS FOUND SPECTROPHOTOMETRICALLY SECOND LIST

A. N. VYSSOTSKY, E. M. JANSSEN, W. J. MILLER, S. J., AND M. E. WALTHER
Leander McCormick Observatory, University of Virginia
Received June 21, 1946

ABSTRACT

Table 1 lists 135 additional dwarf M stars found on objective-prism plates. Tables 2 and 3 give further information concerning the dwarfs of the first list. Proper motions have been derived in 52 cases in which they had not been previously determined.

The accompanying list of dwarf M stars requires little explanation, since it forms a continuation of the list published three years ago.[1] Each star was discovered by its characteristic appearance on our spectral plates, without any knowledge of its proper motion or of its dwarf character as established elsewhere. The 40 stars of Table 1, whose numbers are printed in boldface type, have previously appeared in lists published by Mount Wilson or McDonald observers.

The majority of the stars in the table were discovered by a systematic survey of the spectral plates. In particular, 77 of the 90 stars credited to observers J, M, W, and T were discovered in this way. In all, 95 plates were thus surveyed, resulting in the discovery of 99 M dwarfs; but 22 of these had been discovered here previously (overlapping plates, etc.). The average of one dwarf to a plate (80 square degrees) is remarkably close for the different observers. However, discoveries are rather more frequent from plates outside the Milky Way, since in crowded regions the characteristic features of the fainter dwarfs are easily masked. All the plates examined were 2-hour exposures made by Vyssotsky.[2]

Proper motions for 49 stars have been determined by comparing the astrographic catalogue position with a recent McCormick plate. Six of these stars have motions greater than half a second of arc, namely, Nos. 93, 158, 161, 179, 206, and 208; of these, the first two are the most noteworthy, with motions of 0".85 and 0".78, respectively.

The column headed "M_v" contains estimates of absolute magnitudes which are explained in the next paper (*Ap. J.*, **104**, 239, 1946). These were all made by the first author for the sake of uniformity, as were also the estimates of spectral subclass.

Since one of the chief values of the list is to furnish an unbiased approach to the characteristics of the motions of these stars, it is of particular importance to exclude any star whose dwarf character is at all doubtful. When a spectrum is found which appears to be that of an M dwarf, the decision to retain it or to reject it must be reached before any attempt is made to find the star's motion; otherwise, there will be a tendency to retain stars which are found to have appreciable motion and to reject, as doubtful, certain stars with small motions. The decision is usually not difficult when the spectrum is favorably exposed or when it appears on more than one plate. However, as the task of obtaining duplicate exposures for all doubtful cases is prohibitive, we have perhaps erred on the conservative side in rejecting many possible dwarfs. It is probable that a number of those thus rejected would be classed as K8. A few K8 stars are included in the present list; these show the "Lindblad depression" but no trace of *TiO* bands. However, in spite of our care, there were 3 stars in the first list (Nos. 7, 52, and 69) which we regarded with

[1] *Ap. J.*, **97**, 381, 1943.

[2] *Ap. J.*, **93**, 425, 1941.

TABLE 1

No.	BD or AC	R.A. 1855.0	Decl. 1855.0	m_v	μ_α	μ_δ	Sp.	M_v	π	Source of Proper Motion	Observer
83.....	+19°20	0h 5m6	+19° 34′	10.7	+0.213	−0.013	M0	7:	.....	McC—AC	W
84.....	+40.45	0 9.4	+40 8	9.4	+0.54	+0.09	M0	7:	+0.083	Ci 20.16	J
85*.....	+43.44	0 10.1	+43 12	7.6	+2.874	+0.400	M2	10.7	+ .284	G. C.	J
86.....	−13.116	0 34.1	−13 59	10.3	+0.018	+0.073	M0	7:	.....	McC—AC	J
87.....	+34.106	0 34.9	+34 45	10.0	+0.264	+0.091	M0	7.6	.....	McC—AC	W
88.....	−19.111	0 37.3	−19 44	10.6	+0.255	+0.011	M0	8.3	+ .057	McC—AC	J
89.....	−23.332	0 44.3	−23 41	8.5	+0.60	−0.32	M0	8.3	+ .070	Ci 20.61	J
90.....	.....	0 54.6	+46 16	10.7	.....	.....	M0	8.3	.....	.....	V
91.....	+79.38	1 8.1	+79 22	9.6	+0.282	−0.087	K8	7:	+ .041	Green. Astr.	J
92.....	*+77.742*	1 22.0	+77 20	10.5	−0.070	+0.090	M0	7:	.....	Green. Astr.	J
93.....	+ *4.2595-239*	1 35.9	+ 3 34	10.0	−0.415	−0.740	M2	9.4	.....	McC—AC	W
94.....	*+29.4398*	1 48.5	+29 6	10.7	−0.139	+0.061	M	8.0	.....	McC—AC	V
95.....	+ 2.348	2 5.1	+ 2 58	10.7	−1.77	−1.88	M0	8.8	+ .094	Ci 20.153	V
96.....	+47.612	2 12.7	+47 12	9.8	+0.032	+0.042	M2	11.1	.....	McC—AC	J
97.....	*+75.1146*	2 52.5	+75 28	9.5	+0.219	−0.050	M0	8.6	+ .051	Green. Astr.	V
98.....	+ 1.543	2 58.9	+ 1 27	8.9	+0.33	−0.85	M0	8.8	+ .058	Ci 18.404	J
99.....	*+45.130-216*	2 59.7	+45 9	10.2	−0.406	−0.304	M0	8.8	+ .076	Ci 20.210	W
100.....	+37.748	3 8.7	+37 42	9.9	+0.49	−0.62	M2	9.4	+ .070	Ci 20.221	V
101.....	−20.643	3 21.3	−20 19	8.1	+0.521	+0.304	M0	8.3	+ .071	Ci 18.456	J
102.....	*+34.344-129*	3 25.8	+34 8	10.5	+0.197	+0.151	M0	7.5	.....	McC—AC	J
103.....	+34.724	3 35.2	+34 30	10.6	−0.205	−0.146	M0	8.3	+ .025	McC—AC	J
104.....	+25.613	3 37.5	+25 47	9.5	+0.34	−0.24	M0	8.3	+ .087	Ci 20.259	J
105.....	*+82.779*	3 44.4	+82 30	11.0	+0.131	−0.236	M0	7.9	+ .037	Green. Astr.	J
106.....	−11.916	4 30.9	−11 20	10.8	−0.216	−0.197	M0	8.3	.....	McC—AC	J
107.....	+18.683	4 34.6	+18 43	9.9	+0.71	−1.05	M2	9.4	+ .104	Ross 33	J
108.....	+25.733	4 38.8	+25 53	10.1	+0.115	−0.084	M0	7.5	.....	McC—AC	J
109.....	+49.1280	4 47.7	+49 37	9.4	+0.110	−0.101	M2	10.2	.....	McC—AC	V
110.....	+52.911	4 51.5	+52 58	9.8	+1.309	−1.514	M2	9.4	+ .059	*A.J.*, **50**, 119	V
111.....	+ *2.2283-259*	4 52.0	+ 1 34	10.0	−0.041	−0.152	M0	8.8	.....	McC—AC	V
112.....	−21.1051	4 56.3	−21 28	8.2	−0.157	−0.264	M2	8.8	+ .132	Yale zone	V
113.....	−23.2363	4 57.3	−23 27	10.1	+0.293	+0.138	M0	8.3	.....	Yale zone	V
114.....	−21.1131	5 12.7	−21 33	9.4	−0.130	−0.039	M0	7.9	.....	McC—AC	J
115.....	*+23.406-689*	5 55.3	+23 2	10.7	−0.048	−0.358	M0	8.3	+ .037	McC 84.31	V
116.....	.....	7 28.9	+34 47	11.4	−0.005	+0.121	M	9:	+ .013	McC 491.14	V
117.....	*+29.26222*	8 40.3	+29 33	11.0	−0.086	−0.067	M0	8.1	.....	McC 120.26	V
118.....	+77.361	9 0.9	+77 50	10.1	−1.059	−0.020	M0	8.3	+ .037	Green. Astr.	J
119.....	+81.297	9 7.4	+81 13	9.5	+0.014	−0.448	K8	7:	+ .058	Green. Astr.	J
120.....	*+76.3952*	9 31.8	+76 43	10.0	+0.061	−0.983	M2	10.2	+ .066	Green. Astr.	V
121.....	+63.869	9 45.4	+63 30	8.8	−0.33	−0.60	M2	10.2	+ .082	Ci 20.553	J
122.....	+33.1931	9 51.3	+33 47	10.8	0.000	+0.078	M0	8.8	.....	McC—AC	M
123.....	+ 3.2316	9 59.4	+ 3 41	9.9	−0.075	−0.086	M0	8.3	.....	McC—AC	J
124.....	*+22.214-129*	10 6.3	+21 50	9.5	−0.097	−0.214	M0	7.9	.....	McC—AC	J
125.....	+78.345	10 10.6	+78 12	10.3	−0.179	−0.116	M0	7.7	+ .020	Green. Astr.	J
126*.....	+87.91	10 16.5	+87 23	10.3	+0.028	−0.009	K8	7.7	.....	Green. Astr.	J
127.....	+ 1.2447	10 21.6	+ 1 38	9.7	−0.60	−0.75	M2	9.4	+ .128	Ci 20.580	J
128.....	*+23.468-46*	10 52.3	+23 36	10.5	−0.40	−0.28	M2	10.7	+ .136	Ross 104	V
129*.....	+22.2302	10 54.9	+22 44	9.9	+0.153	−0.040	M2	8.8	.....	McC—AC	V
130.....	+ *8.86-89*	11 16.0	+ 7 53	10.0	+0.208	−0.051	M0	8.3	.....	McC—AC	V
131*.....	+ *8.86-62*	11 21.0	+ 8 22	9.7	−0.24	−1.13	K8	7:	+ .034	Ci 18.1412	V
132.....	+63.965	11 22.9	+63 56	9.9	+0.084	+0.011	M0	8.8	.....	McC—AC	J
133.....	+23.2359	11 24.2	+23 28	10.3	−0.61	−0.05	M0	8.8	.....	Ross 903	V
134.....	+40.2442	11 28.9	+40 2	10.2	+0.469	−0.387	M0	8.3	+ .034	Furuhj. 33	V
135.....	+36.2219	11 43.6	+36 3	10.3	.....	.....	M2	10.2	.....	.....	J
136.....	+29.2228	11 47.4	+29 33	10.8	+0.212	−0.288	M0	8.6	.....	McC—AC	V
137.....	+55.1519	12 5.0	+55 18	9.6	+0.249	+0.076	M2	10.2	.....	McC—AC	V
138.....	.....	12 10.7	+47 24	11.5	−0.70	−0.04	M	8:	.....	Ross 917	J
139.....	+28.2110	12 15.3	+28 25	10.8	−0.146	−0.013	M0	8.6	.....	McC—AC	V
140.....	+13.2618	12 53.6	+13 8	9.9	−0.69	0.00	M0	8.8	.....	Ci 20.755	J
141.....	+21.2486	12 59.2	+21 31	9.1	−0.063	+0.064	M0	8.3	.....	Yale zone	M
142*.....	+48.2108	13 13.5	+48 33	8.7	+0.141	−0.015	M2	9.4	.....	2d Green. 1925	V
143.....	+11.2576	13 22.6	+11 11	9.4	+1.01	−1.09	M2	10.2	+ .123	Ci 20.782	J
144*.....	*+18.1204-96*	13 25.7	+17 32	10.5	+0.304	−0.225	M	11:	.....	McC—AC	V
145.....	− 7.3646	13 27.2	− 7 36	9.3	−0.38	0.00	K8	7.5	.....	Ross 478	J
146.....	− 3.3508	13 32.6	− 3 28	9.7	−0.38	+0.48	M0	7.7	+ .048	Ci 20.794	J
147.....	− 5.3763	13 39.9	− 5 23	10.5	−0.36	−0.59	M0	7.7	+ .032	Ci 20.806	J

TABLE 1—*Continued*

No.	BD or AC	R.A. 1855.0	Decl. 1855.0	m_v	μ_α	μ_δ	Sp.	M_v	π	Source of Proper Motion	Observer
148	*+79°4347*	13h54m4	+79° 37′	10.5	−0.267	+0.100	M0	7.7	.....	Green. Astr.	J
149	*+16.799-62*	13 55.1	+16 13	10.0	+0.117	−0.016	M2	8.6	.....	McC—AC	V
150	*+14.1105-9*	13 55.3	+14 26	10.0	+0.105	−0.093	M0	8.6	.....	McC—AC	V
151	+26.2536	14 5.0	+26 52	10.7	−0.032	+0.172	M0	7.9	.....	McC—AC	M
152	+81.465	14 11.5	+81 18	10.3	+0.172	−0.534	M0	8.1	+0.070	Green. Astr.	J
153*	+24.2733	14 19.0	+24 19	9.0 9.5	+0.786	−1.118	M0 M0	8.8 8.8	+ .056	Yale zone	M
154	+24.2735	14 21.3	+24 29	10.7	−0.48	+0.08	M0	8.3	+ .045	Ci 20.860	M
155*	+20.3009 +20.3010	14 35.9	+20 7	9.5 10.2	−0.25	−0.18	M0 M0	8.2 8.6	+ .025	*A.J.*, **48,** 80	M
156	+22.2742	14 37.6	+22 48	10.2	+0.024	+0.125	M0	7.9	.....	McC—AC	M
157	+16.2708	14 47.6	+16 41	10.5	+0.310	−0.144	M0	8.3	.....	McC—AC	V
158	+ 6.2986	14 57.8	+ 6 13	10.4	−0.604	−0.496	M0	8.6	.....	McC—AC	J
159	− 7.4003	15 11.9	− 7 11	10.9	−1.32	−0.04	M	8:	+ .151	Ci 20.923	M
160	*+15.647-70*	15 28.1	+14 23	10.0	+0.156	−0.017	M0	7.9	.....	McC—AC	M
161	+55.1823	16 13.8	+55 39	10.2	+0.113	−0.492	M0	8.8	.....	McC—AC	J
162	+67.935	16 16.5	+67 35	8.7	−0.494	+0.090	M0	8.8	+ .093	Ci 18.2184	J
163	*+48.1595-89*	16 19.9	+48 42	10.7	+1.14	−0.44	M2	8.8	+ .134	Ci 20.986	V
164	−12.4523	16 22.2	−12 18	10.6	0.00	−1.24	M2	10.7	+ .255	Wolf 1061	J
165*	+45.2505	17 7.9	+45 55	9.5	+0.24	−1.54	M2	11.6	+ .144	Ci 20.1023	J
166	−12.4699	17 8.2	−12 1	10.0	−0.144	−0.017	M0	8.6	.....	McC—AC	M
167	+42.2810	17 8.6	+42 31	9.9	−1.021	−0.322	M2	9.8	+ .032	Furuhj. 47	J
168	−14.4622	17 14.5	−14 48	10.4	−0.107	−0.251	M	8:	.....	McC—AC	M
169*	*+19.997-273*	17 31.4	+18 39	9.8	+0.94	+1.02	M0	9.4	+ .113	Ci 18.2347	J
170*	+23.3151	17 31.8	+23 3	9.6	−0.153	−0.156	M0	8.3	.....	McC—AC	V
171	+43.2796	17 39.5	+43 28	10.2	−0.001	−0.616	M2	11.2	+ .102	Furuhj. 49	J
172	+71.851	17 40.7	+71 24	9.2	−0.108	+0.325	K8	7:	+ .062	Green. Astr.	T
173*	+46.2361	17 41.6	+46 54	10.2	−0.015	+0.021	M0	9.1	.....	McC—AC	J
174	− 6.4663	17 42.8	− 6 0	10.1	+0.001	−0.133	M2	9.4	+ .078	McC 651.1	V
175	*+50.1784-39*	17 43.0	+50 8	10.0	+0.12	−0.34	M0	7.9	.....	Wolf 1386	M
176	− 3.4233	17 57.4	− 3 2	9.0	+0.564	−0.333	M2	10.7	+ .130	Yale zone	M
177	−12.4935	18 1.4	−12 3	9.6	+0.063	−0.202	M2	9.4	.....	McC—AC	M
178	+18.3606	18 8.9	+18 27	9.9	+0.063	+0.089	M0	9.4	+ .062	McC—AC	J
179	+13.3578	18 9.4	+13 53	10.3	+0.098	−0.491	M0	8.1	.....	McC—AC	J
180	+26.3215	18 11.9	+26 37	9.1	+0.343	+0.100	K8	7:	.....	Yale zone	V
181	−11.4672	18 25.4	−11 44	10.3	−0.323	−0.245	M0	8.8	+ .053	Yale zone	M
182	+45.2743	18 31.0	+45 36	10.2	+0.458	+0.363	M0	8.6	+ .081	Furuhj. 50	M
183	+79.590	18 35.9	+79 19	10.2	+0.036	+0.363	M0	7.5	+ .032	Green. Astr.	T
184*	+59.1915	18 41.2	+59 26	9.6	−1.329	+1.896	M2	11.2	+ .282	Ci 18.2456	J
185	+17.3729	18 42.5	+17 18	9.0	−0.389	−0.428	K8	7.9	+ .059	Ci 18.2463	V
186	*+16.247-80*	18 45.4	+16 28	10.5	−0.28	−0.54	M2	9.4	+ .084	Ross 160	M
187	+10.3724	18 48.1	+10 48	9.3	+0.12	−0.01	M0	8.3	.....	Wolf 1509	M
188*	+ *8.142-393*	18 48.5	+ 8 14	10.5	+0.106	−0.079	M2	9.1	.....	McC—AC	M
189	*+75.7125*	18 49.0	+75 48	10.7	−0.099	+0.176	M0	8.3	+ .006	Green. Astr.	V
190	+ 5.3993	18 50.9	+ 5 46	9.6	−0.217	−1.228	M2	9.4	+ .079	Ci 18.2475	M
191	*+75.7157*	19 2.0	+75 6	10.5	+0.092	−0.088	M0	7.9	.....	Green. Astr.	T
192*	+33.3339	19 3.6	+33 50	9.1	−0.06	+0.08	K8	7:	.....	E. B. Lex.	V
193	+24.3692	19 9.3	+24 38	10.3	+0.23	+0.23	M0	8.6	.....	Ross 735	M
194	− *2.326-200*	19 11.9	− 1 52	10.5	+0.156	+0.092	M0	7.9	.....	McC—AC	V
195	+ 0.4241	19 25.2	+ 0 17	10.4	+0.216	+0.050	M0	7.9	.....	McC—AC	V
196	+ 4.4157	19 27.4	+ 4 15	10.4	+0.51	+0.27	M0	8.1	+ .081	Ci 18.2556	V
197*	+31.3767	19 40.7	+31 41	9.4	+0.486	−0.404	M0	8.6	+ .084	*A.J.*, **50,** 119	M
198*	*+20.1080-2078*	19 56.5	+19 42	10.2	+0.185	−0.012	M0	7:	.....	McC—AC	V
199	+61.2068	20 50.3	+61 39	8.9	0.00	−0.77	M0	9.4	+ .138	Ci 18.2707	V
200*	*+39.883-87*	20 54.5	+39 30	10.2	+0.615	−0.268	M0e	8.8	+ .097	Furuhj. 54	M
201	−20.6185	21 12.0	−20 26	9.1	−0.181	−0.742	M0	7.9	+ .046	Ci 18.2770	J
202*	−13.5945	21 22.0	−13 8	9.3	+1.018	−0.263	K8	7.9	+ .048	Ci 18.2790	J
203*	+27.4120	21 31.5	+27 4	10.0	+0.44	0.00	M2	8.1	+ .085	Ci 20.1299	M
204	*+75.8347*	21 57.2	+74 55	10.5	+0.222	+0.037	M0	8.3	.....	Green. Astr.	V
205	+ *7.166-62*	22 3.5	+ 7 12	11.0	+0.25	+0.06	M0	&8	.....	Wolf 1003	W
206*	*+27.66379*	22 7.8	+27 9	10.4	−0.207	+0.554	M0	8.6	.....	McC—AC	V
207*	+56.2783	22 22.8	+56 58	9.6	−0.80	−0.34	M2	9.8	+0.258	Ci 18.2922	W
208	+ 8.4887	22 25.7	+ 8 37	9.9	+0.543	+0.158	M2	9.1	.....	McC—AC	W
209	*+24.44-11*	22 41.6	+23 58	10.9	+0.177	+0.013	M	7.9	.....	McC 321.18	M
210	− 7.5871	22 42.8	− 7 52	10.1	−0.124	+0.123	M2	8.8	.....	McC—AC	J
211	+57.2735	23 17.9	+57 5	10.1	0.00	−0.22	M2	9.4	.....	Ross 302	J
212*	−13.6464	23 40.9	−13 48	9.6	+0.204	+0.051	K8	7.7	.....	McC—AC	V

TABLE 1—*Continued*

No.	BD or AC	R.A. 1855.0	Decl. 1855.0	m_v	μ_α	μ_δ	Sp.	M_v	π	Source of Proper Motion	Observer
213.....	+28°4660	23h45m8	+28° 13′	9.8	+0.141	+0.048	M0	8.3	.....	McC—AC	V
214.....	+45.4378	23 51.2	+45 55	9.5	+0.65	0.00	M0	8.8	+0.″058	Ci 18.3143	J
215*.....	+13.5195	23 53.8	+13 9	9.9	+0.008	+0.160	M0	8.3	.....	McC—AC	V
216*.....	+44.4548	23 57.6	+44 59	10.1	+0.843	−0.151	M2	10.2	+0.089	Furuhj. 63	J
217*.....	+45.4408	23 58.1	+45 1	8.1	+0.832	−0.144	M0	8.8		Furuhj. 1	J

NOTES TO TABLE 1

McC—AC denotes a motion derived by comparing a recent McCormick plate with the AC position; McC followed by a number denotes a star in the general proper-motion program of this observatory.

Stars whose numbers are given in boldface type have previously appeared on the lists published by Mount Wilson or McDonald observers. Stars with asterisks are those for which remarks are made below.

Observer "T" is Mr. C. P. Thornton, an undergraduate student at this university, who volunteered his help in the search.

85. Groom. 34 = ADS 246 AB (Δm = 3m0).
114. Companion d = 4.″9, Δm = 2 mag.
126. Second plate: K5.
129. Second plate: M0.
131. Mount Wilson spectrum G7 belongs to the star preceding this by 68″ (letter of Dr. A. H. Joy).
142. ADS 8862 = H_u 644, Δm = 0m8; rapid binary (see *Harvard Ann. Card*, No. 703, 1945); P. Baize (*B.S.A.F.*, **54**, 148, 1940) finds 50-year period and dynamical parallax of 0.″10.
144. Double, Δm = 0m5, d = 2.″9; Humason and Joy (letter) classify the components as M2 and M3, and Kuiper (letter) as M4+ and M4+.
149. Alden finds this double; Δm = 0m3, d < 1″.
153. βGC 6869.
155. +20.°3010 is ADS 9352 = H_u 575; Δm = 0m5, d = 0.″5; (see also van de Kamp, *A.J.*, **48**, 80, 1939).
165. Close double, Δm = 0m3, d < 1″ (Kuiper, *Ap.J.*, **95**, 201, 1942).
169. Second plate: M2.
170. ADS 10675, d = 4″, Δm = 0m2.
173. Also found independently by Miller on another plate.
184. ADS 11632, Δm = 0m8, d = 17″; second plate: M5.
188. Second plate: M0.
192. Second plate: M0.
197. Double, Δm = 1m0, d = 2.″5 (van de Kamp, *Pub. A.S.P.*, **48**, 313, 1936).
198. Second plate: K8.
200. Double, Δm = 2 mag. (Kuiper, *Ap.J.*, **95**, 201, 1942).
202. Second plate: M0.
203. Second plate: M0.
206. Second plate: M2.
207. ADS 15972 = Krüger 60, Δm = 1m5.
212. Second plate: M0.
215. Double, Δm = 0m5, d = 12″; common proper motion.
216 and 217. ADS 48, F and AB; common proper motion; parallax assumed to be the same for both stars.

some mistrust. Subsequently, duplicate exposures of these 3 have become available on overlapping plates, which confirm the dwarf character of the first 2 but indicate that No. 69 is not a dwarf. In the present list it appears possible that we may have been mistaken about No. 126; on the other hand, No. 173, whose motion is very small, shows marked dwarf characteristics on two plates.

ADDITIONS TO THE FIRST LIST

Table 2 contains new estimates of spectral subclass to supersede those published in the previous paper. This brings the spectral classification of both lists to the same system. Estimates of M_v are also given in Table 2. In addition, we have listed all trigonometric parallaxes now available for these stars, the great majority of the new determinations having been made at this observatory.

Three stars of the first list were published without proper motions, which have now been measured and listed in Table 3. These are motions relative to the reference stars, of course, as are most of the other motions in the two lists. If we reduce the motion of star No. 63 to absolute by allowing for the parallactic motion of the reference stars, we obtain: $\mu_\alpha = -0.''002$, $\mu_\delta = +0.''003$; and yet the star is undoubtedly a dwarf. Further details concerning it have been published elsewhere.[3] Apparently, it will be a very near neighbor of the sun in 500,000 years.

[3] *Pub. A.S.P.*, **58**, 166, 1946.

TABLE 2

No.	Sp.	M_v	π	No.	Sp.	M_v	π	No.	Sp.	M_v	π
1*.....	M0	7:	+0".087	28.....	M0	7.9	.....	55*....	M2	8.8	+0".048
2.....	M2	10.2	.092	29.....	M0	7.5	.....	56.....	M0	7.9	.....
3.....	M0	8.6	.....	30.....	M0	8.3	+0".082	57.....	M0	8.8	.077
4.....	M2	9.4	.081	31.....	M0	7.9	.....	58.....	M0	8.3	.060
5.....	M0	8.8	.....	32.....	K8	7.7	.060	59.....	K8	8.3	.046
6*.....	M0	7.8	.029	33.....	M2	9.4	.....	60*....	M0	7.5	.....
7.....	K8	7:	.028	34*....	M2	8.8	.042	61.....	M0	7:	.055
8.....	M0	8.6	.079	35.....	M2	10.2	.174	62.....	M2	10.2	.070
9.....	M2	9.8	.168	36.....	M	8.8:	.....	63.....	M0	8.8	.083
10.....	M0	8.3	.063	37.....	M0 M0	8.8 8.8	.062	64.....	M2	9.4	.067
11.....	K8	7:	.028	38*....	M2	10.2	.120	65.....	M2	10.6	.170
12.....	M0	7.5	.068	39.....	M0	8.6	.....	66.....	K8	7.5	.017
13.....	M0	8.8	.073	40.....	M0	7.9	.....	67.....	M0	8.8	.044
14.....	M0	8.6	.060	41.....	M0	8.3	.....	68†....	M0	8.3	.033
15.....	M0	8.3	.031	42.....	M0	8.6	.....	70*....	M2	8.8	.....
16*.....	M0	9.1	.050	43.....	M0	8.8	.061	71.....	K8	6.5:	.....
17.....	M5	13:	.262	44.....	M2	9.4	.....	72*....	M0	7.5	.083
18*.....	K8	7:	.057	45.....	M2	9.4	.....	73.....	M	9:	.114
19.....	M0	7.9	.030	46.....	M2	11.2	.086	74.....	M2	9.4	.061
20.....	M2	9.4	.057	47.....	M0	8.3	.....	75.....	K8	7:	.....
21.....	M0	7.7	.037	48.....	M0	8.3	.....	76.....	M0	7.9	.033
22.....	K8	7:	.052	49.....	M2	9.4	.....	77.....	M0	8.3	.034
23.....	M0	7.9	.028	50.....	M0	8.3	.....	78*....	M0	8.1	.....
24.....	M0	7.9	.018	51*....	M2	8.8	.....	79*....	M0	7.9	.....
25.....	M0	8.8	.015	52.....	M0	8.3	.....	80.....	M2e	9.4	.155
26.....	M2	10.2	.099	53*....	M0	8.3	+0.069	81.....	M0	8.3	.....
27.....	M2	10.2	+0.078	54.....	M0	8.8	.....	82*....	M2	11.2	+0.167

*Alternate images on overlapping spectral plates usually agree as to spectral subclass; however, for the following stars, estimates from alternate (less favorably exposed) images are as indicated: 1, K5; 6, K8; 16, M2; 18, M0; 34, M0; 38, M0; 51, M0; 53, K8; 55, M0; 60, K8; 70, M0; 72, K8; 78, M2; 79, K8; 82, M0.

† Star No. 69 has been omitted from this table because a better image on an overlapping plate indicates that it is not a dwarf.

TABLE 3

Star No.	μ_α	μ_δ	Source
3.....	−0".006	+0".131	McC–AC
63.....	− .002	+ .008	McC–AC
79.....	+0.045	−0.085	McC–AC

We wish to thank Dr. Joaquin Gallo, of the Tacubaya Observatory, for kindly furnishing us with the astrographic catalogue positions of stars Nos. 3, 106, 166, and 177; these occur in Tacubaya zones for which the catalogues were not yet published at the time that we needed the positions. Also we are greatly in debt to Director H. L. Alden, of this observatory, for furnishing us with the values of many parallaxes in advance of their regular publication.

MOTIONS AND ABSOLUTE MAGNITUDES OF DWARF M STARS

A. N. VYSSOTSKY
Leander McCormick Observatory, University of Virginia
Received June 21, 1946

ABSTRACT

Approximate estimates have been made of the absolute magnitudes of all dwarf M stars thus far discovered spectrophotometrically. Table 1 gives the McCormick calibration-curve, as well as the comparison of the McCormick absolute-magnitude scale with those of the Mount Wilson and the McDonald observers.

After the motion of each star has been reduced to 10 parsecs, a solution for solar motion yields $A = 275°$, $D = +44°$, $V_\odot = 23$ km/sec. The distribution of the peculiar motions in three directions is presented graphically in Figure 1. There is a fairly well-marked asymmetry of the motions in the direction of galactic rotation for velocities considerably smaller than 63 km/sec. This is to be expected if the mass of the galaxy is rather highly concentrated toward its center.

From a discussion of the motions and spectra of a random sampling of ninth- and tenth-magnitude stars of classes M0 and later, it is found that approximately 3 per cent are dwarfs and that the percentage of stars of intermediate luminosity must be considerably smaller.

The two published lists of dwarf M stars found at this observatory on the prismatic camera plates[1,2] contain 216 objects, for which 118 trigonometric parallaxes and 214 proper motions are available. It is hoped to have perhaps twice as many of these stars in a few years, when the surveying of our plates is finished. However, a discussion of the present material is desirable at this time, in order to supplement the discussion of our general proper-motion program now being completed.

When proper motions are discussed, it is usually advantageous to know the individual stellar distances so that all the motions may be reduced to the same distance. For this purpose an attempt has been made to estimate the absolute magnitudes of our stars in the manner described in the next section and to derive their individual distances from the modulus $(m - M)$. However, if a trigonometric parallax of 0".060, or larger, was available, it has been used for the reduction in preference to the distance modulus.

LUMINOSITY CLASSIFICATION

A rapid inspection on our plates of the spectra of a number of dwarf M stars whose luminosities have been determined previously either at Mount Wilson or at McDonald indicates that the following four characteristic features are correlated with the luminosity: (1) the intensity of the *TiO* bands; (2) the intensity of λ 4227 of *Ca* I; (3) the relative intensity of the continuous spectrum immediately to the violet of λ 4227 as compared with that to the red, i.e., the strength of the "Lindblad depression"; and (4) the sharpness of the break in the intensity of the continuous spectrum at the G-band.

In a re-examination of the spectra of all 216 stars, the intensity of each of these features has been estimated on an arbitrary scale with grades from 0 to 4. Grade 4 corresponds to the greatest intensity in the first three criteria; however, in the case of the fourth, the grades were assigned in reverse order, since the sharper the break at the G-band, the higher the luminosity.

In every case all notations were removed from the plates so that the intensity estimates were made without any knowledge of the star's identity. Whenever more than one spectrum of the same star was available, independent estimates were made from each spectrum. Spectra of three dM5 stars not independently discovered at this observatory were also examined, in order to provide more estimates for stars of fainter luminosities.

[1] *Ap. J.*, 97, 381, 1943. [2] Preceding paper.

Since these are absolute-intensity estimates in uncalibrated spectra, they are, of necessity, rather rough. However, from the 105 cases in which we had more than one spectrum of the same star, it was found that intensity estimates of features 1 and 2 are to some extent complementary. Apparently, when the spectrum is located in a portion of the plate where the best focus is slightly to the violet of its normal position, the *TiO* bands appear weaker and λ 4227 appears stronger, whereas the situation is reversed when the best focus is shifted slightly to the red. Again, estimates of features 3 and 4 also tend to be complementary; for, on a plate which has a higher contrast than average, the grade assigned to feature 3 will be too large and that to feature 4 will be too small. Consequently, grade estimates for features 1 and 2 were combined, as were those for features 3 and 4.

It was possible to compare these grade estimates for 46 stars with absolute magnitudes assigned at Mount Wilson,[3] and a very satisfactory correlation was found. Thus the average residual of the plotted points from the smoothed regression of M_{MtW} on grade estimates 1 + 2, was $0^m.45$; it was $0^m.50$ when grade estimates 3 + 4 were used. In both cases the correlation is much better among the earlier types (K8 and M0) than among the M2 and M5 stars. Comparisons were also made, with absolute magnitudes

TABLE 1

I	M_{McC}	M_{MtW}	M_{McD}	I	M_{McC}	M_{MtW}	M_{McD}
6.....	7.6	7.8	.....	10.....	9.4	9.2	9.6
7.....	7.9	8.0	7.8	11.....	10.2	9.9	10.3
8.....	8.3	8.3	8.4	12.....	11.2	10.7	11.1
9.....	8.8	8.7	9.0	13.....	12.2	.....	11.9

inferred from the spectral types assigned to 42 stars by Kuiper.[4] The correlation was somewhat less satisfactory here, the corresponding average residuals amounting to $0^m.78$ and $0^m.65$, respectively.

It appeared justifiable, therefore, to add together the grade estimates of all four criteria to obtain a single luminosity index, I, which was then calibrated against absolute magnitudes by means of the 107 stars for which trigonometric parallaxes were available at that time. The resulting relation is given in Table 1, as is also the relation between the index and the absolute magnitudes on the Mount Wilson and McDonald scales. It is seen that the three are in good agreement at the bright end of the scale but that the Mount Wilson estimates of the fainter stars tend to be somewhat brighter than the other two.

Absolute magnitudes corresponding to the various observed values of I are listed in Tables 1 and 2 of the preceding paper. Intermediate values, such as 9.1, occur when estimates have been made from more than one spectrum of a star. It is evident from an inspection of the relation just given between I and M_{McC} that the estimates for absolute magnitudes fainter than $9^m.4$ are pretty rough. However, since good trigonometric parallaxes are available for most of these stars, it has not been necessary to use many of these poorer estimates. On the other hand, there are several stars for which the value of I is less than 6 and for which values of M had to be extrapolated; such estimates are followed by a colon.

[3] *Mt. W. Contr.*, No. 511, 1935.

[4] For the spectrum absolute-magnitude-curve, see *Ap. J.*, **87**, 593, 1938; for the individual spectral classifications see *Ap. J.*, **87**, 592, 1938; **89**, 548, 1939; **91**, 269, 1940; **92**, 126, 1940; **95**, 201, 307, 1942; **96**, 315, 1942; **97**, 275, 1943; **98**, 209, 1943.

SOLAR MOTION

The proper motion of each star may now be reduced to 10 parsecs. Thus, if the trigonometric parallax, π, is equal to 0".060 or larger, the star's motion is multiplied by $0''.100/\pi$. In all other cases it is multiplied by $10^{0.2(m-M)}$. Here, for uniformity, the value, M_{McC}, described in the last section, is always used.

These reduced proper motions have been combined into 42 groups, each group containing from 4 to 6 stars. Thus we have 84 observation equations, from which the following elements of solar motion are derived:

$$X = +0''.03 \pm 0''.04 , \qquad A = 275° \pm 7° ,$$

$$Y = -0.33 \pm 0.04 , \qquad D = +44° \pm 5° ,$$

$$Z = +0.33 \pm 0.04 , \qquad (h/r) = 0''.47 \pm 0''.04 .$$

Here (h/r) is the value of the secular parallax reduced to 10 parsecs; but, since most of the motions which we have used are relative, a correction must be applied to allow for the secular parallax of the reference stars, which is approximately 0".01. The correction, then, would be 0".02, since the mean factor used to reduce the observed motions to 10 parsecs was 2.0. Consequently, we find $0''.49 \pm 0''.04$ as the corrected value of (h/r); and, multiplying by 4.74, we obtain as the solar velocity,

$$V_\odot = 23 \pm 2 \text{ km/sec} .$$

PECULIAR MOTIONS

When the residuals from the solar-motion solution were computed, it was found that the 21 stars whose absolute magnitudes are the most uncertain have considerably larger residual motions than the average. These are the stars whose estimated absolute magnitudes are listed with colons in Tables 1 and 2 of the preceding paper, with the exception of the six whose trigonometric parallaxes equal or exceed 0".060. Although these 21 stars were used with full weight in the solution for the solar motion where they introduce no systematic error, they have been omitted from the computations concerning the velocity ellipsoid, since they would exaggerate the dispersions. However, they have been included, with distinguishing designation, in Figure 1.

The dispersions along the axes of the velocity ellipsoid were computed in the same manner as in a previous paper,[1] except that in this case all the motions are reduced to 10 parsecs. Briefly, the dispersion along any axis is derived from the appropriate peculiar-motion components of stars whose positions in the sky are 60° or more from the vertex of the axis. Thus there were 112 stars suitably situated to contribute to the determination of the dispersion along the *a*-axis, there were 98 for the *b*-axis and 81 for the *c*-axis.

Figure 1 shows the frequency distribution of the components parallel to each of the axes. In the case of the *a*-axis it appears that there are relatively too many large motions for a strictly Gaussian distribution. As to the distribution parallel to the *b*-axis, it seems to be even less Gaussian, for a fairly definite asymmetry is apparent. Bearing in mind that a motion of 1 second at 10 parsecs corresponds to 47 km/sec, we find that the largest component in the direction of the galactic rotation is 39 km/sec, belonging to star No. 146, whereas there are 8 stars with fairly well-determined motions which are larger than 40 km/sec in the opposite direction, the largest belonging to Nos. 110 and 147. Two additional large motions in this direction are less well determined, the largest amounting to 166 km/sec for star No. 131.

It might possibly be supposed that these ten stars are not representative dwarfs but very underluminous stars whose absolute magnitudes have been incorrectly estimated and that a very large parallactic motion has been mistaken for the *b*-component of the

peculiar motion. As it happens, however, it is possible to refute this supposition immediately, since trigonometric parallaxes are fortunately available for 8 of the 10 stars. Although only three of the parallaxes exceed 0".060, still they convincingly confirm the motions as derived; the average velocity component of the 8 stars as computed from their parallaxes amounts to 76 km/sec, whereas the average value originally computed exceeds this amount by less than 1 km/sec.

Figure 1 seems to indicate that the asymmetry along the *b*-axis does not appear suddenly at 63 km/sec but rather gradually among considerably smaller velocities. As will be

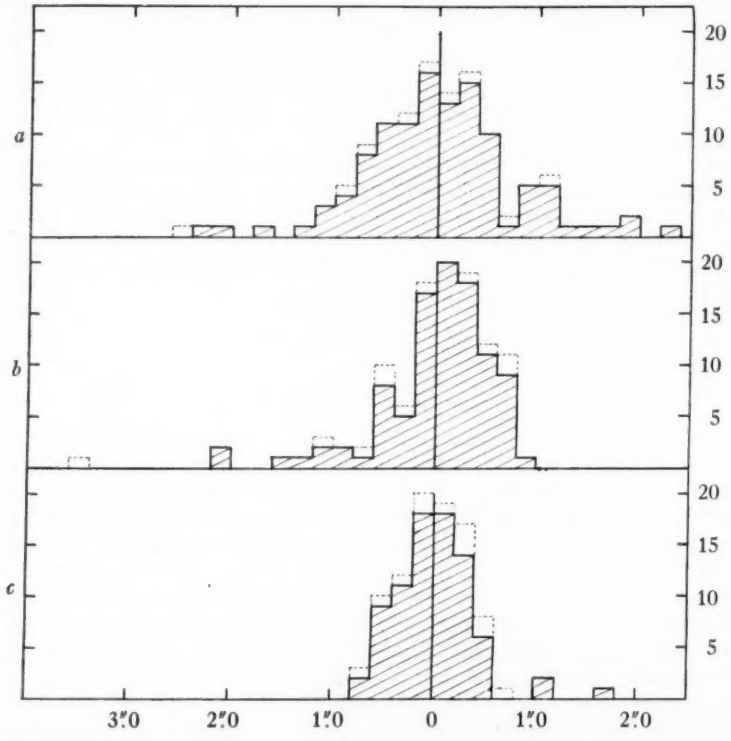

FIG. 1.—Showing the distribution of reduced peculiar motions: (*a*) in the direction of the galactic center (*right*) and anticenter (*left*); (*b*) in the direction of the galactic rotation (*right*) and in the opposite direction (*left*); (*c*) in the direction of the north galactic pole (*right*) and of the south pole (*left*). Dashed outlines indicate motions of lower weight.

reported elsewhere, a similar asymmetry has been found in the motions of the G dwarfs of our general proper-motion program. This lends considerable additional weight to the evidence[5] that the stellar motions in our vicinity indicate a relatively high concentration of mass toward the galactic center; for such a distribution of velocities along the *b*-axis, in which the asymmetry is apparent among velocities well below 63 km/sec, is what is to be expected when the gravitational attraction toward the galactic center varies approximately with the inverse square of the distance, a situation which is illustrated in the Bottlinger diagram.[6] The fact that the dwarf M stars discussed here are a rather homo-

[5] *Monthly Astronomical Newsletter*, September, 1944, p. 2.

[6] *Veröff., U.-Sternw. Berlin-Babelsberg*, Vol. **10**, No. 2, 1933.

geneous group and that they are fairly representative of many of our nearest neighbors gives added importance to this point.

The dispersions along the axis of the velocity ellipsoid have been computed in two ways. Following the procedure outlined in an earlier paper,[1] we find:

$$\sigma_a = 34 \text{ km/sec} ; \quad \sigma_b = 23 \text{ km/sec} ; \quad \sigma_c = 16 \text{ km/sec} .$$

However, since there is an excess of large peculiar motions over those expected in a Gaussian distribution, it is of interest to compute the dispersions by squaring the individual components (instead of multiplying the square of the mean of the components by $\pi/2$). This variation in the procedure yields

$$\sigma_a = 37 \text{ km/sec} ; \quad \sigma_b = 25 \text{ km/sec} ; \quad \sigma_c = 17 \text{ km/sec} .$$

A RANDOM SAMPLING OF FAINT M STARS

We may now investigate the relative frequency of giants, intermediates, and dwarfs among ninth- and tenth-magnitude M stars selected at random. For this purpose we find material in the general proper-motion program just being completed at this observatory. The program includes 782 small sample regions scattered from the north pole to declination $-25°$, comprising a total area of just about 400 square degrees. The total number of stars classified as M0 or later in this area amounts to 89 in the ninth-magnitude group (8^m5–9^m4) and to 131 in the tenth-magnitude group (9^m5–10^m4). One star of the first group and 6 of the second are recognized as dwarfs by the characteristic features of their spectra. When these dwarfs are excluded, the secular parallax of the remaining 88 stars of ninth magnitude is found to be $0''.006 \pm .''001$, and that of the 125 tenth-magnitude stars, $0''.004 \pm .''001$. In the case of such very small secular parallaxes the influence of systematic errors of the fundamental reference system may be considerable; however, if we disregard this possibility, we find a value of -0^m5 as the mean absolute magnitude of the first group and -0^m3 as that of the second. This would lead us to infer that the number of M stars of intermediate luminosity must be relatively small among stars of ninth and tenth apparent magnitudes. Since the matter is of some importance, we may approach it from a different angle.

In the first place, it is not impossible that the spectra of intermediate M stars resemble those of dwarfs, in which case we should be able to distinguish certain of them by their unexpectedly small parallaxes, particularly in the case of the M2 stars. Now there are 57 M2 stars in our two lists, and parallaxes have been obtained for 40 of them; however, only 3 of these could possibly be suspected of being intermediates on the basis of their parallaxes. Even so, they may rather more probably be normal dwarfs. In the case of the K8 and M0 stars the differentiation cannot be so definite, but there is not one which, at present, can be categorically identified as an intermediate.

On the other hand, if the intermediate spectra do not resemble dwarf spectra, then it will be worth while to look for intermediate motions among the 220 M stars of our general proper-motion program. The frequency distribution of the total motions of these stars is indicated in the second column of Table 2. Here the 7 dwarfs have the seven large motions. For comparison the next column gives the distribution of the total (unreduced) motions of the 143 stars in our two lists of dwarf M stars which are classified as M0 or later and which are in the same range of apparent magnitudes as the 220 stars of the random sampling, namely, 8^m5–10^m4. It is seen that the 7 dwarfs of the random sample have motions comparable with the motions in the two published lists of dwarf M stars; but, aside from these, there are no motions in the random sample greater than $0''.045$. The question is: How many intermediate stars are in this group with small motions?

To find the answer to this question we first investigate the distribution of total motions that we might expect to find among a group of M giants at a distance of approximately 1,000 parsecs. If we disregard the errors of measurement, these will have a dis-

persion about 0".005, but the distribution will not be strictly Gaussian because the distribution of the parallactic motions is not at all Gaussian. However, the dispersion caused by errors of measurement is approximately twice as large as that of the true motions, for the probable error of measurement averages about 0".0065. The combined effect, then, of the true motions and the errors will be not very different from a Gaussian distribution with a probable error of about 0".0075. Accordingly, the fourth column of Table 2 gives the computed frequencies of the "motions" of 213 stars in such a two-dimensional Gaussian distribution. The agreement between the observed and the computed distributions is only fair, but, as mentioned previously, the true distribution is known to be not strictly Gaussian.

TABLE 2

Total Proper Motion	Distribution of Total Motions in:			Observed *minus* Computed
	Random Sample	List of M Dwarfs	Gaussian Distribution	
0".000–0".004	16	1	20	− 4
0.005–0.009	57	.....	51	+ 6
0.010–0.014	53	.....	56	− 3
0.015–0.019	31	.....	44	−13
0.020–0.024	23	.....	25	− 2
0.025–0.029	18	1	12	+ 6
0.030–0.034	10	.....	4	+ 6
0.035–0.039	4	.....	1	+ 3
0.040–0.044	1	.....	.....	+ 1
0.045–0.049	.....	.....	.....	.....
0.050–0.059	.....	1	.....	.....
0.060–0.069	.....	.....	.....	.....
0.070–0.079	.....	1	.....	.....
0.080–0.089	.....	2	.....	.....
0.090–0.099	.....	2	.....	.....
0.100–0.199	3	33	.....	.....
0.200–0.399	.....	33	.....	.....
0.400–0.799	3	42	.....	.....
0.800–1.599	1	20	.....	.....
1.600–3.199	.....	5	.....	.....
3.200–6.399	.....	2	.....	.....
Total	220	143	213	0

The excess of the frequency of the observed motions over those computed between 0".025 and 0".045 may possibly be attributed to the presence of subgiants but would hardly indicate the presence of many intermediate M stars; for, if we assume that the absolute magnitude of the intermediates averages about $+4^m.5$, it may be shown that nearly half of them would be expected to have motions between 0".045 and 0".100; but there are no observed motions at all in this interval. We conclude, then, that among the 220 stars of the random sample there are probably not more than 2 or 3 with absolute magnitudes between $+3^m.0$ and $+6^m.0$; and this conclusion is in agreement with the inference from the secular parallaxes mentioned at the beginning of this section.

I am indebted to Dr. E. T. R. Williams for valuable discussion and suggestions in connection with this work. My thanks are also due to Miss Caroyl Beddow and to Miss Dorothy Watson for help in the computations.

ON THE INTERSTELLAR REDDENING IN THE REGION OF THE NORTH POLAR SEQUENCE AND THE NORMAL COLOR INDICES OF A-TYPE STARS

W. W. MORGAN AND W. P. BIDELMAN
Yerkes Observatory
Received July 17, 1946

ABSTRACT

The long base-line colors of Stebbins and Whitford, when used in conjunction with spectral types on the system of the Yerkes spectral atlas, indicate that the white stars of the North Polar Sequence brighter than the seventh magnitude are unaffected sensibly by interstellar reddening. This confirms the earlier result of Keenan and Babcock. The NPS stars are used to determine normal colors for classes A0–F0, and it is found that the unreddened color for class A0 on the international system is in the neighborhood of −0.04 mag. This is about 0.10 mag. less blue than the value which has been in general use.

The colors of the "metallic-line" stars ζ Lyrae A and NPS 4 show that the spectral type determined from the metallic lines corresponds to the intrinsic color of these peculiar objects; the low intensity of the K line appears to be the most abnormal feature.

I. NEW EVIDENCE ON THE PROBLEM OF THE REDDENING OF THE BRIGHTEST STARS OF THE NORTH POLAR SEQUENCE

Undoubtedly the most accurate colors which have yet been determined for stars of various spectral types are those which have been obtained by Stebbins and Whitford in their recent "Six-Color Photometry of Stars."[1] Their work includes the brightest white stars of the North Polar Sequence, together with colors on the same system for some of the A-type stars nearest the sun. Since, in addition to being of very high internal accuracy, the colors of Polar Sequence stars and near-by A dwarfs are on the same system, no reduction of any kind is necessary for a comparison of the two groups; the only additional data needed are accurate spectral types on an identical system for Polar Sequence stars and comparison stars.

It should be emphasized that the accidental and systematic accuracy of the spectral types is as important in the determination of small color excesses as is the precision of the color measures themselves. The spectral types of the brighter Polar Sequence stars were determined some time ago by Keenan[2] on a system which is identical with that of the Yerkes *Atlas of Stellar Spectra*.[3] Since a number of the unreddened stars measured by Stebbins and Whitford are included in the Yerkes *Atlas*, it is possible to make a direct comparison between the colors and spectral types of the A stars in the Polar Sequence and in the general neighborhood of the sun, without making systematic reductions of any kind.

The standard stars used are included in Table 1; the types in every case are those published in the Yerkes spectral atlas. The color equivalent listed is the "Violet minus Infrared," taken from Stebbins and Whitford's paper; only stars observed at least twice are included. The last column gives the estimated distance of the comparison stars from the sun from trigonometric parallaxes and recent Yerkes spectroscopic parallax investigations. The only star in the list for which there appears to be any question as to whether its observed color represents its intrinsic color is β Persei, the B8 standard. The most distant star among the standards is γ Ursae Minoris, which is located at a distance of

[1] *Ap. J.*, **102**, 318, 1945.

[2] *Ap. J.*, **91**, 113, 1940.

[3] Morgan, Keenan, and Kellman, *An Atlas of Stellar Spectra*, 1943.

the order of 70 parsecs; the other comparison stars are all situated within 50 parsecs of the sun.

The Polar Sequence stars of early type (except NPS 4) which were measured by Stebbins and Whitford are listed in Table 2. The columns give the name of the star, the spectral type according to Keenan, and the V − I color index with the number of observations. The star NPS 4 has been omitted because it has a "metallic-line" spectrum, that is, the type from the K line is considerably earlier than that from the metallic lines.

TABLE 1

COLOR STANDARDS, B8–dG0

Star	m	Sp$_{MKK}$	V−I	Distance (Pc)	Notes
β Per	2.2	B8 V	−1.88 (2)	30	1
α Lyr	0.1	A0 V	−1.85 (4)	8	2
γ UMi	3.1	A3 II–III	−1.54 (2)	70	2,3
γ Boo	3.0	A7 III	−1.32 (2)	25	.....
α Aql	0.9	A7 V	−1.30 (4)	5	2
α Cep	2.6	A7 V	−1.24 (2)	13	.....
ζ Lyr B	5.9	F0 V	−1.08 (3)	40	.....
ϵ Cep	4.2	F0 V	−1.07 (18)	20	.....
β Cas	2.4	F2 III	−0.97 (2)	14	.....
78 UMa	4.9	F2 V	−0.86 (2)	25	.....
β CVn	4.3	G0 V	−0.30 (2)	9	.....
β Com	4.3	G0 V	−0.37 (2)	8	.....

NOTES

1. The normal color for main-sequence B8 stars is probably between −1.90 and −1.97, as found from other stars whose spectral types have recently been redetermined at Yerkes.

2. A number of spectrograms of different dispersions show that there can be no doubt that the spectral type of Altair is considerably later than that of Vega and that the type of γ Ursae Minoris is intermediate between the two. The spectral lines of Altair and γ Ursae Minoris are very broad and ill defined; this tends to make them appear faint to the eye on spectrograms of high dispersion.

3. The distance is uncertain because of the incomplete state of the calibration of spectroscopic absolute magnitudes for early A stars situated above the main sequence.

TABLE 2

COLORS OF WHITE POLAR SEQUENCE STARS

Star NPS	Spectrum (Keenan)	V−I	Star NPS	Spectrum (Keenan)	V−I
1	A2	−1.73 (10)*	6	A3	−1.23 (3)
2	B9	−1.84 (2)	2s	F2	−0.95 (2)
3	F0	−1.17 (3)	3s	F4	−0.70 (6)
5	A5	−1.56 (2)			

* There are slight differences in the values for some of the North Polar Sequence stars which are given in Tables 3 and 10 of Stebbins and Whitford's paper. The values from Table 3 have been listed here. NPS 4 has been omitted.

The stars in Tables 1 and 2 are plotted in Figure 1. It is seen that, with the exception of the faintest of the Polar Sequence stars—NPS 6—there is no evidence for any appreciable interstellar reddening for the bright Polar Sequence stars. The line has been drawn at the approximate position at which the Polar Sequence stars would be located if they had undergone an interstellar reddening of 0.1 mag. on the international system; this would correspond to about 0.3 mag. on the V − I scale, according to the conversion factor mentioned by the photoelectric observers.

Recent observations at Yerkes confirm Keenan's spectral type for NPS 6 and indicate that it is probably located slightly above the main sequence, with $M \sim 0.5$. This

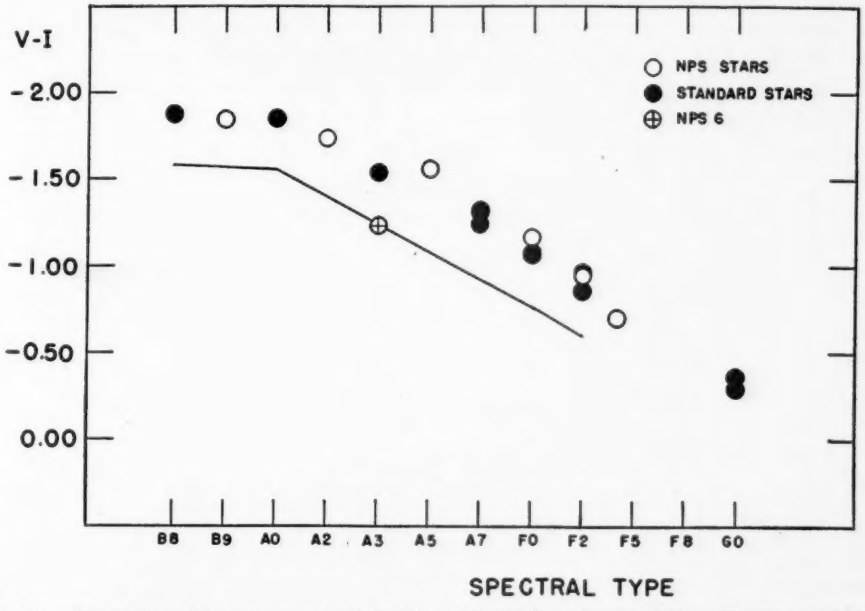

FIG. 1.—The relationship between color (Stebbins, Whitford) and spectral type (Keenan, and Yerkes spectral atlas). The open circles are the brightest white stars of the North Polar Sequence; the crossed circle is NPS 6; filled circles represent standard stars whose spectral types are published in *An Atlas of Stellar Spectra*. The "metallic-line" star NPS 4 is not plotted. The line is drawn at the approximate position at which stars reddened 0.1 mag. on the international system would lie.

would make it probably the most distant of the stars listed, with a distance of around 200 parsecs.

The result that selective absorption first becomes appreciable at distances of about 200 parsecs in the region of the North Polar Sequence was arrived at by Keenan and Babcock[4] from a combination of their spectral types with the colors determined earlier by Stebbins, Huffer, and Whitford.[5] The present investigation, which has the advantage of colors of longer base line and a better selection of standard stars, confirms the results of Keenan and Babcock; for the white Polar Sequence stars brighter than the seventh magnitude there seems to be no evidence of selective absorption effects. The accuracy of the long base-line colors and spectral types, the directness with which the comparison can be made, and the proximity of the standard stars to the sun make this result seem conclusive.

The number of stars plotted is small; in spite of this, the standard stars define a

[4] *Ap. J.*, 93, 64, 1941. [5] *Ap. J.*, 94, 215, 1941.

color–spectral-type relationship with considerable accuracy. We have purposely limited the stars in Table 1 to unreddened objects for which types have been published in the Yerkes spectral atlas. An investigation now in progress indicates that the long base-line colors and the more accurate spectral types now being determined confirm the conclusion reached by one of us some years ago[6]—that, if effects of interstellar reddening and occasional spectral peculiarities are allowed for, the colors of the stars are uniquely defined by their spectral types and absolute magnitudes. For the O and B stars and for the supergiants the complication of interstellar reddening is very serious; it is doubtful whether any northern star earlier than type B3 can be considered entirely unaffected by interstellar reddening.

Table 3 lists the standard stars of classes B3–G2 for which there are at least two observations of color and which are considered to be sensibly unreddened. No supergiants or peculiar stars have been included. The star η Ursae Majoris is the nearest of the northern early B stars; its distance is probably not greater than 30 parsecs. The columns are the same as in Table 2.

TABLE 3

COLOR STANDARDS B3–G2

Star	Sp_{MKK}	V−I	Star	Sp_{MKK}	V−I
η UMa	B3 V	−2.40 (2)	α Aql	A7 V	−1.30 (4)
ν And	B5 V	−2.23 (2)	α Cep	A7 V	−1.24 (2)
τ Her	B5 IV	−2.31 (2)	ζ Lyr B	F0 V	−1.08 (3)
18 Tau	B7 V	−2.06 (2)	ϵ Cep	F0 V	−1.07 (18)
β Per	B8 V	−1.88 (2)	β Cas	F2 III	−0.97 (2)
27 Tau	B8 III	−1.97 (2)	78 UMa	F2 V	−0.86 (2)
ω^2 Aqr	B9	−1.88 (2)	HR 5110	F4 III	−0.62 (2)
2 Cet	B9	−1.92 (2)	31 Com	F8 II–III	−0.13 (2)
ι CrB	A0	−1.94 (2)	HR 7955	F8 V	−0.42 (2)
α Lyr	A0 V	−1.85 (4)	χ Her	F9 V	−0.31 (2)
69 Her	A2	−1.66 (2)	β CVn	G0 V	−0.30 (2)
γ UMi	A3 II–III	−1.54 (2)	β Com	G0 V	−0.37 (2)
γ Boo	A7 III	−1.32 (2)	HR 483	G2 V	−0.24 (2)

The color standards are plotted in Figure 2; the star 31 Comae is omitted because late F giants are intrinsically reddened, relative to main-sequence stars. It is seen that the stars listed define a spectrum-color relationship similar to that found from the smaller number of standards used in Figure 1.

II. THE NORMAL COLOR INDICES FOR A-TYPE STARS ON THE INTERNATIONAL SYSTEM

We may now derive normal color indices for classes A0–F0, if we assume that the colors of the six stars listed in Table 4 are normal for their spectral types. These stars have been observed many times, and their colors on the international system are known with considerable accuracy. In Table 4 we list three sets of color indices: (1) the values given in *Transactions of the International Astronomical Union*, **1**, 69, 1922; (2) the colors on the international scale derived by Stebbins and Whitford[7] in 1938 from a comparison of their photoelectric colors with the revised color indices given by Seares[8] in the same year; and (3) the 1945 values resulting from the most recent revision of the colors of these stars by Seares.[9]

[6] *Ap. J.*, **87**, 460, 1938.

[7] *Ap. J.*, **87**, 237, 1938.

[8] *Ap. J.*, **87**, 257, 1938.

[9] *Ap. J.*, **101**, 15, 1945.

The relationship of color index to spectral class for each of these three determinations is shown in Figure 3. The straight line drawn for the 1945 series is the result of a least-squares solution; the 1938 curve was drawn freehand, while that for the 1922 series represents a quadratic least-squares solution.

Although the number of stars is small, the accuracy of the observational data is high, and no reductions are necessary to derive normal colors for the various spectral subdivisions; the only assumption necessary is that effects of selective absorption are negli-

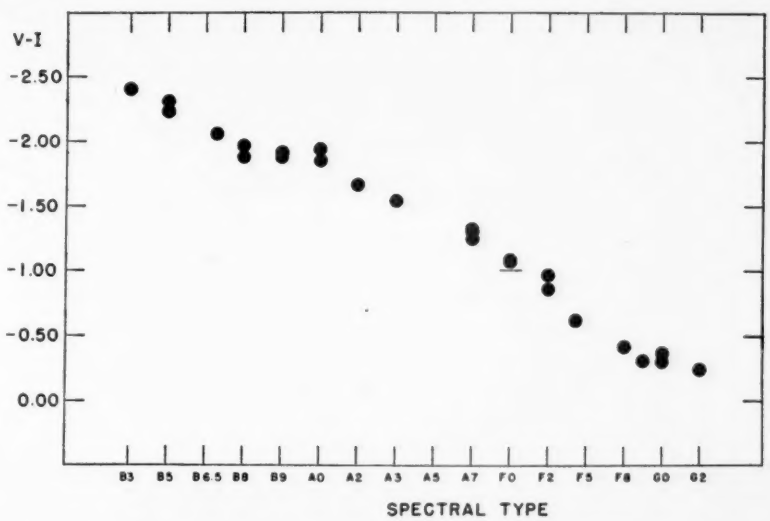

FIG. 2.—The relationship between color (Stebbins, Whitford) and spectral type (recent determinations at Yerkes on the system of the spectral atlas) for unreddened stars of luminosity classes III–V in the spectral range B3–F5. Main-sequence stars are also plotted for types F8–G2. Only stars having at least two observations for color have been included. The spacing of the types on the abscissa has been arranged so that equal intervals correspond approximately to equal accuracy in the determination of the spectral types.

TABLE 4

COLOR INDICES OF POLAR SEQUENCE STARS

Star NPS	Spectrum (Keenan)	C.I. 1922	C.I. 1938	C.I. 1945	Star NPS	Spectrum (Keenan)	C.I. 1922	C.I. 1938	C.I. 1945
1.....	A2	+0.03	+0.03	+0.03	5.....	A5	+0.01	+0.05	+0.03
2.....	B9	−0.04	−0.08	−0.11	2s.....	F2	+0.17	+0.21	+0.15
3.....	F0	+0.22	+0.10	+0.18	3s.....	F4	+0.29	+0.29	+0.23

gible. The colors obtained are given in Table 5. The normal color on the international system for class A0 is therefore probably between −0.02 and −0.05. If spectral class A2 were used for zero point, the normal color index could also be considered zero.

It should be emphasized that these normal colors apply only to spectral types on the system of the Yerkes spectral atlas; this system is based on the HD types for the brightest stars. In the case of the types listed by Stebbins and Whitford[10] there are

[10] *Ap. J.*, **102**, 318, 1945.

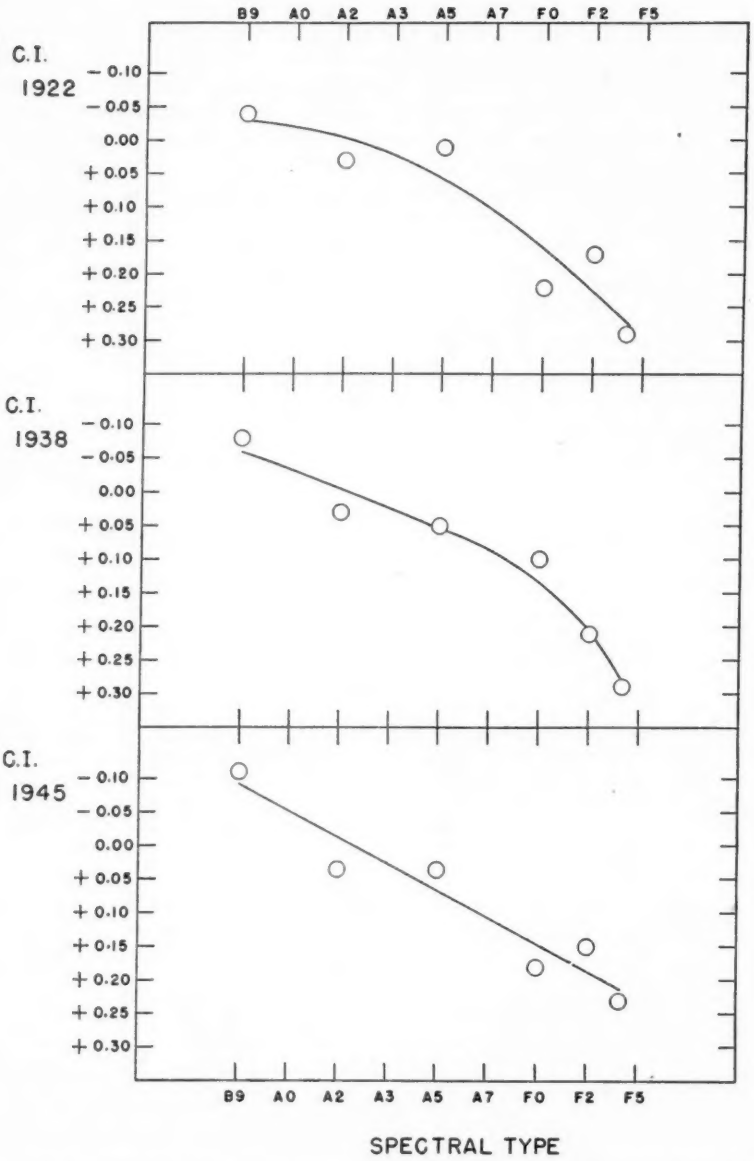

FIG. 3.—The relationship between color index (international system) and spectral type (Yerkes spectral atlas system) for the unreddened stars of the Polar Sequence. NPS 4 has been omitted because of the composite nature of its spectrum. The three diagrams correspond to three sets of values for the color indices.

marked differences from the types in Table 1. In Figure 4 the types listed by the photoelectric observers are plotted for the same stars included in Figure 1. There is an indication of a negative color excess for the Polar Sequence stars when the spectral types listed by Stebbins and Whitford are used.

TABLE 5

NORMAL COLORS ON INTERNATIONAL SYSTEM FOR A0–F0 STARS

Spectral Type MKK	C.I. from 1922 Values	C.I. from 1938 Values	C.I. from 1945 Values	Spectral Type MKK	C.I. from 1922 Values	C.I. from 1938 Values	C.I. from 1945 Values
A0.....	−0.02	−0.03	−0.05	A5.....	+0.06	+0.05	+0.07
A2.....	0.00	0.00	−0.01	A7.....	+0.10	+0.09	+0.11
A3.....	+0.02	+0.02	+0.03	F0.....	+0.16	+0.13	+0.15

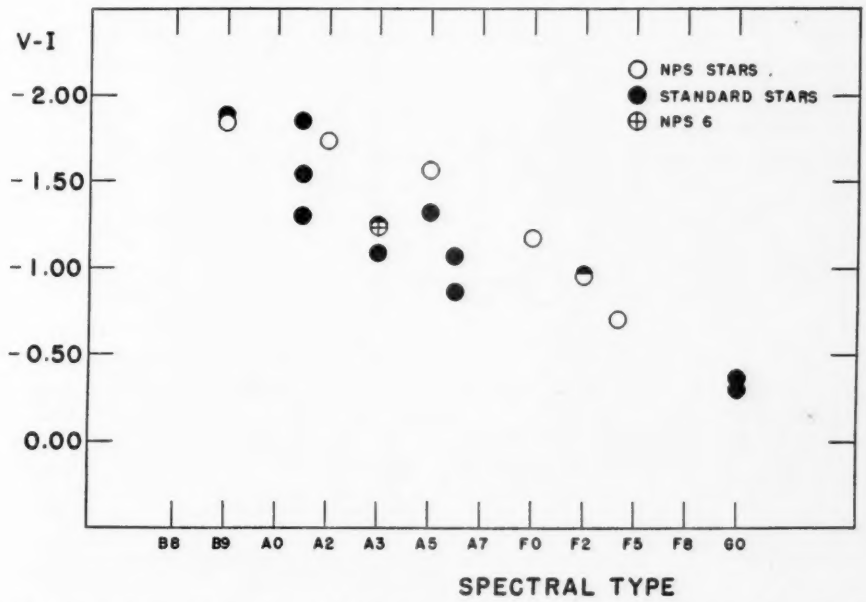

FIG. 4.—The relationship between color (Stebbins, Whitford) and spectral type (tabulated by Stebbins and Whitford). The stars and notation are the same as in Fig. 1.

III. THE COLOR OF THE METALLIC-LINE A STARS ζ LYRAE A AND NPS 4

The spectrum of NPS 4 closely resembles that of ζ Lyrae A; in each case the K line is abnormally weak in comparison to the many metallic lines present. The spectral type from the K line is about A3, while the strength of the metallic lines indicates a type of around A7. The two stars are plotted with respect to the standards of Table 1 in Figure 5. The colors appear to correspond to the metallic-line type rather than to the type from the K line. This conclusion is confirmed from colors of other metallic-line stars, and it seems definite that the type derived from the metallic lines should be used for stars of this peculiar class in investigations of color temperature and interstellar reddening.

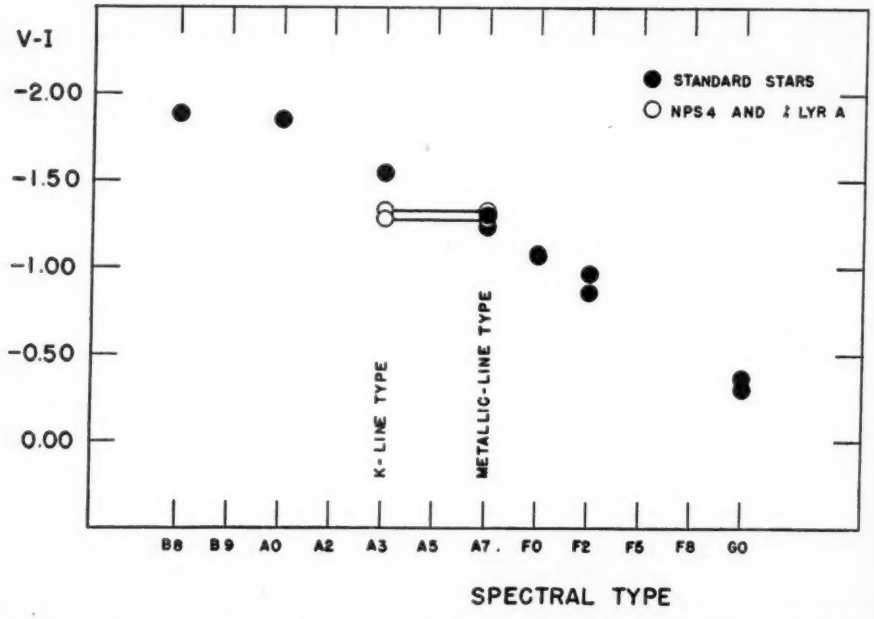

FIG. 5.—The colors of the "metallic-line" stars ζ Lyrae A and NPS 4. The spectral types are on the system of the Yerkes spectral atlas. It is seen that the colors correspond to the type from the metallic lines; if the K line were used for determining the spectral type of these stars, a spurious reddening effect could be introduced. The distance of ζ Lyrae A is in the neighborhood of 40 parsecs; that of NPS 4 is of the order of 80 parsecs.

SPECTROGRAPHIC OBSERVATIONS OF FOURTEEN ECLIPSING BINARIES*

OTTO STRUVE
McDonald and Yerkes Observatories
Received June 15, 1946

ABSTRACT

The spectra and the velocity-curves of the following stars have been determined: AQ Cas, X Tri, ST Per, RS Cep, DN Ori, RW Gem, XZ Pup, RX Hya, T LMi, WW Cyg, SW Cyg, W Del, TW Lac, and Y Psc. Bright lines of *H* were found in RS Cep, SW Cyg, W Del, and DN Ori. The absorption lines of AQ Cas show remarkable, and as yet unexplained, variations in the intensities of the absorption lines of *H* and *He* I. A statistical discussion of all eclipsing variables with $\Delta m_1 \geqslant 1.4$ mag. shows that their mass ratios m_1/m_2 are, on the average, of the order of 5.

This paper is a continuation of earlier work on the spectra and velocity-curves of eclipsing variables.[1] As in the preceding paper, the principal purpose of the work was to find new systems whose spectra have bright *H* lines during the primary eclipse. This aspect of the problem has already been discussed elsewhere,[2] and the amount of informa-

TABLE 1*

THE OBSERVING PROGRAM

No.	Star	1945		Period (Days)	Char.	Magnitude			*D*	*d*	Sp.	Remarks	No. of Plates
		a	*δ*			*M*	A_1	A_2					
1.....	AQ Cas	1h15m30s	+62° 5!7	11.72	A	10.0	1.0	0.3	47h	10h	.....	Long *P*; sec?	28
2.....	X Tri	1 57 25	+27 37.1	0.97	A	8.8	2.2	.2	4.3	0.2	A3a	Deep total; var *P*?	42
3.....	ST Per	2 56 35	+38 58.1	2.65	A	9.2	2.2	0	8.7	0	A	Total; sec? Sm *k*? Br † dense?	30
4.....	RS Cep	4 56 24	+80 10.0	12.42	A	10.2	1.7	....	9.6	.....	A	Short ecl; long total; sec?	54
5.....	DN Ori	5 57 26	+10 13.2	12.97	A	8.9	1.4	0	<36.	7.9	A	*P* to be halved? sec? *D*? *d*?	45
6.....	RW Gem	5 58 08	+23 08.8	2.87	A	9.6	2.0	.2	12.0	1.6	B8	Total	33
7.....	XZ Pup	8 11 10	−23 47.2	2.19	A	7.4	3.4	?	10.5	0	A0	Vis range?	48
8.....	RX Hya	9 03 00	− 8 02.6	2.28	A	9.0	2.7	.1	8.2	0	A2	Good light-curve	35
9.....	T LMi	9 45 13	+33 32.3	3.02	A	10.2	2.4	0	8.4	0	A	Deep; var *P*; A and K tp	30
10.....	WW Cyg	20 02 10	+41 26.1	3.32	A	9.8	3.7	.1	12.0	0.7	A2	Deep total; var *P*; sec?	37
11.....	SW Cyg	20 05 15	+46 08.2	4.57	A	9.3	2.5	....	11.7	2.0	A2	Deep total; A and K; † var *P*	37
12.....	W Del	20 35 10	+18 05.7	4.81	A	9.9	2.2	0.1	12.3	2.1	A	Deep total; var *P*	36
13.....	TW Lac	22 28 15	+54 21.2	3.04	A	11.5	1.8	....	8.0	3.0	.....	Deep total?	29
14.....	Y Psc	23 31 37	+ 7 37.1	3.77	A	9.2	3.0	....	>10.	1	A2	Range? *d*?	36

* The data for *M*, A_1, A_2, *D*, *d*, and Sp. are from H. Schneller, *Kat. u. Eph.*, 1941 (*Kl. Veröff. Berlin-Babelsberg*, No. 22).
† The remarks are from R. S. Dugan, *Contr. Princeton U. Obs.*, No. 15, 1934.

tion collected is sufficient for an understanding of the phenomena involved. The stars were selected from Dugan's *Finding List*,[3] and are listed in Table 1. Nearly all spectrograms were obtained on 103*a*-O film with the *f*/2 Schmidt camera and two glass-prism spectrographs attached to the 82-inch reflector. The dispersion was 76 A/mm at $H\gamma$; the slit width was 0.10 mm, which was projected to 0.018 mm on the film. A few spectro-

* *Contributions from the McDonald Observatory, University of Texas*, No. 126.

[1] *Ap. J.*, **103**, 76, 1946. [2] *Observatory*, **66**, 208, 1946 [3] *Contr. Princeton U. Obs.*, No. 15, 1934.

grams of WW Cyg taken during the total eclipse were obtained with the $f/1$ Schmidt camera, giving a dispersion of 152 A/mm at $H\gamma$. In a few cases the slit was made slightly wider, up to 0.2 mm. The length of the slit was usually between 2 and 3 mm, which gave a width of between 0.36 and 0.50 mm on the films. I am indebted to Dr. W. H. Hiltner for several of the spectrograms used in this work.

The photometric elements used for computing the phases are given in Table 2. Several sets of these elements no longer predict the eclipses accurately. These cases are discussed separately for each star. Photometric orbits have been determined for 10 of the 14 stars. These are listed in Table 3, which has been taken from S. Gaposchkin's data.[4] The star lines used for the determination of the radial velocities are given in Table 4. Table 5 gives the radial velocities, and Table 6 the approximate spectrographic elements of the orbits. In the following paragraphs we discuss each star separately.

TABLE 2*

PHOTOMETRIC ELEMENTS

No.	Star	Epoch JD	Period	Remarks†
1	AQ Cas	2426282.43	$11^d.7203$	
2	X Tri	2422772.78708	0.971535	*a*
3	ST Per	2419030.5038	2.6483615	
4	RS Cep	2417140.469	12.4204	
5	DN Ori	2425502.58	12.9652	
6	RW Gem	2418302.654	2.865500	
7	XZ Pup	2425850.9434	2.192306	
8	RX Hya	2419819.4890	2.2815954	
9	T LMi	2423856.323	3.0199007	
10	WW Cyg	2416981.299	3.317700	*b*
11	SW Cyg	2418440.758	4.5728184	
12	W Del	2418183.243	4.8060	*c*
13	TW Lac	2424387.334	3.03754	
14	Y Psc	2425495.522	3.765903	

* The phases were computed without the use of the remarks. The elements are from H. Schneller, *Kat. u. Eph.*, 1941 (*Kl. Veröff. Berlin-Babelsberg*, No. 22).

† Remarks: $a = +0^d.00237 \sin 0°.1309E$; $b = +0^d.025 \sin 0°.085\,(E + 360°)$; $c = -0^d.6 \cdot 10^{-5}E^2$.

TABLE 3

PHOTOMETRIC ORBITS

No.	Star	P	A_1	A_2	Ecl.	L_b	r_b	k	i	γ	Sol.	Sp_b	Sp_γ	Reference*
2	X Tri	$0^d.97$	2.4	0.2	t	0.87	0.29	0.87	89°	8.6	D	A3	(G5)	13, 80, 37 38, 52
3	ST Per	2.65	2.2	.....	t	.87	.13	.45	80	33.0	D	A	(K0)	19
4	RS Cep	12.42	1.7	.....	t	.78	.08	.41	88	22.0	D	A	(G2)	70
6	RW Gem	2.86	2.0	.1	t	.84	.21	.73	90	10.0	D	A	(F9)	18, 70
8	RX Hya	2.28	2.7	.05	tp	.93	.20	.79	86	20.0	.....	A2	(K0)	13
9	T LMi	3.02	2.5	0.04	tp	.96	.22	.93	87	28.2	D	A5	(K3)	51
10	WW Cyg	3.32	3.7	.....	t	.97	.17	.58	82	86.0	D	A2	(K4)	18, 70, 25
11	SW Cyg	4.57	2.7	.....	t	.91	.17	.65	87	24.0	D	A2	(G9)	70, 20
12	W Del	4.81	2.7	.....	t	.92	.17	.71	86	22.0	D	A	(G7)	70, 61, 18
14	Y Psc	3.77	3.4	.....	tp	0.97	0.18	0.77	86	67.0	D	A2	(K1)	20

* 13: Dugan, *Princeton Contr.*, No. 14, 1933; 80: M. B. Shapley, *Harvard Bull.* No. 840, 1926; 37: Kopal, *A.N.*, **247,** 118, 1932; 38: *Krat. Engelhardt Obs. Kasan Bull.*, No. 3, 1934; 52: Modest and Martin, *Ap. J.*, **79,** 361, 1934; 19: Fetlaar, *B.A.N.*, No. 209, 1930; 70: H. Shapley, *Princeton Contr.*, No. 3, 1915; 18: Fetlaar, *B.A.N.*, No. 108, 1926; 51: McDiarmid, *Princeton Contr.*, No. 7, 1921; 25: Gaposchkin, *Veröff. Berlin-Babelsberg*, Vol. **9,** Part V, 1932; 20: Fetlaar, *Utrecht Res.*, No. 9, 1923; 61: Russell, Fowler, and Borton, *Ap. J.*, **45,** 306, 1917.

[4] *Harvard Mono.*, No. 5, 1938.

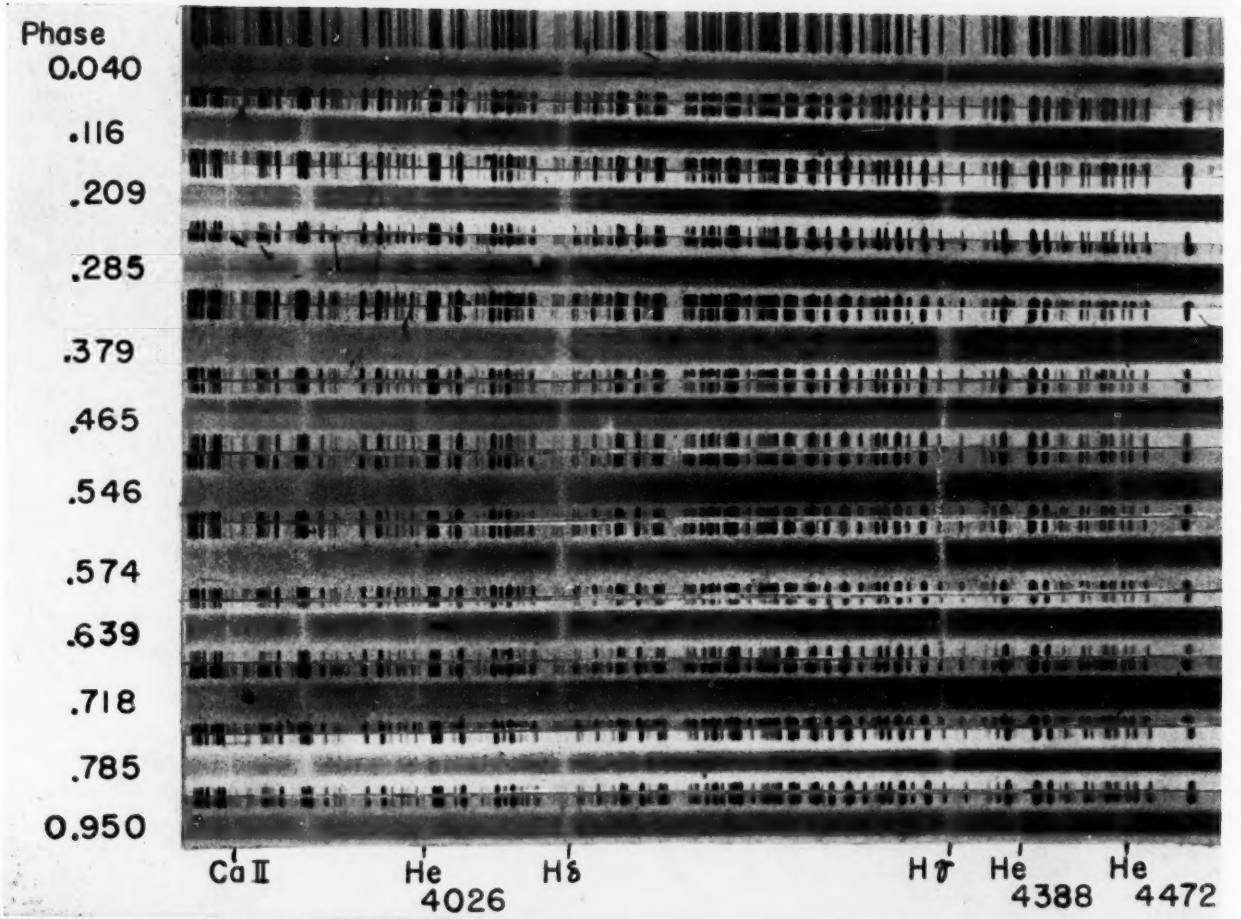

THE SPECTRUM OF AQ CASSIOPEIAE

1. *AQ Cassiopiae.*—The spectrum of this star is very remarkable and will be investigated in much greater detail as soon as possible. The spectral type, outside of eclipse, is B3, but the absorption lines undergo very large variations in intensity. At principal eclipse, phases 0.037 *P* and 0.040 *P*, the *H* lines are weak and narrow; *He* I is weak, and *Mg* II 4481 is relatively strong. There are no emission lines at *Hβ*, but otherwise the *H* absorption cores are too faint and narrow for spectral type B9 which is inferred from the ratio of *He* I/*Mg* II. At phases between 0.2 and 0.4 *P*, the absorption lines of *H* and *He* I are double, with the stronger components on the violet sides. The ratio is not very large, varying between $V/R = 2$ and $V/R = 1$, on different spectrograms. On a few spectrograms *He* I 4026 shows $V/R = 0.5$, but this is rare and probably means only that the difference is not large. In the mean, we can put $V/R = 1.5$. On all these spectrograms, from 0.1 *P* to 0.4 *P*, the lines of *H* and *He* I have their normal, diffuse appearance.

TABLE 4

LIST OF STAR LINES

Element	λ	No. of Star	Element	λ	No. of Star
Ti II.....	3913.46	3, 4, 5, 14	*Fe* II.....	4233.16	2, 3, 4, 5, 8, 9, 11, 13, 14
Ca II.....	3933.67	1, 2, 3, 4, 5, 6, 7, 8, 9, 10, 11, 12, 13, 14	*Cr* I+*Ti* II...	4290.03	2, 4, 5, 6, 8, 14
			Ti II.....	4290.26	3, 5, 11
Fe I.....	3956.68	8	*Sc* II.....	4314.09	2, 3, 4, 5, 6, 8, 11, 14
Fe I.....	4005.25	2, 3, 4, 5, 8	*Sc* II+*Fe* I...	4325.39	2, 3, 4, 5, 6, 8, 11, 12, 14
He I.....	4009.27	6	*Hγ*.....	4340.47	1, 2, 3, 4, 5, 6, 7, 8, 9, 10, 11, 12, 13, 14
He I.....	4026.22	1, 6, 10			
Fe I.....	4045.82	2, 3, 4, 5, 6, 8, 9, 11, 12, 14	*Fe* II.....	4351.77	2, 3, 4, 5, 8, 11, 12, 14
			Fe I..	4383.55	14
Fe I.....	4063.60	2, 3, 4, 5, 6, 8, 11, 12, 14	*He* I.....	4387.93	1, 6
Ni II.....	4067.04	2, 3, 8, 14	*Ti* II.....	4395.04	2, 3, 4, 5, 8, 12, 14
Fe I.....	4071.75	2, 3, 4, 5, 8, 11, 14	*Ti* II.....	4399.77	2, 3, 4, 5, 8, 12
Sr II.....	4077.71	2, 3, 4, 5, 6, 8, 11, 12, 13, 14	*Fe* I.....	4404.77	14
			Fe I.....	4415.13	14
Hδ.....	4101.74	1, 2, 3, 4, 5, 6, 7, 8, 9, 10, 11, 12, 13, 14	*Fe* I.....	4435.01	4, 14
			Fe I+*Ti* II...	4443.09	2, 3, 4, 5, 8, 11, 14
Fe II.....	4171.86	2	*Ti* II.....	4468.49	4
Ti II+*Fe* II..	4172.70	3, 4, 5, 7, 8, 14	*He* I.....	4471.51	1, 6, 10
Fe II.....	4178.85	2, 3, 4, 5, 8, 14	*Mg* II.....	4481.23	2, 3, 4, 5, 7, 8, 9, 10, 11, 12, 13, 14
Sr II.....	4215.52	2, 3, 4, 5, 8, 11, 14			
Ca I.....	4226.73	2, 3, 4, 5, 6, 8, 9, 11, 12, 13, 14			

At phases 0.465 and 0.467 *P*, the absorption lines of *H* and *He* I are exceedingly strong and have the characteristic appearance associated with large turbulence. The central intensities of these lines are high, but their edges are sharp, and the usual Stark wings are absent for *H*. These lines resemble the *H* and *He* I lines in AX Mon, except that there are no strong emission lines in AQ Cas. On a few spectrograms I have suspected weak, broad emission borders at *Hβ* and *Hγ*, but the evidence is not conclusive. At this stage the spectrum is totally different than before. The phases are close to secondary minimum but photometrically this has only $\Delta m_2 = 0.3$ mag., as compared to $\Delta m_1 = 1.0$ mag. for the primary minimum. At phases from 0.546 *P* to 0.642 *P*, the character of the spectrum remains about the same as at 0.467 *P*, though the turbulent appearance of the contours gradually gives way to more normal lines of *H* and *He* I, all single and all of great intensity. These lines have large negative velocities. Then, at phases 0.697, 0.699, 0.718, and 0.785 *P*, the *H* lines have their normal washed-out appearance, and *He* I is very weak. All lines are single and have large negative displacements. This appearance persists at phases 0.950 and 0.952 *P*, where the displacements are less and where, in fact, the

TABLE 5

RADIAL VELOCITIES

AQ CASSIOPEIAE

PLATE G $f/2$	DATE	U.T.	PHASE		Ca II	VELOCITIES (KM/SEC)		SINGLE L
			In Days	In Period		Comp. I	Comp. II	
	1945							
6620	Sept. 25	11:53	3.346	0.285	−26.6	−130.0	+125.8	.....
6668	Oct. 8	6:48	4.413	.377	−22.3	−115.8	+127.7	.....
6669	8	7:23	4.438	.379	−19.2	−178.1	+100.7	.....
6675	12	6:50	8.415	.718	−27.2	.....	.....	−177.1
7165	Nov. 16	4:52	8.173	.697	−24.2	.....	.....	−193.1
7166	16	5:23	8.194	.699	−28.0	.....	.....	−200.7
7190	17	5:29	9.198	.785	− 9.4	.....	.....	−180.8
7206	19	4:02	11.138	.950	−36.0	.....	.....	−124.2
7207	19	4:33	11.160	.952	−36.0	.....	.....	− 93.9
7227	20	4:28	0.435	.037	−18.1	.....	.....	− 16.8
7228	20	5:16	0.468	.040	−25.7	.....	.....	− 35.7
7246	21	2:45	1.364	.116	−29.6	.....	.....	−108.2
7247	21	3:24	1.391	.119	−33.5	.....	.....	− 75.4
7265	22	4:51	2.451	.209	−30.0	−122.8	+106.2	.....
7266	22	5:32	2.480	.212	−30.1	−151.1	+ 78.8	.....
7281	23	2:09	3.339	.285	−30.3	−124.3	+130.3	.....
7282	23	2:52	3.368	.287	− 7.6	−110.3	+154.4	.....
7283	23	3:29	3.394	.290	−26.6	−133.6	+144.1	.....
7303	24	7:36	4.566	.390	−15.7	−133.7	+ 73.5	.....
7304	24	8:17	4.594	.392	−15.7	−173.3	+108.9	− 24.9
7317	25	4:45	5.447	.465	−41.7	.....	.....	− 46.2
7318	25	5:24	5.474	.467	−15.9	.....	.....	− 7.8
7339	26	3:39	6.401	.546	−23.8	.....	.....	−105.4
7340	26	4:11	6.423	.548	−16.2	.....	.....	− 70.5
7364	27	4:50	7.450	.636	−28.0	.....	.....	−135.3
7365	27	5:42	7.487	.639	−12.9	.....	.....	−122.8
7366	27	6:32	7.521	.642	−24.3	.....	.....	−142.0
	1946							
7412	Jan. 24	1:50	6.724	0.574	−48.9	.....	.....	−106.6

χ TRIANGULI

PLATE G $f/2$	DATE 1945	U.T.	PHASE		VELOCITIES (KM/SEC) ALL LINES
			In Days	In Period	
6829	Oct. 26	8:42	0.234	0.241	−122.5
6830	26	8:58	.246	.253	−120.9
6831	26	9:11	.255	.262	−113.0
6840p	27	3:04	.028	.029	− 18.2
6841	27	3:27	.044	.045	− 48.7
6842	27	3:48	.058	.060	− 56.0
6843	27	4:08	.072	.074	− 58.2
6859	28	3:37	.080	.082	− 52.8
6860	28	3:52	.090	.093	− 50.0
6882	29	4:42	.153	.157	− 83.5
6883	29	4:56	.163	.168	−89.5
6903	30	5:17	.206	.212	− 89.2
6904	30	5:49	.228	.235	−123.1
6917	31	6:29	0.284	0.292	−111.2

TABLE 5—*Continued*

x TRIANGULI—*Continued*

Phase G *f*/2	Date 1945	U.T.	Phase		Velocities (Km/Sec) All Lines
			In Days	In Period	
6933	Nov. 1	6:15	0.303	0.312	−106.5
6952	2	5:44	.310	.319	−113.6
6953	2	6:02	.322	.331	− 98.7
6972	3	7:26	.410	.422	− 63.0
6987	4	5:28	.356	.366	− 94.7
7007	5	5:51	.401	.413	− 70.6
7038	7	6:20	.478	.492	− 27.5
7039	7	6:36	.489	.503	− 15.0
7058	8	6:11	.500	.515	− 4.5
7073	10	6:06	.553	.569	+ 15.9
7104	13	5:26	.610	.628	+ 59.5
7105	13	5:42	.622	.640	+ 72.2
7149	15	8:26	.792	.815	+ 98.2
7150	15	8:42	.803	.827	+ 98.4
7167p	16	5:50	.713	.734	+109.2
7168	16	6:07	.725	.746	+107.6
7208	19	5:01	.764	.786	+105.6
7209	19	5:17	.775	.798	+ 97.0
7250	21	5:55	.859	.884	+ 81.4
7251	21	6:10	.869	.894	+ 74.7
7285	23	5:02	.879	.905	+ 70.0
7286	23	5:22	.893	.919	+ 49.2
7288	23	6:56	.958	.986	+ 50.8
7289	23	7:37	.014	.014	+ 12.3
7290	23	8:24	.047	.048	− 40.0
7319p	25	6:10	.011	.011	+ 3.2
7341	26	4:50	.955	.983	+ 47.1
7342	26	5:18	0.004	0.004	+ 29.5

ST PERSEI

Plate G *f*/2	Date 1945	U.T.	Phase		Velocities (Km/Sec) All Lines
			In Days	In Period	
6827	Oct. 26	7:57	1.598	0.603	−19.2
6828	26	8:19	1.614	.609	−16.1
6849	27	9:08	0.000	.000	−70.4
6850	27	9:42	0.023	.009	−86.7
6864	28	7:34	0.934	.353	−71.5
6884	29	5:19	1.841	.695	−22.3
6885	29	5:40	1.855	.700	−28.4
6905p	30	6:44	0.252	.095	−47.5
6918	31	6:28	1.240	.468	−56.9
6934	Nov. 1	6:37	2.247	.848	−26.1
6935	1	7:00	2.263	.854	− 8.6
6954	2	6:25	0.589	.222	−85.0
6955	2	6:47	0.605	.228	−79.6
6970	3	5:54	1.568	.592	−30.8
6971	3	6:49	1.606	.606	−35.5
6988	4	6:04	2.575	.972	−43.2
6989p	4	7:02	2.615	.987	−57.0
6990	4	7:59	0.007	.003	−81.1
6991	4	8:41	0.036	0.014	−89.4

TABLE 5—*Continued*

ST PERSEI—*Continued*

Plate G *f*/2	Date 1945	U.T.	Phase		Velocities (Km/Sec) All Lines
			In Days	In Period	
7008	Nov. 5	6:24	0.941	0.355	−64.7
7040	7	6:59	0.317	.120	−65.1
7041	7	7:19	0.331	.125	−55.4
7106	13	6:04	0.982	.371	−71.2
7107	13	6:27	0.998	.377	−67.4
7169	16	6:26	1.348	.509	−51.8
7170	16	6:43	1.360	.514	−51.3
7210	19	5:44	1.671	.631	−21.9
7229	20	6:03	0.036	.014	−81.5
7343	26	5:50	0.730	.276	−98.8
7344	26	6:09	0.743	0.281	−82.2

RS CEPHEI

Plate G *f*/2	Date	U.T.	Phase		Velocities (Km/Sec)	
			In Days	In Period	All Lines*	*Ca* II
	1945					
6832	Oct. 26	9:58	8.056	0.649	+10.1	+13.6
6851	27	10:32	9.080	.731	+11.4	+20.3
6867	28	9:37	10.042	.809	− 3.8	− 5.7
6868	28	10:26	10.076	.811	−17.4	+ 1.9
6889	29	8:34	10.998	.885	−19.4	+ 1.7
6890	29	9:53	11.053	.890	−11.3	− 9.7
6906	30	10:19	12.071	.972	−15.4	.....
6907	30	11:43	12.129	.977	−25.4	.....
6919	31	7:55	0.550	.044	−26.1	−20.8
6920	31	8:55	0.592	.048	−12.1	−13.9
6936	Nov. 1	7:51	1.547	.125	−25.2	−21.0
6937	1	8:48	1.587	.128	−22.6	−43.9
6956	2	7:26	2.530	.204	−34.9	−40.1
6973	3	8:19	3.567	.287	−36.4	−36.5
6992	4	9:33	4.618	.372	−28.3	−21.6
7009	5	7:52	5.548	.447	−46.1	−63.0
7010	5	9:40	5.623	.453	−28.0	−40.9
7021	6	8:12	6.562	.528	−19.3	−15.2
7022	6	9:09	6.601	.531	−16.8	−29.7
7042	7	8:07	7.558	.609	− 1.2	+ 3.7
7043	7	9:05	7.598	.612	− 0.3	− 0.1
7059p	8	7:35	8.536	.687	+ 9.4	.....
7074	10	7:02	10.513	.846	−11.4	− 8.5
7075	10	8:20	10.567	.851	−11.4	− 0.9
7091	11	6:58	11.510	.927	−10.8	−12.5
7092v.p	11	8:48	11.587	.933	−42.2	.....
7093	12	9:52	0.211	.017	− 5.5	− 8.9
7094	12	11:13	0.267	.021	−21.0	.....
7108	13	7:12	1.100	.089	−17.7	−20.6
7109	13	8:06	1.138	.092	−23.2	−31.3
7129	14	7:07	2.097	.169	−22.6	−17.0
7130	14	8:14	2.143	.173	−34.8	−46.8
7146	15	6:57	3.090	.249	−43.5	−58.4
7171	16	7:22	4.107	0.331	−38.1	−65.4

* Except *Ca* II.

TABLE 5—*Continued*

RS CEPHEI—*Continued*

Plate G *f*/2	Date	U.T.	Phase		Velocities (Km/Sec)	
			In Days	In Period	All Lines*	*Ca* II
	1945					
7172	Nov. 16	8:08	4.139	0.333	−43.2	−54.8
7211	19	6:56	7.089	.571	−15.2	−32.6
7230	20	7:00	8.092	.652	+ 5.7	+ 0.6
7231	20	7:41	8.120	.654	+ 0.6	+15.1
7252	21	7:01	9.092	.732	+ 5.4	+37.7
7267	22	6:06	10.054	.809	−16.6	+18.3
7268	22	6:48	10.083	.812	−10.0	+18.3
7287	23	6:04	11.053	.890	−13.3	− 4.0
7300	24	3:46	11.957	.963	− 9.8	.....
7301	24	4:51	12.002	.966	−10.8	.....
7302	24	6:26	12.068	.972	−24.5	.....
7307	24	10:13	12.226	.984	−41.4	−37.8
7308	24	11:03	12.260	.987	−34.5	−49.3
7322	25	7:50	0.705	.057	−20.5	− 8.3
7323	25	8:32	0.735	.059	−14.4	− 0.7
7345	26	6:56	1.668	.134	−29.6	−30.6
7346	26	7:48	1.704	.137	−19.1	− 0.9
7367	27	7:25	2.688	.216	−45.6	−57.1
7368	27	8:10	2.719	.219	−39.7	−61.4
	1946					
7419	Jan. 25	2:19	11.794	0.950	−28.7	.....

DN ORIONIS

Plate CQ	Date	U.T.	Phase		Velocities (Km/Sec)		
			In Days	In Period	All Lines	*Ca* II and *H*	*Fe* II
	1944						
4042	Dec. 6	8:05	3.161	0.244	−21.4	−35.9	−36.4
4053	7	5:35	4.057	.313	+19.6	+19.6	+43.8
4055	7	8:35	4.182	.323	− 0.9	−17.0	−13.8
	1945						
7131	Nov. 14	9:11	9.111	.703	+24.6	+22.6	+32.5
7132	14	9:40	9.131	.704	+12.8	+13.2	+25.6
7147	15	7:37	10.045	.775	+16.3	+24.0	+24.6
7148	15	7:59	10.061	.776	− 4.0	− 2.8	−12.5
7173	16	8:49	11.095	.856	+ 4.2	+19.4	+24.1
7174	16	9:09	11.109	.857	+21.5	+19.8	+22.8
7191	17	7:27	12.038	.928	+19.8	+36.0	− 2.7
7192	17	8:30	12.082	.932	+14.3	+25.8	+20.0
7193	18	6:36	0.038	.003	+10.3	− 4.3	+12.7
7194	18	7:37	0.080	.006	+ 2.6	+12.2	+25.5
7195	18	8:38	0.123	.009	+24.7	+11.0	+41.1
7196	18	9:40	0.166	.013	+17.7	+17.3	− 4.6
7197	18	10:42	0.209	.016	+ 9.4	+11.9	+ 3.5
7198	18	11:36	0.246	.019	+20.6	+ 4.5	+28.9
7199	18	12:18	0.275	.021	+21.6	+22.2	+32.6
7212	19	8:24	1.113	.086	− 1.3	+18.8	− 7.2
7213	19	8:51	1.132	.087	− 4.1	+ 9.1	−15.2
7232	20	8:19	2.110	0.163	+ 1.9	+10.7	− 2.7

TABLE 5—*Continued*

DN ORIONIS—*Continued*

Plate CQ	Date	U.T.	Phase		Velocities (Km/Sec)		
			In Days	In Period	All Lines	*Ca* II and *H*	*Fe* II
	1945						
7253	Nov. 21	8:16	3.107	0.240	+12.8	+ 4.0	+ 2.9
7254	21	9:14	3.148	.243	+11.5	+13.9	+ 1.3
7269	22	7:44	4.085	.315	+10.6	+ 1.4	+13.6
7270	22	7:59	4.096	.316	+17.9	+17.2	−14.6
7291	23	9:16	5.149	.397	+ 0.5	0.0	+ 7.6
7292	23	9:48	5.171	.399	− 6.8	− 4.1	− 2.4
7293	23	10:13	5.189	.400	− 5.3	− 8.7	− 5.4
7305	24	9:00	6.138	.473	− 3.5	− 6.4	+15.6
7306	24	9:19	6.151	.474	− 0.7	− 5.7	− 1.6
7320	25	6:46	7.045	.543	− 3.8	− 8.0	+ 2.1
7321	25	7:05	7.058	.544	+ 4.6	− 3.6	+ 8.5
7347	26	8:26	8.114	.626	+13.5	+ 8.4	+12.4
7348	26	8:42	8.125	.627	− 0.3	+11.8	+ 5.5
7349	26	9:01	8.139	.628	− 3.0	+12.2	−23.5
7369	27	8:52	9.132	.704	+ 4.6	+14.0	+11.4
7370	27	9:15	9.148	.706	− 0.7	+13.8	+ 6.2
	1946						
7384	Jan. 20	1:29	10.964	.846	− 6.3	+14.0	+10.6
7385	20	2:03	10.987	.847	−12.5	+ 6.7	−26.6
7393	21	2:14	11.995	.925	−30.6	−18.6	−47.1
7394	21	2:45	12.017	.927	+ 3.1	+12.8	+33.9
7404	23	2:52	1.056	.081	+ 3.5	+ 2.2	+ 3.8
7413	24	2:48	2.054	.158	− 2.0	+17.7	+14.0
7420	25	3:35	3.086	.238	− 0.6	− 3.8	+ 3.9
7421	25	4:04	3.106	0.240	− 0.7	+ 4.5	+ 8.6

RW GEMINORUM

Plate G *f*/2	Date 1945	U.T.	Phase		Velocities	
			In Days	In Peorid	All Lines*	*Ca* II
6833	Oct. 26	10:50	1.640	0.572	+41.9	+29.4
6834	26	11:18	1.660	.579	+42.2	+32.3
6865	28	8:11	0.665	.232	−75.9	+29.1
6866	28	8:42	0.686	.239	−61.3	+29.1
6887	29	7:05	1.619	.565	+21.6	+31.9
6888	29	7:35	1.640	.572	+24.8	+35.7
6921	31	9:43	0.863	.301	−40.3	+24.1
6938	Nov. 1	9:36	1.858	.648	+58.0	+27.6
6839	1	10:01	1.875	.654	+47.3	+34.4
6857	2	8:12	2.800	.977	−30.3	.....
6858	2	8:51	2.827	.987	+ 1.4	.....
6859p	2	9:34	2.857	.997	+ 0.8	.....
6860	2	10:22	0.024	.009	+ 2.4	.....
6861	2	11:13	0.059	.021	−36.6	.....
6862	2	11:57	0.090	.032	−56.5	+23.2
6874	3	9:26	0.985	.344	−41.5	+37.6
7011	5	10:54	0.181	.063	−11.1	+32.9
7044	7	9:54	2.139	0.746	+87.3	+32.2

* Except *Ca* II.

TABLE 5—*Continued*

RW GEMINORUM—*Continued*

Plate G *f*/2	Date 1945	U T.	Phase		Velocities	
			In Days	In Period	All Lines*	*Ca* II
7076	Nov. 10	9:26	2.255	0.787	+65.0	+24.4
7110	13	8:56	2.368	.826	+50.7	+26.3
7111	13	9:30	2.392	.835	+60.3	+23.3
7151	15	9:13	1.514	.528	+ 3.0	+10.9
7152	15	9:43	1.535	.536	+ 0.7	+12.5
7175p	16	9:34	2.529	.883	+52.8	+28.7
7233	20	9:14	0.785	.274	−83.4	+20.2
7234	20	9:36	0.800	.279	−67.4	+23.1
7271	22	8:33	2.756	.962	− 0.1	+41.3
7272	22	9:07	2.780	.970	−21.4	.....
7324	25	9:20	0.057	.020	−64.3	+39.9
7325	25	9:55	0.081	.028	−83.3	+ 2.5
7350	26	9:28	1.062	.371	−56.2	+24.1
7351	26	9:52	1.079	.377	−62.5	+17.3
7371	27	9:46	2.075	0.724	+65.8	+23.6

XZ PUPPIS

Plate G *f*/2	Date 1945	U.T.	Phase		Velocities (Km/Sec) All Lines
			In Days	In Period	
6852	Oct. 27	11:16	1.146	0.523	+ 9.2
6870	28	11:26	2.153	.982	+ 70.1
6871	28	11:36	2.160	.985	+ 66.3
6892	29	11:12	0.952	.434	− 50.3
6893	29	11:30	0.964	.440	− 25.2
6924	31	11:15	0.761	.347	− 63.0
6925	31	11:26	0.768	.350	− 45.7
6942	Nov. 1	11:22	1.766	.806	+118.6
6943	1	11:32	1.773	.809	+ 85.8
6994	4	11:12	0.375	.171	− 11.9
6995	4	11:19	0.380	.173	− 14.6
6996	4	11:26	0.384	.175	+ 19.4
7027	6	12:24	0.232	.106	− 8.2
7048	7	12:18	1.227	.560	+ 10.4
7049	7	12:28	1.234	.563	+ 22.2
7081	10	12:19	2.036	.929	+ 89.8
7082	10	12:26	2.041	.931	+ 84.9
7083	10	12:33	2.046	.933	+ 75.7
7114	13	10:49	0.589	.269	− 55.5
7115	13	10:56	0.594	.271	− 49.6
7134	14	10:32	1.577	.719	+ 74.2
7135	14	10:39	1.582	.722	+ 73.7
7153	15	10:06	0.367	.167	− 19.5
7154	15	10:13	0.372	.170	− 36.5
7176	16	9:55	1.359	.620	+ 31.1
7177	16	10:01	1.363	.622	+ 41.3
7215	19	10:26	2.189	.998	+ 59.9
7216	19	10:39	0.006	.003	+ 64.9
7217	19	10:51	0.014	.006	+ 61.6
7219	19	11:44	0.051	.023	+ 63.3
7220	19	12:00	0.062	0.028	+ 54.4

TABLE 5—*Continued*

XZ PUPPIS—*Continued*

Plate G $f/2$	Date 1945	U.T.	Phase		Velocities (Km/Sec) All Lines
			In Days	In Period	
7221	Nov. 19	12:20	0.076	0.035	+ 67.0
7237	20	10:46	1.011	.461	− 38.0
7238	20	10:52	1.015	.463	− 28.7
7255	21	10:36	2.004	.914	+ 77.8
7256	21	10:57	2.018	.920	+ 83.8
7275	22	11:28	0.847	.386	− 59.2
7276	22	11:34	0.851	.388	− 60.9
7294	23	10:41	1.814	.827	+ 81.8
7295	23	10:49	1.820	.830	+ 97.5
7309	24	11:37	0.661	.302	− 72.4
7310	24	11:43	0.665	.303	− 65.8
7326	25	10:22	1.609	.734	+ 89.3
7327	25	10:30	1.615	.737	+ 89.1
7352	26	10:14	0.411	.187	− 12.0
7353	26	10:20	0.416	.190	− 19.6
7372	27	10:12	1.410	.643	+ 43.8
7373	27	10:20	1.416	0.646	+ 35.1

RX HYDRAE

Plate G $f/2$	Date 1945	U.T.	Phase		Velocities (Km/Sec) All Lines
			In Days	In Period	
6853	Oct. 27	11:35	1.471	0.645	+ 39.9
6869	28	11:03	0.166	.073	− 20.7
6891	29	11:04	1.167	.511	+ 1.5
6922	31	10:33	0.857	.376	− 26.2
6923	31	10:51	0.876	.384	− 32.3
6940	Nov. 1	10:35	1.865	.817	+ 38.4
6941	1	11:02	1.884	.826	+ 33.6
6977	3	11:46	1.633	.716	+ 36.7
6978	3	12:14	1.653	.724	+ 29.0
6997	4	11:48	0.353	.155	− 18.1
6998	4	12:16	0.372	.163	− 29.5
7023p	6	10:15	0.007	.003	− 30.5
7024p	6	10:53	0.033	.014	− 44.6
7025p	6	11:25	0.056	.025	− 26.4
7026	6	11:57	0.078	.034	− 22.9
7047	7	12:01	1.081	.474	− 2.9
7079	10	11:38	1.783	.781	+ 39.0
7080	10	12:00	1.798	.788	+ 33.4
7112	13	10:05	0.155	.068	− 32.0
7113	13	10:28	0.171	.075	− 26.6
7133	14	10:12	1.160	.508	− 1.5
7156	15	12:00	2.235	.980	+ 21.8
7178	16	10:18	0.882	.387	− 25.1
7179	16	10:39	0.897	.393	− 23.5
7218	19	11:16	1.641	.719	+ 33.4
7235	20	10:02	0.308	.135	− 38.5
7236	20	10:26	0.325	.142	− 34.9
7257	21	11:52	1.384	.607	+ 18.8
7273	22	10:04	0.027	0.012	− 1.7

TABLE 5—*Continued*

RX HYDRAE—*Continued*

Plate G *f*/2	Date 1945	U.T.	Phase		Velocities (Km/Sec) All Lines
			In Days	In Period	
7274	Nov. 22	10:56	0.064	0.028	− 10.2
7328	25	10:47	0.776	.340	− 36.4
7329	25	11:08	0.791	.347	− 34.0
7330	25	11:30	0.806	.353	− 32.9
7354	26	10:35	1.768	.775	+ 35.4
7355	26	10:44	1.774	0.778	+ 54.2

P LEONIS MINORIS

Plate G *f*/2	Date 1945	U.T.	Phase		Velocities (Km/Sec) All Lines
			In Days	In Period	
6854	Oct. 27	12:10	2.644	0.876	+ 35.3
6872	28	12:08	0.623	.206	+ 1.0
6894	29	12:05	1.620	.536	− 3.4
6926	31	12:03	0.599	.198	+ 3.7
6944	Nov. 1	12:08	1.603	.531	+ 9.3
6975	3	10:18	0.506	.168	− 15.3
6976	3	11:04	0.538	.178	+ 1.8
6993	4	10:33	1.517	.502	− 5.6
7045	7	10:40	1.501	.497	− 11.3
7046	7	11:24	1.532	.507	− 13.6
7077	10	10:12	1.462	.484	− 9.4
7078	10	10:58	1.494	.495	+ 1.8
7116	13	11:29	1.495	.495	− 13.5
7117	13	12:14	1.527	.506	− 18.1
7136	14	11:16	2.486	.823	+ 24.4
7137	14	12:07	2.522	.835	+ 29.8
7155	15	10:42	0.443	.147	− 4.1
7180	16	11:20	1.469	.486	− 8.8
7181	16	12:12	1.505	.498	− 5.4
7214	19	9:47	1.385	.459	+ 7.4
7239	20	11:26	2.453	.812	+ 49.0
7240	20	12:16	2.488	.824	+ 29.2
7277	22	12:13	1.467	.486	− 21.9
7296	23	11:45	2.448	.811	+ 27.6
7311	24	12:17	0.450	.149	− 7.0
7331	25	12:11	1.446	.479	+ 3.1
7356	26	11:29	2.416	.800	+ 10.5
7357	26	12:18	2.450	.811	+ 38.6
7374	27	11:02	0.378	.125	− 22.8
7375	27	12:01	0.419	0.139	− 13.8

TABLE 5—*Continued*

WW CYGNI

Plate G *f*/2	Date 1945	U.T.	Phase		Velocities	
			In Days	In Period	All Lines*	*Ca* II
6838	Oct. 27	1:29	0.545	0.164	−23.4	− 6.9
6856	28	1:25	1.542	.465	+21.5	+ 0.7
6874	29	1:09	2.531	.763	+80.2	+ 0.7
6875	29	1:40	2.552	.769	+75.7	+ 8.3
6896	30	1:09	0.213	.064	−23.8	− 7.1
6897	30	1:40	0.234	.075	−27.8	− 7.1
6909	31	1:13	1.216	.367	−62.3	−25.5
6910	31	1:46	1.239	.373	−59.2	−10.2
6928	Nov. 1	1:07	2.212	.667	+42.1	−10.3
6946	2	1:08	3.212	.968	+74.8	.....
6947	2	1:44	3.237	.976	+70.0	.....
6948	2	2:38	3.275	.987	+50.2	.....
6949	2	3:44	0.003	.001	−16.5	.....
6950	2	4:30	0.035	.011	−19.3	.....
6964	3	1:20	0.903	.273	−70.9	−25.6
6980	4	1:28	1.908	.576	+ 5.0	+ 0.1
7000	5	1:03	2.891	.873	+58.9	+ 3.9
7012	6	2:42	0.642	.194	−47.9	− 3.8
7029	7	0:58	1.570	.474	+11.1	−14.4
7030	7	1:28	1.591	.480	−20.3	+ 0.1
7051	8	1:09	2.578	.778	+78.2	+15.4
7061	9	1:06	0.258	.078	−21.8	− 3.7
7068	10	1:14	1.263	.381	−23.9	−29.7
7088p	11	3:13	2.346	.707	+37.6	+15.2
7097	13	0:56	0.933	.281	−65.6	−14.5
7119	14	0:48	1.927	.581	+ 9.9	+ 7.6
7120	14	1:14	1.945	.586	+34.9	− 3.8
7158	16	1:12	0.627	.189	−57.1	−10.6
7159	16	1:38	0.645	.194	−60.6	−14.5
7203	19	1:53	0.337	.102	−36.2	.....
7204	19	2:25	0.360	.109	−21.2	− 7.6
7242	21	0:43	2.289	.690	+71.9	+11.7
7243	21	1:12	2.309	.696	+57.7	+15.5
7279	23	0:52	0.977	.294	−59.2	−21.7
7280	23	1:26	1.001	.302	−53.7	− 7.3
7334	26	0:50	0.659	.199	−43.8	−25.5
7335	26	1:18	0.678	0.204	−42.0	−14.2

* Except *Ca* II.

SW CYGNI

Plate G *f*/2	Date 1945	U.T.	Phase		Velocities (Km/Sec) All Lines
			In Days	In Period	
6839	Oct. 27	2:28	3.371	0.737	+30.5
6861p	28	4:40	4.462	.976	+12.0
6862	28	5:41	4.505	.985	− 3.5
6876	29	2:08	0.784	.171	−40.2
6877	29	2:29	0.798	.175	−32.7
6898	30	2:08	1.784	.390	−11.8
6899	30	2:34	1.802	.394	−19.6
6911	31	2:15	2.789	0.610	+ 4.8

TABLE 5—*Continued*

SW CYGNI—*Continued*

Plate G *f*/2	Date 1945	U.T.	Phase		Velocities (Km/Sec) All Lines
			In Days	In Period	
6912	Oct. 31	2:37	2.804	0.613	−12.3
6929	Nov. 1	1:37	3.762	.823	+56.2
6965	3	1:52	1.200	.262	−48.6
6966	3	2:15	1.216	.266	−39.4
6981	4	1:58	2.204	.482	−15.1
6982	4	2:16	2.216	.485	−34.7
7013	6	3:09	4.253	.930	+41.4
7031	7	1:55	0.629	.138	− 7.4
7032	7	2:17	0.644	.141	−24.3
7052	8	1:37	1.616	.353	−35.0
7053	8	2:00	1.632	.357	−21.6
7062	9	1:42	2.620	.573	−12.3
7069	10	1:59	3.632	.794	+56.1
7085	11	1:07	0.023	.005	−30.7
7086	11	1:53	0.054	.012	−54.4
7087	11	2:34	0.083	.018	−90.3
7098	13	1:24	2.034	.445	−24.6
7099	13	1:46	2.050	.448	−18.1
7121	14	1:38	3.044	.666	+17.1
7122	14	1:54	3.055	.668	+22.1
7184	17	1:28	1.465	.320	−25.6
7185	17	1:39	1.473	.322	−20.4
7223	20	0:53	4.441	.971	+37.7
7224	20	1:40	4.473	.978	− 7.1
7225	20	2:41	4.516	.988	−20.1
7259	22	0:45	1.862	.407	−10.3
7260	22	1:12	1.881	.411	−15.3
7359	27	0:44	2.289	.501	−11.4
7360	27	1:06	2.304	0.504	−18.3

W DELPHINI

Plate G *f*/2	Date 1945	U.T.	Phase		Velocities (Km/Sec) All Lines
			In Days	In Period	
6844	Oct. 27	4:47	0.312	0.065	− 8.1
6857	28	2:14	1.206	.251	−17.9
6878	29	3:02	2.239	.466	+ 1.3
6879	29	3:33	2.261	.470	+ 3.8
6900	30	3:12	3.246	.675	+40.9
6901	30	4:08	3.285	.684	+43.5
6913	31	3:08	4.244	.883	+45.1
6930	Nov. 1	2:11	0.398	.083	+ 7.6
6967	3	2:49	2.424	.504	+14.3
6983	4	2:40	3.418	.711	+47.9
6984	4	3:02	3.433	.714	+61.7
7003	5	2:23	4.406	.917	+26.9
7004	5	2:52	4.426	.921	+41.2
7014	6	3:32	0.648	.134	+20.8
7033	7	2:48	1.618	.337	− 8.0
7034	7	3:17	1.638	.341	+ 1.5
7054	8	2:31	2.606	0.542	+13.1

TABLE 5—*Continued*

W DELPHINI—*Continued*

Plate G *f*/2	Date 1945	U.T.	Phase		Velocities (Km/Sec) All Lines
			In Days	In Period	
7055	Nov. 8	3:02	2.627	0.547	+21.9
7063	9	2:15	3.595	.748	+58.1
7064	9	2:50	3.619	.753	+54.6
7071	10	3:40	4.654	.968	+53.7
7100	13	2:15	2.789	.580	+35.0
7123	14	2:18	3.791	.789	+48.3
7124	14	2:40	3.806	.792	+43.5
7139	15	0:54	4.733	.985	+43.2
7140	15	1:25	4.754	.989	+29.6
7141	15	2:10	4.785	.996	+12.1
7142	15	3:07	0.019	.004	−14.9
7201	19	0:46	3.921	.816	+54.8
7202	19	1:14	3.940	.820	+56.1
7261	22	1:48	2.158	.449	+10.4
7262	22	2:16	2.177	.453	+ 5.6
7336	26	1:46	1.351	.281	+ 4.0
7337	26	2:15	1.371	.285	+ 5.4
7361	27	1:34	2.342	.487	+ 6.3
7362	27	2:01	2.361	0.491	− 0.3

TW LACERTAE

Plate G *f*/2	Date 1945	U.T.	Phase		Velocities (Km/Sec) All Lines
			In Days	In Period	
6916	Oct. 31	5:17	0.276	0.091	−28.0
6932p	Nov. 1	5:24	1.281	.422	+15.0
6969	3	4:37	0.211	.069	−24.0
6986	4	4:19	1.199	.395	−37.2
7036	7	4:33	1.171	.386	+ 8.2
7037	7	5:33	1.212	.399	−21.0
7057	8	4:54	2.185	.719	+22.2
7065	9	4:06	0.115	.038	− 3.2
7072	10	4:57	1.150	.379	−19.2
7089	11	4:12	2.119	.698	+40.1
7090	11	5:25	2.170	.714	+11.1
7102	13	3:31	1.053	.347	−31.9
7103	13	4:35	1.097	.361	−41.8
7127	14	4:16	2.084	.686	+26.0
7128	14	5:34	2.138	.704	+20.0
7144	15	5:10	0.084	.028	−20.1
7145	15	5:59	0.118	.039	−16.7
7163	16	3:16	1.005	.331	−23.2
7164	16	4:06	1.040	.342	−12.3
7189	17	3:54	2.031	.669	+42.6
7205	19	3:12	0.964	.317	−31.3
7226	20	3:38	1.982	.653	+34.9
7248	21	4:25	3.015	.993	−32.4
7249	21	5:21	0.017	.006	−25.5
7263	22	3:00	0.919	.303	−33.5
7264p	22	3:54	0.956	.315	−60.0
7284	23	4:16	1.972	.649	− 6.8
7316	25	3:58	0.921	.303	−41.0
7338	26	2:57	1.879	0.619	+43.6

TABLE 5—*Continued*

γ PISCIUM

Plate G *f*/2	Date 1945	U.T.	Phase		Velocities (Km/Sec) All Lines
			In Days	In Period	
6845	Oct. 27	5:24	1.272	0.338	−26.6
6858	28	3:04	2.175	.578	+18.3
6880	29	4:02	3.215	.854	+49.9
6881	29	4:21	3.228	.857	+46.8
6902	30	4:44	0.478	.127	−24.3
6914	31	3:40	1.434	.381	− 9.8
6915	31	4:02	1.449	.385	− 9.5
6931	Nov. 1	4:28	2.467	.655	+34.9
6951	2	5:18	3.502	.930	+17.5
6968	3	3:27	0.659	.175	−39.1
6985	4	3:30	1.661	.441	+ 1.5
7005	5	3:35	2.664	.707	+39.8
7006	5	5:16	2.734	.726	+36.4
7015	6	4:07	3.687	.979	+32.5
7016	6	4:43	3.712	.986	−10.3
7017	6	5:15	3.734	.992	−28.9
7018	6	5:55	3.762	.999	+ 4.9
7019	6	6:38	0.026	.007	−13.9
7020p	6	7:15	0.052	.014	−37.1
7035	7	3:47	0.908	.241	−31.8
7056	8	3:35	1.899	.504	+ 5.9
7070	10	2:48	0.101	.027	−16.1
7101	13	2:45	3.099	.823	+30.3
7125	14	3:06	0.347	.092	−15.2
7126	14	3:27	0.362	.096	−14.4
7160	16	2:05	2.305	.612	+23.2
7161p	16	2:21	2.316	.615	+57.0
7162	16	2:37	2.327	.618	+38.0
7186	17	2:06	3.306	.878	+28.7
7187	17	2:27	3.320	.882	+48.5
7188	17	2:52	3.337	.886	+32.3
7244	21	1:48	3.527	.937	+22.4
7245	21	2:07	3.540	.940	+24.1
7313	25	1:32	3.750	.996	−12.3
7314	25	2:34	0.027	.007	−13.6
7315	25	3:10	0.052	0.014	−25.1

lines might have been expected to look similar to those of phases near 0.45 *P* and 0.55 *P*. Yet, in reality, the difference is enormous.

We can probably conclude that the star is a binary, consisting of two components of types B3 and B9, respectively. The B9 star, being the fainter of the two, is producing a total eclipse of the B3 star at principal eclipse. The great strengthening of the *H* and *He* I lines from 0.46 *P* and 0.64 *P* must be due to a gaseous stream associated with the system.

At the present time we shall interpret the velocity-curve as is shown in Figure 1. The *Ca* II line is interstellar and gives a mean velocity of −25.1 km/sec from twenty-eight plates. Too much significance should not be attributed to the fact that, in Table 6, $K_1 > K_2$. We have already seen that the negative absorption component is the stronger at phase 0.25 *P* as well as at phase 0.75 *P*. Hence it is difficult to decide which star should be regarded as the primary.

Mrs. Cecilia Payne-Gaposchkin informed me, after this discussion was completed,

that, from a very large number of Harvard plates, the period of AQ Cas should be corrected to 11.72092 days, as determined by Mrs. Woodward, and that the minima seem about equally spaced and the secondary minimum seems about half as deep as the primary.

2. *X Trianguli.*—On October 27 and November 23, the brightness of the variable was compared to that of two neighboring stars, in the periscope finder of the spectrograph. On both occasions the middle of the eclipse occurred about 36 minutes later than the predicted phase of 0.000, as computed with the elements of Table 2 but without the use of the *sine* term. The spectrum is of class A3, in full light, with many fairly sharp lines and with very broad *H* lines. At principal minimum the type is about G3, also with fairly sharp lines; but on all my spectrograms there is some evidence of blending with the A3

TABLE 6

ELEMENTS OF SPECTROGRAPHIC ORBITS

No.	Star	P (Days)	Char.	γ (Km/Sec)	K_1 (Km/Sec)	K_2 (Km/Sec)	e	T (Phase of Min. Vel.)	T (Phase of Peri-astr.)	ω (De-grees)	$\frac{m_2^3}{(m_1+m_2)^2}\sin^3 i \odot$	$a_1 \sin i$ (Km)
1..	AQ Cas	11.72	Circ.	−20	160	120	0	0.25 P	.....	.....	4.985	25.8×10^6
2..	X Tri	0.97	Circ.	− 5	110	.....	0	.27 P	.....	.....	0.134	1.47×10^6
3..	ST Per	2.65	Circ.	−50	33	.....	0	.25 P	.....	.....	0.008	0.94×10^6
4..	RS Cep	12.42	Ell.	−21	36	.....	0.14	.....	0.71 P	341	0.058	6.08×10^6
5..	DN Ori	12.97	Circ.	+ 8	13	.....	0	.45 P	.....	.....	0.003	2.32×10^6
6..	RW Gem	2.87	Circ.	+ 5	65	.....	0	.25 P	.....	.....	0.082	2.56×10^6
7..	XZ Pup	2.19	Ell.	+22	75	.....	.10	.....	.50 P	200	0.094	2.24×10^6
8..	RX Hya	2.28	Circ.	0	40	.....	0	.25 P	.....	.....	0.015	1.25×10^6
9..	T LMi	3.02	Circ.	+ 5	25	.....	0	.35 P	.....	.....	0.005	1.04×10^6
10..	WW Cyg	3.32	Circ.	+ 8	68	.....	0	.30 P	.....	.....	0.108	3.10×10^6
11..	SW Cyg	4.57	Ell.	− 1	43	.....	.30	.....	.85 P	20	0.033	2.58×10^6
12..	W Del	4.81	Ell.	+19	30	.....	.20	.....	.78 P	0	0.013	1.94×10^6
13..	TW Lac	3.04	Circ.	− 3	33	.....	0	0.25 P	.....	.....	0.011	1.38×10^6
14..	Y Psc	3.77	Ell.	+ 6	37	.....	0.12	.....	0.03 P	103	0.019	1.90×10^6

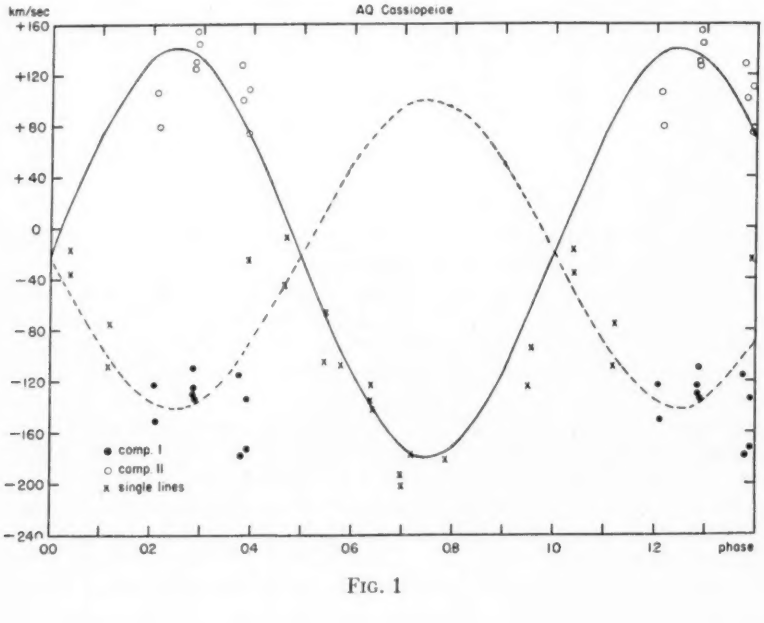

FIG. 1

spectrum—probably because the totality lasts only 0.2 hour. Although the lines of the A3 star are fairly narrow, they are not perfectly free of rotational broadening. This is also supported by the rotational disturbance of the velocity-curve. The range of this disturbance and the appearance of the lines suggest a value of $V_{rot} = 50$ km/sec. This would correspond to a radius of the A3 star of $r = 0.7 \times 10^6$ km, a value which is not unreasonable if compared to the radius of the sun. However, the value of $a_1 \sin i$ of the A3 component around the center of gravity of the system is 1.5×10^6 km, so that the size of the A3 component is probably relatively small. The G3 component is not visible outside of eclipse. The velocity-curve in Figure 2 is quite symmetrical and suggests a circular orbit. It is, however, shifted by about 0.02 P from the predicted phases, which

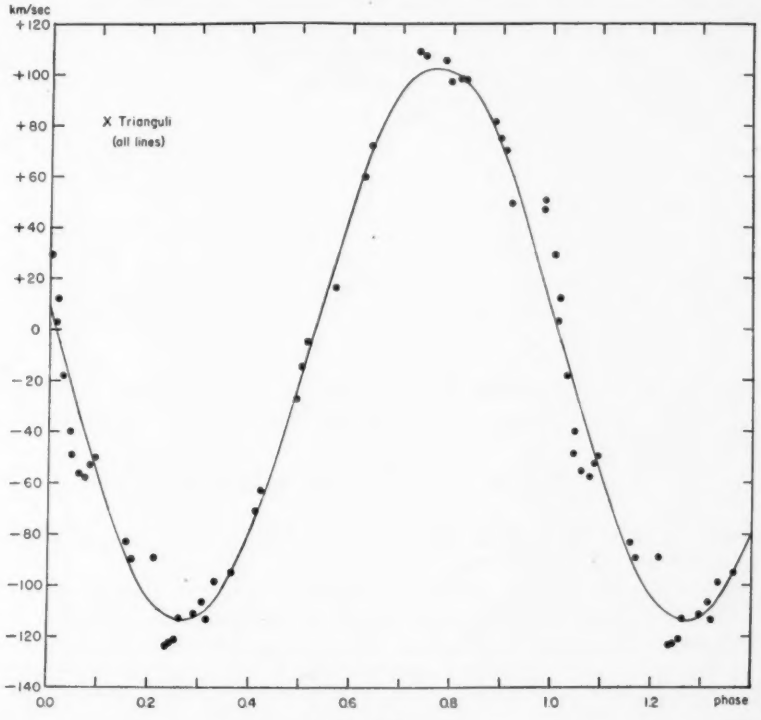

FIG. 2

agrees in sense and amount with the estimated phase of mid-eclipse, which was shifted by +36 minutes, or +0.024 P, from the predicted phase. It must be remembered that in computing the phases we omitted the periodic term. The spectrum shows no bright lines at principal minimum. The rotational disturbance of the velocity-curve begins at about phase 0.96 P and ends at 0.08 P. The middle of the disturbance occurs at phase 0.02 P, in exact agreement with all other evidence.

3. *ST Persei.*—On October 27 and November 4 the variable was compared with a neighboring star in the periscope finder of the 82-inch telescope, and the eclipse was found to occur about 45 minutes, or 0.012 P, earlier than was predicted with the elements of Table 2. In full light the spectrum is of class A3, with many sharp lines and with H lines broadened by Stark effect. During the principal eclipse the spectrum of a star of late type G or K becomes visible. There are no bright lines. The late-type spectrum predominates at phase 0.987 P. At phases 0.972 and 0.000 P, the A and G stars are

blended. There is a strong indication of an appreciable negative rotational disturbance in the velocity-curve, in Figure 3, between phases 0.000 *P* and 0.020 *P*. No observations were secured prior to phase 0.972 *P*, where a positive disturbance would have been expected. The orbit is essentially circular.

4. *RS Cephei.*—Dugan listed the duration of eclipse as 25 hours and that of totality as 11 hours. The data by Schneller in Table 1 must be seriously in error. Estimates of the brightness in the periscope finder suggested, on October 30 and November 24, that the principal mid-eclipse occurred about 11 hours earlier than was predicted from the elements of Table 2. Professor Balfour S. Whitney, of the University of Oklahoma, has observed this star and has found a preliminary value for the epoch of mid-eclipse

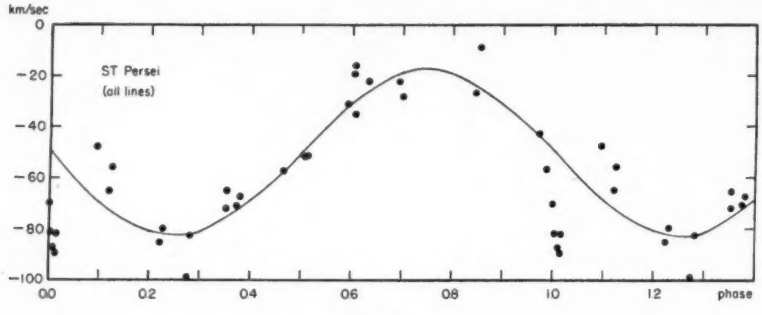

FIG. 3

JD 2431820.84, which "is probably within one or two hundredths of a day of the true minimum." This is about 13 hours earlier than the predicted time. Whitney gives a preliminary set of elements:

$$\text{Princ. Min.} = \text{JD } 2417140.469 + 12^{d}41994\,E\,.$$

His observations also show that the duration of totality is approximately 0.5 day and that of the entire eclipse may be roughly 1 day.

The spectral type of RS Cep, outside of eclipse, is A5, with strong and fairly sharp lines of *Ca* II, *Fe* II, *Ti* II, and *Mg* II, and less pronounced lines of *Fe* I, *Sr* II, *Ca* I, etc. The *H* lines are strong and have wings produced by Stark effect, but the entire appearance of the spectrum suggests a higher luminosity than the preceding stars, X Tri and ST Per. The spectrum resembles that of RW Per, VW Cyg, and AQ Peg,[5] in all of which strong emission lines of *H* were previously found during the principal eclipse. The possibility that emission lines would be found in RS Cep was apparent after the first few spectrograms had been obtained: on these films $H\beta$ had the appearance of an abnormally faint and narrow absorption line, possibly flanked by very weak emission borders. A panchromatic film obtained on October 29 showed that $H\alpha$ is a fairly strong emission line outside of eclipse. During the eclipse the emission lines become very strong. Between first and second contacts, at our phase 0.950 *P*, the red emission components are strong, and the violet components are absent. Mid-eclipse takes place at phase 0.956 *P*. At phase 0.963 *P* both components are present, but the sum of their intensities is less than that of one component before or after. The violet component is slightly stronger. The emitting *H* ring must be somewhat larger in diameter than the eclipsing star: the bright lines never completely disappear. At phases 0.966, 0.972, and 0.977 *P* the violet components are exceedingly strong, and the red components are weak. At this stage several lines of *Fe* II also show violet emission borders. At phases 0.984 and

[5] *Ap. J.*, **103**, 87, 1946.

0.987 *P* the emission lines become rapidly weaker. They are not seen at phases 0.017 and 0.927 *P*.

The spectral type of the eclipsing star, as shown by the absorption lines at phases 0.950–0.972 *P* is about G, with very strong and well-defined lines. It is, however, not normal because of the presence of strong, sharp *H* absorption cores and because of the blending with emission lines of *H* and *Fe* II.

The velocity-curve (Figs. 4 and 5) shows a surprisingly large amount of scatter, considering the strength and the sharpness of the lines. This phenomenon seems to be characteristic of all stars with relatively strong emission lines at minimum: it has already been commented upon in the case of RW Per, VW Cyg, and AQ Peg. There is also a pronounced asymmetry—alike in all four stars: the minimum is broad and shallow and falls

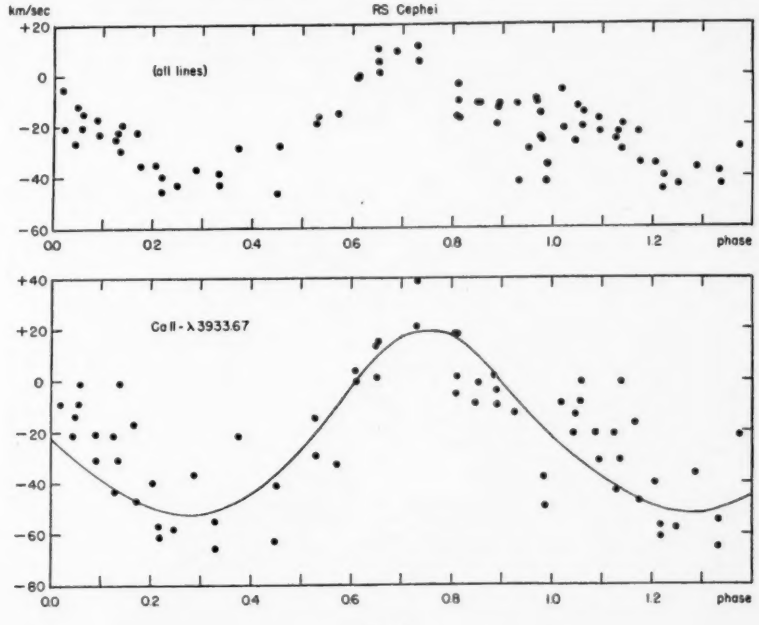

FIG. 4

near phase 0.3 *P*. The spectrographic elements were derived from the *Ca* II curve. But the separate plots for *Fe* I, *Fe* II, and *Ti* II show the same general trend of the velocity-curve. Only the measurements of *Ca* I and *Sr* II scatter widely, probably because of the faintness of these lines; but, at least in the case of *Ca* I, the trend of the curve is probably also the same as for *Ca* II. Hence we can conclude that all absorption features come from the same, A5, component of the binary.

5. *DN Orionis*.—The eclipse on November 18 occurred at about the predicted time, although observations could be started only at the predicted time of mid-eclipse. I have been unable, thus far, to observe the first half of the eclipse. Outside of eclipse, the spectral type is A2, with strong lines of *H*, which are somewhat broadened by Stark effect but, nevertheless, suggest a higher luminosity than such stars as TW Lac, T LMi, Y Psc, or X Tri and resembles RS Cep not only in the appearance of the *H* lines outside of eclipse but also in the relative strength of the *Fe* II lines. All lines, especially those of *Ca* II, *H*, and *Fe* II, are well measurable and should give reliable results. The metallic lines are slightly broadened by rotation. On a few early spectrograms *Hβ* looked ab-

normally narrow and faint. I therefore suspected that bright lines might appear at the principal eclipse. During the total phase of the eclipse the spectrum is of type gF5, with very sharp and strong metallic lines, among which *H*, *Ca* I, *Fe* I, *Ca* II, and *Sr* II are outstanding. On all films, from 0.003 *P* to 0.021 *P*, there is a fairly strong red emission component at $H\beta$. At phases 0.003, 0.006, 0.009, and 0.013 *P*, I also suspect the presence of a very weak violet emission component. At phases 0.006 and 0.009 *P* there are faint red emission components of $H\gamma$ and $H\delta$. The absorption line of $H\beta$, and to a lesser

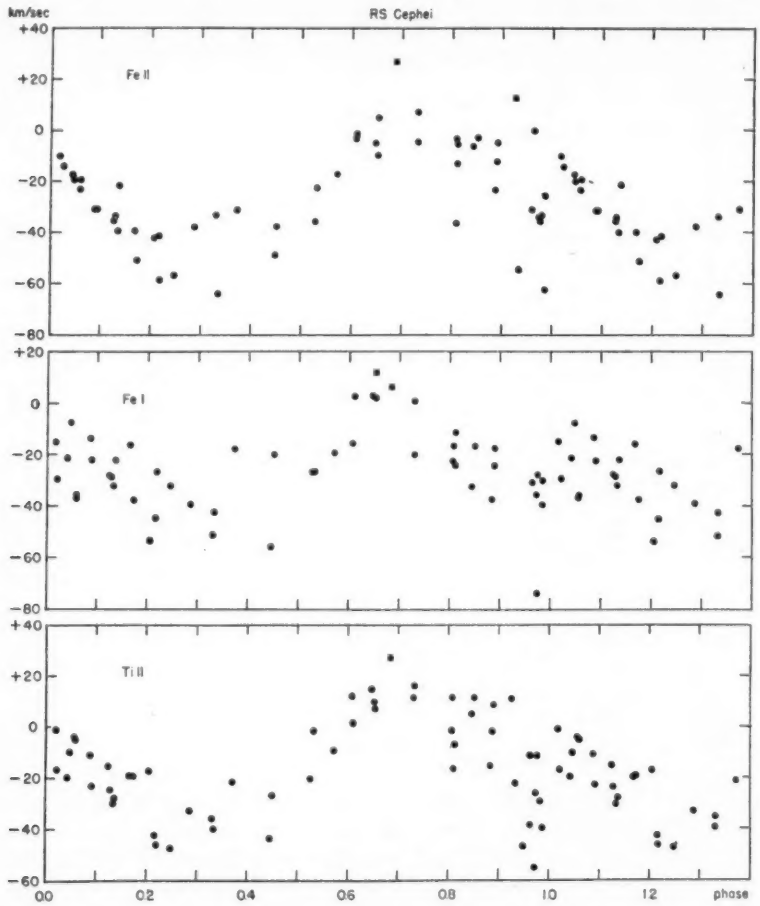

FIG. 5

degree of $H\gamma$ and $H\delta$, is a very sharp and narrow core, similar to those observed in extended atmospheres.

It is of interest that in DN Ori the violet emission component is the stronger after mid-eclipse, while the opposite behavior has been observed in all other eclipsing variables having gaseous rings (the peculiar variable W Serpentis is an exception). The discussion of this phenomenon must be postponed until we have secured spectrograms during the first half of the eclipse.

The radial velocities are extremely discordant—much more so than in other stars with comparable lines. The means of all lines show little variation within the 13-day

cycle. I have included in Table 5 several $f/2$ films, obtained in January, 1946, and also three plates taken in 1944 with the 500-mm camera and quartz prisms by S. Gaposchkin. These are not included in the diagrams (Fig. 6). An attempt to use a period of $\frac{1}{2}P$ gave unsatisfactory results. There is no indiction whatever that the lines may be blended: their widths at phase 0.25 and 0.75 P are exactly the same as at phase 0.50 P. Moreover, we know from the spectrum at principal eclipse that *Fe* II is weak in the fainter, F5, star. Hence these lines, at least, should be unblended in the A2 star. However, a separate plot for *Fe* II shows no more variation than the combined curve for

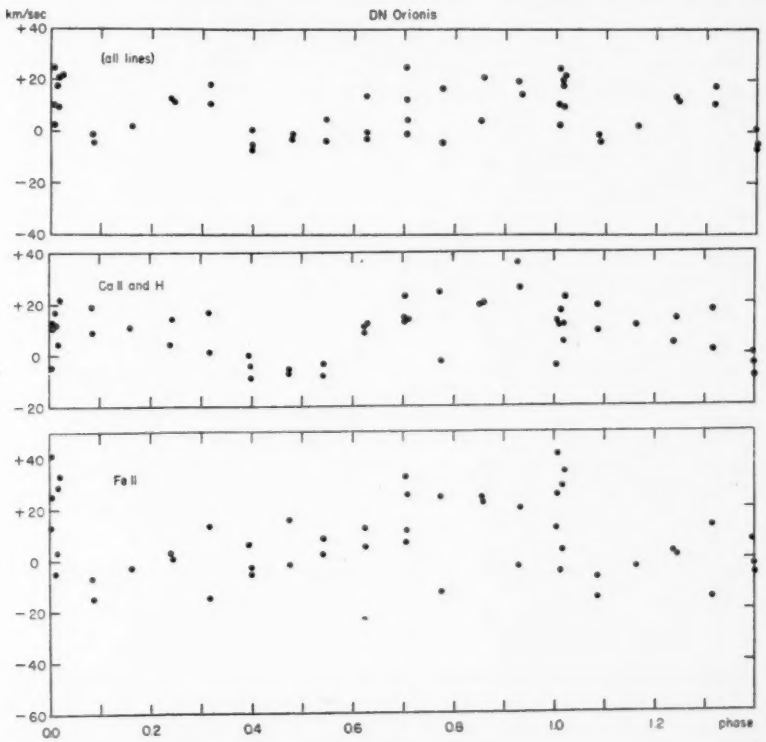

FIG. 6

H and *Ca* II. The latter shows a very slight tendency for a minimum at about phase 0.45 and a maximum at about phase 0.90 P. I have made no attempt to draw the curve; the elements in Table 6 merely represent the semi-amplitude of the curve. There is no reasonable explanation of the shift from the normal position of the minimum at 0.25 P, and the curve may not represent binary motion.

Mrs. C. Payne-Gaposchkin has very kindly communicated to me the results of twelve epochs of minimum determined from 150 recent Harvard plates. Her conclusion is that "they are satisfied by the published period; the minimum is well defined."

We have already seen that the spectrum does not suggest the presence of any appreciable amount of blending during full light. Since the principal eclipse is total, we infer from

$$L_2 = 1 - \lambda_1 ,$$

that $L_2 = 0.28$ and $L_1 = 0.72$. The value of Δm_1 corresponding to λ_1 was taken to be 1.4 mag. and was not corrected for the possible ellipticity of the stars. However, from the light-curve it is probable that blending can play only an unimportant role.

6. *RW Geminorum.*—The eclipse occurred approximately at phase 0.993 *P*, or 28 minutes earlier than the predicted time. The spectral type in full light is B5, with sharp interstellar *Ca* II lines. At principal minimum the type is roughly F5. There were no bright lines. There is a strong indication of a negative rotational disturbance during the partial phase following totality, but the only plate taken before totality, at phase 0.962 *P*, does not show a corresponding positive disturbance. The velocity-curve in Figure 7 is symmetrical and the orbit approximately circular. The mean velocity from the interstellar *Ca* II lines is +23.3 km/sec, from twenty-six spectrograms.

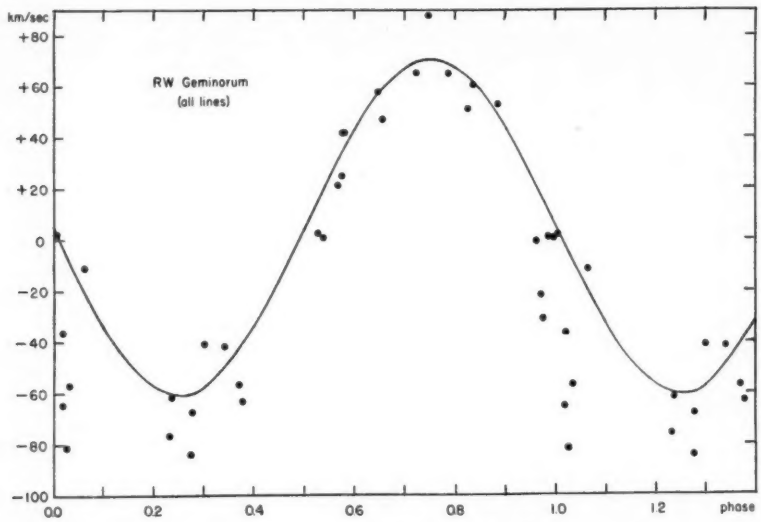

FIG. 7

7. *XZ Puppis.*—Numerous attempts to observe this star at minimum failed completely. It was only after the end of this series of observations that I obtained from Balfour S. Whitney a new determination of the epoch of mid-eclipse, at

$$\text{Princ. Min.} = \text{JD } 2431776.955\,,$$

which is almost exactly 5 hours, or 0.113 *P*, later than the time predicted with the elements of Table 2. The revised elements are

$$\text{Princ. Min.} = 2425850.943 + 2^{d}.192383E\,.$$

This shift is also clearly seen in the velocity-curve, which reaches minimum at about phase 0.35 *P* and maximum at about phase 0.85 *P*. The spectrum outside of eclipse is of type A0, with broad and strong *H* lines; fairly strong, but rotationally broadened, *Ca* II and *Mg* II 4481; and a few weak lines of *Fe* II; etc. Only one plate, at phase 0.106 *P*, was accidentally taken near mid-eclipse. The *H* lines are weaker and much narrower, and there are a few fairly narrow metallic lines of *Fe* II and *Fe* I; *Ca* I is stronger than outside of eclipse. But this spectrum is probably a blend, with the normal A0 star still predominating. The velocity-curve in Figure 8 suggests a small amount of asymmetry,

with a maximum that is slightly broader than the minimum. This would place ω at about 200° and make e of the order of 0.1.

8. *RX Hydrae.*—The eclipse took place at approximately the predicted time. The spectrum in full light is about A8, with broad *H* lines and many fairly strong lines of *Ca* II, *Ca* I, *Fe* II, *Fe* I, *Sr* II, *Ti* II, etc. At mid-eclipse the metallic lines look slightly stronger, but the spectrum is still essentially that of the brighter, A8, star. There are no emission lines. The velocity-curve in Figure 9 is symmetrical.

9. *T Leonis Minoris.*—The period of this star is so nearly equal to 3 days that no observations during the eclipse were possible in the interval covered by this work. The spectrum outside of eclipse is of type A0, with strong, Stark-broadened *H* lines; with fairly strong, narrow *Ca* II lines; and with faint, narrow lines of *Mg* II 4481, *Ca* I 4226, *Fe* I, *Fe* II, etc. The radial velocities in Figure 10 appear in three groups and are suitable only for a preliminary determination of the semi-amplitude of the velocity-curve. If

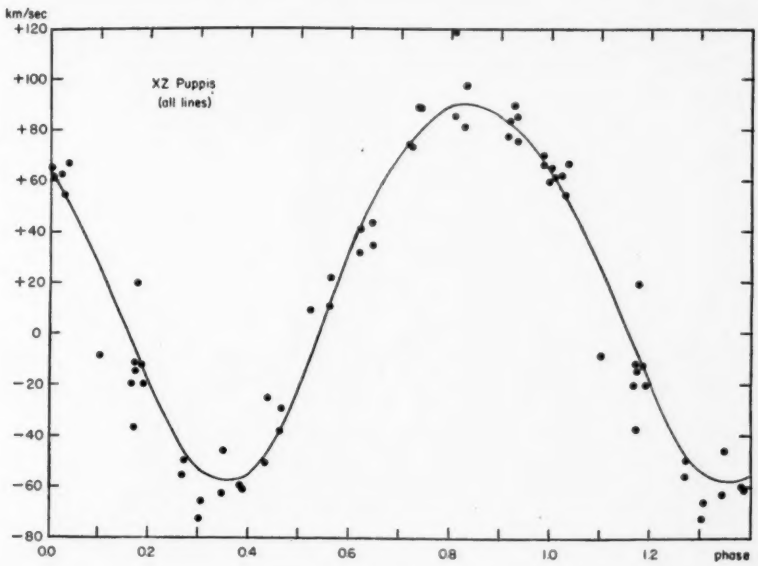

FIG. 8

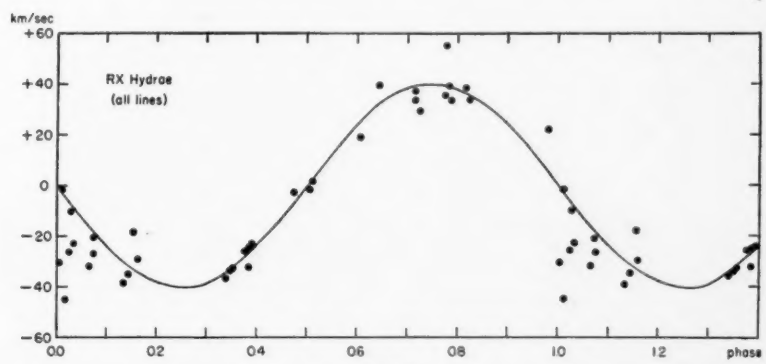

FIG. 9

the observations are to be explained by a circular orbit, then we should be compelled to shift the phase of minimum radial velocity to about 0.35 P. We cannot, as yet, verify the reality of this shift: an eccentric orbit could have satisfied the results equally well.

10. *WW Cygni.*—The eclipse on November 2 was well observed and occurred within about 4 minutes of the time predicted with the elements of Table 2, but without the use of the periodic term. Because of the faintness of the star at mid-eclipse, three spectrograms were obtained with the $f/1$ Schmidt camera and with exposure times of 60, 55, and 25 minutes. The middle exposure, at phase 0.001 P, shows a late-type spectrum, perhaps of class G, but there are no bright lines. It is probable that, even on this plate, the blending with the brighter component, of class B8, with diffuse lines of *He* I and *Mg* II is appreciable. The *Ca* II lines are sharp and are mostly of interstellar origin. There is, however, some indication that this interstellar line is blended with one of stellar origin. The mean velocity from the *Ca* II lines is −6.0 km/sec, from thirty-one spectrograms. The velocity-curve in Figure 11 looks slightly shifted to the right; the reason for this is not clear. Otherwise, it is essentially symmetrical.

11. *SW Cygni.*—The principal eclipse occurred roughly on time, though a few estimates at the finder on October 28 suggested that it took place about 1 hour earlier than

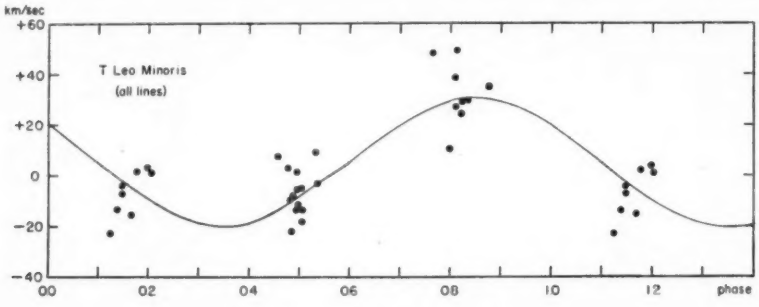

FIG. 10

was predicted. The spectral type in full light is A2, with strong and Stark-broadened lines of H, strong *Ca* II, and very faint and diffuse lines of *Mg* II 4481 and *Fe* II. At phase 0.930 P, the spectrum is normal. At phase 0.971 P, a spectrum of late type is blended with that of the A star, but there are no bright lines. At phase 0.976 P, the late-type spectrum is stronger, and I suspect a very weak red emission component of $H\beta$. At phase 0.978 P, the red emission component is stronger and can be seen at $H\beta$ and $H\gamma$, but not at other lines. At phases 0.985 P and 0.988 P the spectrum is about K0, and the red emission component at $H\beta$ is again somewhat weaker. At 0.005 P the red emission component is absent, but a fairly strong violet component is visible at $H\beta$ and $H\gamma$. At 0.012 P the violet emission is very weak, and at 0.018 P it is absent. At this phase the absorption features still represent a blend of the A2 and K0 spectra. The succession of phenomena during the eclipse suggest that the middle occurred about at phase 0.994 P, which is about 0.7 hour earlier than the predicted time. The maximum intensity of the H emission lines is small compared to that of RS Cep. The velocity-curve in Figure 12 is unsymmetrical and shows a large rotational disturbance. Again the general character of the curve is similar to that of other eclipsing variables with emission lines: the minimum is broad and shallow, and the maximum is narrow.

12. *W Delphini.*—On November 15 the eclipse occurred about 60–90 minutes later than had been predicted with the elements of Table 2, but without the use of the E^2 term. Outside of eclipse the spectral type is A0 or B9, with very strong, Stark-broadened lines of H and with weak and somewhat diffuse lines of *Ca* II and *Mg* II 4481. There is

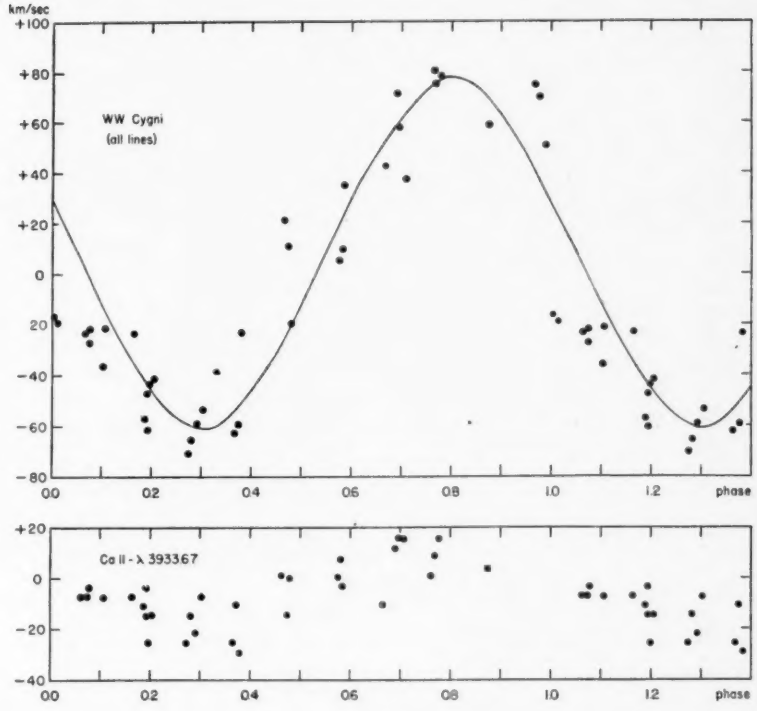
km/sec
+100
+80
+60
+40
+20
0
20
−40
−60
−80
WW Cygni
(all lines)
00
02
04
06
08
10
12
phase
+20
0
−20
−40
Ca II - λ 393367
00
02
04
06
08
10
12
phase

FIG. 11

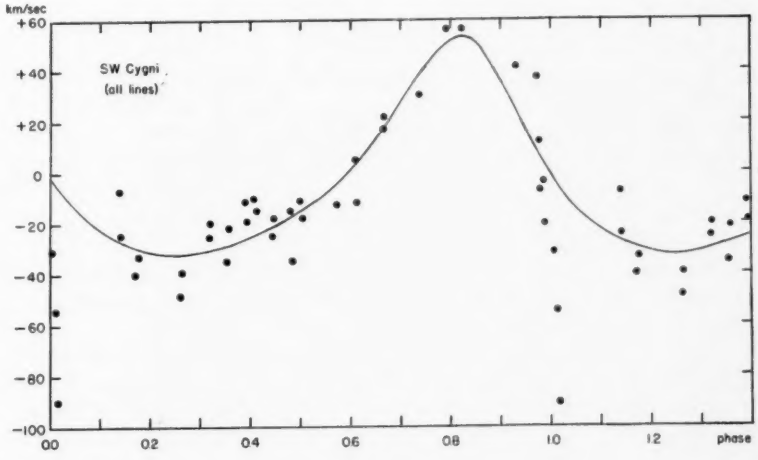
km/sec
+60
+40
+20
0
−20
−40
−60
−80
−100
SW Cygni
(all lines)
00
02
04
06
08
10
12
phase

FIG. 12

an indication of very weak and diffuse lines of *He* I 4471 and 4026. The spectrum is still normal at phases 0.985 *P* and 0.989 *P*, although the absorption lines may be slightly narrower than outside of eclipse. At phase 0.996 *P* a late-type spectrum is blended with that of the A0 star, and *Hβ* shows a very weak red emission component. At phase 0.004 *P* the spectrum is about G5, and the red emission component is still fairly visible. At phase 0.014 *P*, on an underexposed film, I suspect that *Hβ* has a very weak violet emission component. At phase 0.065 *P* the spectrum is again A0, but the lines of *Ca* II and *Mg* II 4481 are sharp and narrow. On this film, of excellent quality, I cannot detect

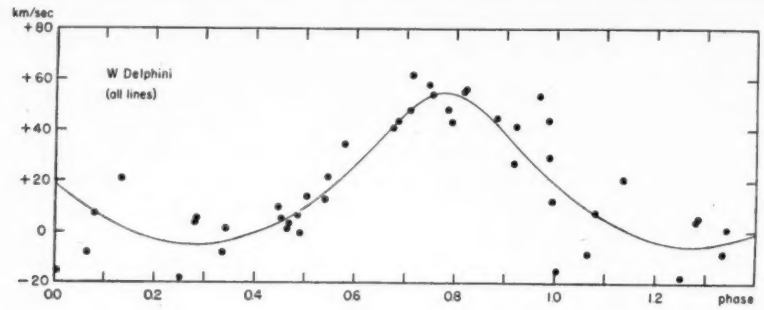

FIG. 13

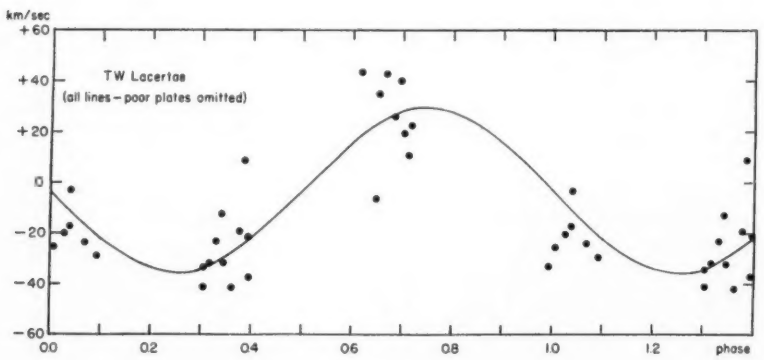

FIG. 14

the lines of *He* I. The velocity-curve in Figure 13 is slightly unsymmetrical, with a broad and shallow minimum and a narrower maximum. The rotational disturbance is pronounced, both before and after totality.

13. *TW Lacertae.*—The distribution of the observations was unfavorable because the period differs little from 3 days. The star appeared faint, as seen in the finder on November 27, at approximately phase 0.95 *P*, but the spectrogram was so underexposed that no features, other than a weak continuum, can be distinguished. The star was normal in brightness at phases from 0.993 *P* to 0.091 *P*. Hence it is probable that the eclipse now occurs 3 or 4 hours earlier than predicted. Outside of eclipse the spectrum is about A2, with strong, Stark-broadened *H* lines, fairly strong *Ca* II, and weak lines of *Mg* II 4481 and *Ca* I 4226. The lines of *Fe* I and *Fe* II are very faint. Because of the poor distribution of the observations and the large scatter of the measurements, we can de-

termine only a preliminary value of the semi-amplitude of the velocity-curve (Fig. 14), assuming the latter to be symmetrical.

14. *Y Piscium.*—The eclipse on November 6 occurred about 30 minutes earlier than the predicted time. The spectrum outside of eclipse is A3, with many sharp, but relatively weak, lines of *Mg* II 4481, *Fe* I, *Fe* II, *Ca* I, *Sr* II, *Ti* II, etc. The *Ca* II lines are strong; *Fe* II is relatively weak. At phase 0.940 *P* the spectrum is normal. At 0.979 *P*, blending with a late-type star is apparent, and at 0.986 *P* the latter is prominent. There are no bright lines. At phases 0.992, 0.996, and 0.999 *P* the spectrum is about K0, and there are no bright lines. On two films at 0.007 *P* the spectrum is mostly K0, but blending with A3 is already noticeable. On both films I suspect an exceedingly weak violet emission component at $H\beta$; but, since I am not certain of it, I have not included this star in my discussion of gaseous shells.[6] At phase 0.014 *P* the A3 star predominates, but the K0 features are still visible. The velocity-curve in Figure 15 is unsymmetrical.

Discussion.—Table 7 contains the mass functions and values of K_1 for those eclipsing variables for which the depths of the primary minima are $\Delta m_1 \geqslant 1.4$ mag. The choice of this limit was arbitrary. It was made in order to be reasonably certain that the lines

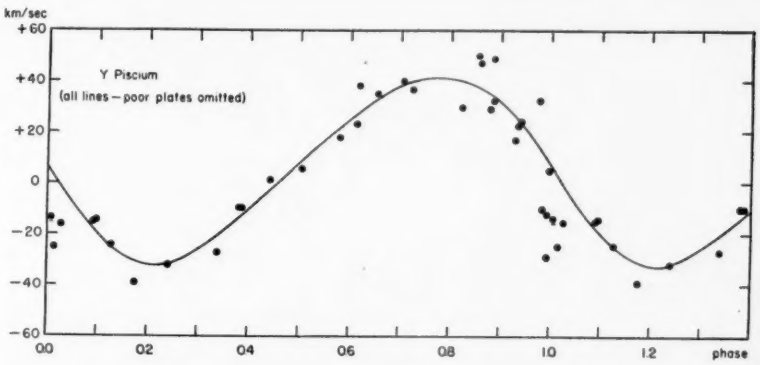

FIG. 15

of the brighter components of the binaries are not affected by blending, outside of the eclipses. In Figures 16 and 17, the values of K_1 have been plotted against log *P*, separately for the A- and B-type stars. RU Cnc was omitted because of its late spectral type; *QY* Aql, of type F0, was included among the A's. Both figures show the limiting curves determined by me many years ago from ordinary spectroscopic binaries.[7] The eclipsing variables fall far below the limiting curve, despite that, for them, $i \approx 90°$. We infer that these systems differ systematically and in a most unexpected manner from ordinary spectroscopic binaries. The mass function

$$f(m) = \frac{m_2^3}{(m_1 + m_2)^2} \sin^3 i = c K_1^3 P (1 - e^2)^{3/2},$$

where $\log c = 3.01642$. In the case of the eclipsing binaries, $\sin^3 i \approx 1$. Hence

$$K_1^3 = P^{-1}(1 - e^2)^{2/3} \frac{m_2}{\left(\frac{m_1}{m_2} + 1\right)^2}.$$

[6] *Observatory*, **66**, 208, 1946.

[7] *M.N.*, **86**, 63, 1925; *Ap. J.*, **66**, 118, 1927.

TABLE 7

MASS FUNCTIONS AND SEMI-AMPLITUDES OF VELOCITY-CURVES FOR 31 ECLIPSING VARIABLES HAVING $\Delta m_1 \geqslant 1.4$ MAG.

Star	Type	P	A_1	A_2	K	$f(m)$	log P
XZ Sgr	A3	3.28	2.8	.....	11	0.0005 ⊙	0.52
DN Ori	A2	12.97	1.4	0	13	.003	1.11
T LMi	A0	3.02	2.4	0.0	25	.005	0.48
ST Per	A3	2.65	2.2	0	33	.008	0.42
RW Per	A5	13.20	2.1	.....	18	.009	1.12
TW Lac	A2	3.04	1.8	.....	33	.011	0.48
UU Oph	A0	4.40	2.4	0	30	.012	0.64
W Del	A0	4.81	2.2	0.1	30	.013	0.68
RX Hya	A8	2.28	2.7	0.1	40	.015	0.36
Y Psc	A3	3.77	3.0	.....	37	.019	0.58
RZ Sct	B2	15.19	1.4	.....	24	.02	1.18
BD Vir	A	2.55	1.4	0.1	42	.02	0.41
AQ Peg	A2	5.55	2.7	0.1	35	.023	0.74
VW Cyg	A3	8.43	2.6	0	34	.033	0.93
SW Cyg	A2	4.57	2.5	.....	43	.033	0.65
QY Aql	F0	7.23	2.9	.....	36	.035	0.86
Y Leo	A3	1.69	3.3	.....	60	.038	0.23
SX Hya	A3	2.90	4.0	.....	50	.040	0.46
RU Cnc	F9	10.17	1.5	.....	34	.042	Omitted
RZ Cas	A0	1.20	1.7	0.1	69	.044	0.08
TX UMa	B8	3.06	2.2	.....	52	.045	0.49
RS Cep	A5	12.42	1.7	.....	36	.058	1.09
TT Hya	A3	6.95	3.6	1.3	41	.070	0.84
RW Gem	B5	2.87	2.0	0.2	65	.082	0.46
U Sge	B9	3.38	2.9	0.1	68	.088	0.53
TU Mon	B5	5.05	1.9	.....	55	.09	0.70
XZ Pup	A0	2.19	3.4	.....	75	.094	0.34
WW Cyg	B8	3.32	3.7	0.1	68	.108	0.52
X Tri	A3	0.97	2.2	0.2	110	.134	9.99
Z Vul	B3	2.45	1.6	0.3	96	.225	0.39
U Cep	B8	2.49	2.4	0.1	120	0.42	0.40

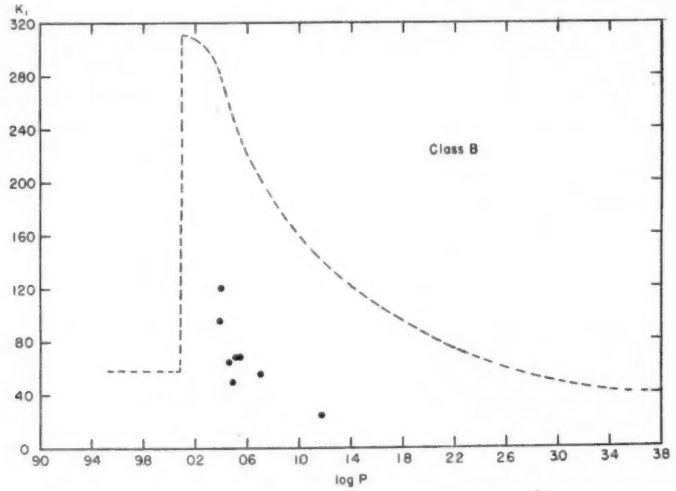

FIG. 16

The relation with P is clearly brought out in both diagrams. It is improbable that the eccentricity differs systematically in the two groups. Hence the difference must arise from the mass ratio or the total mass. We cannot definitely distinguish between these two possibilities. But it is much more likely that the total masses are normal. Assuming $m_2 = 1\odot$, we conclude that for $m_1/m_2 = a$,

$$\frac{(a+1)^{2/3}(\text{sp. bin.})}{(a+1)^{2/3}(\text{ecl. var.})} = \frac{K_1(\text{ecl. var.})}{K_1(\text{sp. bin.})} \sim 0.3 .$$

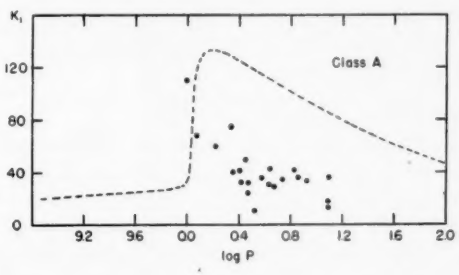

FIG. 17

If, for the limiting curve, $a = 1$, then we obtain for the eclipsing variables a mass ratio a of the order of 10. If $m_2 \neq 1\odot$ for the ordinary spectroscopic binaries, then we can only find

$$a(\text{ecl. var.}) = 12\left[\frac{m_2(\text{ecl. var.})}{m_2(\text{sp. bin.})}\right]^{1/2} - 1 .$$

Thus, for m_2 (ecl. var.) $= 1\odot$; m_2 (sp. bin.) $= 4\odot$, we find

$$a(\text{ecl. var.}) = 5 .$$

It is clear that selection favors small values of a in the process of discovering new spectroscopic binaries, while there is no such favoring in the process of discovering eclipsing variables having large values of Δm_1.

SPECTROSCOPIC OBSERVATIONS OF θ AQUILAE*

CARLOS U. CESCO AND OTTO STRUVE
Yerkes and McDonald Observatories
Received July 10, 1946

ABSTRACT

The spectroscopic orbit of θ Aquilae based on 12 Coudé spectrograms has been derived. The elements show appreciable differences when compared with those previously determined by other observers. Apparent variations of the intensities of the lines are accounted for by a blending effect.

INTRODUCTION

Several spectroscopic binaries have been observed to show peculiar variations in the intensities of the lines. A study using spectrograms of the highest dispersion available is desirable in order to obtain further evidence concerning this phenomenon. The star θ Aquilae has the additional interest that a new determination of its orbit, using spectrograms of high dispersion, would improve our knowledge of this system. In view of these considerations, the star was placed on the observing program of the McDonald Observatory.

THE ORBIT

The spectroscopic orbit of θ Aql has been determined by several investigators.[1] On only a few of their spectrograms were the lines of the secondary visible. Errors in their elements, due to the blending of the lines, were to be expected. The elements derived in this paper seem to confirm this fact.

Of the 20 spectrograms (see Table 1) secured with the coudé spectrograph attached to the 82-inch reflecting telescope of the McDonald Observatory (a combination which gives a dispersion of 3.8 A/mm at λ 4405), only 12 were used for radial velocity—namely, those on which the blending of the lines was not appreciable. The determinations of radial velocity were obtained by measuring, whenever possible, all the lines given in Table 2.

By repeated trials the set of elements given in Table 3 was derived. Corrections to these elements were then computed by a least-squares solution, using the method suggested by King.[2] Each individual plate gave two observational equations. No attempt was made to attach weights according to the quality of the plates; weight 1 was assigned to each individual measure. The final elements are given in Table 4, where, for comparison, the elements derived by Harper,[3] Baker,[4] and Luyten, Struve, and Morgan[1] are also given. In Figure 1 the final computed velocity-curve is shown, together with the measured radial velocities.

From the times of nodal passage, as calculated for the four solutions, we have computed a new value for the period,

$$P = 17.12426 \pm 0.00012 \text{ (p.e.)},$$

which slightly improves the representation of the observations.

* *Contributions from the McDonald Observatory, University of Texas*, No. 124.

[1] See Luyten, Struve, and Morgan, *Pub. Yerkes Obs.*, Vol. 7, Part IV, 1939.

[2] See Harper's paper, *Pub. Dom. Ap. Obs.*, 1, 327, 1914.

[3] *J.R.A.S. Canada*, 6, 265, 1912.

[4] *Pub. Allegheny Obs.*, 2, 41, 1910.

As a matter of illustration, we computed the values of γ and of the mass ratio, r, using O. C. Wilson's method.[5] We obtained

$$\gamma = -28.10 \pm 0.49 \text{ (m.e.) km/sec}$$

and

$$r = 1.243 \pm 0.019 ,$$

in very good agreement with our adopted values.

TABLE 1

RADIAL VELOCITIES OF θ AQUILAE

Plate Cd	Emulsion (Eastman)	Exposure Time	Date (1945)	U.T.	JD 2431+	Primary		Secondary	
						Velocity (in Km/Sec)	O−C	Velocity (in Km/Sec)	O−C
599	103a-O	1:35*	June 24	8:30*	630.854	.....	.....	.....	.....
603	103a-O	2:00	25	6:52	631.786	.....	.....	.....	.....
608	103a-O	1:30	26	7:35	632.816	.....	.....	.....	.....
615	103a-O	1:30	27	9:30	633.896	− 2.49	−0.26	− 59.74	+0.29
620	IIa-O	1:36	28	8:53	634.870	+17.34	−0.85	− 81.88	+3.64
625	103a-O	1:35	29	7:33	635.815	+47.42	+1.05	−118.25	+2.45
631	IIa-O	2:00	30	7:51	636.827	+ 5.24	+0.68	− 69.96	−1.45
637	IIa-O	2:10	July 1	10:05	637.920	.....	.....	.....	.....
638	IIa-O	2:03	4	10:14	640.926	−52.86	+0.33	+ 5.77	+2.19
642	IIa-O	2:20	5	8:25	641.851	−55.88	−3.84	+ 3.96	+1.81
647	IIa-O	3:30	6	8:15	642.844	−52.40	−2.28	+ 0.01	+0.26
650	IIa-O	≈3:00	7	8:58	643.874	−48.13	−0.57	− 0.75	+2.70
651	IIa-O	2:40	9	9:51	645.910	.....	.....	.....	.....
656	IIa-O	2:37	10	9:13	646.884	.....	.....	.....	.....
661	IIa-O	3:00	12	8:45	648.865	.....	.....	.....	.....
664	IIa-O	2:20	13	7:33	649.815	.....	.....	.....	.....
671	IIa-O	1:50	16	8:09	652.840	+42.31	−1.68	−117.94	−0.20
672	IIa-O	2:00	16	10:16	652.928	+47.41	+1.28	−123.01	−2.61
676	IIa-O	2:01	17	7:48	653.825	+10.81	−3.32	− 80.11	+0.35
677	IIa-O	1:59	17	9:55	653.913	+ 6.69	−0.69	− 71.38	+0.66

* Hours and minutes.

TABLE 2

STAR LINES USED FOR THE DETERMINATION OF RADIAL VELOCITIES

Fe II	4351.762	*Mg* II	4481.240	*Fe* II	4515.345
Mg II	4390.585	*Ti* II	4501.274	*Ti* II	4533.967
Ti II	4395.035	*Fe* II	4508.285	*Ti* II	4549.628
Ti II	4443.804				

TABLE 3

PRELIMINARY ELEMENTS OF θ AQUILAE

P = 17.12431 days
K_1 = 52 km/sec
ω_1 = 32°.2
e = 0.60
T = JD 2431636.3

K_2 = 65 km/sec
ω_2 = 212°.2
γ = −28.1 km/sec

[5] *Ap. J.*, **93**, 29, 1941.

VARIATIONS OF THE LINES

The spectrum of the primary component has been classified as A0 or B9s; the spectrum of the secondary is, roughly speaking, of the same class. A spectrum taken on July 16 at 10^h16^m—at about the time of maximum velocity (see Pl. X)—shows the lines of the primary definitely stronger than those of the secondary. Accordingly, on the plates taken on July 9 and 10 we should expect the red component to be the weaker; and on the plate taken on July 13, after the star had crossed the γ-axis, the blue component should be the weaker. A close inspection of the plates, especially in the region $\lambda\lambda$ 4500–4530 shows that, in fact, the contrary is true. This is especially pronounced for the weaker lines, on July 13, for example, $\lambda\lambda$ 4501, 4508, 4515, 4534. The contours of these lines appear almost double, with a strong and sharp violet component, which is flanked on the red side by a faint and diffuse component.

TABLE 4

ORBITAL ELEMENTS OF θ AQUILAE

	Allegheny (1910)	Ottawa (1912)	Yerkes (1934)	Yerkes (1945)
γ	−30.5 km/sec	−25.9 km/sec	−25.0±0.9 (p.e.) km/sec	− 27.94±0.23 (p.e.) km/sec
K_1	46.0±1.1 (p.e.) km/sec	49.5 km/sec	42.6±1.1 km/sec	51.01±0.84 km/sec
K_2				63.68±0.97 km/sec
e	0.681±0.012	0.691	0.615±0.021	0.607±0.011
ω_1	14.9 ±1°5	27°0	21.5 ±1°9	34.45±2°30
ω_2				214.45±2°30
T	JD 2418261.914±0.04	JD 2417731.377	JD 2427646.198±0.09	JD 2431636.344±0.042
T_Ω	.812	.201	.004	.010
$a_1 \sin i$				9.5×10^6 km
$a_2 \sin i$				11.9×10^6 km
$m_1 \sin^3 i$				0.75⊙
$m_2 \sin^3 i$				0.60⊙

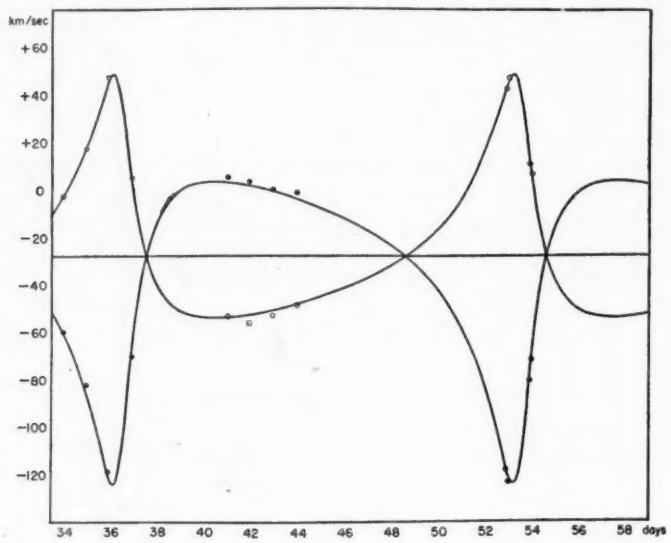

FIG. 1.—Velocity-curves of θ Aquilae

PLATE X

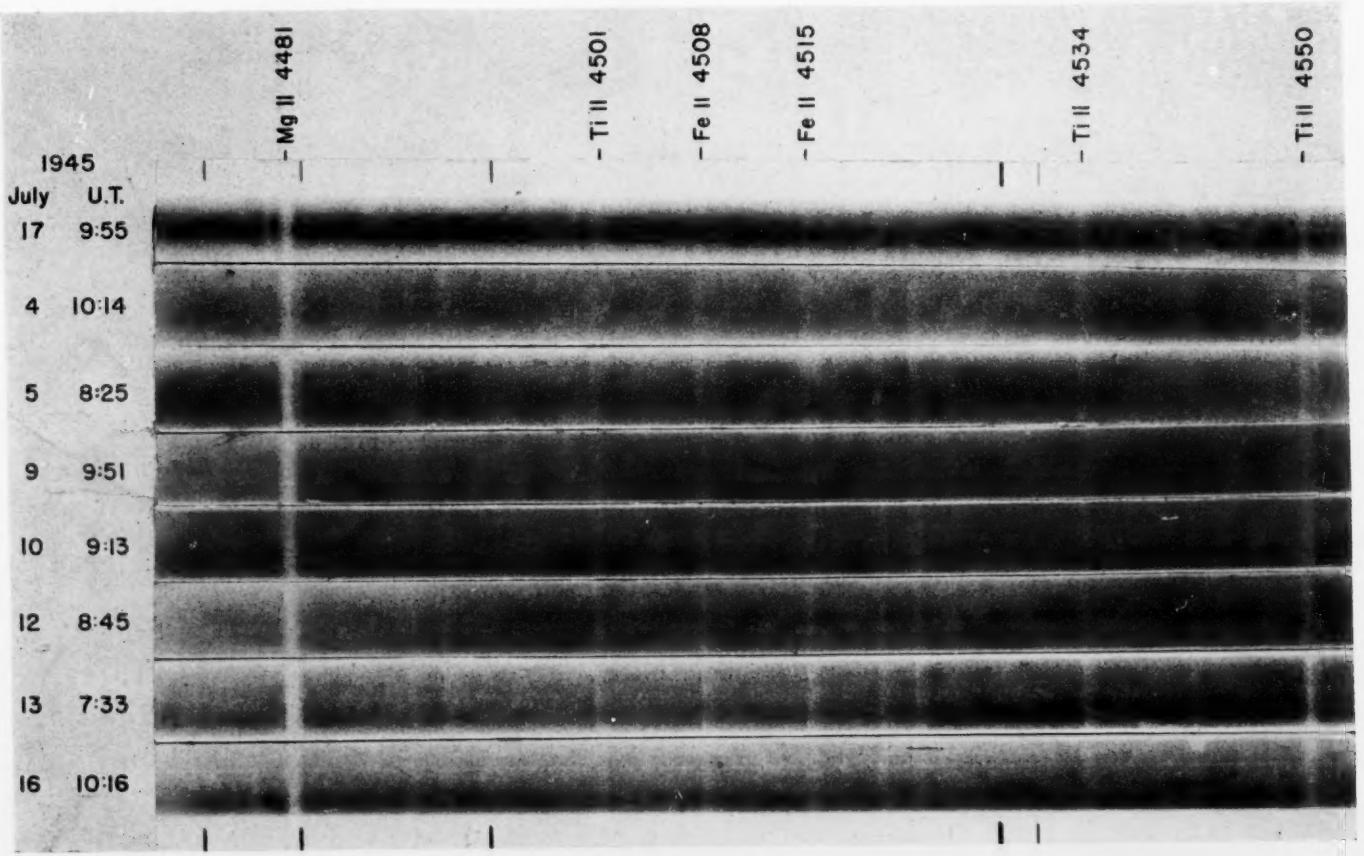

THE SPECTRUM OF θ AQUILAE

UNIV. OF MICH.

This phenomenon is so striking that a somewhat more detailed study of it appears justified. In Figure 2 we have shown the orbits of the two components of θ Aql and the relative positions of the components on July 10 and July 13. The line of sight is perpendicular to the line of nodes. It is immediately seen that there is no orbital or geometrical reason for the sharp components of the lines to be symmetrical with respect to the time of γ velocity. Because of the large eccentricity this point in the orbit is far removed from conjunction.

This circumstance makes it appear very probable that the effect is due to blending—despite the fact that visual inspection of the plates at first made us doubt this interpretation because of the rather conspicuous tendency of the fainter lines on July 13 to look double.

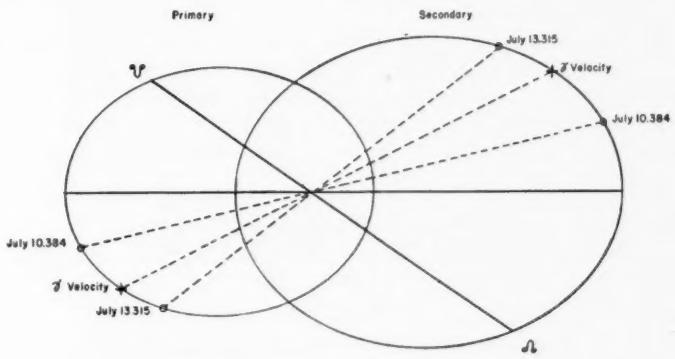

FIG. 2.—Orbits of θ Aquilae

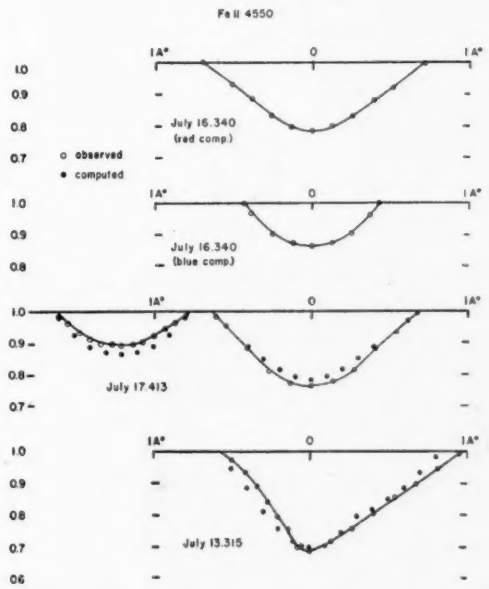

FIG. 3.—Line contours of *Fe* II + *Ti* II 4550 in θ Aquilae

In Figures 3 and 4 we have shown the measured contours of λ 4481 and λ 4550, together with those computed when the lines are blended. The assumption was made that the brightnesses of the two stars remain the same and that the contours do not vary as a function of phase. It will be seen that, for these relatively strong lines, blending satisfactorily accounts for the observations.

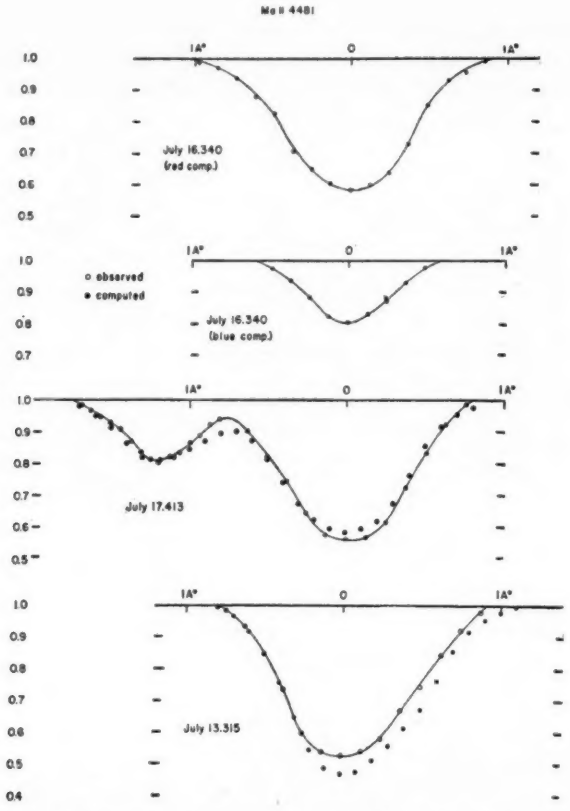

FIG. 4.—Line contours of *Mg* II 4481 in *θ* Aquilae

There is an indication that the fainter spectroscopic component has a somewhat narrower contour, even after allowing for the difference in equivalent width. This is seen in Figures 3 and 4, as well as in Plate X. This fact undoubtedly accounts for the sharp violet component which is so prominent on July 13.

SPECTROSCOPIC OBSERVATIONS OF ζ^1 URSAE MAJORIS*

CARLOS U. CESCO
Yerkes and McDonald Observatories
Received July 10, 1946

ABSTRACT

The spectroscopic orbit of ζ^1 UMa has been determined from 11 Coudé spectrograms. The new orbit agrees well with previous determinations. The intensities of the lines have also been investigated.

INTRODUCTION

Variations of the intensities of the lines of ζ^1 Ursae Majoris were announced by Miss Maury in 1898.[1] In a very complete study of the spectrum of this star, L. Hadley[2] mentions, however, that no variation in the relative intensity of the spectral lines was observed. A similar result was found by R. M. Petrie in a recent paper.[3] In order to determine whether variations are now present, the star was placed on the observing program of the McDonald Observatory.

Fourteen spectrograms were obtained with the Coudé spectrograph attached to the 82-inch reflecting telescope of the McDonald Observatory (a combination which gives a dispersion of 3.8 A/mm at λ 4405). Some of them were calibrated by means of a wedge slit.

THE ORBIT

As a by-product of this investigation a new determination of the orbit of ζ^1 UMa was obtained. Only spectrograms in which the blending of the lines was not conspicuous were used for the determination of radial velocity. Table 1 lists the lines as measured for

TABLE 1

STAR LINES USED FOR THE DETERMINATION OF RADIAL VELOCITIES

Fe II	4351.762	*Ti* II	4501.274	*Ti* II	4533.967
Fe I	4404.752	*Fe* II	4508.285	*Fe* II	4541.523
Ti II	4443.804	*Fe* II	4515.345	*Ti* II	4549.628
Mg II	4481.240				

radial velocity; an average of eight or nine of these lines was measured. On Plate Cd 663, of poor quality, only five lines of the primary and six of the secondary were measured. The radial velocity given for each plate (Table 2) is the straight mean of all the measured lines. No attempt at weighting according to the quality of the plates was made.

After a series of trials, the set of preliminary elements given in Table 3 was determined. Differential corrections for these elements were then computed by a least-squares solution with the method suggested by King.[4] The final elements are given in the last column of Table 4. The radial velocities are plotted in Figure 1, together with the computed velocity-curve.

* *Contributions from the McDonald Observatory, University of Texas*, No. 127.

[1] *Ap. J.*, **8**, 173, 1898.

[2] *Pub. U. Mich. Obs.*, **2**, 76, 1916. An interesting historical review of the observations of this star can be found in this paper.

[3] Unpublished. Presented at a meeting of the American Astronomical Society.

[4] See Harper's paper in *Pub. Dom. Ap. Obs.*, **1**, 327, 1914.

Previous determinations of the orbit of this star have been made by Eberhard[5] and Hadley.[2] Our results are in fairly good agreement with theirs. Table 4 also contains the elements derived by Hadley (those based on the Ann Arbor observations as well as those based on the Potsdam observations) and Eberhard's elements. A new value was derived for the period, using the times of periastron passage computed from the orbits of Eberhard, Hadley (Ann Arbor), and Cesco:

$$P = 20.53860 \pm 0.00003 \text{ (m.e.) days .}$$

TABLE 2

RADIAL VELOCITIES OF ζ^1 URSAE MAJORIS

PLATE CD	EMULSION (EASTMAN)	EXPOSURE TIME (MINUTES)	DATE (1945)	U.T.	JD 2431+	PRIMARY		SECONDARY	
						Velocity (in Km/Sec)	O − C	Velocity (in Km/Sec)	O − C
606	103*a*-O	60	June 26	4:26*	632.685	+42.15	−1.66	−58.62	−0.76
618	IIa-O	60	June 28	5:06	634.712	+49.30	−0.44	−62.55	+1.39
623	IIa-O	60	June 29	4:05	635.670	+31.47	+0.80	−44.54	−0.22
629	IIa-O	60	June 30	4:11	636.674	−36.62	−0.77	+24.57	+0.74
635	IIa-O	75	July 1	5:00	637.708	−80.21	−1.47	+66.55	−1.25
640	IIa-O	70	July 5	4:08	641.672	−42.56	−1.62	+29.58	+0.54
646	IIa-O	86	July 6	5:28	642.728	−30.90	+0.15	+24.74	+5.84
649	IIa-O	≈150	July 7	5:30	643.729	.....	.....	.....	.....
654	IIa-O	74	July 10	4:35	646.691	.....	.....	.....	.....
659	IIa-O	84	July 12	4:11	648.674	.....	.....	.....	.....
663	IIa-O	157	July 13	4:24	649.683	+20.62	+1.00	−34.26	−1.20
665	IIa-O	75	July 15	3:03	651.627	+32.91	−0.05	−46.25	+0.48
669	IIa-O	71	July 16	4:13	652.676	+38.88	−1.30	−54.02	+0.12
674	IIa-O	72	July 17	3:45	653.656	+45.56	−0.93	−59.93	+0.68

* Hours and minutes.

TABLE 3

PRELIMINARY ELEMENTS OF ζ^1 URSAE MAJORIS

$P = 20.53644$ days
$K_1 = 67.5$ km/sec
$\omega_1 = 104°$
$e = 0.56$
$T = \text{JD}2431636.6$
$K_2 = 67.5$ km/sec
$\omega_2 = 284°$
$\gamma = -6.86$ km/sec

TABLE 4

ORBITAL ELEMENTS OF ζ^1 URSAE MAJORIS

	Potsdam (1901) (Eberhard)	Ann Arbor (1912) (Hadley)	Potsdam (as Computed by Hadley)	McDonald (1945)
γ	.....	−7.22 km/sec	−12.06 km/sec	−6.39 ± 0.41 (m.e.) km/sec
K_1	.....	71.65 ± 0.69 (p.e.) km/sec	66.05 ± 0.77 (p.e.) km/sec	65.33 ± 0.88 km/sec
K_2	.....	69.21 ± 0.56 km/sec	67.76 ± 0.98 km/sec	66.99 ± 0.88 km/sec
e	0.502	0.53248 ± 0.00530	0.54058 ± 0.00805	0.541 ± 0.006
ω_1	101.3°	105°35′9 ± 1°33′8	99°39′3 ± 1°50′9	103°29 ± 1°13
ω_2	.....	285°35′9 ± 1°33′8	279°39′3 ± 1°50′9	283°29 ± 1°13
T	1901, March 28.88	5.9088 ± 0.0483 days*	5.5356 ± 0.0546 days*	JD 2431636.591 ± 0.032
T_Ω	1901, March 26.414	3.463 days*	.....	34.297
$a_1 \sin i$	.....	17.31×10^6 km	15.8×10^6 km	15.3×10^6 km
$a_2 \sin i$	.....	16.39×10^6 km	15.9×10^6 km	15.7×10^6 km
$m_1 \sin^3 i$	.....	1.83⊙	1.57⊙	1.42⊙
$m_2 \sin^3 i$	.....	1.79⊙	1.46⊙	1.39⊙

* From 1912, March 10.000 G.M.T.

[5] *A.N.*, **136**, 17, 1894.

PLATE XI

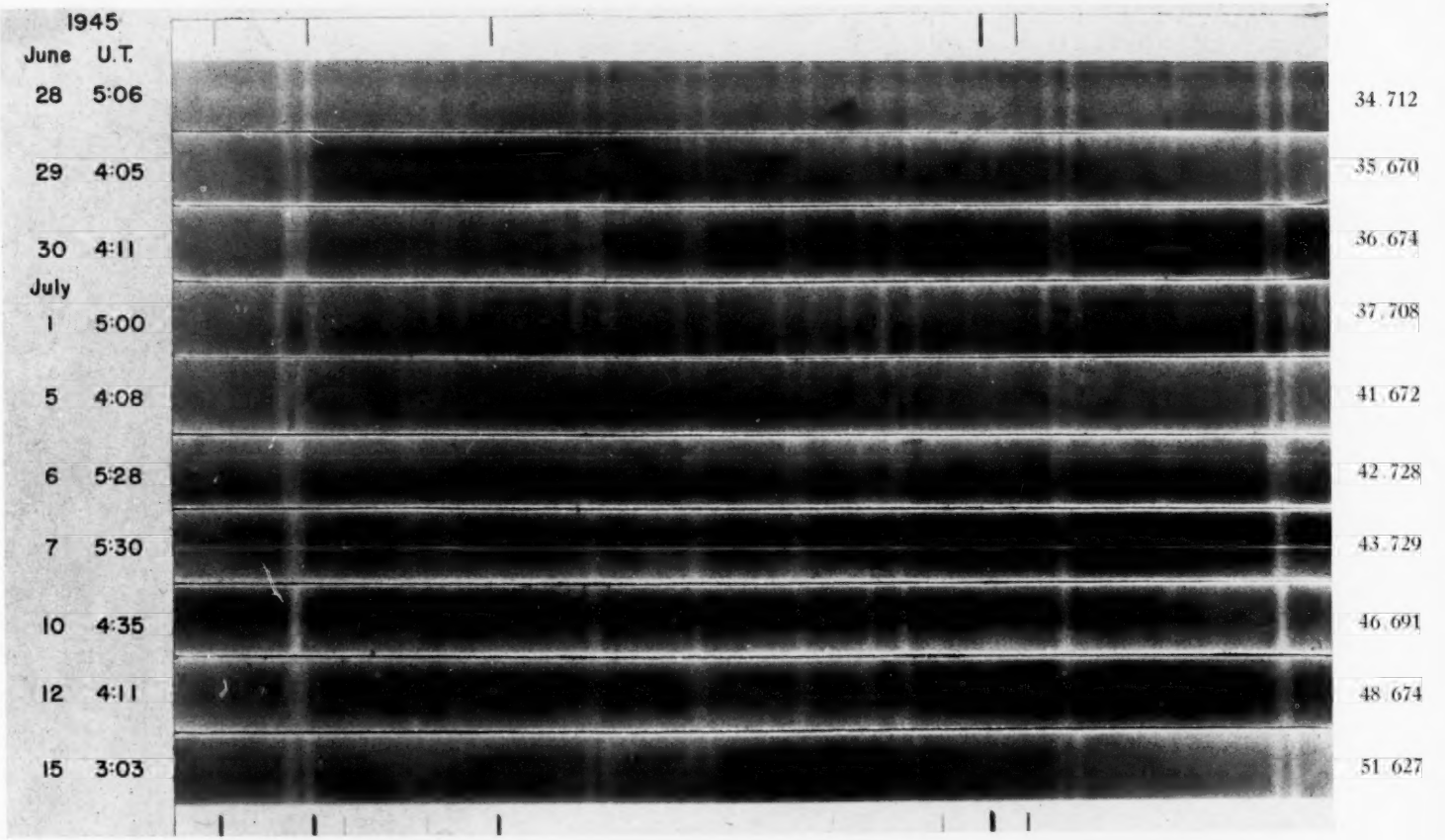

THE SPECTRUM OF ζ^1 URSAE MAJORIS

PHOTOMETRY OF THE LINES

Microphotometric tracings of some of the plates were used to derive the equivalent widths of the lines *Mg* II 4481.240 and *Fe* II + *Ti* II 4549.628. Table 5 contains the measured equivalent widths. There are no conspicuous variations with phase, but the primary is a little stronger than the secondary.

The measured contours show very clearly what is also apparent upon visual inspection of Plate XI. The secondary component is broader and slightly shallower than the primary. In this connection an interesting phenomenon is observed on the spectrograms

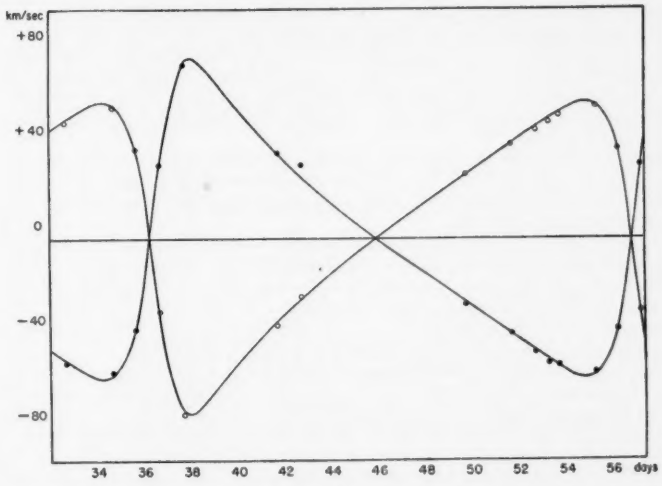

FIG. 1.—Velocity-curve of ζ^1 Ursae Majoris. Abscissae are counted from JD 2431600. Open circles represent the measured velocities of the primary, dots those of the secondary.

TABLE 5

MEASURED EQUIPMENT WIDTHS IN ζ^1 URSAE MAJORIS

PLATE CD	Mg II 4481		Ti II 4550		PLATE CD	Mg II 4481		Ti II 4550	
	Primary	Secondary	Primary	Secondary		Primary	Secondary	Primary	Secondary
618.....	0.220	0.213	0.191	0.182	635.....	0.240	0.259	0.239	0.210
623.....	0.291	0.281	0.208	0.186	640.....	0.259	0.248	0.212	0.188

of July 7, before γ-velocity, and of July 12, after γ-velocity. When the two components are well separated, it is difficult to decide which is the stronger, and accurate measures are required to decide this point. But on July 7 the strong violet component is flanked by a very weak red component, while on July 12 the strong red component is flanked by a very weak violet component. This is probably caused by the blending of two contours which are not alike in shape.

The greater broadening of the lines of the secondary *looks* like an effect of more rapid axial rotation of the fainter component, but it could also be produced by a difference in limb-darkening. Hence it is not possible to derive additional information from this effect.

THE RADIAL VELOCITIES OF FIFTY GLOBULAR STAR CLUSTERS*

N. U. MAYALL
Lick Observatory
Received July 15, 1946

ABSTRACT

Radial velocities determined with a low-dispersion (430 A/mm at $H\gamma$) spectrograph attached to the 36-inch Crossley reflector are reported for fifty globular clusters. The list is substantially complete to $\delta = -40°$ for the equipment used. All the velocities are for the integrated light of the clusters. At least four satisfactory spectrograms were obtained for each cluster; the residuals from the mean velocity for each cluster indicate an average internal probable error for a single plate of ± 22 km/sec. From an independent series of higher-dispersion spectra (130 A/mm at $H\gamma$) of fifteen clusters observed with the 36-inch refractor and from a comparison with velocities determined elsewhere, it is found that, in general, the systematic errors are small, only several km/sec. The average differences without regard to sign, however, indicate that the final velocities may be uncertain by 15–20 km/sec, especially for clusters observed only with low dispersion.

Of the fifty velocities measured, nineteen are positive and thirty-one negative; all of them fall within the previously known range from +291 to −360 km/sec. The excess of negative velocities is due to selection, for the majority of the observed clusters are located in galactic longitudes (145°–325°), where the solar-motion component is negative.

The spectral types, although difficult to estimate because of the composite and peculiar nature of the spectra, appear to range from A5 to G5, with an average of F7.6, but there is a preponderant number (thirty) included in the smaller interval from F8 to G5. Comparison with Stebbins and Whitford's photoelectrically measured color classes shows little variation of color with spectral class, after the effect of space reddening is removed by the cosecant law previously deduced from the color observations.

On the basis of a number of solar-motion solutions it is found that (1) no K-term is indicated; if one is introduced into the solution based on fifty clusters, $K = -7.9 \pm 18.8$ km/sec; (2) there is no appreciable deviation of the computed apex from the one generally assumed at galactic longitude 55° and latitude 0°; (3) the solar motion with respect to the clusters, $V_\oplus$, averaged from four different ways of treating the 50 velocities, is $V_\oplus = 175 \pm 25$ km/sec, but this value probably is too small because of observational selection; (4) from separate solutions for the two groups of clusters in the hemispheres containing the apex and antapex and from a discussion of the degree of completeness in the two groups, it is concluded that the most probable value for the solar motion, with allowance for the clusters of unknown velocity, is $V_\oplus = 200 \pm 25$ km/sec. The mean residual motion without regard to sign is 101 km/sec.

A cluster solar motion smaller by about 75 km/sec than hitherto obtained from half as much data suggests re-examination of the question of the sun's orbital velocity, $V_\odot$. From a consideration of the most recent material for galactic objects, it is concluded that $V_\odot = 280 \pm 40$ km/sec, i.e., unchanged from values heretofore generally adopted. The local group of nebulae, with certain qualifications because of the possibility of red-shifts and a component of the motion of the galaxy as a whole being included in their radial velocities, provide a check on $V_\odot$. Several solar-motion solutions yield the round number $V_\odot = 300 \pm 25$ km/sec, so that there now seems to be a real difference of $V_\odot - V_\oplus = 80$–100 km/sec between the sun's motion with respect to the galactic center and to the system of globular clusters. The most obvious interpretation of the difference is that the cluster system partakes in the general galactic rotation and that it may, for dynamical reasons, be appreciably flattened.

Attempts to find, in the peculiar velocities, evidence of a general or differential rotation of the cluster system have led to inconclusive results. The reasons are partly the inaccurate distances for a number of clusters, but especially the large dispersions in velocity and in distance from the galactic plane. Nevertheless, the photometric distances for many clusters are still too imperfectly known to rule out the possibility of a small amount of flattening of the system for reasonable values of space absorption. The elliptical outline of the projected distribution of the clusters in the Andromeda nebula indicates that a globular-cluster system may be appreciably flattened. This circumstance suggests radial-velocity determinations for the clusters in that spiral as probably the most direct means for further investigation of the dynamics of a system of globular clusters.

I. PREVIOUS WORK

The only extensive series of observations hitherto made to determine the radial velocities of the globular star clusters is represented by the pioneer work of V. M. Slipher,[1]

* *Contributions from the Lick Observatory*, Ser. II, No. 15. The principal results of this paper were presented orally at the dedication of the Mexican National Astrophysical Observatory at Tonanzintla, Puebla, Mexico, February 20, 1942.

[1] *Pop. Astr.*, **26**, 8, 1918; **30**, 11, 1922; **32**, 622, 1924. A preliminary announcement was made in *Pub. A.A.S.*, **3**, 331, 1918.

who published the velocities for seventeen clusters from 1918 to 1924. In 1919, Sanford[2] published the velocities for three clusters, but two of them had already been observed by Slipher; with this exception, there are no velocities reported for additional clusters from 1918 to 1934.[3] Within this interval there are a few new measures reported by Pease,[4] Strömberg,[5] and Moore,[6] but they refer to objects previously observed by Slipher. In 1934, Humason[7] published velocities for three clusters and Baade[8] for one. A year later Edmondson[9] reported velocities of four more clusters, two of which were based on unpublished measures by Humason and two on spectrograms obtained by Slipher. Thus, as recently as 1935, when the present work was undertaken, radial velocities were available for only twenty-six clusters. Since this number represents but one-fourth of the known globular clusters and since these objects play a unique and important role in the structure and dynamics of the galaxy, it was apparent that further radial-velocity measures were desirable. It is the purpose of this paper to give such measures for as many clusters as could be observed at Mount Hamilton within a reasonable time.

During 1935–42, radial velocities were obtained for fifty clusters, and this number closely approaches the practicable limit for the instrumental equipment employed. While it would be possible to add a few more objects to the list, it could be accomplished, under existing conditions, only by the expenditure of a disproportionate amount of time. The exposure times were so long and the difficulties of working at very low altitudes were so considerable for the last few clusters observed that the program seemed to have reached the point at which the law of diminishing returns became operative.

II. DIFFICULTIES AFFECTING SPECTROSCOPIC OBSERVATION

The determination of radial velocities of globular clusters is a curiously difficult problem for several reasons, which merit a brief discussion because they shed light on the causes for the slow accumulation of data. First, although these objects are relatively bright—their average photographic magnitude, according to Christie,[10] is 9.5, with a range from 4.6 to 12.9—there is only a rather small number of them in which the light is sufficiently concentrated toward the center to permit observations with ordinary stellar spectrographs. For the majority of clusters the light is distributed over an area much larger than that of the slit. Consequently, a fairly bright total magnitude does not always mean that exposures, even of the order of several hours with ordinary stellar spectrographs, will record the spectra of the globular clusters.

A second difficulty in the determination of radial velocities of globular clusters is that the distribution in the sky of the clusters is unfavorable for an observer in the north temperate zone. There are approximately seventy clusters north of declination $-40°$; of this number, forty-seven, or 65 per cent, lie between declination $-10°$ and $-40°$; and thirty-four, or 72 per cent of them, fall between right ascensions 16 and 19 hours. Be-

[2] *Ann. Rep. Director Mt. W. Obs.*, 1919.

[3] C. D. Perrine has reported that spectrograms have been obtained at Córdoba, with the 30-inch reflector, for a number of southern clusters; but, so far as the writer knows, the velocities have not been published. The following list of references appears to be the only information available on such important observations: *Pub. A.A.S.*, **7**, 165, 193, 1932 (24 plates with a small spectrograph, mostly of globular clusters); **8**, 63, 1936 (23 plates of 8 globular clusters); **8**, 162, 1936 (1 plate of NGC 1851, 4 of NGC 104); **8**, 271, 1936 (10 plates of 3 globular clusters).

[4] *Pub. A.S.P.*, **40**, 342, 1928.

[5] *Ap. J.*, **61**, 353, 1925; *Mt. W. Contr.*, No. 292.

[6] *Pub. Lick Obs.*, **18**, 217, 1932.

[7] *Pub. A.S.P.*, **46**, 357, 1934.

[8] *Ap. J.*, **82**, 410, 1935; *Mt. W. Contr.*, No. 529.

[9] *Lowell Obs. Bull.*, **3**, No. 88, 143, 1935.

[10] *Ap. J.*, **91**, 8, 1940; *Mt. W. Contr.*, No. 620.

cause of this remarkably high concentration in a relatively small area, it is not possible to observe the majority of the globular clusters for more than a few months during the year. The consequence is that a number of years is required to accumulate spectroscopic observations for a considerable number of clusters.

A third factor which increases the difficulties of spectroscopic observation is the fact that many of these clusters are partially obscured by interstellar matter, as the photoelectric measures of color by Stebbins and Whitford[11] have shown. The obscuration is more pronounced for blue light than for red, as is well shown on photographs taken by Baade[12] with the 100-inch reflector on Mount Wilson. Pictures such as Baade's clearly show that many clusters are abnormally weak in actinic light; and this circumstance combines with the average low altitude of the clusters to make work difficult in the ordinary photographic region.

Finally, the composite nature of the spectra and the velocity dispersion in each cluster blend and broaden, respectively, the spectrum lines. The result is that only a few lines of rather poor visibility are available for radial-velocity measurement.

The combination of these several difficulties means that the observer is obliged to use, for most clusters, spectrographs giving low dispersion, of the order of 300–500 A/mm. As a consequence, the radial velocities of globular clusters not only are difficult to determine but are, for the most part, unobtainable with high accuracy. This was especially true when, as in the present investigation, the aim was to get velocities from the integrated light of the clusters. The question of the spectra and velocities of the individual stars, however important and interesting it may be, had to be passed over because the cluster stars are too faint for the available equipment. In making the observations the clusters were intentionally placed out of focus and allowed to drift on the slit. In this way spectra of the integrated light, of satisfactory width, and of uniform density perpendicular to the direction of dispersion, were obtained.

III. OBSERVATIONAL MATERIAL

Forty-nine of the clusters were observed with the nebular spectrograph[13] used in the prime focus of the 36-inch Crossley reflector. The optical parts of this spectrograph consist of two 60° UV glass prisms and an $f/1.3$ camera lens, with the combination giving a dispersion at $H\gamma$ of 430 A/mm. Plate XII shows the spectrograph as it is mounted in the telescope; with this apparatus the effective southern limit for exposures of several hours is reached at about declination $-38°$. Since there is a bright and concentrated cluster (NGC 1851) located at $\delta = -40°$, which it was important to observe because of its nearness to the antapex of the solar motion, it was necessary to observe it, the fiftieth cluster, with the lowest-dispersion (130 A/mm at $H\gamma$) stellar spectrograph attached to the 36-inch refractor. This latter equipment was also used to observe as many of the other clusters as possible, the aim being to obtain a check on the velocities determined with the Crossley low-dispersion apparatus. Table 1 lists the radial velocities for the individual spectrograms obtained with both telescopes.

While the data in Table 1 are self-explanatory, a few remarks should be made concerning the velocities obtained with the Crossley low-dispersion spectrograph. It may be noted that, in general, four and occasionally five low-dispersion plates were obtained for each cluster and that each plate was measured only once. This procedure was adopted because experience demonstrated that most of the error of a low-dispersion radial-velocity determination is inherent in the spectrograms, i.e., the error of measurement is small

[11] *Ap. J.*, **84**, 132, 1936; *Mt. W. Contr.*, No. 547.

[12] *Pub. A.A.S.*, **9**, 31, 1937; *Trans. I.A.U.*, **6**, 452, 1938. Two of Baade's photographs of a reddened cluster—one taken in blue light and the other in red light—are reproduced by B. J. and P. F. Bok in *The Milky Way*, p. 145, Philadelphia: Blakiston, 1941.

[13] *Pub. A.S.P.*, **48**, 14, 1936.

PLATE XII

PLATE XII

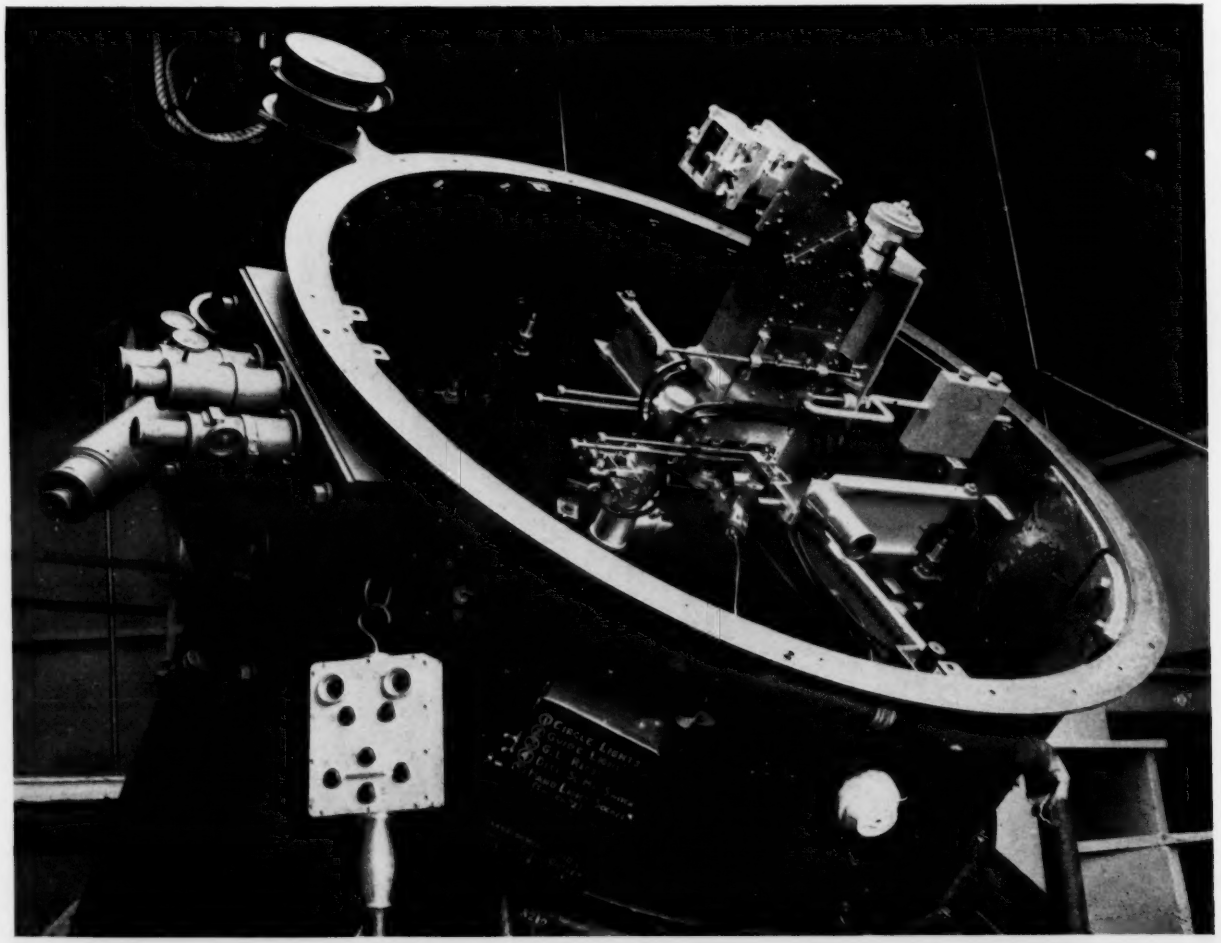

NEBULAR SPECTROGRAPH MOUNTED AT THE PRIMARY FOCUS OF THE CROSSLEY 36-INCH REFLECTOR

PLATE XIII

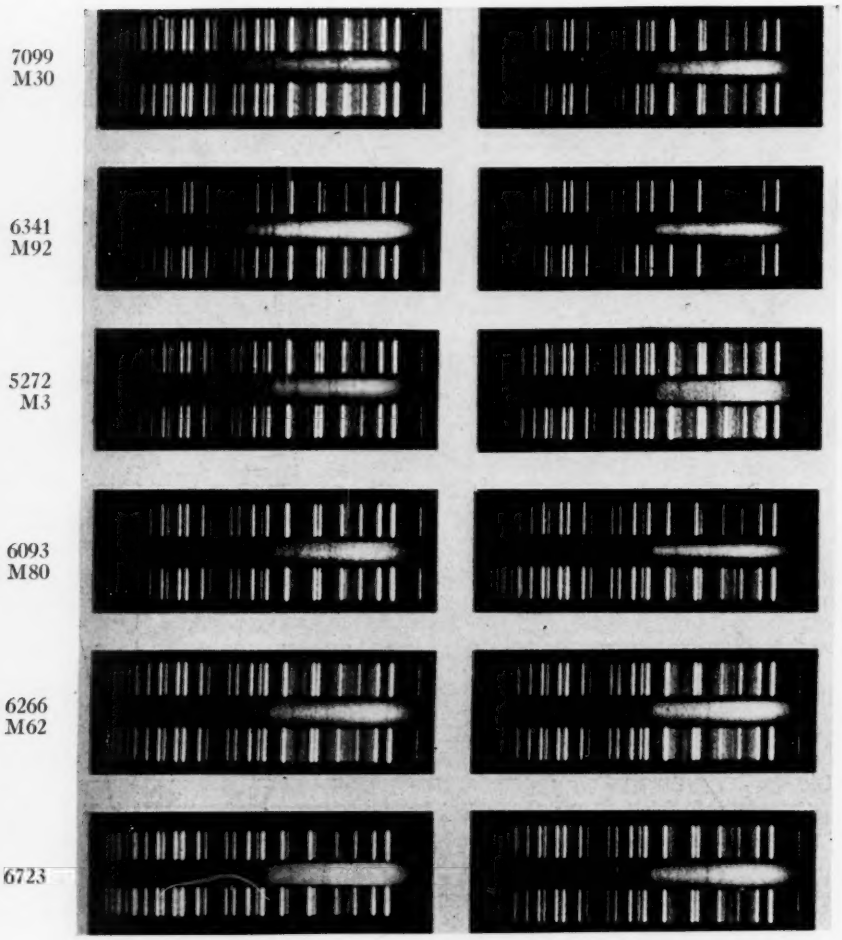

TYPICAL SPECTRA OF GLOBULAR STAR CLUSTERS

Linear dispersion of original negatives, 430 A/mm at *H;* enlargement, ×8.9

TABLE 1

RADIAL VELOCITIES OF GLOBULAR CLUSTERS FROM INDIVIDUAL SPECTROGRAMS

Cluster NGC	Date of Observation*	Exp. (Min.)	Velocity (Km/Sec)	Telescope
1851	1939 Nov. 18	180	+302	
	1939 Nov. 19	240	+277	
Mean			+290	36-inch
1904 (M 79)	1937 Oct. 10	60	+196	
	1938 Jan. 24	60	+255	
	1939 Jan. 11	60	+252	
	1939 Jan. 11	60	+245	
Mean			+237	Cr.
	1936 Nov. 9	270	+206	36-inch
2298	1941 Jan. 26	180	+ 20	
	1941 Jan. 28	210	+ 48	
	1941 Jan. 29	210	+ 72	
	1941 Jan. 30	210	+144	
	1941 Feb. 1	210	+ 36	
Mean			+ 64	Cr.
2419	1941 Feb. 2	600	+ 35	
	1941 Mar. 16+	420	+ 61	
	1941 Mar. 18+	450	− 30	
	1941 Mar. 20+	540	− 20	
Mean			+ 14	Cr.
4147	1935 Apr. 26	150	+232	
	1937 Mar. 16	180	+200	
	1938 Feb. 25	180	+184	
	1938 Apr. 21	180	+149	
Mean			+191	Cr.
4590 (M 68)	1937 May 14	210	−108	
	1939 Feb. 21	180	−109	
	1939 Feb. 22	180	−109	
	1939 Feb. 23	180	−140	
Mean			−116	Cr.
5024 (M 53)	1935 May 3	90	− 87	
	1937 May 28	60	− 66	
	1938 Feb. 26	60	− 87	
	1938 Apr. 22	90	− 55	
Mean			− 74	Cr.
	1938 May 3+	1110	−108	36-inch
5272 (M 3)	1935 May 4	90	−121	
	1937 May 30	30	−180	
	1938 Apr. 19	30	−144	
	1938 Apr. 19	30	−163	
Mean			−152	Cr.
	1936 Feb. 28	300	−177	
	1936 Mar. 1	285	−157	
Mean			−167	36-inch
5634	1935 May 3	90	− 56	
	1937 May 29	120	− 52	
	1938 Feb. 25	135	− 45	
	1938 Feb. 26	180	− 98	
Mean			− 63	Cr.

* A plus sign (+) after the date indicates that the exposure extended over several nights.

TABLE 1—*Continued*

Cluster NGC	Date of Observation*	Exp. (Min.)	Velocity (Km/Sec)	Tele-scope
5694	1935 May 30	120	−202	
	1937 May 31	225	−188	
	1938 June 2	240	−198	
	1938 June 25	180	−161	
Mean			−187	Cr.
5824	1935 May 4	60	− 68	
	1937 May 13	60	− 18	
	1938 July 16	60	− 49	
	1938 July 17	60	− 96	
Mean			− 58	Cr.
5904 (M 5)	1935 May 26	30	+ 68	
	1935 June 29	20	+ 74	
	1938 Apr. 19	37	+ 89	
	1938 July 16	20	− 6	
Mean			+ 56	Cr.
	1936 Mar. 22	300	+ 61	36-inch
5986	1939 May 25	180	− 16	
	1939 June 13	180	+115	
	1940 May 3	185	− 98	
	1940 June 2	210	+ 9	
Mean			+ 2	Cr.
6093 (M 80)	1935 May 26	40	+ 43	
	1935 June 29	80	− 3	
	1938 July 17	30	+ 8	
	1938 July 22	35	+ 21	
Mean			+ 17	Cr.
	1936 June 21	285	+ 12	36-inch
6171	1937 June 4+	360	−192	
	1937 July 1+	360	−120	
	1938 July 18	333	−121	
	1938 July 20+	364	−154	
Mean			−147	Cr.
6205 (M 13)	1937 June 30	30	−223	
	1937 July 11	30	−244	
	1938 July 4	35	−217	
	1938 July 4	36	−239	
Mean			−231	Cr.
	†1914 May 27+	645	−221	
	1936 June 15	270	−217	
Mean			−219	36-inch
6218 (M 12)	1935 May 26	180	+ 30	
	1937 May 16	110	+ 57	
	1938 May 26	180	+ 19	
	1938 June 28	120	+ 39	
Mean			+ 36	Cr.
6229	1935 May 31	60	−210	
	1937 June 30	91	−149	
	1938 May 25	120	−122	
	1938 July 30	120	−166	
Mean			−162	Cr.
	1936 June 17	405	−144	36-inch

† The spectrograms of 6205 (M 13) and of 7078 (M 15), taken in 1914, were obtained by W. H. Wright.

TABLE 1—*Continued*

TABLE 1—*Continued*

Cluster NGC	Date of Observation*	Exp. (Min.)	Velocity (Km/Sec)	Tele-scope
6254 (M 10)	1937 July 4	180	+104	
	1937 Aug. 5	120	+ 45	
	1938 July 22	120	+ 40	
	1938 July 23	150	+ 71	
Mean			+ 65	Cr.
6266 (M 62)	1935 May 31	60	− 63	
	1937 May 14	60	−134	
	1937 July 12	59	−158	
	1937 Aug. 11	58	− 88	
Mean			−111	Cr.
	1938 May 28	285	− 64	36-inch
6273 (M 19)	1935 June 7	60	+153	
	1937 May 14	70	+120	
	1937 July 12	87	+140	
	1937 July 28	84	+ 54	
Mean			+117	Cr.
	1938 June 23+	605	+116	36-inch
6284	1937 May 17	225	+ 34	
	1939 June 22	240	− 15	
	1939 June 23	330	+ 19	
	1939 July 6+	240	+ 51	
Mean			+ 22	Cr.
6293	1937 July 5	120	− 50	
	1937 Aug. 9	120	− 54	
	1938 July 2	110	− 82	
	1938 July 26	120	−107	
Mean			− 73	Cr.

Cluster NGC	Date of Observation*	Exp. (Min.)	Velocity (Km/Sec)	Tele-scope
6304	1936 July 25	90	−102	
	1940 June 26	180	− 41	
	1940 June 27	185	−115	
	1940 June 29	175	−117	
	1940 June 30	170	−117	
Mean			− 98	Cr.
6333 (M 9)	1937 July 7	180	+237	
	1937 Aug. 12	180	+196	
	1938 July 27	180	+221	
	1938 July 28	180	+244	
Mean			+224	Cr.
6341 (M 92)	1937 June 12	23	−114	
	1938 July 31	40	− 86	
	1938 Aug. 1	20	−137	
	1938 Aug. 1	20	−114	
Mean			−113	Cr.
	1936 May 24	300	−110	
	1936 June 19	180	− 78	
Mean			− 94	36-inch
6356	1937 July 10	120	+ 78	
	1938 June 3	140	+ 31	
	1938 June 6	180	+ 2	
	1938 June 7	180	+ 12	
Mean			+ 31	Cr.
6402 (M 14)	1937 June 11	328	−106	
	1937 July 31+	510	−149	
	1940 June 7	390	−125	
	1940 June 8	390	−104	
Mean			−121	Cr.

TABLE 1—*Continued*

Cluster NGC	Date of Observation*	Exp. (Min.)	Velocity (Km/Sec)	Telescope
6440	1940 July 1	355	−183	
	1940 July 3	360	−130	
	1940 July 4	350	−148	
	1940 July 6+	450	− 73	
	1940 July 9	360	−115	
Mean			−125	Cr.
6441	1937 May 15	60	− 59	
	1937 July 5	90	− 80	
	1938 Aug. 15	90	− 78	
	1938 Aug. 19	90	− 64	
Mean			− 70	Cr.
6544‡	1940 Aug. 27	210	+ 3	
	1940 Aug. 28	210	− 9	
	1940 Aug. 29	195	− 34	
	1940 Sept. 1	195	− 8	
Mean			− 12	Cr.
6624	1935 June 10	60	+105	
	1938 July 31	120	+ 58	
	1938 Aug. 16	110	+ 62	
	1938 Aug. 18	123	+ 50	
Mean			+ 69	Cr.
6626 (M 28)	1936 July 25	60	− 4	
	1937 July 13	60	+ 7	
	1938 July 30	100	− 26	
	1938 Aug. 18	110	− 15	
	1938 Aug. 19	90	+ 25	
Mean			− 3	Cr.
6637 (M 69)	1937 July 14	60	+ 89	
	1937 Aug. 13	140	+ 90	
	1938 Aug. 23	120	+ 97	
	1938 Aug. 24	152	+158	
	1938 Aug. 25	120	+ 39	
Mean			+ 95	Cr.
6638	1937 June 6	180	− 27	
	1937 Aug. 8	240	− 55	
	1938 Aug. 26	180	− 20	
	1938 Aug. 27	180	+ 24	
	1938 Aug. 28	180	+ 7	
Mean			− 14	Cr.
6652	1937 Aug. 29	180	−129	
	1938 July 4	154	−124	
	1938 Aug. 20	180	−139	
	1938 Aug. 22	180	−105	
Mean			−124	Cr.
6656 (M 22)	1937 July 14	90	−170	
	1937 July 27	60	−173	
	1938 June 26	60	−148	
	1938 July 4	56	−156	
Mean			−162	Cr.
6681 (M 70)	1937 July 12	92	+218	
	1938 June 25	90	+203	
	1938 June 26	60	+219	
	1939 Aug. 14	90	+154	
Mean			+198	Cr.

‡ Crossley reflector photographs taken in red light leave little doubt that NGC 6544 is a globular cluster; a similar conclusion, for different reasons, has also been reached by P. Collinder (*Ann. Lund Obs.*, No. 2, p. 340, 1931).

TABLE 1—*Continued*

† Crossley reflector photographs taken in red light leave little doubt that NGC 6544 is a globular cluster; a similar conclusion, for different reasons, has also been reached by P. Collinder (*Ann. Lund Obs.*, No. 2, p. 340, 1931).

TABLE 1—*Continued*

Cluster NGC	Date of Observation*	Exp. (Min.)	Velocity (Km/Sec)	Telescope
6712	1936 Aug. 11	180	− 67	
	1937 July 10	230	−127	
	1938 June 30	165	−175	
	1938 July 29	208	−155	
Mean			−131	Cr.
6715 (M 54)	1935 June 1	35	+ 95	
	1936 July 18	30	+131	
	1938 June 26	30	+ 86	
	1938 July 3	33	+139	
Mean			+113	Cr.
	1936 Aug. 12	120	+100	36-inch
6723	1940 July 10	210	+ 8	
	1940 July 25	180	+ 16	
	1940 July 26	180	+ 1	
	1940 July 27	210	− 37	
Mean			− 3	Cr.
6779 (M 56)	1935 July 26	205	−188	
	1936 Aug. 13	180	−130	
	1937 July 12	135	−201	
	1937 Aug. 12	180	−210	
Mean			−182	Cr.
6838 (M 71)§	1937 July 8	180	− 58	
	1937 Sept. 28	300	−144	
	1938 June 28	300	− 62	
	1938 July 22	255	− 55	
Mean			− 80	Cr.
6864 (M 75)	1935 June 8	55	−224	
	1937 July 5	45	−229	
	1937 Oct. 9	45	−222	
	1938 June 25	45	−186	
Mean			−215	Cr.
	1935 July 8	180	−232	36-inch
6934	1935 June 7	60	−266	
	1937 July 3	60	−395	
	1937 July 6	75	−355	
	1937 July 13	120	−416	
Mean			−358	Cr.
6981 (M 72)	1937 Aug. 5	285	−281	
	1937 Aug. 9	300	−317	
	1937 Sept. 29+	300	−230	
	1938 July 23	260	−269	
Mean			−274	Cr.
7006	1935 July 8	260	−394	
	1937 July 13	220	−309	
	1937 Oct. 9	240	−368	
	1938 July 21	240	−322	
Mean			−348	Cr.
7078 (M 15)	1937 Aug. 13	16	−135	
	1937 Aug. 13	16	−159	
	1938 July 29	15	− 87	
	1938 July 29	15	−125	
Mean			−126	Cr.

§ Although Shapley (*Star Clusters*, p. 233) includes NGC 6838 (M 71) in his catalogue of galactic clusters, it is here considered to be a globular cluster, for the following reasons: (1) J. Cuffey (*Pub. A.A.S.*, **10**, 122, 1941), from star counts on 36-inch reflector plates, found a diameter of 23 minutes of arc and a population of between three and four thousand stars. (2) Crossley reflector plates suggest the presence of a rich background of faint stars, typical of globular clusters. (3) R. J. Trumpler (*Lick Obs. Bull.*, **14**, No. 420, 175, 1930) did not include M 71 in his preliminary catalogue of open-star clusters because of its exceptional richness, which would set it apart from all the other known galactic clusters.

TABLE 1—*Continued*

Cluster NGC	Date of Observation*	Exp. (Min.)	Velocity (Km/Sec)	Tele-scope
	†1914 Aug. 16+	840	− 86	
	1936 July 26	120	−107	
Mean.....	.....	.....	− 96	36-inch
7089 (M 2).....	1935 June 30	32	+ 39	
	1935 Sept. 24	15	− 6	
	1937 Aug. 29	20	+ 15	
	1937 Sept. 30	20	+ 24	
Mean.....	.....	.....	+ 18	Cr.
	1936 July 26	120	+ 8	36-inch
7099 (M 30).....	1935 June 10	20	−178	
	1937 July 6	30	−128	
	1937 Sept. 30	30	−217	
	1938 June 26	30	−147	
Mean.....	.....	.....	−168	Cr.
	1936 Aug. 12	300	−163	36-inch

compared with the "plate error."[14] The latter presumably is composed chiefly of photographic and instrumental effects, whose influence is more likely to be lessened by single measures of a number of plates than by several measures of but one or two plates.

Plate XIII reproduces some typical low-dispersion spectrograms, in which the principal point to be noticed is the scarcity of absorption lines suitable for radial-velocity measurement. The two most prominent ones (near the center of the illustrations) are the *H* and *K* lines; the fainter are $H\gamma$, G-band, $H\delta$, and some blends to the violet of the calcium pair. Since the wave lengths of these blends were found from measures of stellar spectra to depend to a large extent upon the type of spectrum, the blends are unsuitable for radial-velocity determinations of objects having a variable degree of spectrum composite-

TABLE 2

COMPARISON OF RADIAL VELOCITIES DETERMINED WITH THE CROSSLEY REFLECTOR AND THE 36-INCH REFRACTOR*

Globular Cluster NGC	Crossley (426 A/Mm) (Km/Sec)	36-Inch (130 A/Mm) (Km/Sec)	Difference Cr.−36-Inch (Km/Sec)
1904 (M 79)	+237	+206	+31
5024 (M 53)	− 74	−108	+34
5272 (M 3)	−152	−167	+15
5904 (M 5)	+ 56	+ 61	− 5
6093 (M 80)	+ 17	+ 12	+ 5
6205 (M 13)	−231	−217	−14
6229	−162	−144	−18
6266 (M62)	−111	− 64	−47
6273 (M 19)	+117	+116	+ 1
6341 (M 92)	−113	− 94	−19
6715 (M 54)	+113	+100	+13
6864 (M 75)	−215	−232	+17
7078 (M 15)	−126	−107	−19
7089 (M 2)	+ 18	+ 8	+10
7099 (M 30)	−168	−163	− 5

* Systematic difference = +0.1 km/sec; average difference = 16.9 km/sec (without regard to sign).

ness. Their exclusion leaves, at most, five lines for measurement; in some cluster spectra only the *H* and *K* lines can be seen in measurable strength. As a general rule, in order to allow for the differing visibilities, the calcium lines were each given double weight, $H\delta$ weight unity, and the G-band and $H\gamma$ each half-weight, when the velocity was deduced for an individual spectrogram. Under these circumstances it is easy to see why globular-cluster velocities, determined by low dispersion of their integrated light, are unlikely to be of high accuracy.

IV. ACCURACY OF THE RADIAL VELOCITIES

The order of accuracy attained with spectra of such small scale may be indicated as follows: From 202 plates of forty-nine globular clusters, the probable error of a single plate was found to be ± 22 km/sec; the mean of 4 plates, accordingly, has a probable error of ± 11 km/sec. Since, however, a probable error deduced in this way merely describes the internal consistency, it was thought desirable to check the external or sys-

[14] The question has been considered in detail in *Lick Obs. Contr.*, Ser. II, No. 1; *Ap. J.*, **95**, 5, 1942.

tematic error by some other means. After a few trial exposures it was found possible to photograph the spectra of sixteen of the brightest and more concentrated clusters with the previously mentioned fast stellar spectrograph used with the 36-inch refractor. Since this instrument gives approximately three times the dispersion of the Crossley nebular spectrograph and since spectrograms obtained with it of standard radial-velocity stars showed no appreciable systematic error, it was thought that a series of plates taken in this manner with the refractor would afford the desired check on the velocities obtained with the reflector. There are fifteen clusters for which it is possible to form the difference: Crossley reflector *minus* 36-inch refractor. Table 2 shows how closely the two groups of velocities agree. With the exception of NGC 6266, for which the difference is 47 km/sec, the two sets of measures agree quite satisfactorily, for the systematic difference is only 0.1 km/sec.

V. COMPARISON WITH OTHER DETERMINATIONS

In order to compare the Lick velocities with those determined elsewhere, it is necessary, first, to combine the data from the two telescopes. Because there were not enough 36-inch refractor spectrograms to give a reliable value of the probable error of a single plate, it was assumed that single refractor plates deserve three times as much weight as single Crossley reflector plates. The assumed ratio of weights depends upon the linear dispersions, which are 130 A/mm and 426 A/mm for refractor and reflector spectrograms, respectively. Since the probable error of a single Crossley reflector plate was found to be ± 22 km/sec, the relative weight of 3 for a single 36-inch refractor plate is equivalent to a probable error of $\pm 22/\sqrt{3} = \pm 13$ km/sec. This value agrees reasonably well with those usually found from measures of stellar spectra having few lines of poor visibility.

When the velocities in Table 2 are combined on the basis of weight 1 for Crossley plates and weight 3 for 36-inch refractor plates, it is found that the total weights indicate internal probable errors of ± 7 to ± 11 km/sec for the mean cluster velocities. To estimate the external probable errors, an attempt has been made to collect in Table 3 all the previously determined radial velocities of globular clusters, for comparison with those measured at Lick.

Examination of the differences in Table 3 discloses several large values: there are two greater than 100 km/sec and seven of 50 km/sec or greater. While it is difficult to know where to draw the line denoting significance, differences of 50 km/sec or greater probably are abnormal, whereas occasional differences of 30–40 km/sec reasonably may be expected because of the natural difficulties attending the determinations. On this admittedly arbitrary basis there are seven clusters for which the various measures appear to be in serious disagreement. In some of these cases, as the result of private correspondence,[15] the discrepancies have been found to be more apparent than real; the circumstances are considered in detail in the following paragraphs.

NGC 5024 (M 53).—Both the Lowell and the Mount Wilson determinations give large differences with the same sign: -76 and -111 km/sec, respectively. The Lowell velocity, -165 km/sec, however, is the weighted mean of two discordant measures, -170 and -83: km/sec, by Slipher and by Edmondson, respectively. On the other hand, the Mount Wilson velocity, -200 km/sec, is regarded with some confidence by Sanford, who obtained it from a single spectrogram (mean dispersion 210 A/mm between *K* and *H*), exposed $16^h\ 30^m$. The Lick velocities, -74 and -108 km/sec, from reflector and refractor plates, respectively, are in fair agreement. The value -108 km/sec is considered especially trustworthy, because it was obtained from an excellent spectrogram of $18^h\ 30^m$

[15] The writer is much indebted to Messrs. Edmondson, Humason, and Sanford for supplementary data, which have been used in this discussion. The additional information has been invaluable in the effort to elucidate the differences in, and to arrive at the most probable values of, the velocities.

TABLE 3

COMPARISON OF GLOBULAR CLUSTER VELOCITIES

CLUSTER (NGC)	LICK		LOWELL*		MT. WILSON		LO.−LI. (KM/SEC)	MT.W.−LI. (KM/SEC)	SOURCE NOTES
	Km/Sec	No. Pl.†	Km/Sec	No. Pl.	Km/Sec	No. Pl.			
1851	+290	(—, 2)	+295	(1)	.....	.....	+ 5	.....	.....
1904 (M 79)	+224	(4, —)	+245	(1)	.....	.....	+21	.....	.....
2419	+ 12	(4, —)	.....	.....	+ 20	(1)	.....	+ 88	1
5024 (M 53)	− 89	(4, 1)	−165	(1)	−200	(1)	−76	−111	2
5272 (M 3)	−161	(4, 2)	−135	(4)	−140	(1)	−26	+ 21	3
					−153	(15)	.....	+ 8	
5904 (M 5)	+ 58	(4, 1)	+ 30	(3)	.....	.....	−28	.....	.....
6093 (M 80)	+ 15	(4, 1)	+ 45:	(1)	.....	.....	+30:	.....	.....
6205 (M 13)	−225	(4, 2)	−240	(1)	−230	(4)	−15	− 5	4
6218 (M 12)	+ 36	(4, —)	.....	.....	+160	(1)	.....	+124	2
6229	−154	(4, 1)	−135	(1)	.....	.....	+19	.....	.....
6254 (M 10)	+ 65	(4, —)	+ 90	(1)	.....	.....	+25	.....	.....
6266 (M 62)	− 91	(4, 1)	− 45	(1)	.....	.....	+46	.....	5
6273 (M 19)	+117	(4, 1)	+ 50	(1)	.....	.....	−67	.....	.....
6333 (M 9)	+224	(4, —)	+225	(1)	.....	.....	+ 1	.....	.....
6341 (M 92)	−105	(4, 2)	−150	(2)	.....	.....	−45	.....	.....
6402 (M 14)	−121	(4, —)	−150:	(1)	.....	.....	−29:	.....	6
6440	−125	(5, —)	.....	.....	−175	(1)	.....	− 50	7
6626 (M 28)	− 3	(5, —)	+ 10	(1)	.....	.....	+13	.....	.....
6656 (M 22)	−162	(4, —)	−135	(2)	.....	.....	+27	.....	8
6779 (M 56)	−182	(4, —)	.....	.....	− 40	(1)	.....	+142	9
6934	−358	(4, —)	−365	(1)	.....	.....	− 7	.....	.....
6981 (M 72)	−274	(4, —)	.....	.....	−180	(1)	.....	+ 94	7
7006	−348	(4, —)	.....	.....	−350	(1)	.....	− 2	7
7078 (M 15)	−118	(4, 2)	−110	(2)	−180	(1)	+ 8	− 62	
					−156	(2)	.....	− 38	10
					− 93	(1)	.....	+ 25	
7089 (M 2)	+ 14	(4, 1)	− 15	(5)	.....	.....	−29	.....	.....
7099 (M 30)	−166	(4, 1)	−155	(1)	.....	.....	+11	.....	.....

* Except as indicated in the notes to the table, velocities in this column are those reported by F. K. Edmondson (*Lowell Obs. Bull.*, **3**, No. 88, 143, 1935) upon the basis of all the spectra measured by him and by V. M. Slipher.

† The first figure denotes the number of Crossley plates, the second, the number of 36-inch refractor plates.

NOTES

1. 2419. W. Baade, *Carnegie Yrbk.*, **33**, 143, 1934; *Ap. J.*, **82**, 396, 1935; *Mt. W. Contr.*, No. 529. The velocity represents a slight revision of the one (+15 km/sec) communicated by M. L. Humason to Edmondson, *Lowell Obs. Bull.*, **3**, No. 88, **143**, 1935.

2. 5024 (M 53) and 6218 (M 12). The Mount Wilson determinations are by R. F. Sanford, *Carnegie Yrbk.*, **18**, 250, 1919, and refer to the nuclei.

3. 5272 (M 3). The first Mount Wilson velocity of −140 km/sec is by Sanford (*ibid.*) and is the mean of velocities found for 4 stars; the velocity supersedes the value −190 km/sec originally given as the mean for 7 stars (*ibid.*, **17**, 213, 1918). The second Mount Wilson velocity, −153 km/sec, is that reported by A. H. Joy (*Ap. J.*, **92**, 396, 1940; *Mt. W. Contr.*, No. 637) for a 15-day Cepheid (Barnard's variable) in the cluster.

4. 6205 (M 13). The Mount Wilson velocity is a mean of plates for four stars, measured by W. S. Adams, Joy, and Humason and quoted by G. Strömberg (*Ap. J.*, **61**, 353, 1925; *Mt. W. Contr.*, No. 292). The attribution to "Sanford—unpublished" in J. H. Moore's "General Catalogue" (*Pub. Lick Obs.*, **18**, 217, 1932) is an error.

5. 6266 (M 62). The velocity originally reported by Slipher (*Pop. Astr.*, **26**, 8, 1918; **30**, 11, 1922; **32**, 622, 1924), −50 km/sec, appears with the wrong sign in Strömberg's compilation (*Ap. J.*, **61**, 353, 1925; *Mt. W. Contr.*, No. 292). The value tabulated here for Lowell represents a correction of this error, which was also included in Edmondson's list.

6. 6402 (M 14). The velocity reported by Edmondson, +150:km/sec, seems to be another case of wrong sign. In a private communication to the writer, Edmondson states that the velocity given for 6402

NOTES TO TABLE 3—*Continued*

is the weakest in his list, that only two lines were measured, and that it is possible that the spectrum was measured backward in the Hartmann comparator. For these reasons and because measures of individual lines in the Lick spectra gave negative velocities without exception, the Lowell velocity is tabulated here as one of approach.

7. 6440, 6981 (M 72), and 7006. The Mount Wilson velocities are by Humason, *Pub. A.S.P.*, **46**, 357, 1934.

8. 6656 (M 22). The velocity originally reported by Edmondson, −100 km/sec, was a mean of the Lowell and (Humason's) Mount Wilson determinations; the value tabulated here is a revision which includes additional data kindly supplied by Edmondson in correspondence with the writer.

9. 6779 (M 56). The Mount Wilson velocity is by Humason, who communicated it to Edmondson (*op. cit.*).

10. 7078 (M 15). The first Mount Wilson velocity, −180 km/sec, is from a measure by Adams of a plate taken by Pease, *Pub. A.S.P.*, **40**, 342, 1928. The second Mount Wilson velocity, −156 km/sec, is from measures by Humason of two plates obtained by Pease (*ibid.*). The velocity is for an emission-line object which Pease considered to be a planetary nebula, possibly associated with the cluster. The third Mount Wilson velocity, −93 km/sec, is a determination by Sanford, referred to by Pease in his note describing the bright-line object.

exposure, dispersion 130 A/mm at $H\gamma$. On the basis of all the evidence, weights were assigned to the several measures as shown in the accompanying tabulation.

	Velocity (Km/Sec)	Rel. Wt.
Lowell (V. M. S.)	−170	1.5
Lowell (F. K. E.)	− 83:	0.5
Mt. W. (R. F. S.)	−200	1
Lick (Cr.)	− 74	4
Lick (36-inch)	−108	3
Adopted	−112	10

NGC 6218 (M 12).—The large difference of +124 km/sec between the Lick and the Mount Wilson measures probably may be wholly discounted. Dr. Sanford has little confidence in his pioneer determination, which was made under poor conditions and with a spectrograph now regarded as very inferior. The velocity +160 km/sec will therefore be omitted from further discussion in the present paper, and for this cluster the adopted velocity = +36 km/sec, weight 4.

NGC 6273 (M 19).—The difference of −67 km/sec between the Lick and the Lowell determinations seems to be real. Slipher's and Edmondson's measures of +30 and +71 km/sec, respectively, are in satisfactory agreement, as are the Lick reflector and refractor results of +117 and +116 km/sec, respectively. With weights of 2 and 7 assigned to the mean Lowell and Lick velocities, respectively, for this cluster, the adopted velocity= +102 km/sec, weight 9.

NGC 6440 and 6981 (M 72).—The differences of −50 and +94 km/sec between the Lick and the Mount Wilson determinations for these two clusters are hardly more than might be expected, since the Mount Wilson velocities were reported to be uncertain by ±50 km/sec. Both the Lick and the Mount Wilson determinations depend only upon measures of small-scale spectra (dispersion 430 A/mm at $H\gamma$), the former upon four or five plates per cluster, the latter upon one plate per cluster.[16] The assignment of unit

[16] That a range as large as 200 km/sec among individual plates may occasionally occur with low dispersion can be seen from the measures listed in Table 1 for NGC 5986; in general, however, the range is of the order of 100 km/sec.

weight to each plate for these two clusters leads to the following adopted velocities: 6440, −133 km/sec, weight 6; 6981 (M 72), −255 km/sec, weight 5.

NGC 6779 (M 56).—The difference of +142 km/sec may represent an extreme example of the circumstances discussed for the foregoing two clusters. The basic spectroscopic material is of the same nature, consisting wholly of small-scale spectra. Although it is an unsatisfactory procedure, about all that can be done in this case is to assign weights on the same basis, which gives for this cluster an adopted velocity = −154 km/sec, weight 5.

NGC 7078 (M 15).—The difference of −62 km/sec between the mean of the Lick plates, —118 km/sec, and the early Mount Wilson velocity, −180 ± 50 km/sec, again seems to be a case of the pioneer determination's being unreliable. The velocity in question depends upon measures of only three lines on a single low-dispersion (about 350 A/mm) spectrogram of poor definition. The other early Mount Wilson velocity, −93 km/sec, was measured by Sanford, who considers it to be worth unit weight. The third Mount Wilson velocity, −156 km/sec, is for a bright-line object whose membership in the cluster remains to be established. Until the matter is clarified by further observations, it seems best not to include it in the average, which is computed as in the accompanying tabulation.

	Velocity (Km/Sec)	Rel. Wt.
Lick	−118	10
Lowell	−110	4
Mt. W.	− 93	1
Adopted	−114	15

With the outstanding cases of discordance in Table 3 treated as described above, there remains a number of differences in velocity which provide the accompanying summary tabulation.

AVERAGES OF DIFFERENCES <50 KM/SEC

	No. Vel.	With Sign (Km/Sec)	Without Sign (Km/Sec)
Lo.−Li.	18	+1.4	21.4
Mt. W.−Li.	7	+2.4	15.3

These results suggest that the systematic differences—those averaged with regard to sign—are satisfactorily small, of the order of only a few km/sec. On the other hand, the average differences without regard to sign indicate that the adopted velocities may be uncertain by an external probable error several times their internal probable error, that is to say, by as much as ±15 to ±20 km/sec. The new velocities reported herein, especially those which depend only upon the low-dispersion Crossley spectrograms, should therefore be used with caution in refined investigations of the motions of individual clusters.

The complete list of adopted velocities, which it is hoped will approximate the most probable velocities based on all available data, is given in Table 4. The system of weighting is as follows: (1) Mount Wilson and Crossley low-dispersion (430 A/mm at $H\gamma$)

spectrograms, each unit weight; (2) Lowell spectrograms (average dispersion 160 A/mm between K and $H\beta$), weight 2; Lick 36-inch refractor plates (130 A/mm at $H\gamma$), weight 3. Joy's velocity for Barnard's variable in NGC 5272 (M 3), based on thirteen plates of 120 A/mm dispersion and on two of 75 A/mm, undoubtedly deserves high weight, although, without knowledge of the velocity dispersion in clusters, it is difficult to know what relative weights to give to a well-determined velocity for a single star and to a less

TABLE 4

RADIAL VELOCITIES OF FIFTY GLOBULAR STAR CLUSTERS

Globular Cluster NGC	Radial Velocity (Km/Sec)	Relative Wt.*	Globular Cluster NGC	Radial Velocity (Km/Sec)	Relative Wt.*
1851	+291	8	6341 (M 92)	−118	14
1904 (M 79)	+231	6	6356	+ 31	4
2298	+ 64	5	6402 (M 14)	−131	6
2419	+ 14	5	6440	−133	6
4147	+191	4	6441	− 70	4
4590 (M 68)	−116	4	6544	− 12	4
5024 (M 53)	−112	10	6624	+ 69	4
5272 (M 3)	−150	24	6626 (M 28)	+ 1	7
5634	− 63	4	6637 (M 69)	+ 95	5
5694	−187	4	6638	− 14	5
5824	− 58	4	6652	−124	4
5904 (M 5)	+ 45	13	6656 (M 22)	−148	8
5986	+ 2	4	6681 (M 70)	+198	4
6093 (M 80)	+ 18	9	6712	−131	4
6171	−147	4	6715 (M 54)	+107	7
6205 (M 13)	−228	16	6723	− 3	4
6218 (M 12)	+ 36	4	6779 (M 56)	−154	5
6229	−150	9	6838 (M 71)	− 80	4
6254 (M 10)	+ 73	6	6864 (M 75)	−222	7
6266 (M 62)	− 81	9	6934	−360	6
6273 (M 19)	+102	9	6981 (M 72)	−255	5
6284	+ 22	4	7006	−348	6
6293	− 73	4	7078 (M 15)	−114	15
6304	− 98	5	7089 (M 2)	− 3	17
6333 (M 9)	+224	6	7099 (M 30)	−164	9

* When the relative weight is 4–6, the velocity depends only upon spectrograms of low dispersion (430 A/mm at $H\gamma$).

accurate velocity for the combined light of many stars. Pending the results for several other bright cluster-variables, which are on Joy's observing program, the velocity for Barnard's variable in M 3 will be given weight 5.

VI. SPECTRAL TYPES

Before proceeding to a discussion of the velocities of the globular clusters, their spectral types will be considered. Estimates were made of all the Lick spectra, and the averages for each cluster are given in Table 5, columns 2 and 3. For comparison, the spectral types estimated at Harvard and at Mount Wilson are given in columns 4 and 5. Data in the remaining three columns are discussed in Section VII.

In making the estimates of spectral type, no attention was paid to the distribution of light in the continuous spectrum, for the reasons set forth in Section II; the classification is based entirely upon a comparison of the intensities of lines in the cluster spectra with those in stellar standards selected from a Mount Wilson list.[17] Estimates made on differ-

[17] *Ap. J.*, **81**, 187, 1935; *Mt. W. Contr.*, No. 511.

TABLE 5

SPECTRAL TYPES AND COLOR CLASSES OF GLOBULAR CLUSTERS

CLUSTER NGC (1)	SPECTRAL TYPE				COLOR CLASS		NO. OF NEB. (8)
	Cr. (2)	36-Inch (3)	Harv.* (4)	Mt. W. (5)	Obs.† (6)	Corr.‡ (7)	
1851	.....	(d)F5	G0	.....	.....	.....	.....
1904	F8	(d)F3	F8	.....	.....	.....	.....
2298	F8	.....	.....	.....	.....	.....	.....
2419	F5	.....	.....	F5§	a9	a3	87
4147	A5	.....	A7?	.....	f6	f5	48
4590	A6	.....	.....	.....	.....	.....	34
5024	F2	A8n	.....	.....	f6	f4	65
5272	F5	(d)F2	G	.....	f8	f6	50
5634	F4	.....	.....	.....	f6	f4	35
5694	A9	.....	.....	.....	f6	f3	39
5824	F4	(d)F5:	F8	.....	f8	f3	12
5904	F6	(d)F7	G?	.....	f8	f6	63
5986	G0	.....	F8	.....	f9	f2	0
6093	F8	(d)F4	K0	.....	f9	f4	6
6171	G2	.....	.....	.....	k0	g7	3
6205	F7	(d)F2	G0	F0‖	f9	f6	34
6218	F7	.....	.....	.....	g1	f7	18
6229	G0	(d)F6	.....	.....	f8	f6	56
6254	G0	.....	.....	.....	g2	f9	0
6266	G1	(d)F6	K0	.....	g5	f1	0
6273	F2	(d)F2	G5?	.....	g3	f2	0
6284	G1	.....	F?	.....	g1	f1	0
6293	A9	.....	G5	.....	g0	a3	0
6304	G3	.....	K?	.....	k0	f0	0
6333	F1	.....	(K)	.....	g4	f5	0
6341	A9	A5n	G5?	.....	f5	f2	43
6356	(g)G2	.....	K0	.....	g7	f8	0
6402	G0	.....	.....	.....	g7	g1	0
6440	G3	.....	.....	G3¶	m	a6	0
6441	G4	.....	K0	.....	g8	f5	0
6544	G1	.....	.....	.....	.....	.....	0
6624	G4	.....	M0	.....	g4	f6	0
6626	G0	.....	G5	.....	g6	f4	0
6637	G5	.....	K2	.....	g7	g1	0
6638	G3	.....	.....	.....	g4	f4	0
6652	G3	.....	K5	.....	g3	f7	0
6656	F6	.....	.....	.....	g2	f3	0
6681	G2	.....	.....	.....	f8	f2	0
6712	G4	.....	.....	.....	g7	f2	0
6715	F7	F0	F8	.....	g1	f6	0

* A. J. Cannon, *Harvard Bull.*, No. 868, 1929.

† Stebbins and Whitford, *Ap. J.*, **84**, 132, 1936; *Mt. W. Contr.*, No. 547.

‡ Corr. color class obtained from calibration of photoelectric C_3 scale (Stebbins and Whitford's Table II, *op. cit.*) and from corr. C.I. = Obs. C.I. − 0.0237 csc *b*.

§ Humason, quoted by Baade, *Ap. J.*, **82**, 396, 1935; *Mt. W. Contr.*, No. 529.

‖ F. G. Pease, *Pub. A.S.P.*, **26**, 204, 1914. Mean for thirty-nine stars.

¶ M. L. Humason, *Pub. A.S.P.*, **46**, 357, 1934.

TABLE 5—*Continued*

Cluster NGC (1)	Spectral Type				Color Class		No. of Neb. (8)
	Cr. (2)	36-Inch (3)	Harv.* (4)	Mt. W. (5)	Obs.† (6)	Corr.‡ (7)	
6723	G3	.....	.....	.....	f7	f2	0
6779	F5	.....	.....	.....	f8	a3	0
6838	(g)G5	.....	.....	.....	.....	.....	0
6864	G1	(d)F8	G0	.....	g1	f8	16
6934	F9	.....	G0	.....	f8	f4	15
6981	G2	.....	.....	G5¶	f8	f6	15
7006	F1	.....	.....	G3¶	f6	f2	50
7078	F0	(d)F0	F	.....	f6	f2	20
7089	F3	(d)F0	F5	.....	f7	f4	25
7099	A6	A7n	F8	.....	f4	f2	27

ent plates of the same cluster ranged over about one-half of a spectral class, with no range greater than one spectral class. For the fifty clusters observed, the average type is F7.6 ± 3.6 (p.e.), with a frequency distribution as shown in the accompanying tabulation.

Sp.	No.	Sp.	No.	Sp.	No.	Sp.	No.
A5	1	F0	1	F5	4	G0	5
A6	1	F1	1	F6	2	G1	5
A7	1	F2	2	F7	1	G2	5
A8	0	F3	1	F8	5	G3	4
A9	3	F4	2	F9	1	G4	3
						G5	2

The cluster spectral types thus appear to be included in the interval from A5 to G5, with a preponderant number (thirty) within the smaller range from F8 to G5. This latter result may not be fairly representative, for two reasons: (*a*) There is an indication of a systematic effect related to the dispersion employed, for the spectral types in column 2, deduced from low-dispersion spectra, average 0.3 spectral class later than those in column 3, deduced from spectra dispersed three times as much. (*b*) There is some suggestion of a fairly compact group of about ten clusters, centered at longitude 330° and latitude −10°, which average nearly G2 and which therefore contribute largely to the frequencies for the later spectral classes.

The spectral-type estimates in column 4 were made by Miss Cannon from objective-prism photographs taken for the *Henry Draper Catalogue*. It is evident from her estimates and from the notes accompanying them that Miss Cannon used the distribution of light in the continuous spectrum, as well as the faintly visible dark lines, to classify the spectra. For this reason and also because Miss Cannon's estimates were made before it was known that the globular clusters are reddened by selective interstellar absorption, we find a number of clusters classified as late as K0–M. In the light of present knowledge, such attributions are mainly of historical interest and are illustrative of the difficulties of classifying objective-prism spectra of objects having an appreciable size.

Of the five Mount Wilson classifications given in column 5, four are by Humason and one by Pease. The latter, in a notable pioneering observation, classified the spectra of thirty-nine individual stars in NGC 6205 (M 13) from three plates exposed from 20 to 30

hours in a focal-plane spectrograph attached to the 60-inch reflector. Pease's average of F0 is in good agreement with the estimate of F2 based on the best Lick spectrogram. There is also entirely satisfactory agreement between Humason's estimates and those based on Crossley spectra of corresponding low dispersion.

Further discussion of the spectral types of globular clusters should be prefaced by the statement that the estimates of type are bound to be somewhat uncertain because of the composite and peculiar nature of the spectra. It was noticed that, in general, the clusters in the range from A5 to about F8 were more difficult to classify than those assigned to classes F8–G5. When the cluster spectra were matched against the standard stellar spectra, it was frequently found that, for a given cluster, its spectral type was uncertain by one-half, or even by as much as one spectral class, depending upon the particular line being matched. Thus the *K*-line in many cases seemed to be "filled in" or to be weaker than one would expect from the intensities of $H + H\epsilon$ and of the G-band. As a rule, the *K*-line yielded the earliest type, $H\delta$ and $H\gamma$ the average, and the G-band the latest. The ultraviolet blends usually suggested an earlier-than-average classification, but they were not an important factor in the estimates because the spectra so often were underexposed to the violet of *H* and *K*. In only two cases (NGC 6356 and 6838) was the *CN* feature at λ3883 seen in sufficient strength to suggest the possibility of giant characteristics in the integrated light. In fact, a dispersion of only 300–450 A/mm for these cluster spectra seems incapable of clearly revealing the spectroscopic differences between giants and dwarfs. In the case of the spectra obtained with the refractor, however, the dispersion was large enough (from 80 to 150 A/mm) to show, in a number of clusters, the *Sr* II lines at λ 4077 and λ4215. Their intensities closely matched those in ordinary dwarfs, a circumstance which has been indicated in column 3 of Table 5 by "(d)."

The weakness of the *K*-line and of the *Sr* II lines in these cluster spectra may be regarded as another example of the different and peculiar spectral characteristics already noted by Morgan, Keenan, and Miss Kellman[18] in the spectra of several high-velocity stars and of the isolated cluster-type variable, RR Lyrae. The conventional spectroscopic absolute-magnitude criteria suggest that these stars are dwarfs, but other evidence indicates that they are giants. The discrepancies, however, have been pointed out by Baade[19] as being but further manifestations of the differences between stars of his population Types I and II. Since the globular cluster stars, those of high velocity, and the RR Lyrae variables all belong to Type II, it is not surprising that they have certain spectral features in common.

VII. COMPARISON OF COLOR AND SPECTRAL CLASSES

Of the last three columns of Table 5, column 6 gives the color class, determined photoelectrically by Stebbins and Whitford;[11] column 7 the color class, corrected for space reddening on the basis of their cosecant relation; and column 8 the number of nebulae, counted on a fairly uniform series of 1-hour Crossley photographs of the clusters. The observed and corrected color classes are shown plotted against the spectral classes in Figure 1, *A* and *B;* the clusters in fields with and without nebulae are indicated by different symbols.

Considering, first, the essentially unreddened clusters—those in fields with nebulae—we see that there is not much variation in color class with spectral class and that the blueness of NGC 2419 apparently sets it apart from the other clusters. Another such case may be NGC 7492, which has a color class of a5 but which is too faint to have been observed with the spectrograph. Considering, next, the reddened clusters, we see that reduction of their colors on the basis of the cosecant relation brings them as a group into general agreement with the unobscured clusters. There are a few exceptions, such as NGC

[18] *An Atlas of Stellar Spectra* ("Astrophysical Monographs"), 1943.

[19] *Ap. J.*, **100**, 137, 1944; *Mt. W. Contr.*, No. 696.

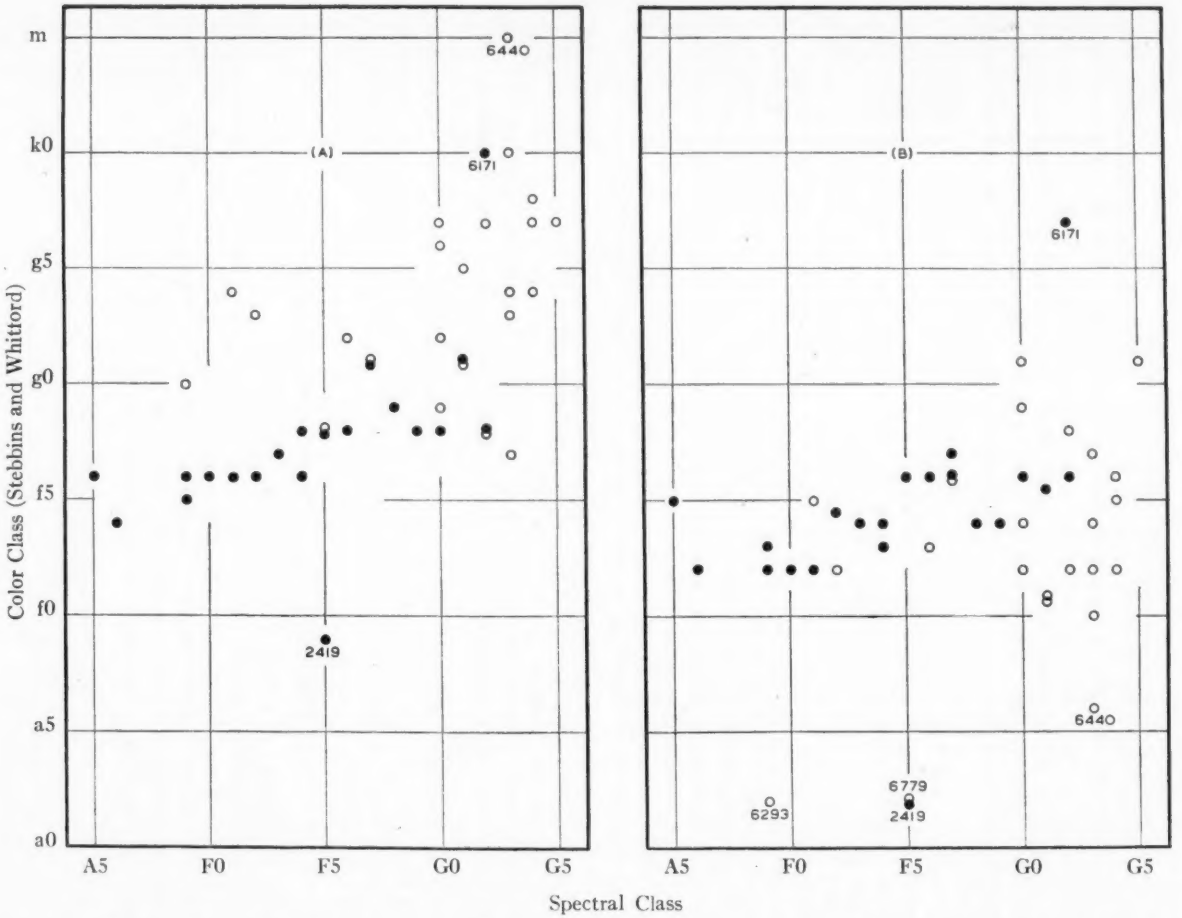

FIG. 1.—Comparison of color and spectral classes of globular clusters. *A*, observed photoelectric color classes. *B*, color classes corrected for space reddening according to cosecant relation. ●, clusters in fields with nebulae. ○, clusters in fields without nebulae.

6293 and 6779, for which the correction seems to be too large, and NGC 6171, for which it appears to be too small. NGC 6440, with the lowest latitude (+2°.4 referred to the Harvard pole), is, of course, extremely sensitive to a cosecant correction, and its departure from the others is hardly significant. On the whole, the use of the cosecant law of reddening seems to have worked satisfactorily in a statistical sense, if not without failure in a few individual cases

The lack of appreciable change in color class with spectral class may be more quantitatively brought out in the accompanying tabulation, in which the exceptional cases mentioned above have been omitted from the averages (figures in parentheses denote numbers of clusters).

AVERAGE COLOR CLASSES CORRECTED FOR SPACE REDDENING

Spectral Class	A5–A9	F0–F4	F5–F9	G0–G5	A5–G5 (Total)
Unobscured clusters	f3.0 (4)	f3.2 (4)	f5.5 (6)	f4.8 (5)	f4.3 (19)
Obscured clusters	.....	f3.5 (2)	f6.0 (2)	f4.7 (16)	f4.7 (20)
All	f3.0 (4)	f3.3 (6)	f5.6 (8)	f4.7 (21)	f4.5 (39)

While there may be a slight suggestion of increasing color with advancing spectral class, it can scarcely be regarded as established with the available data. The average color class is f4.5 ± 1.8 (p.e.), which may be compared to F7.6 ± 3.6 for the average spectral class; the difference, 3.1 ± 4.0, clearly has little significance.

The foregoing comparison supports the working hypothesis that there appears to be no close relationship between color and spectral type of the integrated light of the globular clusters. In other words, the integrated spectral class probably cannot be inferred with safety from the color class, at least when the latter is based on the very compressed photoelectric scale of C_2. It would therefore be unprofitable to obtain from the integrated spectral types "normal" color indices and to use the latter to obtain color excesses from the measured color indices. The evidence at hand suggests that probably the best procedure for determining color excesses of the globular clusters is the one already followed by Stebbins and Whitford in deriving their cosecant law of reddening, namely, to assume the same intrinsic color for all clusters. Since they used a color corresponding to spectral class F6, which is precisely the mean of the average color and spectral classes found above, there is good reason, as far as the cluster spectra are concerned, to accept the color excesses as derived by Stebbins and Whitford for the globular clusters.

VIII. SOLUTIONS FOR THE SOLAR MOTION

In order to show at a glance the nature of the basic data now available for determinations of the solar motion referred to the globular clusters, the distribution of the radial velocities in galactic longitude is shown in Figure 2. The first point to be noted is the spread in the velocities; they range from −360 to +291 km/sec, and in this respect the new material agrees with what was previously known. A second fairly evident feature is that there are more negative than positive velocities; in fact, the center of gravity on the velocity axis falls at −58 km/sec. A third characteristic in the distribution of motions is the apparent lack of velocities between galactic longitudes 40° and 190°, and again between longitudes 230° and 300°. The first of these gaps, in the general direction opposite to that of the galactic center, is quite real; there is but a single cluster known throughout a region including more than one-third of the sky. The second vacancy is simply due to the fact that most of the globular clusters in this region cannot be observed from the north temperate zone.

classes corrected for space reddening according to cosecant relation. ●, clusters in fields with nebulae. ○, clusters in fields without nebulae.

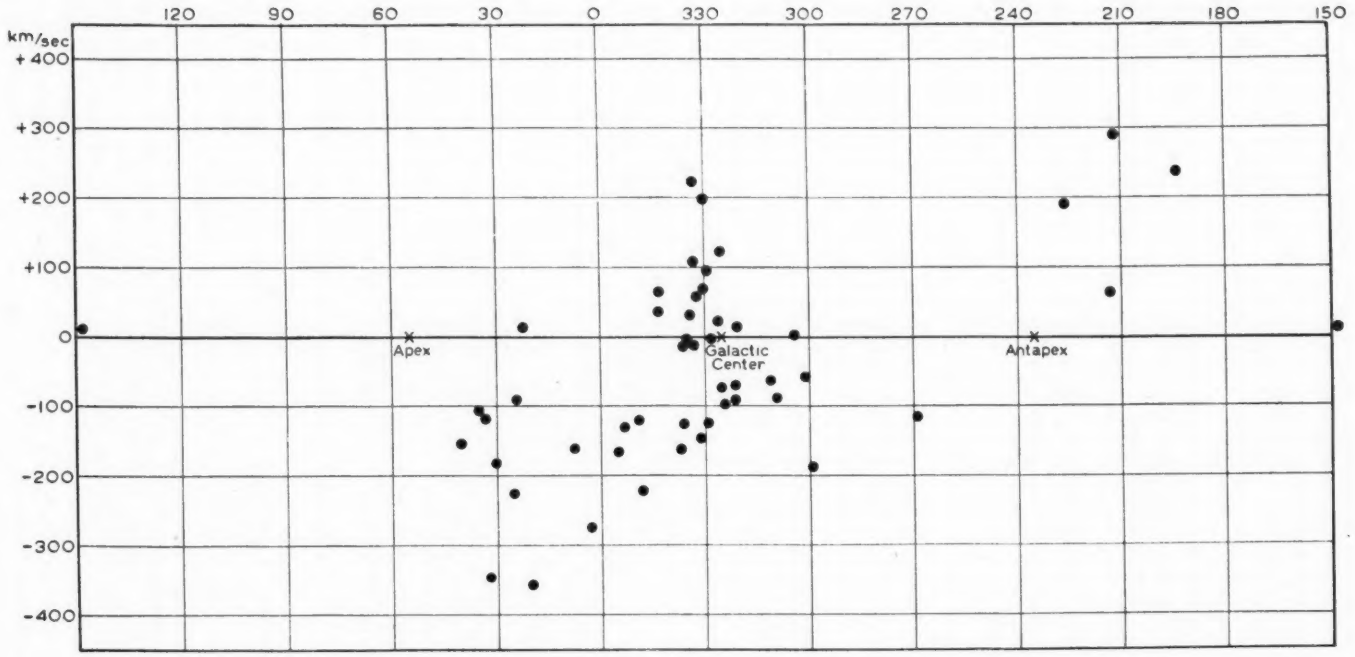

FIG. 2.—Observed radial velocities of 50 globular star clusters, plotted against galactic longitude

With this picture of the distribution of globular cluster radial velocities before us, it may appear rather discouraging to attempt to find the solar motion referred to the system of the globular clusters, hereafter denoted by $V_\oplus$. According to current ideas, the sun moves in a circular orbit around a galactic center located near longitude 325°. Viewed from the north galactic pole, the motion is clockwise; the apex is therefore at longitude 55°, the antapex at 235°. Since the globular clusters are not found in abundance at either of these places but, instead, are highly concentrated around a point halfway between, where the solar-motion component is small, it is evident that a solar-motion solution based on this body of material can hardly be expected to yield results of high precision. Moreover, the problem is not made easier by the large velocity dispersion in the motions of the clusters. Nevertheless, despite these natural difficulties, we shall proceed to a consideration of the results obtained from a number of solar-motion solutions based on these fifty velocities, if for no other reason than that a number of references are to be found in the literature to similar solutions based on only eighteen to twenty-six velocities.

As the first step in the solar-motion solutions, the velocities in Table 4 were corrected for a local solar motion of 20 km/sec toward the conventional apex at $\alpha = 271°$ and $\delta = +28°$; by this procedure any solar motion deduced from the cluster velocities is referred to a moving co-ordinate system whose rotational velocity about the galactic center corresponds to the average motion of the near-by stars.

From preliminary solutions made with about forty velocities (see S. Chandrasekhar, *Principles of Stellar Dynamics*, p. 3 ["Astrophysical Monographs"], University of Chicago Press, 1942), it became apparent that the solar motion from increased material was going to be nearly 100 km/sec smaller than that obtained from the earlier investigations of Strömberg[20] and of Edmondson,[9] who used eighteen and twenty-six velocities, respectively. Strömberg's result[21] was $V_\oplus = 272 \pm 45$ km/sec toward an apex in galactic longitude $70° \pm 7°$ and latitude $+13° \pm 7°$; while Edmondson's was $V_\oplus = 261 \pm 40$ km/sec toward $67° \pm 6°$ and $+1° \pm 8°$. In order to make these results comparable with those deduced from the additional data— improved or corrected velocities are now available for some of the clusters used in the earlier work —Strömberg's and Edmondson's solar-motion solutions were repeated with the newer data. The results from these solutions and from a number of others now to be discussed are given in Table 6. In this table all the results depend upon the assumption that $K = 0$, since a first solution based upon fifty velocities yielded a K-term of -7.9 ± 18.8 km/sec.

For each of the six groups of clusters noted in column 1 of Table 6, four solar-motion solutions were made: (1) velocities given equal weight; (2) velocities assigned the weights listed in Table 4; (3) co-ordinates of the apex included as unknowns; (4) apex assumed at longitude 55°, latitude 0°. The first two groups of clusters with eighteen and twenty-six members, respectively, have already been described; the third group of fifty clusters includes all those for which velocities are now available; the fourth group of thirty-four clusters and the fifth group of sixteen clusters contain, respectively, those clusters which lie in the hemispheres centered on the assumed apex and those centered on the corresponding antapex; the sixth group of forty-seven clusters omits three whose velocities may have unduly decreased the solar motion.

To consider, first, the solutions for the first three groups, it is evident on the basis of the probable errors involved that there is hardly any appreciable deviation from an apex at longitude 55° and latitude 0°. While it might appear from the values in column 6 that the apex could have an appreciable northerly latitude, the latter is due almost entirely to the influence of the two clusters NGC 5272 (M 3) and NGC 6205 (M 13). These

[20] *Ap. J.*, **61**, 353, 1925; *Mt. W. Contr.*, No. 292.

[21] Strömberg actually made four solutions, with and without a K-term and with and without grouping the velocities. The result quoted here is from the solution with $K = 0$ and without grouping, since Strömberg obtained K-terms with probable errors as large as K. Both Strömberg's and Edmondson's values for the solar motion have been corrected here for the local motion of the sun.

two objects at the high latitudes of +78° and +40° and with velocities having the high assigned weights of 24 and 16, respectively, contributed nearly 20 per cent to the weight of the solar-motion component perpendicular to the galactic plane. With M 3 and M 13 each given the average weight of 7, a modified solution with the weighted velocities gave +9°.2 ± 8°.1 for the apex latitude; this value agrees closely with +8°.2 ± 8°.8 obtained from the fifty equally weighted velocities The values of the apex longitude in columns 3 and 4 show no significant deviation from 55°; the somewhat larger values previously obtained from fewer velocities are not substantiated by the increased data. On the whole, it may be concluded on the basis of these fifty globular-cluster velocities that probably there is no large deviation of the solar motion from a direction at right angles to the center of the galaxy or from the galactic plane.

The evidence for a solar motion considerably smaller than heretofore derived is to be found in the third line of columns 7, 8, 9, and 10 of Table 6. The average of the four solutions based on fifty velocities is $V_\odot = 174 \pm 23$ km/sec, with the four solutions giving values in the range from 168 to 180 km/sec. These results may be contrasted with the

TABLE 6

SOLAR-MOTION SOLUTIONS ($K=0$) FOR GLOBULAR CLUSTERS

Solution	No. of Cl.	Galactic Co-ordinates of Apex (Harv. Pole)				Solar Motion (Km/Sec), $V_\odot$			
		Longitude		Latitude		Apex from Sol.		Apex $l=55°$, $b=0°$	
(1)	(2)	Equal Wt. (3)	Weighted (4)	Equal Wt. (5)	Weighted (6)	Eq. Wt. (7)	Wtd. (8)	Eq. Wt. (9)	Wtd. (10)
1. Strömberg	18	69°.9 ± 6°.1	60°.9 ± 8°.5	+ 8°.5 ± 7°.0	+19°.1 ± 7°.7	264 ± 42	205 ± 37	219 ± 37	194 ± 31
2. Edmondson	26	61.8 ± 5.3	54.8 ± 7.0	0.0 ± 6.3	+11.6 ± 6.4	264 ± 34	214 ± 31	237 ± 29	201 ± 27
3. Mayall	50	51.3 ± 6.8	50.1 ± 5.5	+ 8.2 ± 8.8	+16.4 ± 6.6	168 ± 23	179 ± 19	171 ± 26	180 ± 23
4. Apex group	34	64.5 ± 4.0	63.6 ± 5.4	− 6.7 ± 7.4	+ 6.7 ± 6.2	248 ± 35	224 ± 31	205 ± 29	178 ± 26
5. Antapex group	16	26.1 ± 18.1	27.4 ± 11.1	+27.3 ± 16.1	+29.2 ± 9.7	133 ± 30	172 ± 25	86 ± 50	135 ± 50
6. NGC 2298, 4590, 5694 omitted	47	57.1 ± 4.8	54.4 ± 5.3	+ 1.3 ± 6.5	+12.2 ± 5.6	219 ± 24	205 ± 22	213 ± 26	192 ± 23

average of those obtained for the two smaller groups investigated earlier by Strömberg and by Edmondson. With the co-ordinates of the apex included as unknowns, an average $V_\odot = 264 \pm 38$ km/sec or 210 ± 36 km/sec is obtained, depending on whether equal weights or assigned weights are used; for the assumed apex, $V_\odot = 226 \pm 33$ or 198 ± 29 km/sec. The comparison clearly shows that, for a small group of eighteen to twenty-six clusters, the solar motion is quite sensitive to the position of the apex and to the assigned weights; in fact, the range from $V_\odot = 264$ to 198 km/sec is five and a half times greater than that for the group of fifty clusters. Such results suggest the influence of observational selection, which has to be fully investigated before a solar motion as small as $V_\odot = 175$ km/sec can be accepted; this question is taken up in the following section.

IX. OBSERVATIONAL SELECTION

Since radial velocities have been determined for only slightly more than half of the known globular clusters, it becomes important to try to estimate the probable effect on the solar motion of those clusters which, because of their positions, contribute most weight to solar-motion solutions. In order to show graphically how different groups of clusters, or even individual clusters, may affect the solar motion, a diagram such as Figure 3 is useful. In this figure the known velocities, corrected for local solar motion, are shown plotted against the cosine of the angular distance from an apex assumed to be at longitude 55° and latitude 0°. The new, the previously known but redetermined, and the

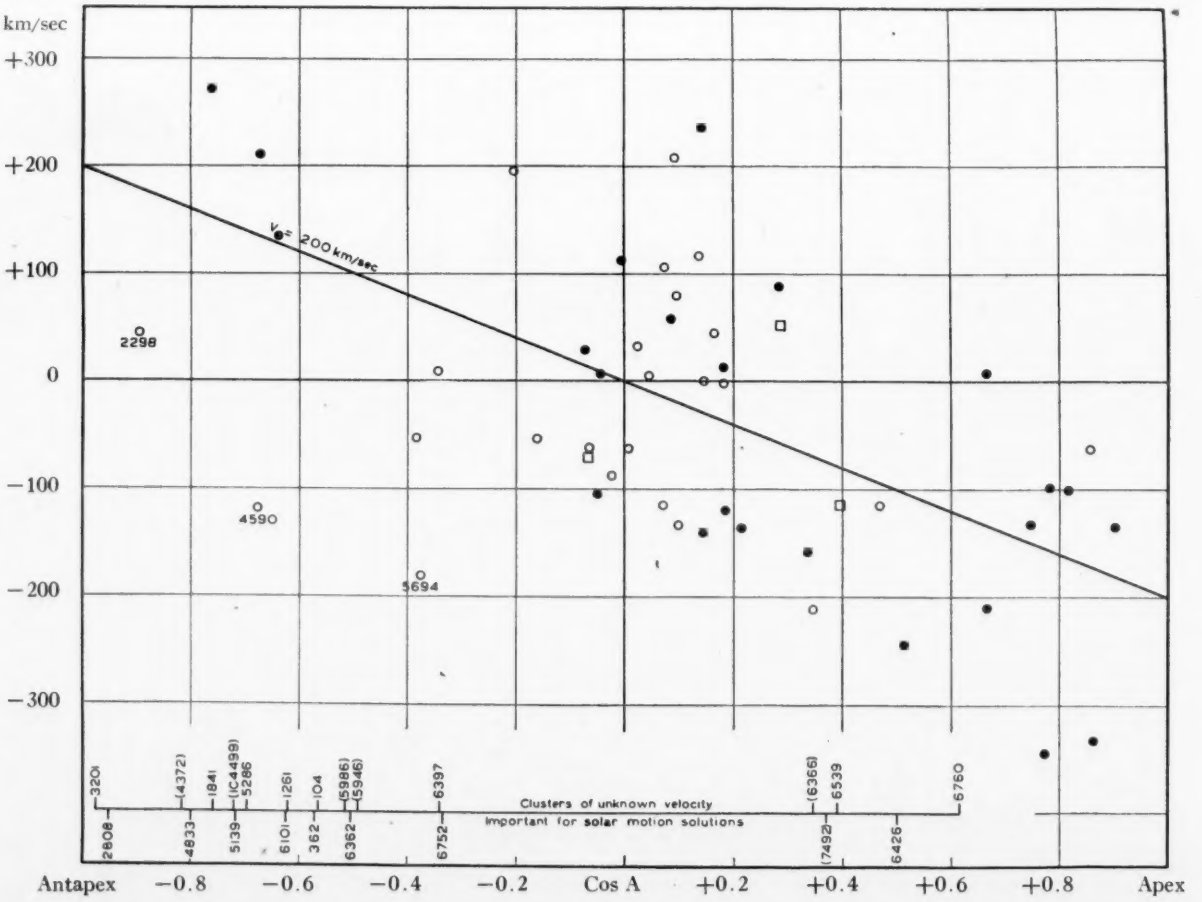

FIG. 3.—Distribution of radial velocities of globular clusters with respect to cosine of apical distance, A. Velocities are corrected for local solar motion, and the apex is assumed to be at $l = 55°$, $b = 0°$. ●, velocities previously known but redetermined. ○, new velocities. □, corrected earlier velocities.

corrected earlier velocities are denoted by different symbols. For the assumed apex, any solar-motion solution of the kind listed in columns 9 and 10 of Table 6 may be represented in the figure by a straight line through the origin. The slope of the line is equal to the solar motion, and the diagram shows a line corresponding to a solution giving $V_\odot = 200$ km/sec. In the lower part of the figure the positions on a horizontal axis are shown for a number of clusters of unknown velocity; they are more fully discussed later in this section.

APEX AND ANTAPEX GROUPS

For reasons soon to become apparent, we shall consider the degree of completeness of the radial-velocity observations for clusters located in the two hemispheres containing the assumed apex and antapex. With the assumed values of $l = 55°$ and $b = 0°$, the clusters then become separated into two g oups, one including longitudes from 325° to 145° (apex group) and the other, 145° to 325° (antapex group).

There are ninety-three entries in Shapley's catalogue of globular clusters.[22] From Crossley photographs it appears that two clusters—NGC 6235 and 6535—probably are not globular, and that four other clusters—NGC 6355, 6401, 6544, and 6838—almost certainly are to be added to the list of globular clusters. Other newly found globular clusters are NGC 5694, discovered by Lampland and Tombaugh[23] and investigated by Baade,[24] and NGC 1841, reported by Shapley and Paraskevopoulos.[25] The two rejections and the six additions give a revised total of ninety-seven globular clusters. Of these, the apex group includes fifty-two, the antapex forty-five. Radial velocities are available for thirty-four clusters in the apex group and for sixteen in the antapex group. Thus there remain eighteen clusters in the apex group and twenty-nine in the antapex group for which velocities are unknown. The percentages of completeness for velocity observations are therefore 65 and 36 per cent for the apex and antapex groups, respectively. These percentages, however, do not fairly indicate the effective completeness in the two groups, because they do not show how the clusters are distributed as regards apical distance. In order to examine this point and to estimate the possibilities for further radial-velocity observations, Table 7 has been prepared.

In Table 7, cosines of apical distances are given for the clusters whose velocities are unknown. The tabulation separates the clusters vertically according to apex and antapex group, with the latter subdivided at $\delta = -40°$, which is near the practicable southern limit for the radial-velocity observations made at Mount Hamilton. In addition to the columnar segregation, the clusters north of $\delta = -40°$ are arranged in three groups according to the estimated difficulty of spectroscopic observation. The first group of eight clusters contains those of least central concentration. They are so little condensed and faint that slit spectra of their integrated light will be extremely difficult, if not impossible, to obtain. For such clusters, observations of individual stars probably will be required for radial-velocity determinations, and a telescope of considerably larger aperture than 36 inches will be needed to make the observations. In the case of the second group of twelve clusters, while their light is not nearly so spread out, it is still too faint and too reddened to encourage radial-velocity observations in the ordinary photographic region. For these clusters the best means for velocity determinations would seem to be spectrographs designed for work in the visual and red spectral regions, although difficulty may be encountered even there because of the very few and faint lines available for measurement; with low dispersion, it is doubtful whether any lines will have visibilities comparable to H and K. The third group includes only four clusters, which probably could be observed in the manner described in Section III; but even they are near the threshold of observation for the equipment employed. Two of these clusters—NGC 6121 (M 4) and 6809

[22] *Star Clusters*, Appen. A, 1930.

[23] *A.N.*, **246**, 171, 1932.

[24] *Pub. A.S.P.*, **46**, 52, 1934.

[25] *Harvard Bull.*, No. 914, 1941.

(M 55)—are so large that they probably should be observed with a telescope of smaller scale than the Crossley.

Turning, now, to the distribution of apical distances, we see from the values of cos A in Table 7 that in the apex group there are very few clusters which have large enough values of cos A (small apical distances) to affect seriously the solar-motion solution. There is only one cluster (NGC 6760) with cos $A = 0.6$, one (NGC 6426) with cos $A = 0.5$, and three (NGC 6366, 6539, and 7492) with cos A between 0.3 and 0.4. Under these circumstances, additional radial-velocity observations for clusters in the hemisphere containing the apex may be expected to have little effect on future solar-motion solutions.

TABLE 7

DISTRIBUTION OF VALUES OF COS A FOR CLUSTERS OF UNKNOWN VELOCITY
(A = Angular Distance from Assumed Apex at $l = 55°$, $b = 0°$)

Character of Clusters	Apex Group		Antapex Group				Character of Clusters
	$\delta > -40°$		$\delta > -40°$		$\delta < -40°$		
	NGC	cos A	NGC	cos A	NGC	cos A	
Faint and insufficiently condensed [8 clusters]	5466	+.205	288	−.014	104	−.564	
	6366	+.346	5053	−.056	362	−.572	
	6426	+.498	5897	−.197	1261	−.621	
	7492	+.368	6144	−.100	1841	−.758	
					2808	−.952	
Sufficiently condensed but faint and greatly reddened [12 clusters]	6287	+.051	6453	−.044	3201	−.976	
	6324	+.044	.....	.....	(4372)	−.817	Southern Hemisphere objects
	6355	+.035	.....	.....	4833	−.800	
	6401	+.101	.....	.....	5139	−.717	
	6517	+.155	.....	.....	5286	−.696	[23 clusters]
	6522	+.052	.....	.....	(IC 4499)	−.720	
	6528	+.061	.....	.....	(5927)	−.491	(Parentheses denote objects of doubtful nature, or of insufficient concentration)
	6539	+.389	.....	.....	(5946)	−.491	
	6553	+.129	.....	.....	6101	−.624	
	6569	+.051	.....	.....	6139	−.257	
	6760	+.614	.....	.....	(6352)	−.273	
					6362	−.504	
Sufficiently bright and condensed [4 clusters]	6316	+.009	6121	−.100	6388	−.206	
	6342	+.138	.....	.....	6397	−.342	
	6809	+.173	.....	.....	(6496)	−.171	
					6541	−.136	
					6584	−.255	
					6752	−.336	

The case is quite different for the clusters in the antapex group, for here we find a number of large values of cos A, which occur in the polar cap south of $\delta = -40°$. Without direct photographs on a scale comparable with Crossley plates, it is difficult to tell how many of these, far-southern clusters with suitably large values of cos A could be observed for radial velocity. From the published descriptions, however, it would appear that at least six clusters (those in parentheses) might be difficult objects for spectroscopic study. Exclusion of these doubtful cases leaves thirteen clusters for which it would be very valuable to have velocities for a definitive solar-motion solution.

To summarize graphically the foregoing discussion, those clusters of unknown velocity which have $|\cos A| > 0.3$ are shown plotted on a horizontal axis in the lower part of Figure 3. The other clusters for which velocities are not available are omitted, because

clusters with $|\cos A| < 0.3$ contribute but little weight to solar-motion solutions; they are mainly of value for determinations of the mean peculiar velocity.

It is evident from the distribution of points on the horizontal axis that the radial-velocity observations in the apex group are substantially complete for solar-motion solutions. Of the five clusters indicated, only two (NGC 6760 and 6539) are likely to provide velocities derived from their integrated light. The other three, as indicated in Table 7, are among the least concentrated and faintest clusters, and it may be some time before velocities of enough individual stars in them are obtained to give satisfactory radial velocities for these clusters. In the antapex group, on the other hand, the distribution of points on the horizontal axis suggests a serious deficiency, whose influence we now attempt to estimate by considering the solutions in the last three lines of Table 6.

Since the radial velocities for the clusters in the apex group are substantially complete, comparison of the solar-motion solutions for the apex and antapex groups (see lines 4 and 5, Table 6) indicates that the deficiency of velocities in the antapex group (*a*) decreases the longitude of the apex, (*b*) increases the latitude of the apex, and (*c*) decreases the solar motion. In fact, the co-ordinates of the apex computed from the smaller group are so different from the assumed apex that use of the latter to calculate the solar motion represents a forced and unwarranted treatment of the observations, as is evident from the exceptionally small solar motions and large probable errors listed in line 5 and columns 9 and 10 of Table 6. The corresponding solar motions in line 4 for the apex group, while they show nearly the same range, do not reach such low values as in the other group; also, the longitude of the computed apex deviates from the assumed apex in the opposite sense. The comparison suggests the conclusion that appreciable deviation from the assumed apex and a smaller solar motion can result from the lack of velocities for those thirteen clusters in the antapex group which have been designated in Table 7 and in Figure 3.

With the aim of allowing quantitatively for the effect on the solar motion of the clusters of unknown velocity in the antapex group, the series of solutions in the last line of Table 6 were made. From an inspection of the distribution of the new velocities indicated in Figure 3, it may be seen that there are three clusters (NGC 2298, 4590, and 5694) whose velocities can appreciably decrease the solar motion. Moreover, these three velocities depend entirely upon low-dispersion Crossley spectrograms, and therefore they may be under suspicion. With these three velocities omitted, the solar motion, based on forty-seven velocities, averages 207 ± 24 km/sec, with a range of 27 km/sec for the four different ways of treating the data; the co-ordinates of the computed apex agree closely with those of the assumed apex.

From the foregoing discussion, we have at this point the following alternative values for the solar motion: (*a*) For fifty clusters, $V_\odot = 174 \pm 23$ km/sec, probably too small because of observational selection. (*b*) For forty-seven clusters, $V_\odot = 207 \pm 24$ km/sec, plausibly corrected for observational selection.

The question which has to be considered before a final value can be given is: How much weight is to be attached to the larger value? It resulted from a procedure involving the use of considerable judgment, and the omission of three velocities may be objected to for at least one reason: the velocity dispersion around the antapex is comparable with that around the apex when all the velocities are included. For example, the range in velocity between NGC 7089 and 6934, 353 km/sec, near the apex, is similar to the velocity range between NGC 1851 and 4590, 390 km/sec, near the antapex. The principal difference in the character of the velocity dispersions in the two groups is that in the antapex group the distribution of residual velocities is asymmetrical: there are nearly twice as many clusters which tend to decrease a solar motion of the order of 175 km/sec as those which help to increase it. This latter circumstance, and the strongly negative average radial velocity of -58 km/sec for all fifty clusters, probably outweigh in importance the reduction in velocity range around the antapex produced by the omission

of the three clusters in question. At all events, until further data become available, we give as the most reliable value for the solar motion referred to the globular clusters:

$$V_{\oplus} = 200 \pm 25 \text{ km/sec}, \quad \text{toward } l = 55°, \ b = 0°.$$

The average of the residual motions without regard to sign (mean peculiar motion) is 101 km/sec.

X. GALACTIC ROTATION AND THE GLOBULAR CLUSTER SYSTEM

In discussions of galactic rotation the sun's orbital velocity often has been considered to be of the order of 275–300 km/sec; and the basis for this figure usually has been given as the solar motion derived from the radial velocities of eighteen to twenty-six globular clusters.[26] It appears from fifty velocities, however, that a significantly smaller solar motion is probable; and hence there is some reason to re-examine the question of the sun's circular velocity of rotation, which hereafter will be designated by $V_{\odot}$ to distinguish it from $V_{\oplus}$.

The underlying supposition in the interpretation of the globular cluster solar motion as the sun's orbital velocity has been that the cluster system is essentially spherical and that it would therefore be expected, for dynamical reasons,[27] to have little if any general rotation. Accordingly, a smaller solar motion of $V_{\oplus} = 200$ km/sec for the clusters suggests two alternative interpretations: either (1) no significant general rotation of a spherical cluster system and a smaller circular velocity ($V_{\odot} = 200$ km/sec) for the sun or (2) an appreciable amount (75–100 km/sec) of systematic rotation for a flattened cluster system and a solar orbital velocity as hitherto assumed ($V_{\odot} = 275$–300 km/sec). The second alternative appears to be more probable on the basis of data from other sources, discussed below.

SUN'S ORBITAL VELOCITY

a) In the theory of galactic rotation as formulated by Oort, his dynamical constants A and B are simply related to the total angular velocity, $V_{\odot}/R_{\odot}$, where $V_{\odot}$ is the sun's circular velocity at the distance $R_{\odot}$ from the galactic center, as follows:

$$V_{\odot}/R_{\odot} = A - B .$$

In the most recent discussion of the radial-velocity and proper-motion material suitable for the study of galactic rotation, R. E. Wilson[28] concluded that the most probable values for A and B are $+0.0177$ and -0.0128 km/sec/parsec, respectively. The sun's orbital velocity and distance from the galactic center are therefore connected as in the accompanying tabulation. The simple theory of galactic rotation thus leads essentially to a numerical dependence of $V_{\odot}$ upon $R_{\odot}$, or vice versa, and a more precise specification of one requires the evaluation of the other by some other means.

$V_{\odot}$ (Km/Sec)	$R_{\odot}$ (Kpc)
200	6.6
250	8.2
300	9.8
350	11.5

[26] The idea that the solar motion with respect to the globular clusters may be principally a reflection of the rotation of the local stellar system around a distant galactic center goes back at least as far as Lundmark's early discussion of the problem (*Mon. Not. R.A.S.*, **84**, 749, 1924).

[27] B. Lindblad, *Upsala Medd.*, No. 3, 1925; *Ark. f. math., ast. och fys.*, **19**, A, No. 21, 1925.

[28] *Ap. J.*, **92**, 170, 1940; *Mt. W. Contr.*, No. 631.

b) One way in which $V\odot$ and $R\odot$ may be separately determined is to use more general formulae for galactic rotation, with observations of objects at greater distances from the sun. A recent example of this procedure is Joy's discussion[29] of his extensive radial-velocity measures of the galactic Cepheids.[30] By using the more general formulae derived by Miss Hayford[31] and by Bottlinger,[32] Joy obtained $R\odot = 10.0$ kpc and $V\odot = 296$ km/sec. Both of these values, however, may be subject to revision because (1) the adopted constant of interstellar absorption, $a = 0.85$ mag/kpc, probably is too large and (2) Bottlinger's formula used to obtain $V\odot$ rested on the assumption that the entire mass of the galaxy is concentrated at the center. In the first case, R. E. Wilson[26] found that $a = 0.65$ mag/kpc brought into agreement the determinations of A from a large body of radial-velocity observations of Cepheids and of other stars, so that Joy's value for $R\odot$ should be increased by 10 per cent, to about $R\odot = 11$ kpc. In the second case, Wyse and Mayall[33] in an investigation of the distribution of mass in the two nearest spirals—M 31 and M 33—found that the rotational velocities in these systems could be represented with a more nearly uniform distribution of mass and concluded that a similar distribution in the galaxy could not be ruled out by the available data. If the assumption of a high central concentration does not hold for the galaxy, Joy's value of $V\odot$ from the Cepheid material could be reduced by as much as 20 per cent, to about $V\odot = 240$ km/sec, for a uniform distribution of mass. Since, however, complete uniformity of distribution is an extreme condition probably not realized in the galaxy, it would seem better merely to give the revised result as $240 < V\odot < 300$ km/sec, with some preference for the lower range. Since these revised values of $R\odot = 11$ kpc and $V\odot \sim 250$ km/sec do not fit the fairly well-established relation between $V\odot$ and $R\odot$ given in paragraph *a*, it would appear that the separate evaluation of them mainly from the available radial-velocity data for stars cannot, at least for the present, be regarded as entirely satisfactory.

c) Oort,[34] from Van de Kamp's[35] data on the density gradient in the globular clusters and from Edmondson's mean peculiar velocity (105 km/sec) for twenty-six clusters, estimated the acceleration in the solar neighborhood to be 2.5×10^{-8} cm/sec^2, and from this obtained $V\odot = 250$ km/sec. While Oort attached no formal probable error to the result, he stated: "This estimate is admittedly uncertain, but the uncertainty is probably not larger than that of the more direct determinations." The latter he considered to be Edmondson's solar motion of 274 km/sec, based on twenty-six cluster velocities, and his own solar-motion solution for the nearest extragalactic nebulae of 365 ± 70 km/sec, which is examined in more detail below in paragraph *e*.

d) Probably the most reliable estimates of $V\odot$ result from the relation between $V\odot$ and $R\odot$ given in paragraph *a*, with values of $R\odot$ deduced from the spatial distribution of globular clusters and of isolated cluster-type variables around the galactic center. In this case the assumption is made that the centroid of the distances of each group, when corrected for space absorption, corresponds to the center of the galaxy. For the clusters, values of $R\odot$ ranging from 5.5 to 10.0 kpc have been determined,[35, 36, 37] with the results depending mainly upon the manner in which corrections for the absorption were applied. Values of $R\odot$ as small as 5.5–7.5 kpc, however, probably represent overcorrection of the cluster distances,[38] and the distance to the galactic center seems more likely to fall in the

[29] *Ap. J.*, **89**, 356, 1939; *Mt. W. Contr.*, No. 607.

[30] *Ap. J.*, **86**, 363, 1937; *Mt. W. Contr.*, No. 578.

[31] *Lick Obs. Bull.*, **16**, No. 448, 53, 1932.

[32] *Veröff. Berlin-Babelsberg*, Vol. **10**, No. 2, 1933.

[33] *Ap. J.*, **95**, 24, 1942; *Lick Obs. Contr.*, Ser. II, No. 2.

[34] *Mon. Not. R.A.S.*, **99**, 375, 1939.

[35] *A.J.*, **42**, No. 989, 161, 1933.

[36] Baade, *Ap. J.*, **82**, 396, 1935; *Mt. W. Contr.*, No. 529.

[37] Stebbins and Whitford, *op. cit.*

[38] McLaughlin, *A.J.*, **51**, No. 1152, 97, 1945.

range of 8–10 kpc. Further support for this conclusion is provided by the isolated cluster-type variables. From the frequency distribution in apparent magnitude of several hundred such variables, located in a fairly unobscured field at $l = 307°$ and $b = -20°$, Shapley[39] derived a value of $R\odot = 9.7 \pm 1.2$ (m.e.) kpc. This nearly independent[40] determination suggests that, for the present, $R\odot$ may not be known more accurately than 9.2 ± 1.2 kpc, and this figure, by the relation between $V\odot$ and $R\odot$ given in paragraph *a*, indicates an orbital velocity for the sun of $V\odot = 280 \pm 40$ km/sec.

e) A value for $V\odot$ closer to 300 km/sec than to 200 km/sec is also suggested by the radial velocities of the nearest extragalactic nebulae, although in this case the interpretation of the observations is complicated by the motion of the galaxy as a whole and by the velocity-distance relation. Since neither of these two disturbing elements can be properly evaluated with scanty data, the early solar-motion solutions[41] involving nebular radial velocities may be passed over without further discussion. In fact, the problem of the sun's and the galaxy's motions remained beclouded until it became known that the sun participates n the galactic rotation and that the galaxy is located in a small group of relatively close nebulae, whose distances of less than a million light-years set them well apart from the next nearest extragalactic systems. Chiefly as the result of investigations by Hubble[42] and by Baade,[43] it has been established that this "local group" contains at least a dozen members. If these form a physically connected group, it might be postulated, as Hubble has done,[44] that the velocity-distance relation may not operate within the local group. He has tested the hypothesis by making separate solar-motion solutions for the local group members and for the nearer field nebulae.[45] From the solar motion found for the field nebulae—300 km/sec toward $l = 63°$ and $b = +35°$ (no correction for galactic rotation)—and from that for the local group—265 km/sec toward $l = 52°$ and $b = -12°$ (no correction for red-shift)—Hubble concluded that either (1) the galaxy with its satellite Magellanic Clouds is a triple system in the general field, but in the neighborhood of a small group of nebulae moving toward it, or (2) the law of red-shifts does not operate within a physically connected system like the local group. The second alternative was considered more likely, because the solar motion for the nebulae became about 150 km/sec toward the north galactic pole when corrections for galactic rotation (assumed $V\odot = 275$ km/sec toward $l = 55°$ and $b = 0°$) were applied, while for the local group it became 475 km/sec toward $l = 58°$ and $b = -19°$ when corrections for red-shifts were included. Since these two motions for the galaxy are mutually incompatible and the correction for galactic rotation probably is of the right order, it would appear that there is little reason to correct radial velocities of local group members for red-shifts observed in the general field.

With the velocity-distance term thus eliminated from the problem, the solar motion referred to the local group members may be regarded in two ways: (1) principally as a relative motion between the group and the galaxy as a whole or (2) mainly as a reflection of the sun's orbital motion around the galactic center.[46] The latter viewpoint would seem

[39] *Proc. Nat. Acad. Sci.*, **25**, 113, 1939.

[40] It is not entirely independent because the photometric distances of the cluster and isolated variables depend upon the assumption of an absolute magnitude $M = 0.0$ pg for all the variables.

[41] Lundmark, *Mon. Not. R.A.S.*, **85**, 865, 1925; Oort, *Bull. Astr. Inst. Netherlands*, **5**, No. 196, 239, 1930; Hubble, *Proc. Nat. Acad. Sci.*, **15**, 168, 1929.

[42] Summarized in *The Realm of the Nebulae*, chap. vi, 1936.

[43] *Ap. J.*, **100**, 147, 1944; *Mt. W. Contr.*, No. 697.

[44] *Ap. J.*, **84**, 270, 1936; *Mt. W. Contr.*, No. 549; also *The Realm of the Nebulae*, p. 151.

[45] *J. Franklin Inst.*, **228**, 142, 1939.

[46] Oort (*Bull. Astr. Inst. Netherlands*, **4**, No. 132, 89, 1927) suggested nearly twenty years ago that the radial velocities of the Magellanic Clouds may be chiefly reflections of the sun's galactic rotation. More recently, R. E. Wilson (*Pub. A.S.P.*, **56**, 102, 1944) computed the space motions of the clouds from the

to have in its favor the higher odds in probability, for it is difficult to imagine that the motions of the nearest neighbors of the galaxy would, purely as the result of chance, indicate a solar motion toward the same apex as that found for the clusters. While the local group solar motion may include a component of the motion of the galactic center, the evidence from Hubble's preliminary solutions indicates that it is small and that the galaxy may be moving more nearly at right angles to the other members of the local group. As Hubble has noted, such a motion for the galaxy cannot yet be regarded as established on the basis of the available material, and further radial velocities of nebulae resolved into their brightest stars will be required to provide a definitive solution. Since current nebular observing programs include numerous late-type, resolved spirals, the motion of the galaxy among the nearer field nebulae should eventually become determinable with good accuracy. Meanwhile, for the present purpose, the solar motion for local group members may be used as a check on the values of the sun's orbital velocity obtained by other methods.

TABLE 8

OBSERVED RADIAL VELOCITIES OF LOCAL GROUP NEBULAE

Object	V (Km/Sec)	Source
Large Mag. Cl.	+276	R. E. Wilson, *Pub. Lick Obs.*, **13**, 188, 1918
Small Mag. Cl.	+168	*Ibid.*, p. 190
NGC 1049*	− 25:	Mayall, this paper
NGC 6822	−150	Humason, *Ap. J.*, **74**, 35, 1931; *Mt. W., Contr.*, No. 426
M 33	−167	Mayall and Aller, *Ap. J.*, **95**, 5, 1942; *Contr. Lick Obs.*, Ser. II, No. 1
M 31	−300	H. W. Babcock, *Lick Obs. Bull.*, **19**, No. 498, 41, 1939.
M 32	−205	Mayall, this paper
NGC 185	−270	
NGC 205	−340	
Prob. members:		
IC 10	−400	Mayall, *Pub. A.S.P.*, **53**, 122, 1941
NGC 6946	−150	Humason, *Ap. J.*, **83**, 10, 1936; *Contr. Mt. W.*, No. 531
IC 342	− 25	*Ibid.*

* Brightest globular cluster in Fornax dwarf (cf. Nos. 47 and 48).

Because of the foregoing considerations and because several additional and improved velocities have become available since Hubble investigated the problem, new solar-motion solutions for comparison with those for the clusters have been made for the local group nebulae. As shown in Table 8, radial velocities are currently at hand for nine accepted members and for three probable members. This list includes some hitherto unpublished velocities; among them that for NGC 1049, the brightest globular cluster[47] in the Fornax dwarf,[48] is an uncertain mean of four spectrograms which gave individual measures ranging from −182 to +71 km/sec.[49]

velocities of the individual nebulae. He found motions of the order of 550–700 km/sec toward $l = 140°$–$148°$ and $b = -32°$ to $-18°$, i.e., nearly at right angles to the line of sight and in the galactic plane. Such large velocities, if confirmed by observations of additional objects in the Magellanic Clouds, would raise serious doubts as to the physical association of the clouds with the galaxy.

[47] Hubble and Baade, *Pub. A.S.P.*, **51**, 40, 1939.

[48] Shapley, *Proc. Nat. Acad. Sci.*, **25**, 565, 1939; also *Galaxies*, pp. 141–49, 1943.

[49] It would be of value to have a velocity for the other and fainter globular cluster, in order to help average out the known large dispersion in cluster velocities; but the spectrographic observation of a fifteenth-magnitude object at $\delta = -35°$ is impracticable for the Crossley reflector.

As in the case of the clusters, the velocities of the local group nebulae were first corrected for a local solar motion of 20 km/sec toward $\alpha = 271°$ and $\delta = +28°$. Solar-motion solutions based on these reduced velocities were then made in the usual manner, and the results are shown in Table 9. In these solutions each velocity was assigned unit weight, since it was found from preliminary solutions that essentially the same results were obtained when the velocities were grouped and weighted. There is also little reason to include a K-term in the solutions, because its value is about the same as its probable error. Thus, for the assumed apex, $K = -21 \pm 24$ or -34 ± 16 km/sec, depending on whether all twelve or only the nine accepted members are used; also, because of the limited data, K is indeterminate when it is included in solutions for the co-ordinates of the apex. For these reasons Table 9 shows results only for the solutions made with $K = 0$.

Although, as indicated in the table, separate solutions were made for all twelve nebulae and for only the nine accepted members, there is very little difference in the results. Also the deviation of the computed apex from the assumed apex is hardly more than the probable error; the small negative latitude cannot be regarded as established on the basis of such limited material. In short, the evidence, as far as it goes, points to an

TABLE 9

SOLAR-MOTION SOLUTIONS ($K = 0$) FOR LOCAL GROUP NEBULAE

No. of Nebulae	Co-ordinates of Apex		Solar Motion (Km/Sec)	
	Gal. Long.	Gal. Lat.	Sol. Apex	$l = 55°$, $b = 0°$
9	$60°.3 \pm 5°.8$	$-14°.1 \pm 4°.4$	308 ± 22	314 ± 23
12	57.4 ± 8.6	-20.4 ± 7.1	301 ± 32	288 ± 27

apex close to $l = 55°$ and $b = 0°$, and to a solar motion, in round numbers, of 300 ± 25 km/sec. Figure 4 shows graphically how such a solar motion[50] fits the observations.

To collect and to assess the foregoing results bearing on the sun's orbital velocity: The best evidence from galactic objects is that $V_\odot = 280 \pm 40$ km/sec, while from the near-by extragalactic systems, $V_\odot = 300 \pm 25$ km/sec. The latter value is to be viewed as more of a check on the former, because of the present uncertainty of the motion of the galaxy as a whole. The net result of the discussion, therefore, is that there is little reason to change the value for $V_\odot$ generally adopted heretofore, that is, we still have $V_\odot =$ 280–300 km/sec. Only now it seems advisable to distinguish between the solar motion with respect to the globular clusters, $V_\oplus$, and to the galactic center, $V_\odot$; for, if the present treatment of the problem is correct, there is a difference of $V_\odot - V_\oplus = 80$–100 km/sec. The most obvious interpretation of the difference is that the cluster system partakes in the general rotation of the galaxy; and, if that is the case, the cluster system may be somewhat flattened; this possibility is briefly considered in the following subsection.

GLOBULAR CLUSTER SYSTEM

Shapley's early work on the distances of the globular clusters led to a spatial distribution for them which was conspicuously elongated in the direction from the galactic center to the sun. As an arrangement which gave an extension in one special direction, it could be regarded with suspicion or expectancy, depending on how much faith was

[50] It is likely that a more accurate value for the solar motion referred to the local group will be forthcoming from the Mount Wilson Observatory when radial velocities, determined with the highest possible dispersion, are published for the local group nebulae (*Carnegie Yrbk.*, **44**, 16, 1945).

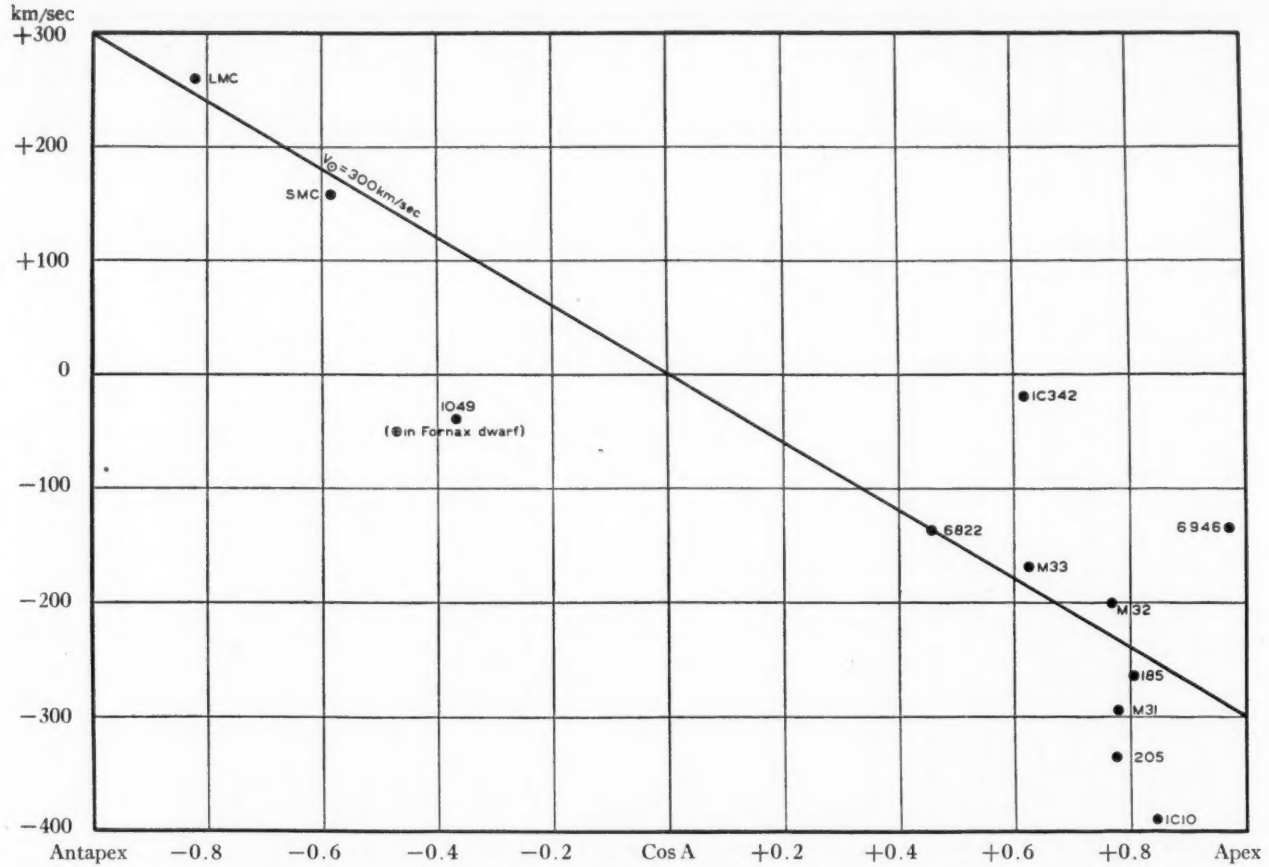

FIG. 4.—Distribution of radial velocities of local group nebulae with respect to cosine of apical distance, A. Velocities are corrected for local solar motion, and the apex is assumed to be at $l = 55°$, $b = 0°$.

placed in the method of deriving the distances. From a skeptical viewpoint the elongation could be ascribed to systematic errors in the distances; from a foresighted attitude, to the effect of some as yet undisclosed agency. The latter in due time was identified as interstellar absorption, and correction of the globular cluster distances for dimming gave considerable support to a spherical distribution.[35, 36]. The amount of the correction is still uncertain,[37] however, and for a number of clusters even the uncorrected distances are inaccurately known, since they depend only upon total magnitudes and diameters. The case for an essentially spherical system does not, therefore, rest upon a very firm foundation in so far as the photometric data are concerned. While it seems certain that the distribution is not nearly so flattened as indicated by no correction for galactic obscuration, the possibility of an appreciable degree of flattening cannot be ruled out by reasonable values for the absorption, of the order of $a = 0.4$–0.6 mag/kpc. Perhaps the strongest evidence that a globular cluster system may be flattened is provided by the apparently elliptical outline of the projected or surface distribution of those 148 nebulous objects in the Andromeda nebula which Hubble has provisionally identified as globular clusters.[51]

A number of attempts[52] have been made to show that the globular clusters participate in various ways in the rotation of the galaxy, but the results in general were inconclusive. The great range in distance from the center, uncertainties in the distances of individual clusters, and especially the large dispersions in velocity and in distance above the galactic plane make inapplicable the simple and approximate theory of galactic rotation; and extension of the theory to include the more general case requires a knowledge of the distribution of mass within the galaxy or of how the circular rotational velocity depends upon distance from the center. Even with the additional radial-velocity data given here, no satisfactory interpretation of the individual peculiar velocities in terms of a differential or general rotation has been found. The reasons are partly because the data are still insufficient and partly because of the large dispersions just mentioned. Probably the most promising way to investigate the general motion of a system of clusters would be to obtain radial velocities for a number of those objects in the Andromeda nebula. Since none of these, however, is brighter than the fifteenth magnitude, the determination of their velocities may be left to a telescope larger than the Crossley 36-inch reflector.

In conclusion, the writer wishes to express his appreciation and gratitude to Messrs. D. M. Popper and L. H. Aller, who, as students at the Lick Observatory, helped to make many of the spectrographic observations, and to Miss Julie M. Vinter Hansen and Mrs. Delia M. Herbig, who, respectively, made the preliminary and final least-squares solutions.

[51] *Ap. J.*, **76**, 44, 1932; *Mt. W. Contr.*, No. 452. The number of such objects has recently been increased to 300 by Baade, who communicated his identifications in advance of publication to Seyfert and Nassau (*Ap. J.*, **102**, 377, 1945).

[52] Edmondson, *op. cit.*, and *Mon. Not. R.A.S.*, **96**, 636, 1936; Mineur, *Mon. Not. R.A.S.*, **96**, 61, 1935; Camm, *Mon. Not. R.A.S.*, **99**, 87, 1938.

NOTES

SOME REMARKS ON THE NOVA PHENOMENON

The general character of the phenomena associated with the novae is such that it is natural to speak of them as explosions on a cosmic scale, an idea which has led to various speculations about the possible subnuclear mechanism which might produce such an explosion.[1] Thus far no definite mechanism of this type seems to have been agreed upon. Still it seems to be of some interest to consider various features of the nova phenomenon that do point to an interior explosion as the most likely cause and to which, thus far, scant reference has been made.

Consider for comparison an underwater explosion of a spherical charge. The first stage after ignition consists in the conversion of the explosive material into an equal volume of extremely hot gas, creating a pressure discontinuity on the surface of the charge. This pressure discontinuity generates, in turn, an expanding spherical shock wave that travels with the appropriate shock-wave velocity. When reaching the surface of the water, the wave breaks through the surface within a certain area, creating what is called "the dome."

The bubble of hot gas that set off the shock wave goes on expanding for a while to reach a maximum size, after which the pressure exerted by the weight of water gets the upper hand and it collapses to a minimum size, at which time it sets off another shock wave intrinsically weaker. The bubble may perform a number of such oscillations while it is being driven upward by its buoyancy, which finally brings it to the surface with a brilliant burst—"the plume"—practically the only thing that the casual spectator sees of the explosion.

From the terrestrial experiment we may pass on to the cosmic analogue and suppose the central part of a star to contain explosive material of a size big enough to set off an explosion on a cosmic scale. The charge becomes ignited somehow, and a spherical shock wave is started on its way outward, reaching the surface of the star nearly simultaneously at all points. If the temperature in the wave front is large enough, the outer part of the star will be flung out into space with a velocity depending upon the intensity of the wave. The dramatic suddenness and violence with which a nova starts its career, in respect to both increase in luminosity and velocity of the surface layer, would seem to require the equivalent of a shock wave for its appropriate description; and from the given data on luminosity and acceleration of the atmospheric shell it should be possible to estimate the energy of the wave.

If the central superhot bubble is not too large, it will be expected to perform oscillations in much the same way as the bubble of an underwater explosion does. However, these oscillations are not easily detected by astronomical observations, because the interior part of the star is more or less screened from view by the shell detached from the star by the first shock wave. However, successive shells have sometimes been observed, indicating the existence of more shock waves generated by continued oscillations.

Obviously, the existence of a superhot bubble of gas near the stellar center is an extremely unstable condition, and, unless everything is perfectly balanced, the bubble will start rising toward the surface—a fact that seems to have been overlooked by earlier writers on novae as exploding stars. Adiabatic cooling may tend to slow down the speed of the rising bubble; but, considering the vast scale of the phenomenon which has been postulated, it must reach the surface in a rather violent manner, be shot out into space

[1] Cf. Baade and Zwicky, *Proc. Nat. Acad. Sci.*, **20**, 259, 1934; F. Cernuschi, *Phys. Rev.*, **56**, 120, 1939.

with a velocity which sometimes may be hyperbolic, and carry the explosion products away from the mother-star, forming a kind of transient binary with rapidly separating components—the nova counterpart of "the plume." This final cataclysm may appear in the observations as a secondary maximum of luminosity and, later on, the shot-off bubble may become visible in the telescope.

Both these features have observational counterparts. It may, in particular, be pointed out that the unidirectional character of the expulsion of the bubble makes it understandable that the secondary maximum, as well as the appearance of a visible companion nebular knot, may be very erratic in character and sometimes be missing altogether.

A further elaboration of the above point of view would seem to involve a study of shock waves in stars as a first prerequisite. It might be possible in this way to obtain an independent estimate of the amount of energy released in the explosion, which may be compared with the observed excess of radiation during the nova stage. Considering the extremely high temperatures involved in a shock wave, it seems necessary to conclude that light-pressure will be by far the biggest part of total pressure and the main agent responsible for the driving-off of the initial shell by the shock wave.

To recapitulate, it may be said that the occurrence of a real explosion seems necessary not only in order to account for the shock-wave type of initiation of novae but still more for the occasional formation of a companion nebular knot and a secondary maximum of luminosity. Moreover, the explosion hypothesis seems flexible enough to allow for the existence of recurrent novae. Other suggested mechanisms for the making of novae may encounter considerably greater difficulties in these several respects.

It should, moreover, not be overlooked that, whatever the explosion mechanism is, it will, if sufficiently violent, provide a high-temperature laboratory which far surpasses that existing in ordinary stars and in which nuclear transformations on a grand scale must take place. The instability and subsequent expulsion of the bubble insures that the explosion fragments are distributed in interstellar space—a circumstance worth keeping in mind when considering the distribution of elements in the universe as well as in speculations about the origin of cosmic rays.[2]

SVEIN ROSSELAND

PRINCETON UNIVERSITY OBSERVATORY
July 3, 1946

NOTE ON THE SPECTRAL AND LUMINOSITY CLASSIFICATION OF STARS FROM SPECTRA OF LOW DISPERSION

In a recent paper on the spectra of the BD stars within 5° of the north pole, J. J. Nassau and Carl K. Seyfert,[1] using spectra of low dispersion, state that they have established criteria for spectral classification as well as for the separation of giants and dwarfs. It may be appropriate to point out that in all essential features the same system for classification and for luminosity criteria has been used at the Uppsala and Stockholm observatories for nearly twenty-five years. The variation of intensity of the cyanogen bands with stellar luminosity was found by the writer[2] at the Mount Wilson and Lick observatories in 1921. A rather complete presentation of the methods in question has been given in a paper by B. Lindblad and E. Stenquist,[3] where a bibliography of seventeen papers on the subject by Y. Öhman, C. Schalén, J. H. Petersson, S. Jungkvist, E. Stenquist, and the writer, published prior to 1933, was presented. Nassau and Seyfert have

[2] Baade and Zwicky, *op. cit.*

[1] *Ap. J.*, **103**, 117, 1946.

[2] *Mt. W. Contr.*, No. 228; *Ap. J.*, **55**, 85, 1922.

[3] *Stockholm Astr. iaktt. och. unders.* (*Stockholm Ann.*), Vol. **11**, No. 12, 1934.

mentioned only the paper by Petersson on the stars in the Carrington zone, making some comparisons with it at the end of their paper.

Later contributions to the development of the luminosity criteria have been given by J. M. Ramberg[4] and B. Lindblad[5] (especially concerning the dwarfs of advanced K and M type) and in the paper by Ramberg on the Hyades and Praesepe to be mentioned later. A general outline of the system has also been given in the report of the Subcommittee on Criteria for Classification of Stellar Spectra in 1935.[6] Criteria in low dispersion for stars of Cepheid character have been investigated by Y. Öhman and W. Iwanowska[7] and by W. Iwanowska.[8] Other effects, for instance the increase of intensity of the *MgH* and *CaH* bands in the dwarfs of late types, as found by Y. Öhman,[9] may be useful in the future but have not yet been included in the general system. A comparison between the effects of luminosity in the cyanogen bands at λ 3883 and λ 4216 has been performed by H. O. Grönstrand.[10] In the early types much information is obtained by measuring the intensity of the lines of hydrogen. Special criteria for the white dwarfs were found by the writer[11] in 1921 and have been discussed more recently by Y. Öhman[12] and J. M. Ramberg,[13] who have both discovered new specimens of this type.

Applications of the methods on a large scale in recent years have been made by E. Stenquist[14] to the Cambridge proper-motion stars; by L. Gratton[15] to the Pleiades region; by Å. Wallenquist[16] to a region of the southern Milky Way in Sagittarius and Ophiuchus; by J. M. Ramberg[17] to the region of the Hyades and Praesepe, and by E. Vanäs[18] and G. Wernberg[19] to selected regions in the northern Milky Way. A preliminary report on the results of an application of the methods to stars in the region of the north galactic pole has been given by K. G. Malmquist.[20] An extensive work by J. M. Ramberg in a selected Milky Way region in Lacerta and Cepheus to a limiting magnitude fainter than $13^{m}0$ has made considerable progress in recent years. A preliminary report on results in Kapteyn's Selected Areas down to the same limiting magnitude has recently been published by T. Elvius.[21]

The variation of the cyanogen absorption with spectral type and luminosity has been studied by T. Setterberg in larger dispersion with the cassegrain spectrograph on the 40-inch reflector of the Stockholm Observatory in a paper which is soon to be published.

[4] *Stockholm Astr. iaktt. och unders*, Vol. **11**, No. 13, 1934.

[5] *Stockholms Obs. Ann.*, Vol. **12**, No. 2, 1935.

[6] *Trans. I.A.U.*, **5**, 181, 1936.

[7] *Stockholm Medd.*, No. 21, 1935.

[8] *Stockholms Obs. Ann.*, Vol. **12**, No. 5, 1936.

[9] *Mt. W. Contr.*, No. 498; *Ap. J.*, **80**, 171, 1934; *Stockholms Obs. Ann.*, Vol. **12**, Nos. 3 and 8, 1936.

[10] *Stockholm Medd.*, No. 50, 1942.

[11] *Loc. cit.*

[12] *Stockholm Medd.*, Nos. 31 and 32, 1937.

[13] *Stockholms Obs. Ann.*, Vol. **13**, No. 9, 90, 1941.

[14] *Nova Acta Reg. Soc. Scient. Uppsala.*, Ser. IV, Vol. **10**, No. 7; *Uppsala Medd.*, No. 72, 1937.

[15] *Stockholms Obs. Ann.*, Vol. **13**, No. 3, 1939.

[16] *Ann. v.d. Bosscha-Sterrenw. Lembang*, **5**, 5, 1939.

[17] *Stockholms Obs. Ann.*, Vol. **13**, No. 9, 1941.

[18] *Uppsala Obs. Ann.*, Vol. **1**, No. 1, 1939.

[19] *K. svensk. vetensk. Handl.*, Vol. **19**, No. 6; *Uppsala Obs., Ann.* Vol. **1**, No. 4, 1941.

[20] *Trans. I.A.U.*, **6**, 459, 1939.

[21] *Stockholms Obs. Ann.*, Vol. **14**, No. 8, 1945.

Especially in the later development of the method, the classifications of the spectra of low dispersion are based as far as possible on real spectrophotometric measurements of the various criteria as regards both spectral type and absolute magnitude. In this way it is possible effectively to avoid errors depending on the apparent brightness of the stars. As a by-product, monochromatic apparent magnitudes of the stars are obtained.

BERTIL LINDBLAD

STOCKHOLM OBSERVATORY, SALTSJÖBADEN
June 19, 1946

THE OCCURRENCE OF CYCLES IN *He* I

ABSTRACT

The relative populations of the 3^3D, 4^3D, and 4^3F levels are computed for different dilution factors and strengths of the lines feeding these levels. It is found that the occurrence of forbidden transitions causes a very slight overpopulation of the 3^3D level. A forbidden line of the type $2^3P - 4^3F$ is found to be intrinsically deeper than a permitted line, such as $2^3P - 4^3D$.

For a three-level cycle, the theory of cycles as developed by Rosseland[1] gives

$$\frac{N_2}{N_1} = \frac{A_{13}A_{32} + A_{12}A_{31} + A_{12}A_{32}}{A_{21}A_{31} + A_{21}A_{32} + A_{23}A_{31}}, \tag{1}$$

where N_1 is the population of level 1, N_2 that of level 2, and A_{ik} is the probability of transition from level i to level k, A_{ki} the probability of transition from level k to i, and $k > i$ at all times. The quantities A_{ik} and A_{ki} are evaluated according to their usual definitions,[2] allowance being made for the presence of a diluted radiation field. The quantity N_3/N_1, where N_3 is the population of level 3, is given by a similar expression.

In computing the relative population of the levels, it is convenient to use the dilution factor W and the ratio b_{31}/b_{32} as parameters. Here b_{ki} is the spontaneous emission coefficient of the transition k to i and occurs in the expressions for A_{ik} and A_{ki}. We may evaluate b_{ki} if the f value of the transition k to i is known. The ratio b_{31}/b_{32} gives the relative strength of the transitions 1–3 and 2–3.

Consider the diffuse series of *He* I. Let level 1 be 2^3P, level 2 be 3^3D, and level 3 be 4^3D or 4^3F. The discussion differs only very slightly in numerical factors for the singlet and the triplet series and thus will be carried through here only for the triplet series. However, there will be a difference between the singlet and the triplet series as regards the absolute population of the upper levels, for the 2^1P level is connected to the ground level of the *He* atom by a permitted transition, whereas the 2^3P level is above a metastable state.

Case I.—Level 3 is 4^3F. Then the transition 1–3, $2^3P - 4^3F$, is forbidden, and the transition 2–3 is a strong permitted line, being the leading member of the $3^3D - n^3F$ series. The probability of spontaneous transition 3–1, b_{31}, will depend on the electric fields present, i.e., on the density of the atmosphere, being practically zero in a supergiant, and in dwarf stars differing from zero by an amount depending on the density of the atmosphere.[3] From a consideration of the theoretical intensity of the $2^3P - 4^3F$ line in weak fields, it seems likely in dwarf stars, where the expected electric fields can be classified as weak, that b_{31}/b_{32} is less than 10^{-3}. In giant stars $b_{31}/b_{32} = 0$.

Table 1 gives the relative population of the 3^3D level, level 2, and the 4^3F level, level 3, for various values of W and b_{31}/b_{32}. The rapid depopulation of the upper levels with increasing dilution is evident. Recall also that N_1 decreases rapidly with increasing dilu-

[1] S. Rosseland, *Theoretical Astrophysics*, p. 145, Oxford: Clarendon Press, 1936.

[2] *Ap. J.*, **88**, 94, 1938.

[3] *Ap. J.*, **100**, 333, 1944.

TABLE 1

LEVEL 3 = 4^3F

W	b_{31}/b_{32}			
	0	10^{-2}	10^{-1}	1
	N_2/N_1			
1.0.....	0.490	0.490	0.490	0.490
0.5.....	.286	.286	.287	.290
0.1.....	.0667	.0668	.0673	.0703
0.05.....	.0340	.0340	.0344	.0361
0.01.....	0.00692	0.00693	0.00701	0.00740
	N_3/N_1			
1.0.....	0.467	0.467	0.467	0.467
0.5.....	.207	.208	.211	.228
0.1.....	.0164	.0168	.0198	.0356
0.05.....	.00456	.00479	.00666	.0163
0.01.....	0.000203	0.000262	0.000710	0.00300

TABLE 2

LEVEL 3 = 4^3D

W	b_{31}/b_{32}			
	1	10	100	∞
	N_2/N_1			
1.0.....	0.490	0.490	0.490	0.490
0.5.....	.290	.287	.286	.286
0.1.....	.0703	.0674	.0668	.0667
0.05.....	.0361	.0344	.0340	.0340
0.01.....	0.00740	0.00701	0.00693	0.00692
	N_3/N_1			
1.0.....	0.333	0.333	0.333	0.333
0.5.....	.163	.179	.184	.185
0.1.....	.0254	.0376	.0404	.0407
0.05.....	.0116	.0188	.0203	.0205
0.01.....	0.00214	0.00378	0.00411	0.00415

tion. This may be seen from the work of Struve and Wurm.[2] For any given dilution factor, however, the population of the 3^3D level is not significantly increased unless the strength of the forbidden line, 2^3P-4^3F, is comparable to that of the permitted line, 3^3D-4^3F. Such a great strength of the forbidden line in the atmosphere of a dwarf star seems improbable. Thus we may conclude that there is no noticeable extra re-emission in the 2^3P-3^3D line in dwarf stars from overpopulation of the upper level caused by uncompensated absorption in the 2^3P-4^3F line and cyclic emission $4^3F\rightarrow3^3D\rightarrow2^3P$. The population of the 4^3F level increases slightly as the strength of the forbidden line increases.

Case II.—Level 3 is 4^3D. Then the transition 1–3 is permitted, and the transition 2–3, being 3^3D-4^3D, is forbidden. Following through the analysis, as in Case I, shows that the possible excess population of the 3^3D level is very small for any reasonable value of the forbidden transition probability, b_{32}. Table 2 gives the relative population of level 2, and of level 3 to that of level 1 for various values of W and of b_{31}/b_{32}.

The fraction N_3A_{31}/N_1A_{13} gives the ratio of the number of emission processes in the line 1–3 to the absorption processes. Since A_{31}/A_{13} is a constant for any given value of the dilution factor W, the change of N_3/N_1 with different relative strengths of the lines 1–3 and 2–3 will give the change in the amount of emission to absorption in the line 1–3 for varying b_{31}/b_{32}. Table 1 shows for dilution factor $W = 0.01$ that, when the transitions 1–3 and 2–3 are of equal strength, the emission to absorption in line 1–3 is 0.00300/0.000262 = 11 times greater than when the line 1–3 has only 10^{-2} times the strength of the transition 2–3. Table 2 shows that, when the transition 1–3 is 100 times stronger than the transition 2–3, then the emission to absorption in line 1–3 is 0.00411/0.00214= 1.9 times stronger than when the lines are of equal strength. Thus when the transition 1–3 is permitted—hence very strong—the ratio of emission to absorption in the line is about 20 times its value when the line is forbidden and very weak. This result indicates that a forbidden line of the type discussed here is intrinsically deeper than a permitted line. The numerical values obtained here are maximum values, since the ideal case of a three-level system is discussed. Also it must be remembered that large dilution and values of b_{31}/b_{32} at all different from zero are mutually exclusive, if the transition 1–3 is forbidden.

ANNE B. UNDERHILL

YERKES OBSERVATORY
July 23, 1946

REVIEWS

Infrared and Raman Spectra of Polyatomic Molecules. By GERHARD HERZBERG. New York: D. Van Nostrand Co., 1945. Pp. 632+xiii. $9.50.

This is the most complete and satisfactory treatise on polyatomic molecules yet to appear and it constitutes a distinct contribution to the literature of molecular physics.

The first chapter, including about fifty pages, presents a general summary of the classical and quantum mechanical problems of rotation for linear, symmetric, spherical, and asymmetric molecules. The array of energy levels appropriate to each is illustrated and described in terms of spin and symmetry properties, statistics, and statistical weights. From these properties the characters of the rotational infrared and Raman spectra are predicted.

Chapter ii provides, in about one hundred and eighty pages, a complete discussion of molecular vibrations. A summary of the classical theory of normal co-ordinates and their symmetry properties introduces the discussion of vibrational eigen-functions and energy levels. The solution of the secular equation is illustrated by many specific examples, employing the assumptions of central forces, of valence forces, and of more general force fields. Force constants and molecular dimensions are tabulated for all the simpler polyatomic molecules which have been studied to date. The effects of anharmonicity, of vibrational interactions, and of isotopic substitutions are clearly presented.

A feature which will be most welcome to many readers is the concise and readable summary of those aspects of group theory which are essential for the description of molecular eigenfunctions and the determination of selection rules. Eighteen tables of symmetry types and characters are included, each appropriate to one or more point group.

In chapter iii vibrational infrared and Raman spectra are discussed, with an encyclopedic summary of all the presently available illustrations. These are classified according to the numbers of atoms per molecule, from three up to twelve, which provides for easy reference. This is a very convenient and valuable feature.

The effects of interaction between vibration and rotation are described in chapter iv. These include selection rules, typical envelopes for unresolved bands, and details of the line structure in resolved bands. The modifications resulting from centrifugal distortion, from internal rotation, and from molecular inversion, and the Coriolis splitting are briefly but adequately treated.

Methods for calculating thermodynamic quantities and the vibrational and rotational contributions to the partition function are reviewed in chapter v. The nature of the liquid and solid states are briefly discussed also.

The text includes a very extensive collection of experimental data, presented in tabular and graphical form, and a bibliography of nearly a thousand titles. The arrangement of material is admirable. Ready reference is provided by the complete subject and author indexes. It is to be regretted that the publishers permitted some of the figures to appear with lettering too small for legibility.

E. F. BARKER

University of Michigan

David Rittenhouse. By J. EDWARD FORD. Philadelphia: University of Pennsylvania Press, 1946. Pp. viii+226. $2.50.

This welcome addition to the series "Pennsylvania Lives" tells a straightforward story of the life and times of David Rittenhouse of Norriton and Philadelphia. Sometimes, indeed, the story seems too straightforward, with little color or excitement, but it is fairly certain that no fact of importance in the life of this early astronomer-patriot has been omitted. An earlier volume of the series, *John Alfred Brashear*, was written in a newspaper style, which made for more excitement but far less accuracy and more offense to astronomers. Only one thousand copies of each of these volumes are printed.

Born in 1732, Rittenhouse was a farmer and obscure clock-maker for thirty-five years. His

clocks were good; many of them in Philadelphia are running today and keeping good time. Rittenhouse was self-taught, yet he became an expert instrument-maker, mathematician, and observer. Most famous of his observations is that of the transit of Venus in 1769. Rittenhouse made his observations from his observatory at Norriton, but a platform erected for another party of observers, in the State House Yard, served as the place from which the Declaration of Independence was read to a public gathering on July 8, 1776.

In 1770 Rittenhouse moved to Philadelphia and into the best social and intellectual circles. He served long as one of the secretaries of the American Philosophical Society and, succeeding Benjamin Franklin, as president of that early learned group. While he delivered many papers before the Society, Rittenhouse was not a good speaker and was ill at ease when the eyes of others were upon him. With his few intimate friends, among whom were Thomas Jefferson and James Madison, he was warm and congenial.

Before Rittenhouse was forty he had built two intricate orreries and eclipse-predictors; one of these was for the College of New Jersey (Princeton), the other for the College of Philadelphia (University of Pennsylvania). The author does not tell the final destinies of these two machines; the one at Princeton was recently a "gear-mine" for miscellaneous unimportant mechanisms, according to reports, but the one at Pennsylvania, restored to operating condition a few years ago at the Franklin Institute, is preserved in the library of the university.

Details of many of the observations of comets, fireballs, and eclipses are given. For example, the British evacuated Philadelphia in mid-June, 1778, and on June 24 Rittenhouse and his scientific friends observed a total eclipse of the sun from the State House Yard observatory. His many surveying expeditions to determine the boundary lines of Pennsylvania and the adjoining states are chronicled in much detail; in this and other passages, however, the biographer has avoided repetitions of dates, and phrases such as "the following year" or "six months later" sometimes send the reader leafing back through several pages to see what year is meant.

In his public life Rittenhouse was for a while in the position of being considered a dangerous radical, but most of his service was in capacities such that there was much work and little opportunity to direct policy. As a tax collector and state treasurer Rittenhouse was able to live quite comfortably. Like Isaac Newton, Rittenhouse was director of the mint. Unlike his English predecessor, however, Rittenhouse did not grow prosperous in the job; through no fault of his this experience was an unhappy one and he resigned, after having the satisfaction of receiving a clean bill of health from an investigating committee.

For fifty years Rittenhouse suffered from what we today call gastric ulcers; this was the cause of his death in 1796. He had made little impression on international science, and even American astronomers today know too little about him. This new biography, which seems completely free of errors of typography or fact, should contribute to his stature.

ROY K. MARSHALL

The Fels Planetarium of
The Franklin Institute

Photometric Atlas of Stellar Spectra. By W. A. HILTNER and ROBLEY C. WILLIAMS. Ann Arbor: University of Michigan Press, 1946. $7.50.

The modern development of astrophysics requires that stellar spectra should be investigated by exact quantitative measurements not only with regard to the wave lengths but also with regard to the intensity profiles of the lines. Publication of the complete photometric record is the only way to make available in an entirely objective way the full amount of information which may be derived from a spectrogram. Moreover, the intensity graph has a pictorial value and speaks directly to the mind as no list of intensities could do.

For these reasons the *Photometric Atlas* of Hiltner and Williams must be considered an important step in stellar photometry. It is composed of an introductory outline and eight small booklets in a portfolio, each booklet giving the detailed record of a typical stellar spectrum on a scale of true intensities. Some of the very best instruments now available have been used for its derivation. The spectra were taken with the excellent coudé spectrograph of the McDonald Observatory and extend from about λ 3920 to λ 6720; the region covered varies a little from star to star. The dispersion increases from 2.1 A/mm near λ 4000 to 14.2 A/mm near λ 6500. The use of the recently introduced gratings would have caused difficulties of ghosts and false light, which are now largely avoided, the more so because the spectrograph lens was coated with

a nonreflecting film. The calibration was obtained by means of a wedge-slit, uniformly illuminated by a photoflood lamp; the exposures were one-fourth those on the spectrum itself. For the photometric reduction the authors made use of the ingenious, direct-intensity reading microphotometer of the University of Michigan. There is no doubt that only a completely automatic instrument could give in a finite time the full record of such beautifully detailed and complicated spectra.

The eight stars selected are typical for the following classes: B8Ia; A0V; A1V; A2Ia; F5Ib; F5IV; K2pec; M2Ib. The curves are reproduced on a scale of 12 A/mm at λ 3900 to 1.3 A/mm at λ 6700. The continuous background is traced at a height of 50 mm above the whole spectrum. The grain of the plate puts a limit to the detection of faint lines; these oscillations are still increased by some inevitable minor imperfections in the direct-intensity photometer. By comparing the record of α CMi to the tracings of the solar spectrum it is found that central deflections of 5 per cent, and more, can be distinguished from the background. However, these lines are so narrow in the reproduction that it is not possible to derive anything like equivalent widths. It is clear that a larger scale would have increased the amount of information to be derived from the spectrograms; but the higher cost of publication would probably have been prohibitive. Moreover, as it is now, the *Atlas* has a handy size, which makes the manipulation of the records particularly convenient.

In order to determine the influence of the instrument, the authors have measured the profiles of some iron-arc lines, which they consider to be intrinsically broadened by Doppler effect alone, and they derive an instrumental half-width of 1.5 mm, corresponding to a half-width of 0.15–0.55 A, according to the spectral region. It is to be noted that the iron lines may have been broadened also by Stark effect and by self-reversal, so that the true instrumental width is perhaps even less than assumed by the authors. An especial feature of this instrumental profile is its very faint tails, which compare favorably with those given by gratings. Doublets can be resolved at about 0.15 A near λ 4000 and at 0.55 A near λ 6000. The position of the continuous spectrum has been determined by preliminary records on a small scale, extending over a wide range of the spectrum. It sometimes deviates from the 100 line by 5 per cent and, of course, becomes very uncertain for the late-type stars. But an exact determination of the background cannot be expected from editors of a survey atlas and should be the subject for special theoretical work. The inclusion of a star like α Ori is especially suited to show the full complication of the intensity record and should be especially appreciated.

It is an important point to ascertain the precision of the photometric calibration. The authors state that a check was made on the calibration-curves and that these were found to vary by no more than 3 per cent.[1] It would have been interesting if some checks had been made also on the photometric reduction as a whole. Is there no influence of the factor 4 between the exposures of the spectra and of the calibrations? No influence of the intermittency due to guiding? It would have been possible, perhaps, to test the combined effect by comparing the records for a strongly and for a less strongly exposed strip of the same spectrum. It is very satisfactory that records have been made in both senses and that no asymmetries in the spectral lines have been detected.

Altogether, it is a continuous joy to "read" these records and to recognize many features, well known from verbal descriptions but now, for the first time, seen in a graphical representation. The enormous amount of work and care devoted to this *Atlas* is amply justified by the wealth of useful information which it discloses. It should be used over and over again by all astrophysicists interested in stellar spectra.

M. MINNAERT

Yerkes Observatory

ERRATUM

In Figure 1, page 138, of this volume, the equivalent widths of the four lines should have been given as follows: λ 4077 = 1.21 A, λ 4045 = 0.99 A, λ 4071 = 0.64 A, and λ 4058 = 0.15 A. In Plate II, the wave length "4068" should be corrected to "4058."

[1] Mr. W. A. Hiltner has pointed out to the reviewer a typographical error: the error limit of 0.15 in log *I* should read "0.015."